UNIVERSITY OF NOTTINGHAM

SCHOOL OF MATHEMATICAL SCIENCES

Learned fear extinction: an interdisciplinary investigation of the neurocircuitry and the potential therapeutic benefit of cannabidiol

Regimantas Jurkus

A thesis submitted to the University of Nottingham for the degree of

DOCTOR OF PHILOSOPHY

SEPTEMBER 2018

ABSTRACT

Fear memory and extinction are psychological processes believed to be dysfunctional in several anxiety disorders. We studied these processes using pharmacological, computational modelling and electrophysiological approaches to understand their neurochemical modulation as well as mediation by several brain areas. First of all, considering the well documented anxiolytic effect of the phytocannabinoid cannabidiol (CBD) in contextual fear memory and innate fear paradigms, we investigated its effects in auditory fear memory and extinction in rats. Our experiment revealed that CBD reduced auditory fear memory expression without impairing extinction. CBD also reduced contextual fear prior to extinction, consistent with previous findings. Our results indicate that CBD reduces learned fear associated with explicit cues, and support the potential use of CBD together with psychological treatments of anxiety disorders in the future.

Fear memory and extinction are mediated by a network of brain areas and their complex interactions. Recent computational fear memory and extinction network models have studied the function of the amygdala and its interaction with cortical areas. However, the role of the ventral hippocampus (VH), an area involved in both fear expression and extinction, in such models has not been addressed. We created a spiking neuron model of prelimbic cortex (PL), involved in fear expression, infralimbic cortex (IL), involved in extinction, and VH. We found that VH inactivation reduced the activity of PL to a larger extent than PL-IL disconnection, whereas PL-IL disconnection reduced the activity of IL to a larger extent than VH inactivation. This finding is consistent with the anxiolytic effect of VH inactivation reported in the literature.

Considering these roles of VH supported by our modelling experiment, we investigated VH interaction with PL and IL in awake behaving rats. Electrophysiological recordings during behavioural testing showed a decrease in PL, IL theta

oscillation power, and a decrease in VH theta and low gamma oscillation power, at extinction recall, compared to fear recall. The theta oscillation synchrony between PL and IL was also decreased during extinction recall, compared to fear recall. These findings add further support to the involvement of VH, PL and PL-IL communication in learned fear expression.

Overall, our findings revealed an anxiolytic effect of CBD in learned fear associated with explicit cues and strengthened the evidence of VH, PL and PL-IL communication involvement in learned fear expression. These results could lead to novel treatment approaches and new therapeutic targets for the processes that are dysfunctional in several anxiety disorders.

The work is dedicated to Aaron Hillel Swartz and Alexanda Asanovna Elbakyan.

The heroes whose crime is that of sharing knowledge with the world.

ACKNOWLEDGEMENTS

First of all, I would like to thank my supervisors, Dr Reuben O'Dea, Dr Carl Stevenson and Professor Markus Owen for their Sisyphean struggle with me during my PhD studies. I would like to thank Dr Reuben O'Dea for his unfaltering patience in explaining the mathematical modelling principles and hearing my misinterpretations of them over and over. I am grateful to Dr Carl Stevenson for the extensive scientific discussions, advice and the unshakeable aura of calm reflection when facing a multitude of my less-than-perfect experiments. Your attitude towards science and life in general is very inspiring! Lastly, Professor Markus Owen's ingenuity in explaining difficult concepts simply was something every scientist should strive for.

Secondly, I would like to thank my friends. I am grateful to my best friend, Karolis. Of all the things we did throughout the years, the last thing I expected was for you to show up on my doorstep with bags of food unexpectedly, just to make sure that I don't starve during the thesis writing. You're the best, bud. A big thanks to Mezida and Vitaly for all those great BBQs and outings. Life would not be the same without you. Thanks to Lucas, my brother from a different mother, who is simply a walking adventure. Your great advice, your awesome tours of Amsterdam and your company in general are second-to-none. Thanks to Priyata, Vincent and John, who supported me with memes, laughter and great conversations. I am forever grateful to all of you.

Last, but not least, I would like to thank my family: mom, dad, little sister, grandpa, aunts, uncles and cousins. You were always there for me. I could not have done this without you. My special thanks goes to my late grandmas, Kristina and Danguolė. Your stories, advice and lessons helped me get through to this point in my life. Only now I begin to grasp the wisdom you have shared with me. I miss you and I wish you were here.

PUBLICATIONS

Jurkus, R., Day, H. L., Guimarães, F. S., Lee, J. L., Bertoglio, L. J. Stevenson, C. W. (2016), 'Cannabidiol regulation of learned fear: implications for treating anxiety-related disorders', *Frontiers in Pharmacology* **7**, 454.

CONTENTS

ACRONYMS AND ABBREVIATIONS

2-AG 2-arachidonoylglycerol

5-HT1A Serotonin receptor type 1A

AB Accessory nucleus

AChE Acetylcholinesterase

AP Anterior-posterior axis

AEA Anandamide

AMPA α-amino-3-hydroxy-5-methyl-4-isoxazoleprionic acid

ANOVA Analysis of variance

BA Basal amygdala

BDNF Brain-derived neurotrophic factor

BLA Basolateral amygdala

CA1 Cornu ammonis 1

CB1 Cannabinoid type 1 receptor

CBD Cannabidiol

CeA Central nucleus of amygdala

CR Conditioned response

CS Conditioned stimulus

dACC Dorsal anterior cingulate cortex

DCS D-cycloserine

DH Dorsal hippocampus

E-Ext Early extinction

FS Fast-spiking interneuron

GABA γ-aminobutyric acid

Hab Habituation

HH Hodgkin-Huxley formalism

IAF Integrate-and-fire model

IL Infralimbic cortex

IN Inhibitory cell

ITC Intercalated cell masses

LA Lateral amygdala

L-Ext Late extinction

LFP Local-field potential

LTD Long term depression

LTP Long term potentiation

LTS Low threshold spiking interneuron

mPFC Medial prefrontal cortex

NMDA N-methyl-D-aspartate

NPY+ Neuropeptide Y expressing interneuron

O-LM Oriens lacunosum-moleculare interneuron

PFC Prefrontal cortex

PL Prelimbic cortex

PTSD Post-traumatic stress disorder

PV Parvalbumin-positive interneuron

TRPV1 Transient receptor potential cation channel subfamily V member 1

US Unconditioned stimulus

vmPFC Ventromedial prefrontal cortex

VH Ventral hippocampus

1

GENERAL INTRODUCTION

1.1 OVERVIEW

Fear conditioning and extinction are believed to be dysfunctional in several anxiety and trauma-related disorders. During fear conditioning an association is made between a dangerous or aversive unconditioned stimulus (US) and its predictor, a neutral conditioned stimulus (CS) which could be a simple cue or a context. This association leads to the previously neutral CS eliciting a defensive response or 'fight-or-flight' behaviour in order to avoid danger. Once the association is complete, extinction learning can take place. During extinction, CS is presented on its own or in many repetitions leading to a diminished defensive response. However, extinction does not delete the CS-US association, since the presentation of CS in a different environment can result in a spontaneous return of the defensive behaviour over time after extinction.

Fear conditioning and extinction involve multiple brain areas, but particularly important ones are the amygdala, prelimbic and infralimbic cortices of the medial prefrontal cortex, and the ventral hippocampus (Calhoon & Tye 2015). The amygdala serves as the association centre for the sensory CS and US inputs representing the conditioned fear. This association takes place in the basolateral part of the amygdala (BLA) (Rogan et al. 1997). BLA projects to the central nucleus of the amygdala, which, in turn, projects to other brain areas, leading to the release of stress hormones, adrenaline and to the expression of defensive behaviour, such as freezing in rodents (LeDoux et al. 1988, Van de Kar et al. 1991, VanElzakker et al.

2014). Prelimbic and infralimbic cortices modulate this activity of the amygdala in opposite ways. The prelimbic cortex indirectly encourages the central nucleus of the amygdala to communicate with other brain areas resulting in fear expression, whereas the infralimbic cortex projects to inhibitory neurons next to the central nucleus of the amygdala and prevents the expression of fear (Vertes 2004, VanElzakker et al. 2014, Berretta et al. 2005). The ventral hippocampus, on the other hand, is involved in both fear expression and extinction as well as the processing of information about the environment which can drive the re-expression of fear to an extinguished CS if it presented in a new environment (Sierra-Mercado et al. 2011, Marek et al. 2018). It is important to understand the interaction between the ventral hippocampus and the two areas of the medial prefrontal cortex at different stages of fear memory and extinction to better understand their role in the process. Therefore, we have investigated the medial prefrontal-ventral hippocampal interactions electrophysiologically at fear recall and extinction recall stages. We have found very little interaction between the areas at these two stages. However, the individual area activity at the stages was consistent with the general consensus of their involvement at fear conditioning and extinction process.

The study of the interaction of the aforementioned and other brain areas involved in fear memory and extinction processing is a highly detailed and temporally-restrictive process. The methods of investigation range from studies of the molecular pathways within cells to understand synaptic plasticity, to electrophysiological recordings of brain activity during fear memory and extinction. Such knowledge is difficult to integrate intuitively as features spanning multiple spatial and temporal scales must be considered, from single cells to large-scale brain networks (Nair et al. 2016). Thus, computational modelling methods of fear networks have been employed to integrate this information and aid understanding of these processes and their influence on fear memory and extinction processing. The most recent branch of models, focusing on biophysical details, has made strides towards understanding fear memory processing, but focused on the amygdala and the medial prefrontal cortex (Pendyam et al. 2013, Fenton 2015). The role of the ventral hippocampus in such models has not been addressed. Thus, we created a spiking

neuron model network that included the ventral hippocampus together with the amygdala and the medial prefrontal cortex. The model verified the ventral hippocampus involvement in learned fear expression that is consistent with biological studies.

Pharmacological approaches have been used to better understand fear memory and extinction processing. This has led to discoveries that, for example, some widely used anxiolytics, such as benzodiazepines, impair fear extinction process (Rothbaum et al. 2014). On the other hand, cannabidiol, a non-psychoactive cannabis plant constituent, can facilitate the extinction process and dampen the expression of certain types of fear memory (Levin et al. 2012, Stern et al. 2012, 2014, 2015, 2017, Gazarini et al. 2015, Song et al. 2016). However, there is very limited data of cannabidiol effects on fear memory related to explicit cues. Therefore, we have investigated the role of cannabidiol in auditory fear conditioning experiment, which showed that cannabidiol is anxiolytic, but does not interfere with the auditory fear extinction process.

Even though most of this research is done in rodents, their fear memory and extinction processing and the areas involved are similar to humans. In fact, the extinction process studied in rodents is the underlying basis for exposure therapy used in the clinic (Stewart & Wrobel 2009, Norberg et al. 2018). It is believed that the pathophysiology of anxiety arises from dysregulation of normal fear memory and extinction processing (Sherin & Nemeroff 2011, Mahan & Ressler 2012, Milad et al. 2007, 2008, 2009). Therefore, a better understanding of fear memory and extinction processing, the functional and time-specific involvement of various brain areas as well as pharmacological targets that can be used to facilitate it could potentially present new and more effective ways of anxiety and trauma-related disorder treatment. In fact, the experiments that we have conducted contribute towards understanding of the ventral hippocampal-medial prefrontal cortex interplay at two important stages of fear memory. Our modelling work is consistent with the anxiolytic effect of VH inactivation reported in biological studies and presents a good starting point to include other areas involved in fear memory and extinction processing. Lastly, our experiment with cannabidiol suggests that it might be

compatible with exposure therapy. Due to the similarity of humans and rodents in fear and extinction processing, the results of our experiments could contribute towards the change in approaches of clinical anxiety and trauma-related disorder treatment.

1.2 ANXIETY AND TRANSLATIONALLY-RELEVANT ANIMAL MODELS

Anxiety disorders are characterised by the expression of fear in non-threatening situations or excessive behavioural and physiological manifestations in response to observed or anticipated danger (Gilmartin et al. 2012). These disorders are the most prevalent mental health disorder group in the European Union, with 14% of the total population affected annually (Wittchen et al. 2011). Addressing these disorders clinically is a challenge since the past 50 years of anxiolytic, fear symptom-aleviating, drug development has delivered little to no new solutions (Griebel & Holmes 2013).

The most recent milestones of anxiolytic drugs can be summarised by serendipitous discovery of the serotonergic drug anxiolytic properties and the licensing of selective-serotonin reuptake inhibitors for the treatment of anxiety disorders in the late 20th century which have dominated the clinical management of anxiety disorder symptoms ever since (Griebel & Holmes 2013, Baldwin et al. 2014).

However, this group of drugs is not a panacea, carrying serious side-effects, including the risk of life-threatening serotonin syndrome, tolerability, efficacy limitations and a delayed onset of action, that is usually accompanied with a transient worsening of the symptoms (Baldwin et al. 2014).

The lack of progress has brought focus to three areas of research:

1. Developing new, or repurposing old, drugs that are compatible with psychological treatment approaches, such as exposure therapy (Myers & Davis 2007, Steckler & Risbrough 2012).

2. Investigation of the cross-communication between the areas involved in fear memory and extinction processing during different stages of the process (Quirk & Milad 2010, Hartley & Phelps 2010, Milad & Quirk 2012, LeDoux 2014, LeDoux & Pine 2016).

3. Employment of computational modelling methods capable of efficiently integrating the available multidimensional information of fear memory and extinction processing to reveal the gaps in knowledge (Nair et al. 2016).

In this thesis introduction I will discuss the current state of fear memory processing research in the light of these three factors. The experiments presented in the following chapters will cover the contribution to each of the promising areas of research sequentially. The thesis will conclude with the discussion of the work I have done and what are the main challenges that lie ahead.

1.2.1 *Limited treatment options for anxiety disorders*

Anxiety and stress-related disorders dominate mental health problems with a lifetime prevalence of 28.8% (Kessler et al. 2005). Specific phobias, social phobia and post-traumatic stress disorder (PTSD) are among the most dominant disorders within the group, with a lifetime prevalence of 12.5%, 12.1% and 6.8% respectively (Kessler et al. 2005).

A recent meta-analysis of effective treatments of PTSD revealed several groups of drugs that were more effective than placebo (Cipriani et al. 2018). These included: selective serotonin reuptake inhibitors (SSRIs) fluoxetine, paroxetine and sertraline; a serotonin-norepinephrine reuptake inhibitor (SNRI) venlafaxine; a trycyclic antidepressant (TCA) desipramine; irreversible monoamine oxidase inhibitor (MAOI) phenelzine; and an antipsychotic risperidone. The best effect was attributed to phenelzine (Cipriani et al. 2018).

SSRIs are associated with a delayed onset of action accompanied by a temporary worsening of anxiety-related symptoms, a plethora of adverse effects ranging from insomnia and sexual dysfunction to increased risk of suicide, and a with-

drawal syndrome once the use is discontinued (Rosen et al. 1999, Dording et al. 2002, Cascade et al. 2009, Fergusson 2005, Tamam & Ozpoyraz 2002, Sinclair et al. 2009). The rest of the remaining drugs, excluding the antipsychotic drug risperidone, rely on the serotonergic system and carry serious associated side effects (Remick et al. 1989, Riediger et al. 2017, Kerr 2001, Stahl et al. 2005, Blythe & Hackett 1999). Risperidone, on the other hand, is associated with side-effects that rely on dopaminergic system ranging from sedation to pseudoparkinsonism and the irreversible involuntary movement disorder – tardive dyskinesia (Muench & Hamer 2010).

All of the drugs listed in the report by Cipriani et al. (2018) have recorded cases of lethal toxicity, with TCAs, MAOIs, SNRIs and, to a lesser extent, SSRI being infamous as drugs of choice in a large number of suicidal single-drug overdoses (Popa et al. 2010, Kopala et al. 1998, Kerr 2001, Isbister et al. 2004, White et al. 2008). Therefore, alternative safer and more effective approaches are urgently needed.

An approach that is safer, albeit less effective than pharmacotherapy in PTSD is repetitive exposure to traumatic cues, also known as exposure therapy (Stewart & Wrobel 2009). Exposure therapy has been shown to be more effective than other psychological interventions, such as relaxation training or eye movement desensitization and reprocessing, in clinical outcomes of PTSD (Taylor et al. 2003).

Interestingly, a meta-study by Wolitzky-Taylor et al. (2008) showed a similar trend in the case of specific phobias since exposure therapy is superior to alternative psychological interventions. Considering the potential side effects of anxiolytic drugs, it is not surprising that psychological interventions are used to treat such disorders (Baldwin et al. 2014).

1.2.2 *Anxiety disorders involve multiple brain areas*

There are no biomarkers of anxiety that would be specific enough to be used for diagnosis (Bandelow et al. 2016). Instead, anxiety disorders are diagnosed based on symptoms by a qualified mental health professionals. Although there are no specific biomarkers useful for diagnosis, PTSD results in significant pathophysiological

changes in the brain: hyper-responsiveness to emotional stimuli in the amygdala, increases in emotional responsiveness and reductions of volume in the hippocampus and decreases in the grey matter and white matter of the prefrontal cortex with accompanying hypo-responsiveness to emotional stimuli among others (Sherin & Nemeroff 2011, Mahan & Ressler 2012). The aforementioned three brain areas are known as the fear memory triad – the essential members of the brain network responsible for the processing of fear learning and memory (Giustino & Maren 2015). In addition to the areas involved, a series of studies with PTSD sufferers have indicated their reduced ability to learn to suppress inappropriately expressed learned fear, suggesting that either the learned fear signal that is too overpowering or the fear suppression signal is too weak (Milad et al. 2007, 2008, 2009).

Such clinical findings regarding impaired learned fear processing and multiple brain area functional dysregulation indicate that anxiety and trauma-related disorders such as PTSD should be studied at a network level and that fear memory processing plays a significant part in the disorder.

1.2.3 *Fear memory and extinction memory competition in classical fear conditioning*

Fear learning and memory in Pavlovian, classical conditioning, terms is the association of a neutral conditioned stimulus (CS), which can range from a simple acoustic tone to an amalgam of sensory inputs, defined as a context, with an aversive unconditioned stimulus (US), such as an electric shock. Fear learning can be categorized into stages, known as acquisition, consolidation, retrieval or expression. Similarly, extinction learning consists of acquisition, consolidation and recall. These stages can be followed by fear renewal and spontaneous fear recall.

During the fear acquisition stage an animal is presented with the CS together with an US to learn and later consolidate the association into long-term memory. When this is achieved, the animal is able to undergo retrieval where it is presented with the CS alone, which serves as the predictor of the US, resulting in a conditioned response (CR), which is usually freezing behaviour in rodent studies.

During the extinction learning stage the CS-only stimulus is presented long enough or in many repetitions so that the CR expression gradually diminishes. This stage is followed by extinction recall, where the presentation of CS results in a diminished CR that is retained from the extinction stage.

It is important to note that extinction learning (i.e. associating safety with CS) extinguishes the expression of defensive behaviour, or freezing, which is a behavioural indicator of fear memory. In other words, extinction training does not overwrite the previous fear learning, but instead suppresses it competitively. In fact, this can be witnessed during fear renewal stage, where an extinguished CS is presented outside the extinction context, in a fear conditioning context or a completely new context, resulting in an increased freezing behaviour. Similarly, an increased defensive behaviour to an extinguished CS can be seen during spontaneous fear memory recall.

Overall, the functional segregation of fear and extinction memory associated to the same CS and the temporally-limited dominance over each other is key to understanding the neuroscience of fear memory, its disorders and their potential treatment.

Classical conditioning model validity

Animal models are evaluated based on specific validity criteria, known as face, construct and predictive validity. Face validity describes how well an animal model measures what it is designed to measure. Construct validity describes how well does the animal model match the pathophysiology or etiology of a disorder. Lastly, predictive validity describes how well does the drug action in the animal model correspond to the drug action in clinical patients.

Pavlovian, or classical, fear conditioning is capable of eliciting a behavioural fear response, its subsequent recall, and suppression as a result of extinction learning, suggesting a robust face validity. This behaviour can be correlated to the level of stress hormones and neural activity in brain areas associated with fear memory. Moreover, the extinction stage of classical conditioning is highly similar to the exposure therapy used to treat anxiety and stress-related disorders, and fear renewal

as well as spontaneous fear recovery seen in classical conditioning is a limiting factor of this psychological treatment. Therefore, classical fear conditioning has a good construct validity. Lastly, the behavioural manifestations of fear in the animal model can be manipulated with pharmaceuticals used in fear memory disorders, suggesting a good predictive validity.

Overall, classical fear conditioning provides a methodologically valid behavioural paradigm to investigate the brain areas and their involvement in the different stages of the fear and extinction learning process underlying anxiety and stress-related disorders.

1.3 NEUROANATOMY OF THE FEAR MEMORY TRIAD

Anxiety and anxiety-related disorders clinically manifest with hyperactivation of the amygdala and associated areas, a phenonmenon that is similar to the activity seen in fear conditioning of healthy individuals (Etkin & Wager 2007). In fact, it is generally accepted that failure to extinguish fear expression is a key aspect of these disorders (Rosen & Schulkin 1998, Santini et al. 2008, Jovanovic et al. 2010).

Neuroimaging studies of PTSD patients highlight impaired extinction recall coinciding with dysfunctional activity in multiple brain areas with the amygdala and the dorsal anterior cingulate cortex (dACC) showing hyperactivity and the hippocampus as well as the ventromedial prefrontal cortex being hypoactive (Milad et al. 2009). However, studies of these areas and their involvement in anxiety and stress-related disorders clinically is restricted to non-invasive techniques.

Fear memory relies on three key brain areas for its formation which are dysfunctional in anxiety and stress-related disorder patients: the amygdala, the hippocampus and the prefrontal cortex (Bishop 2007).

Initial stages of delay fear conditioning, defined by discrete CS and co-terminating US association are mostly reliant on the amygdala; trace fear conditioning, in which a discrete CS terminates and is then followed by a lagging US requires more input from the medial prefrontal cortex and the hippocampus for the association to take place, whereas contextual fear conditioning relies on the

amygdala-hippocampal interaction for the acquisition of fear memory (Gilmartin et al. 2014).

Our understanding of how this circuit works in terms of fear memory processing is beginning to emerge and is one of the main topics of interest of today's neuroscience.

1.3.1 *Amygdala*

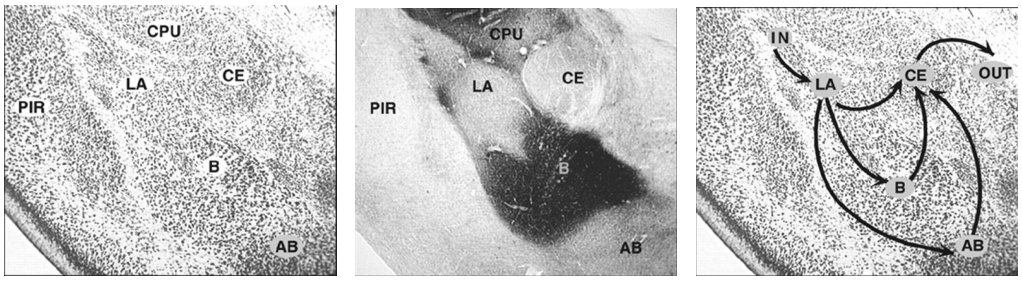

(a) Nissl-stained slice (b) AChE-stained slice (c) Amygdala pathways

Figure 1 – The different regions of the amygdala, including the lateral amygdala (LA), basal (B), accessory basal (AB), and central nuclei (CE). It is surrounded by the piriform complex laterally (PIR) and the caudate putamen (CPU) dorsally. Panels 1a and 1b show Nissl-stained and acetylcholinesterase-stained (AChE-stained) adjacent slices, respectively. The pathways within the amygdala are shown in panel 1c. Adapted from LeDoux (2000).

Since the seminal experiments with temporal lobectomy of rhesus monkeys in 1937, the amygdala has been known to be involved in the expression and modulation of fear (Klüver & Bucy 1937, cited in Hermans et al. 2014). Nowadays the amygdala is known as a complex of several nuclei located in the temporal lobe, subdivided based on their cytoarchitecture, projections and functions (Figure 1).

The basolateral complex (BLA) of the amygdala is composed of basal (BA), accessory basal (AB) and lateral (LA) nuclei and sometimes referred to as the deep nuclei of the amygdala (Sah et al. 2003). The intercalated nuclei (ITC) of the amygdala are found between BLA and the central nucleus of the amygdala (CeA). The latter is formed of the centromedial (CeM), centrolateral nuclei (CeL) and a portion of the bed nucleus of the stria terminals (BNST). The aforementioned

areas are accompanied by the cortical nuclei, the anterior amygdala area and the amygdalo-hippocampal area.

Fear memory research has mostly focused on BLA, the area of fear memory CS and US input convergence and locus of initial fear memory formation, CeA, which drives the expression of defensive, "fight-or-flight" behaviour, and ITC, which exert inhibitory control over CeA.

Contextual, tone and shock input convergence

When an animal is undergoing a fear conditioning paradigm to learn the association of CS and a US, relevant inputs arrive and converge in the lateral nucleus of the amygdala (LA) in the basolateral complex (Blair 2001, Barot et al. 2008, Hashikawa et al. 2013).

In the case of the auditory cued conditioning, the tone information arrives through both a direct and indirect pathway, through the thalamus and the auditory cortex, respectively (Romanski & LeDoux 1993, Doron & Ledoux 1999, Ferrara et al. 2017, Kim & Cho 2017a).

During contextual fear conditioning, the contextual CS reaches BLA from the dorsal hippocampus indirectly, relying on the ventral hippocampus CA1 and the subiculum for transmission (Fanselow 2000, LeDoux 2000).

The US, in the form of shock, pathway to LA has been unknown for some time, but recent evidence suggests reliance on intact lateral and ventro-lateral parts of the periaqueductal gray (LPAG and VLPAG), which is one of the key areas in the brain for processing pain (Assareh et al. 2017).

Input association

Once these signals converge in BLA, an association of the information can take place. In fact, Rogan et al. (1997) showed that in auditory fear learning the CS following fear conditioning evokes a type of activity in the lateral nucleus of BLA that is similar to the induction of long-term potentiation (LTP), the molecular model thought to underlie synaptic plasticity. This places BLA at the centre of the initial memory formation.

As mentioned above, fear extinction is a repeated or prolonged CS presentation in the absence of the previously associated US, resulting in a diminished CR (Fitzgerald et al. 2014a). In other words, it is the ability of the brain to override the aversive experience-context or experience-cue association to stop the expression of fear responses and avoidance behaviours when a context or a cue no longer can accurately predict danger. It involves increasing the inhibitory tone in the amygdala by engaging local GABAergic neurotransmission (Paré et al. 2004).

LTP-like activity in BLA is also important for extinction learning, since interference with glutamatergic NMDA signalling impairs the acquisition of extinction training (Falls et al. 1992, Mao et al. 2006). Therefore, LTP-like activity in BLA is important for both fear and extinction learning processes.

BLA synapses onto ITC show NMDA-dependent LTP and LTD, suggesting that ITC could be the main site of plasticity associated with fear extinction (Royer & Pare 2002). Lesions to ITC impair the expression of extinction (Likhtik et al. 2008). Therefore, while LTP-like activity in BLA is important for both fear expression and extinction, it relies on its projections to ITC for the latter process.

Fear memory input associations within BLA give rise to three distinct populations of neurons that exhibit emotional state-specific activity in response to CS (Herry et al. 2008). Specifically, fear memory trace neurons of BLA exhibit increased firing rate during high fear stage, extinction memory trace neuron activity is the highest during low fear stage, whereas extinction-resistant memory trace neurons fire at both high and low fear states (Herry et al. 2008).

Defensive behaviour

BLA, upon receiving sensory inputs representing a fearful situation, sends an excitatory signal via the projection to the central nucleus of the amygdala, inducing an output of the information to the hypothalamus, PAG, and the bed nucleus of the stria terminalis, engaging vigilance, freezing behaviour and the sympathetic "fight-or-flight" response (VanElzakker et al. 2014, LeDoux et al. 1988, Van de Kar et al. 1991).

1.3.2 *Medial Prefrontal Cortex*

The prefrontal cortex is divided into medial (mPFC), lateral and ventral PFC, each containing additional subdivisions (Uylings & van Eden 1990). Rodent mPFC lesions revealed its involvement in attention, working memory and emotional regulation (Vertes 2006, Kesner & Churchwell 2011).

Rodent mPFC can be seen in Figure 2. This area can be further subdivided into the dorsal anterior cingulate (dACC), prelimbic (PL), infralimbic (IL) and medial orbital cortices (Uylings & van Eden 1990, Heidbreder & Groenewegen 2003, Hoover & Vertes 2007). PL is homologous to human dACC and IL is homologous to human vmPFC (Quirk & Beer 2006).

mPFC in contextual fear memory

Zelinski et al. (2010) showed that lesions to IL and PL prior to contextual fear conditioning affected only extinction recall, whilst lesions to the ventromedial orbital PFC resulted in impaired extinction with increased levels of generalized anxiety. However, such experiments should be performed with separate lesions to IL or PL as the two areas seem to have discrete effects in fear memory.

However, the mPFC involvement in acquisition is still debated as, on one side, there is electrophysiological evidence of its involvement in fear memory acquisition, but, on the other hand, there seems to be a lack of behaviourally relevant confirmation of such involvement.

PL involvement in correct context discrimination was shown in a food-reward paradigm exploiting conflicting context-response tasks (Marquis et al. 2007). It could be possible that PL is involved in determining a better danger-predicting cue when presented with conflicting context cues. The closest evidence in support of this notion was seen in Antoniadis & McDonald (2006), where damage to mPFC, covering PL, IL and the anterior cingulate cortex, resulted in a lack of contextual fear discrimination.

An additional experiment with separate lesions to each of the three areas could help determine if PL, any other area, or a combination of them underlie

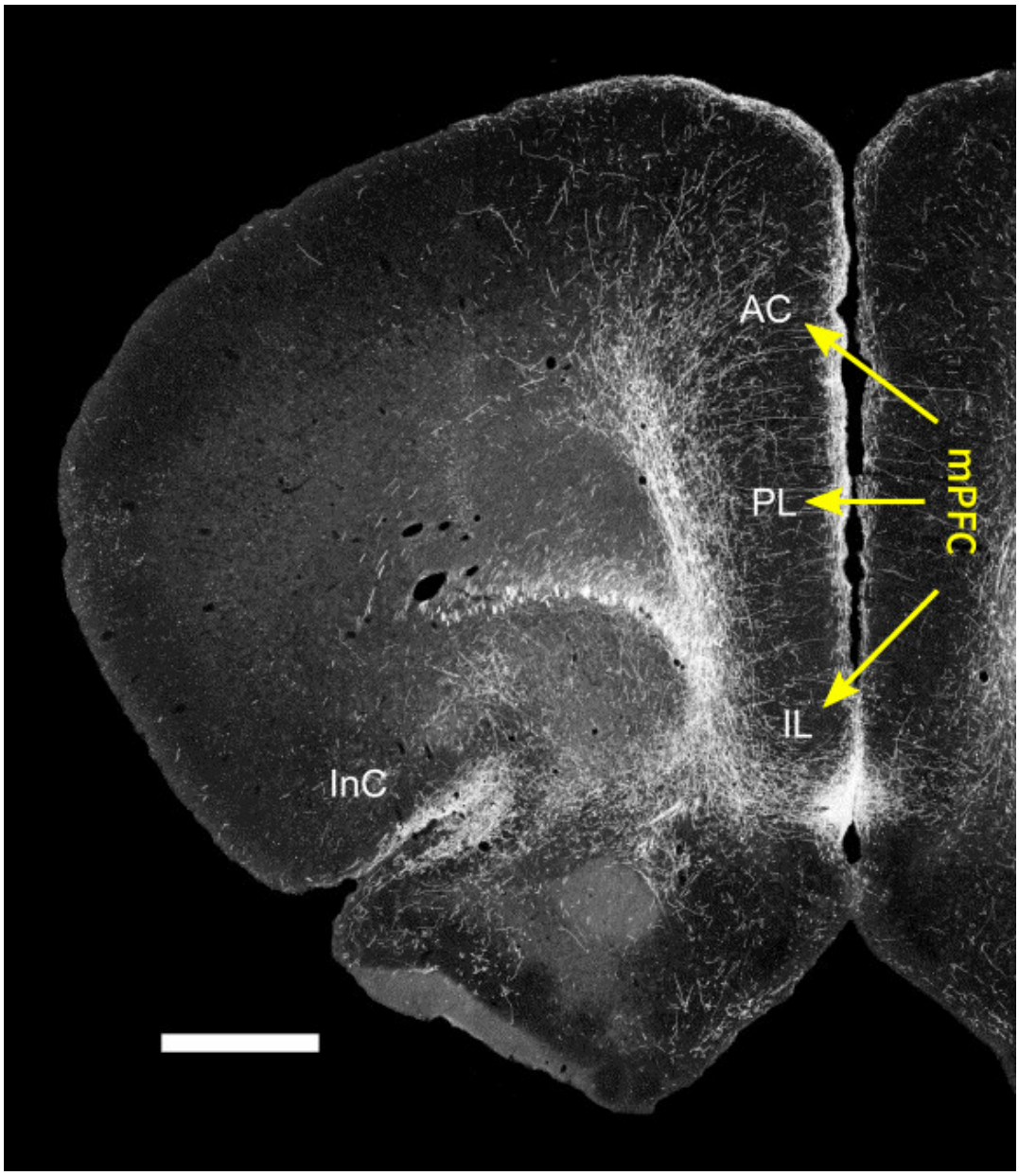

Figure 2 – Labelling patterns of mPFC resulting from PHA-L injection into the nucleus reuniens of the thalamus. AC, anterior cingulate cortex; IL, infralimbic cortex; InC, insular cortex; PL, prelimbic cortex. Adapted from Vertes (2006).

this effect. This would reveal more information regarding the role IL and PL play in contextual fear memory processing. Laurent & Westbrook (2009) have carried out experiments which clearly indicated that PL is responsible for fear memory retrieval and IL is responsible for extinction, especially its consolidation and retrieval, during contextual fear conditioning.

mPFC in explicit-cue fear memory

Early studies in fear conditioning using explicit cues showed that IL activity during extinction recall is inversely proportional to the fear expressed by the animal (Milad & Quirk 2002). Stimulation of this area prior to fear extinction results in reduced defensive behaviour during conditioned cue presentation (Milad & Quirk 2002). Interestingly, however, electrolytic lesions to IL did not produce extinction expression deficits, but impaired its recall after a long delay (Quirk et al. 2000). Similarly, Chang & Maren (2010) showed that IL lesions impair extinction retention. Pharmacological inactivations of IL produced impairments of extinction retention as well (Fontanez-Nuin et al. 2011, Santini et al. 2012). Chronic intermittent alcohol administration disrupted fear extinction and severely affected its retention (Holmes et al. 2012). A study by Kim et al. (2010) linked extinction deficits to reduced activity in IL and showed that stimulation of IL facilitated extinction. Finally, both Do-Monte et al. (2015) and Bukalo et al. (2015) used optogenetic silencing and electrical stimulation, respectively, to show that IL is not necessary during extinction retrieval. Therefore, IL is necessary for extinction learning, in particular its acquisition and, consequently, retention, but not the extinction retrieval.

Conversely, stimulation of PL increases defensive behaviour and impairs extinction learning (Vidal-Gonzalez et al. 2006). This was confirmed with pharmacological inactivation of these areas using muscimol, a $GABA_A$ agonist, which showed that that inactivation of IL impaired extinction acquisition and recall, whereas inactivation of PL resulted in impaired fear expression (Sierra-Mercado et al. 2011). These studies show that PL is involved in promoting fear expression and IL in extinction learning and retention, similarly to its involvement in contextual fear memory processing.

1.3.3 *Hippocampus*

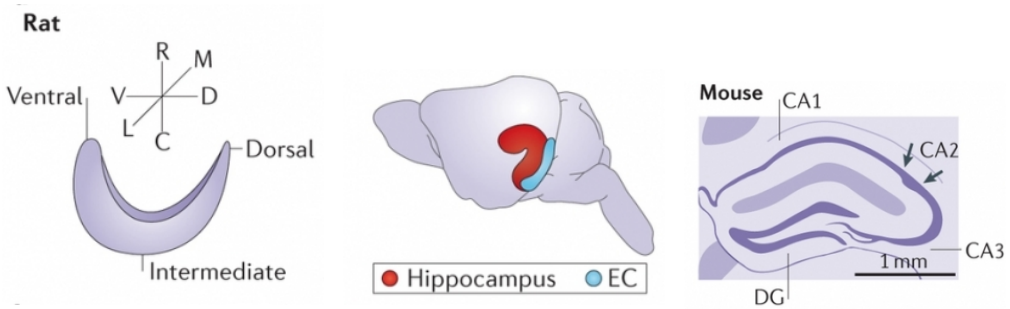

(a) Rat hippocampus longitudinal axis

(b) Location of Hippocampus in the rat brain

(c) Murine hippocampal structure

Figure 3 – Orientation of the rodent hippocampus longitudinal axis, its location in the rodent brain as well as an illustration of Nissl-stained cross-section of the mouse hippocampus. A, anterior; C, caudal; D, dorsal; DG, dentate gyrus; EC, entorhinal cortex; L, lateral; M, medial; P, posterior; R, rostral; V, ventral. Adapted from Strange et al. (2014).

The hippocampus is a brain structure associated with spatial navigation and memory (Buzsáki & Moser 2013). Located in the medial temporal lobe, in close proximity to the entorhinal cortex, it is surrounded by associated structures of the subiculum and the hippocampal formation containing the dentate gyrus (Squire & Zola 1996). The hippocampus proper – the Ammon's horn, or Cornu Ammonis, can be further subdivided into three areas (CA1 – CA3; see Figure 3c).

In rodents, the hippocampus is located along the ventral-dorsal axis, which is perpendicular to the human hippocampus, that stretches along the anterior-posterior axis (Strange et al. 2014). Interestingly, however, the lack of anatomical conservation across species is not reflected functionally, as the ventral hippocampus of rodents corresponds to the anterior hippocampus in humans (Strange et al. 2014).

There is a considerable discussion regarding the anatomical boundaries of the ventral and dorsal parts of the hippocampus, with some researchers suggesting simple division, while others preferring the ventral, medial and dorsal segments (Strange et al. 2014).

Regardless of the nebulous anatomical boundaries, the dorsal and ventral parts of the hippocampus play important and functionally distinct roles in the processing fear memory. Therefore, in the following parts the dorsal and ventral hippocampus will be considered separately.

Dorsal Hippocampus and the assembly of a context

For more than 20 years it has been clear that the hippocampus is important for the acquisition stage of contextual fear memory as lesions in the hippocampus impaired the acquisition of contextually dependent fear-motivated place preference (Selden et al. 1991). The dorsal hippocampus (DH), in particular, was shown to have a temporally-limited (1 day) role in early contextual fear recall, which is later taken over by other areas, with evidence pointing to the amygdala (Kim & Fanselow 1992, Rudy et al. 2004).

This temporal limitation of the hippocampus-mediated recall was confirmed using excitotoxic lesions, resulting in retrograde amnesia with lesions done one day after conditioning (Maren et al. 1997). Lesions to the hippocampus prior to conditioning, on the other hand, does not consistently produce anterograde amnesia, inability to create new memories, suggesting that other areas compensate when its function is impaired (Anagnostaras et al. 2001). Anagnostaras et al. (2001) explain that the dorsal hippocampus is likely to act as a centre for the formation of robust context representation in the neural circuitry. Contexts guide the retrieval of specific CS-US associations made within them (Bouton 1993). After this context is formed in the brain it acts as a single CS rather than a complex modality of sensory inputs, thus it can be passed on to different areas and, after the initial period, be recalled independently of the hippocampus. Alternatively, the animal associates a single, accurate predictor of a shock with the CS, which it might do preferentially after the context assembling mechanism becomes impaired (which would essentially mean a failure to produce a complete context).

This appears to be the case in the experiments done by Wiltgen (2006) who show that rats with DH lesions appear to learn contextual conditioning, albeit slower than rats with intact DH, and suggest that it is not necessary for the acqui-

sitions of the contextual fear. However, the authors do not present any evidence against discrete context element-US association taking place in lesioned rats (Wiltgen 2006). In fact, a study done by Frankland et al. (1998) reveals that DH-lesioned rodents are able to learn contextual fear in agreement with Wiltgen (2006), but fail to discriminate between fear and non-fear contexts. This is described as dual representation, which states that a context can be represented as a set of distinct elements or, preferentially, as an amalgam of the elements formed by the hippocampus, with the latter potentially enabling incomplete context pattern completion improving fear prediction accuracy (Rudy & O'Reilly 2001). A DH lesioning study by Matus-Amat (2004) supports the role of this dual representation model in contextual fear conditioning.

However, the dorsal hippocampus is not involved in the long-term storage of context memory since remote pre-exposure of context has been shown to prevent retrograde amnesia caused by a dorsal hippocampus lesion (Anagnostaras et al. 1999). This extensive DH role in contextual fear involves glutamatergic NMDA receptors (Young et al. 1994, Bast et al. 2003). Overall, DH plays a crucial, but temporally-limited role in context formation during contextual fear memory training.

Intact dorsal hippocampus is also important for processing contextual information in explicit-cue fear memory, as lesions to it prior to fear training or after extinction training impairs contextually regulated fear renewal by potentially interfering with its acquisition and/or expression (Ji & Maren 2005). This could be interpreted as translationally-relevant evidence towards a hippocampal role in the etiology and therapy of fear memory disorders since they rely on extinction-based interventions, such as exposure therapy, which, while effective at reducing fear, have a limited long-term benefit as gradual return of the initial symptoms or fear renewal outside of clinical setting is not uncommon (Baldwin et al. 2014, Craske et al. 2014, Vervliet et al. 2013). Specifically, patients who experience therapeutic benefit of exposure therapy in a clinical setting but undergo a fear relapse outside of it are experiencing a hippocampus-dependent phenomenon. Such fear renewal process requires an intact ventral hippocampus (Orsini et al. 2011).

Ventral hippocampus

DH relies on the ventral hippocampus (VH) to send the contextual information to the amygdala and mPFC, however, the role of VH in the fear network is not limited by this. In fact, VH plays an important role in unconditioned fear expression as lesions to the area reduce fear expression and neuroendocrine stress responses in innate fear paradigms (Kjelstrup et al. 2002). The ventral subiculum of VH sends direct projections to the central nucleus of the amygdala, which is responsible for controlling the expression of fear behaviour (Canteras et al. 1992). In addition to this, Sierra-Mercado et al. (2011) showed that VH is involved in both fear expression and fear extinction in auditory fear memory. In fact, studies indicate the role of VH in auditory fear expression, with lesions or infusions resulting in auditory fear memory expression impairment (Maren & Holt 2004, Hunsaker & Kesner 2008). This suggests that VH is involved in both auditory fear expression and extinction.

However, VH-CeA projections are secondary to the major efferents of VH-BLA and VH-mPFC, with the former having reciprocal afferents (Canteras et al. 1992, Vertes 2004, Hoover & Vertes 2007, Herry et al. 2008, Arszovszki et al. 2014, Ciocchi et al. 2015). Since VH is so heavily connected to the two aforementioned areas involved in the processing of fear memory, it is not surprising to find evidence of VH involvement as well.

A study by Zhang et al. (2014) showed that increasing inhibitory tone in VH with muscimol seems to impair defensive behaviour in an innate fear paradigm and contextual, but not auditory, fear conditioning. This is largely in agreement with Bast et al. (2001) who highlighted the fact that while intra-VH muscimol inhibits contextual fear memory by pharmacologically increasing the inhibitory tone, auditory fear is only affected by intra-VH tetrodotoxin, which completely prevents synaptic transmission, suggesting a lack of interneuronal involvment in auditory fear memory compared to contextual fear memory processing in VH (Bast et al. 2001). The importance of interneurons in contextual fear memory appears to be related to the findings of Lovett-Barron et al. (2014). The group

pinpointed the input filtering role of dendrite-targeting parvalbumin-positive (PV) interneurons, which, if disabled, cause increased firing in the hippocampal CA1 during US arrival and, thus, impair contextual fear conditioning. Conversely, however, inactivation of the glutamatergic ventral hippocampal neurons were showed to impair the consolidation of contextual fear memory (Zhu et al. 2014). Therefore, a balance between PV interneuron and glutamatergic neuron activity in the ventral hippocampus is necessary for the contextual fear conditioning to take place.

In summary, the evidence suggests that the ventral hippocampus is involved in all of the stages of contextual fear memory with particular importance of VH interneurons in mediating its function. In contrast, VH is also involved in auditory fear conditioning, but the inhibitory tone is secondary to the synaptic plasticity and activity of pyramidal cells in the area.

1.3.4 *Interactions between VH, PL, IL and amygdala during fear memory*

PL-BLA and IL-ITC interactions are important for opposing fear and safety drives

The medial prefrontal cortex represents a key area required for top-down regulation of the amygdala function (Kim et al. 2011). PL is involved in fear memory expression or retrieval in both contextual and explicit cue fear memory paradigms, with increased stimulation increasing the expression of defensive behaviour (Laurent & Westbrook 2009, Vidal-Gonzalez et al. 2006, Sierra-Mercado et al. 2011). The role of PL in fear expression can be related to its interaction with the amygdala.

PL sends excitatory projections to the lateral amygdala, which, in turn, extends excitatory projections to BLA, indirectly affecting the output to CeA and, thus, positively modulating the CS-US association and promoting fear memory expression (Vertes 2004, VanElzakker et al. 2014). This pathway underlies the PL functional role in fear expression.

In contrast to PL, IL is involved in extinction learning acquisition and retention of both contextual and explicit-cues (Laurent & Westbrook 2009, Vidal-

Gonzalez et al. 2006, Sierra-Mercado et al. 2011). Interestingly, both Do-Monte et al. (2015) and Bukalo et al. (2015) recently presented evidence suggesting that IL is not involved in auditory extinction recall. Early studies showed that stimulation of mPFC resulted in decreased CeA neuron responses to inputs from areas such as BLA (Quirk et al. 2003). Such effect depends on IL projections to the inhibitory GABAergic ITC neurons. These ITC neurons receive excitatory glutamatergic projections from IL (Berretta et al. 2005). In fact, ITC is highly responsive to the inputs arriving from IL (Amir et al. 2011). The excited ITC inhibit CeA, stopping the output of the amygdala, therefore, suppressing the downstream effectors that elicit fear. Recent data also suggest that IL also targets BLA, which then recruits ITC and inhibits CeA output (Orsini et al. 2011, Knapska et al. 2012, Cho et al. 2013, Strobel et al. 2015). Therefore, IL has at least two pathways to prevent fear expression by suppressing the output of CeA. In fact, the suppression signal originating from IL competes with an opposing signal coming from BLA of the amygdala, responsible for enforcing the CS-US association (VanElzakker et al. 2014).

This duality of fear expression and its suppression signals in the amygdala and their competition, or lack thereof, is what underlies the mechanistic aspects of healthy fear memory and its pathology, and the amygdala-mPFC interactions described here are important for that fear versus safety competition.

Fear memory triad

Section 1.3.4 describes that IL plays an important role during extinction. Rosas-Vidal et al. (2014) showed that brain-derived neurotrophic factor (BDNF), a protein implicated in long term memory, in IL is necessary for the extinction of conditioned fear and could be manipulated to suppress fear memories.

Surprisingly, however, extinction training resulted in increased ventral hippocampal BDNF, and not IL BDNF, and, intra-VH BDNF facilitated IL target excitability (Rosas-Vidal et al. 2014). A study by Sotres-Bayon et al. (2012) showed that the ventral hippocampus is capable of inhibiting PL activity following extinction training by targeting PL interneurons. Disabling VH at this stage resulted increased PL glutamatergic projection neuron activity and fear expression (Sotres-Bayon

et al. 2012). The double-edged effect of IL facilitation and PL inhibition following extinction learning demonstrates VH importance in learned fear suppression.

Conversely, intact signalling from VH to PL and BA is essential for contextual regulation of explicit-cued fear renewal (Orsini et al. 2011). If the inhibitory tone in the ventral hippocampus is increased, the context-regulated fear renewal is inhibited (Hobin et al. 2006). This contextually-regulated fear retrieval is reliant on dual-projecting VH neurons that terminate at both PL and BA (Jin & Maren 2015, Kim & Cho 2017b). These seemingly opposing functions governed by VH following fear extinction suggest a presence of a complex intra-VH mechanism that gates fear expression and its suppression. Indeed, a study by Nguyen et al. (2017) shows that impairments in VH LTP results in fear memory specificity deficits.

VH sends projections to fear memory trace neurons in BLA, is interconnected with extinction-resistant memory trace neurons, but does not seem to project onto or receive input from extinction memory trace neurons (Herry et al. 2008). It sends strong direct projections to PL and IL of mPFC that terminate on both pyramidal cells and interneurons, and can induce an LTP that is reversible (Jay & Witter 1991, Jay et al. 1992, 1996, Burette et al. 1997, Tierney et al. 2004). These direct projections are accompanied by an indirect, reciprocal pathway through the nucleus reuniens (Varela et al. 2014, Griffin 2015).

Interestingly, however, both PL and IL do not project directly onto VH and, therefore, have to rely on the entorhinal cortex, BLA or the nucleus reuniens for communication with VH (Vertes 2004, Cenquizca & Swanson 2007, Vertes et al. 2007, McGarry & Carter 2017). These findings, together with Senn et al. (2014) suggestion of informational segregation between BLA-PL and BLA-IL brings to light the pivotal role of VH as a gate that controls fear and extinction dominance in the fear memory network following extinction training.

VH, mPFC and BLA interaction in fear renewal

When it comes to explicit-cue fear conditioning, a good example of mPFC involvement in fear memory processing is contextually controlled fear renewal,

where an extinguished discrete CS is presented in a new context, resulting in an increased fear.

In order for fear renewal to take place an intact network of the ventral hippocampus, the basal amygdala and PL is required as evidenced by a study done by Orsini et al. (2011). The authors postulated two models for convergent signal integration, with one model integrating the signals in the basal amygdala and the other in PL. This work was extended by three studies looking into VH, mPFC and BLA interactions in fear memory renewal. Jin & Maren (2015) investigated Fos, a molecular marker of neuronal activity, expression in VH neurons projecting to PL and BA following extinction. It was found that dual projecting VH neurons were more likely to express Fos than neurons projecting to either area only (Jin & Maren 2015). Wang et al. (2016) looked into the engagement of VH neurons projecting to PL and IL. They found that Fos expression was similar in VH neurons to projecting to PL, IL or both when the animal was tested in a context triggering fear renewal (Wang et al. 2016). Finally, Marek et al. (2018) revealed that during fear renewal a population of neurons projects to PV-positive interneurons within IL, causing feed-forward inhibition of its projections to the amygdala. They recreated the findings with GABAergic agonists and antagonists in IL (Marek et al. 2018). This shows a compeletely novel mechanism involved in fear renewal where IL inhibition playing a key part.

Overall, the different, specific neuron-dependent mechanisms are slowly emerging as contributors within the mPFC, VH and BLA network. However, more research is necessary to investigate the gating mechanisms underlying these processes and how can they be targetted for potential anxiolytic development.

Electrophysiological aspects of VH-PL and VH-IL projections in fear memory processing

Activity in the hippocampus is electrophysiologically defined by the presence of synchronous theta oscillations (4-12 Hz) (Buzsáki & Draguhn 2004). These oscillations have been shown to entrain excitatory and inhibitory single-unit firing as well as gamma (30-150 Hz) oscillations in the ACC and PL of the medial pre-

frontal cortex (Sirota et al. 2008). Hippocampal theta to prefrontal slow gamma coupling enhancement is proportional to the successful working memory task completion and appears to be an indicator of increasing spatial memory task difficulty (Tamura et al. 2017). However, these interactions play a big role in fear memory and behaviour.

Electrophysiological recordings of local-field potentials (LFP) in rodents have shown that theta oscillation synchrony between the ventral hippocampus and the medial prefrontal cortex predict anxiety-like behaviour and this phenomena relies on direct VH – mPFC input. (Adhikari et al. 2010, Padilla-Coreano et al. 2016). Disrupting this synchrony between the two areas by blocking gap-junctions results in anxiolytic effect (Schoenfeld et al. 2014). Suppression of hippocampal theta activity is also believed to be a predictively valid electrophysiological indicator of anxiolytic effect when it comes to innate fear (Yeung et al. 2012).

When it comes to fear memory, CA1-LA theta synchrony is detected after fear conditioning and coincides with fear expression (Seidenbecher et al. 2003). This synchrony appears to be temporally restricted so that only consolidated fear memory coincides with the synchrony, as opposed to immediate or remote recall (Narayanan et al. 2007). A study by Lesting et al. (2011) showed that IL-LA-CA1 displays theta synchrony during fear expression that is disrupted during extinction training. Extinction recall coincides with a return in LA-IL and CA1-IL coupling, with CA1-LA remaining low (Lesting et al. 2011).

Interestingly, the consolidation of learned fear seems to rely on the hippocampal-BLA and BLA-mPFC theta synchrony (Popa et al. 2010). However, the area of mPFC recorded from in this study is located at the PL and IL border, making it difficult to predict individual contributions of these areas (Popa et al. 2010, Paxinos & Watson 1998). Nevertheless, the causality analysis between the three areas before and after conditioning showed hippocampal theta entrainment, or synchronisation, to both BLA and mPFC (Popa et al. 2010). Upon extinction recall this hippocampal theta dominance shifts over to IL (Lesting et al. 2013). These synchrony studies suggest that hippocampal CA1 theta plays a key role in fear

dominance during fear memory, whereas IL theta dominance indicates successful extinction training.

The role of PL in this divergent function is largely neglected since these synchrony studies focused on whole mPFC or IL exclusively. Recently, Fenton et al. (2014a) showed an opposing trend in PL and IL theta activity. Specifically, PL theta was more active during high-fear early extinction and IL theta was more active during low-fear late extinction. Considering the importance of the hippocampus-mPFC theta synchrony involvement in anxiety-like behaviour, the next step would be to compare CA1-IL and CA1-PL oscillatory behaviour during the high fear conditioning recall and low fear extinction recall stages of fear memory and extinction paradigm.

Interestingly, another, higher frequency band seems to be involved in fear memory and extinction processing too. Prefrontal cortex gamma oscillations (30 – 120 Hz) are involved in attention and working memory (Benchenane et al. 2011). The prefrontal cortex is interconnected with other areas, including the hippocampus, within which gamma oscillations play a role in fear memory and extinction (Likhtik et al. 2014, Wang et al. 2015). Hippocampal gamma oscillations arise due to inhibitory neuron activity and is involved in directing the communication between it and other areas involved in memory processing (Buzsáki 2001, Gloveli et al. 2005, Hájos & Paulsen 2009, Montgomery & Buzsáki 2007, Buzsáki & Wang 2012). The inhibitory neurons involved in these oscillations can inhibit ventral hippocampal CA1 pyramidal cells and contribute to their synchronisation (Cobb et al. 1995, Miles et al. 1996, Freund & Buzsáki 1996). A study by Albrecht et al. (2013) showed that fear conditioning and its recall reduced kainate-induced ventral hippocampal gamma oscillations in rodent brain slices *ex vivo*. Similarly, recent evidence suggest that lower frequency gamma oscillations in the prefrontal cortex are involved in fear extinction, with enhanced PL gamma oscillations coinciding with fear extinction deficits (Fitzgerald et al. 2014b). Similarly, increased gamma oscilations in human homolog of IL coincide with successful fear extinction recall, whereas baseline gamma oscillations within the area indicate fear extinction recall failure (Mueller et al. 2014). A study by Fenton et al. (2016) showed reduced PL gamma

oscillations during extinction and its recall, while IL had increased gamma oscillations during extinction recall. However, VH-PL and VH-IL interactions within this frequency band are yet to be determined.

1.3.5 *Summary*

The ventral hippocampus, prelimbic and infralimbic cortices are all involved in fear memory processing. The prelimbic cortex is associated with fear expression, the infralimbic cortex is associated with extinction learning, whereas the ventral hippocampus is involved in both fear expression and extinction as well as contextually-controlled fear renewal. Electrophysiological data suggests that PL and IL have opposite activity patterns during high and low fear states, but the influence of the hippocampus on these two areas, specifically their synchrony at high and low fear states is not clear.

1.4 COMPUTATIONAL APPROACH TO INVESTIGATING FEAR NETWORKS

The previous sections focused only on a fraction of the number of areas involved in fear memory processing, namely the amygdala, hippocampus and prelimbic as well as infralimbic cortices of the medial prefrontal cortex.

However, fear learning and memory has been studied experimentally for decades with a plethora of disciplines. Some of these disciplines cover universal molecular level features of synaptic plasticity and long-term potentiation (Blair 2001). Other disciplines focus on the brain areas and their projections involved in the fear circuitry (Hoover & Vertes 2007). These areas and their interactions are studied in awake behaving animals using electrophysiological recordings as well as neuroimaging in patients (Tovote et al. 2015, Sehlmeyer et al. 2009).

These advanced techniques used together with rodent fear behaviour paradigms have revealed a large number of brain areas involved in anxiety-related behaviours (Calhoon & Tye 2015; Figure 4). Some of the areas include detailed

local micro-circuits with specific functions. Temporal aspects of specific area involvement have to be considered too, making cohesive representation of fear memory processing difficult to grasp intuitively (Calhoon & Tye 2015, Nair et al. 2016). Therefore, computational neural network modelling approaches have been increasingly used to integrate the features spanning multiple spatial and temporal scales of fear memory processing networks. Such models generate predictions using computational experiments which can be verified in animal models, which have become an efficient and inexpensive approach to complement the research done *in vivo*.

Computational models of fear memory can be classified into different groups based on the types of neurons used. Earliest models have largely relied on the neuronal activity abstractions focusing on the connectivity aspects instead. These were followed by a focus on biophysical details of neurons leading to a number of biophysical model networks. Finally, some of the most recent models try to reach the middle ground by using spiking neuron models focusing on action potentials as opposed to all the biophysical aspects of specific neurons.

Subsection 1.4.1 will summarise the different types of neuron models. Subsection 1.4.2 will outline models of synapses and plasticity. The rest of the section will overview the firing-rate, biophysical and phenomenological models of fear memory networks.

1.4.1 *Models of firing rate and spiking neurons*

Firing-rate models approximating neuronal populations

Firing-rate models approximate neuronal activity by describing the average firing rate of neuronal populations, as opposed to considering the dynamics of individual neurons. These neuronal approximations are modelled as abstract units with values reflecting low to high firing rates in the monitored population. Such approximations of neuronal activity were used in the fear memory network models at the end of 20th century due to their extremely low computational cost (Armony

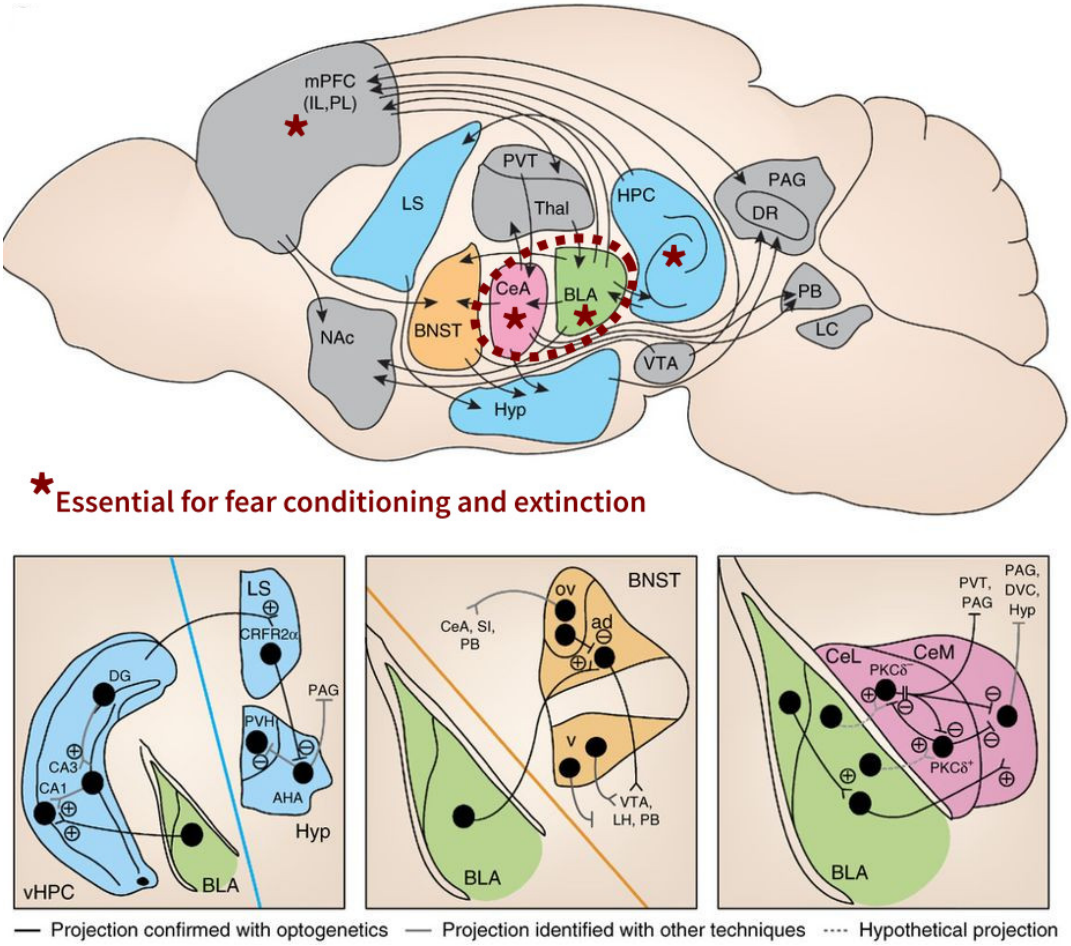

Figure 4 – Neural circuitry of the brain areas involved in rodent fear behaviour processing. (Top) is the saggital view of rodent brain including the long-range projections playing a role in fear. The two major parts of the amygdala are indicated by the red ellipse. (Bottom left) Septal and hippocampal micro-circuits. (Bottom middle & right) Extended amygdala microcircuits of BLA-BNST and BLA-CeA, respectively. ad, anterodorsal nucleus of BNST; AHA, anterior hypothalamic area; BLA, basolateral amygdala; BNST, bed nucleus of the stria terminalis; CeA, central amygdala; CeL, lateral subdivision of the central amygdala; CeM, centromedial subdivision of the amygdala; CRFR2α, type 2 corticotropin releasing factor receptor; DR, dorsal raphe nucleus; DVC, dorsal vagal complex; HPC, hippocampus; Hyp, hypothalamus; IL, infralimbic division of mPFC; LC, locus coeruleus; LH, lateral hypothalamus; LS, lateral septum; mPFC, medial prefrontal cortex; NAc, nucleus accumbens; ov, oval nucleus of BNST; PAG, periaqueductal gray; PB, parabrachial nucleus; PL, prelimbic division of mPFC; PVH, paraventricular nucleus of the hypothalamus; PVT, paraventricular thalamus; SI, substantia innominata; Thal, thalamus; v, ventral nucleus of BNST; vHPC, ventral hippocampus; VTA, ventral tegmental area. Adapted from Calhoon & Tye (2015).

et al. 1995, 1997a,b). The firing-rate models allowed researchers to focus on the connections between the studied areas, leading to models of these types being named "connectionist" (Armony et al. 1995, 1997a, Li et al. 2009, Nair et al. 2016).

Action potential and spiking neuron models

Neurons are electro-chemically polarised excitable cells. Their defining feature is the ability to conduct a wave of depolarisation, or an action potential, along an axon leading to neurotransmitter release into a synapse. Hodgkin and Huxley in their landmark experiments investigating the action potential generation in a giant squid axon revealed contributions of sodium and potassium ionic currents conducted across the neuronal cell membrane (Hodgkin & Huxley 1952a,b,c,d). Together with Eccles they received a Nobel Prize in Physiology or Medicine in 1963 for this work.

These discoveries lead to a formalism defining a neuron as a compartment covered with a membrane that conducts ionic currents (Hodgkin & Huxley 1952a,b,c,d). The initial Hodgkin-Huxley (HH) formalism focused only on two main ionic currents, but it can be extended to ten or more types of currents seen in various neurons within the brain, whether they are thalamic relay cells, motoroneurons or hippocampal pyramidal cells (Hodgkin & Huxley 1952d, McCormick & Huguenard 1992, Purvis & Butera 2005, Golomb et al. 2006).

The strength of the formalism is that electrophysiological aspects of any neuron can be accounted for in the formalism recreating it in detail computationally. The main trade-off for its richness in detail is its computational cost, relying on the computations of multiple currents and gating variables for each current. An example of this expense can be seen in the computational experiment by Bezaire et al. (2016), which modelled a full scale biophysical CA1 of the rat hippocampus. It consisted of approximately 340000 pyramidal HH neurons, 28000 HH interneurons and just under 5.2 billion synapses. It took a 4 hour computation time on a supercomputer with 3000 microprocessors and 4 TB of RAM to simulate the network activity for just 4 seconds (Bezaire et al. 2016).

It is questionable if the electrophysiological detail provided by the Hodgkin-Huxley formalism is a good justification to use a computationally expensive model of a neuron when modelling large-scale networks. Precisely this type of argument is made by the proponents of integrate-and-fire or other phenomenological neuronal models (Izhikevich 2004). They represent the other extreme of spiking neuron models compared to the HH formalism, since they are the simplest possible representation of a spiking neuron.

IAF models focus on the action potential as opposed to the various currents that participate in its generation. Their underlying simplicity makes IAF models an excellent choice for large-scale neuronal networks, where the focus is on the general activity of neuronal populations. While there are several different models of IAF neurons, they are all defined by two features: a variable describing the membrane potential with a stable resting potential and incoming synaptic current integration leading to the firing of the neuron. An IAF model created by Izhikevich (2003) describes the spike generation dynamics of the membrane potential V and an adaptation variable, u, evolving for $V < V_{\text{peak}}$:

$$c\frac{dV}{dt} = k(V - V_r)(V - V_t) - u + I_{\text{syn}}(t), \tag{1}$$

$$\frac{du}{dt} = a[b(V - v_r) - u], \tag{2}$$

where a is the inverse of the time constant of the u dynamics, b measures how strongly the variable u is coupled to voltage, v_r is the membrane resting potential, and V_t is the instantaneous threshold potential and V_{peak} is the maximal potential. Once the spike is emitted (i.e. $V = V_{\text{peak}}$) the variables are reset to

$$V \leftarrow c, \tag{3}$$

$$u \leftarrow u + d. \tag{4}$$

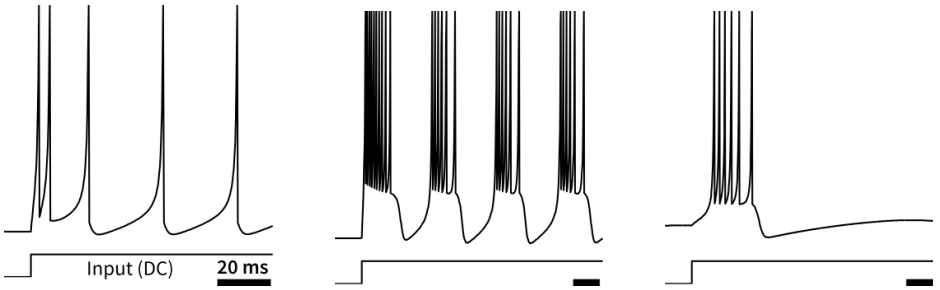

(a) Tonic Spiking (b) Tonic Bursting (c) Phasic Bursting

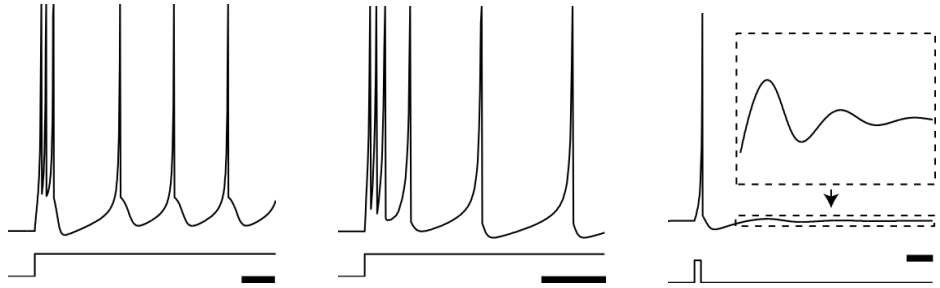

(d) Mixed Mode (e) Spike Frequency Adaptation (f) Subthreshold Oscillations

Figure 5 – Examples of biological properties of spiking neurons recreated with the Izhikevich IAF spiking neuron model. These dynamics depend on the values of a, b, c and d. Each horizontal bar reflects a 20-ms interval. Adapted from Izhikevich (2004).

.

The unit firing dynamics are governed by the recovery time constant a as well as its sensitivity to subthreshold oscillations, b, which also determines if the adaptation variable governs amplifying (i.e. $b < 0$) or resonant (i.e. $b > 0$)) dynamics (for details see Izhikevich (2007) p. 273 – 319). The addition of an adaptation variable u provides the neuron with ability to generate subthreshold oscillations, firing adaptation and bursting dynamics.

Figure 5 shows several examples of firing patterns recreated by the model. When compared to other IAF models or HH, Izhikevich model is able to reproduce various neuronal dynamics, lacking electrophysiological detail that is outweighed by a nearly two orders of magnitude lower computational cost (13 FLOPS vs 1200 FLOPS per ms, Izhikevich (2004); see Figure 6).

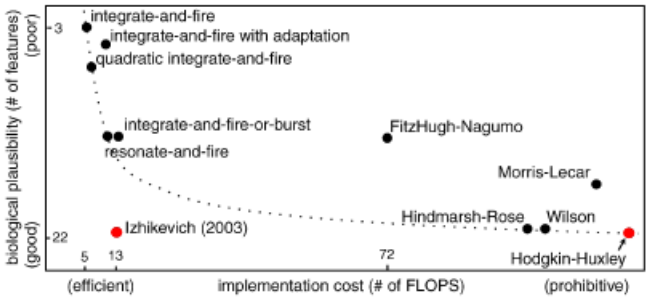

Figure 6 – Comparison of computational cost and model features of various types of spiking neuron models. Izhikevich model and HH formalism are marked with red dots. Adapted from Izhikevich (2004).

1.4.2 *Synaptic conductance and plasticity*

Synaptic models

Interneuronal communication relies on the synaptic conductance. The presynaptic neuron releases neurotransmitters into the synaptic cleft, which open the ligand-gated ion channels on the post-synaptic neuron and depolarise or hyperpolarise it.

There are various ways of modelling the synaptic conductance dynamics, and one of the most detailed methods uses the currents arising from excitatory glutamatergic AMPA and NMDA neurotransmition relying on their ligand-gated cation channels as well as the inhibitory GABAergic neurotransmission reliant on $GABA_A$-ligand gated anion channels on the post-synaptic neuron. These neurotransmitter receptors display nearly linear current-voltage relationships and can be modelled using ohmic conductance g_{syn} (Roth & van Rossum 2009). Such conductance can be modelled with a system of two coupled differential equations describing fast binding, τ_{rise}, and slow dissociation, τ_{decay} of the ligand-receptor complex:

$$g_{\text{syn}}(t) = \bar{g} f g(t), \tag{5}$$

where f is the normalization factor so that $\bar{g}$ is the peak amplitude of the current

$$f = \frac{1}{-e^{(t_{\text{peak}}-t_0)/\tau_{\text{rise}}} + e^{(t_{\text{peak}}-t_0)/\tau_{\text{decay}}}}. \tag{6}$$

The dynamics of g is determined from:

$$\frac{dg}{dt} = -\frac{g}{\tau_{\text{decay}}} + h, \tag{7}$$

$$\frac{dh}{dt} = -\frac{h}{\tau_{\text{rise}}} + h_0\delta(t_0 - t), \tag{8}$$

where h_0 is the scaling factor.

This conductance, g_{syn}, when multiplied with a difference between the postsynaptic neuron membrane voltage and reversal potential, $V - E_{\text{ligand}}$ gives the synaptic current:

$$I_{\text{syn}} = g_{\text{syn}}(t)[V(t) - E_{\text{ligand}}] \tag{9}$$

This type of model allows for accurate description of synaptic conduction temporal aspects.

Models of Hebbian plasticity

Models of fear memory undergo learning. One of the most biophysical models of learning is defined by the changes in synaptic weights or synaptic plasticity. According to Hebb (1949), synaptic plasticity depends on the persistent or repetitive presynaptic neuron's stimulation of the postsynaptic neuron. This was recorded experimentally by Bliss & Lømo (1973) showing that transient increases in presynaptic and postsynaptic neuron activity causes a long-term potentiation of the synapse (LTP). A low level of activity, or lack of synchrony between the presynaptic and postsynaptic neuron, results in an opposite process, LTD, resulting in decreases of synaptic strength, sometimes called 'anti-Hebb' process (Lisman 1989).

This bidirectional modulation of synaptic weights relies on the influx of calcium and its interaction with Ca^{2+}/calmodulin-dependent protein kinase II within the neuron (Lisman 1989, Lisman et al. 2002). The synaptic neuron activity-dependent calcium influx has become the basis for spike timing-dependent plas-

ticity (STDP) models (Shouval et al. 2002a). This is expressed as a synaptic weight governing rule:

$$\dot{w} = \eta\left([Ca^{2+}]\right)\left(\lambda_{\text{rise}}\Omega\left([Ca^{2+}]\right) - \lambda_{\text{decay}}w\right) \tag{10}$$

where λ_{rise} and λ_{decay} are scaling and decay factors with the term $\lambda_{\text{decay}}w$ preventing the saturation of the synaptic weight w. η and Ω are calcium-dependent learning rate and plasticity direction governing functions, respectively:

$$\Omega = \begin{cases} 0 & \text{if } [Ca^{2+}] \leqslant \theta_d, \\ \alpha\left([Ca^{2+}] - \frac{\theta_p+\theta_d}{2}\right)^4 - 0.1 & \text{if } \theta_d < [Ca^{2+}] < \theta_p, \\ \frac{1.2}{1+\exp(-35(-\theta_p-0.045))-0.2} & \text{if } [Ca^{2+}] \geqslant \theta_p, \end{cases} \tag{11}$$

$$\eta = \begin{cases} \frac{1}{1+\exp 13(-[Ca^{2+}])+5.5} & \text{if } [Ca^{2+}] < 0.389, \\ \frac{1}{1.25+\exp(9.2(-[Ca^{2+}])+4)-0.2} & \text{if } [Ca^{2+}] \geqslant 0.389. \end{cases} \tag{12}$$

The thresholds θ_d and θ_p define the boundaries of medium and large influx of calcium, leading to reduction or increase of synaptic weight, respectively.
Such model of synaptic plasticity is one of the most biophysically detailed models available and used in a number of fear memory network models (Vlachos et al. 2011, Pendyam et al. 2013, Fenton 2015).

1.4.3 *Computational models of fear memory*

Connectionist and firing-rate models of the fear memory network

A number of abstract models of fear memory that ignore the concepts of spiking neurons have been created focusing on specific nuclei of the amygdala and inputs arriving to it to study fear memory processing.

Armony et al. (1997b) studied the processes of conditioned stimulus or tone arrival to the amygdala and tone discrimination dependence on the auditory cortex and the auditory thalamus. The model predicted that the thalamo-amygdala pathway is sufficient for the discrimination of different conditioning stimuli since

the auditory cortex was not necessary. Vlachos et al. (2011) used a firing rate model to study the basal amygdala activity during fear conditioning and extinction. The model received inputs of CS, US and were split to receive one of the two different contexts reflecting stages of fear memory and extinction. It resulted in different activation of two neuronal populations, resembling fear and extinction memory trace neuronal populations described by Herry et al. (2008). Ball et al. (2012) created a firing-rate neuron model of the lateral amygdala receiving tone and shock inputs seen in classical fear conditioning. The model made predictions on tone and shock input densities, how the cells without direct sensory inputs might produce conditioned responses and the means to prevent fear learning stimulus generalization, where a non-conditioned CS is similar to a conditioned CS and elicits a conditioned response, through the balance between excitatory and inhibitory activity potentiation (Ball et al. 2012). Models like these reflect the computational counterparts of the amygdalo-centric view in fear memory processing that dominated the field of neuroscience for decades (Nair et al. 2016). A few of these "connectionist" models extended beyond the amydala and included cortical as well as limbic structures that play important roles in fear memory processing. Krasne et al. (2011) designed a firing rate model of the amygdala with inputs from the cortex, the hippocampus and the thalamus. Fear and extinction learning in the model relied on synaptic plasticity arising due to neuromodulation of the lateral and basal amygdala by the cortical, hippocampal and thalamic inputs. The model was capable of mimicking various stages of classical fear conditioning, including renewal, and made predictions about the role and temporal specificity of the hippocampus and the amygdala nuclei involvement in fear memory. However, due to the firing rate abstractions of neuronal activity, such results do not describe neuronal interactions within populations and are, therefore, limited in their scope. Navarro-Guerrero et al. (2012) built a model of auditory fear conditioning involving the amygdala, mPFC, the auditory cortex, the auditory thalamus and the ventral tegmental area. The model, intended to be used for robotics, was able to learn both aversive and rewarding stimuli as well as temporal relationships between the stimuli and predicting cues.

In a similar vein a model by Moustafa et al. (2013) designed an analogue neuron network of BLA, ITC and CeA of the amygdala as well as vmPFC (IL) and the hippocampus. The hippocampus served as the context processing area, delivering inputs to both vmPFC and BLA. These three areas received CS and US. BLA was delivering inputs to CeA, whereas vmPFC projected to ITC cells that inhibited CeA. The model, relying on the temporal difference learning, was sufficient to reproduce conditioning, extinction and contextual-regulation. It also showed that lesioning vmPFC impaired extinction, while the hippocampus damage affected extinction in a safe context.

In general, these models focusing on the generalised firing rate representations lack biological realism of spiking neurons and their interaction. Specifically, these types of approximations lack biological realism. Such limitation is being addressed by spiking neuron network models.

Biophysical models of fear memory network

Similarly to the connectionist models described in the section 1.4.3, biophysical modelling studies of fear memory can subdivided into two groups: those focused on the amygdala and its role in fear memory, and those that also include cortical areas involved in fear memory processing.

Li et al. (2009) created a HH model of the LA consisting of 8 pyramidal cells and 2 interneurons. This small network was able to learn CS-US associations and highlighted the sites of plasticity important for fear memory processing as well as the role of NMDA receptors in extinction learning (Li et al. 2009). Another model by Li et al. (2011) modelled the intercalated cells of the amygdala, composed mostly of GABAergic interneurons. These cells receive an input from the infralimbic cortex which leads to inhibition of CeA output and, consequently, blocks fear expression. However, there is a robust autoinhibition circuit within ITC. The model showed that a transient IL input is capable of overcoming this inhibition level within ITC and cause increased firing rates in the area capable of inhibiting CeA (Li et al. 2011).

A series of studies investigated the lateral amygdala and the principles of LA pyramidal cell recruitment into fear memory trace (Kim et al. 2013a,b, 2016, Feng

et al. 2016). Kim et al. (2013a) showed that the recruitment consisted of two conditions, a high intrinsic excitability of pyramidal interneurons and the involvement of competitive synaptic interactions within LA so that highly excitable neurons strengthen their interconnections with each other due to plasticity and recruit interneurons that inhibit the plasticity of other pyramidal cells. Another study by the group dismissed fear memory dependence on plasticity of the thalamic and cortical inputs as well as that of LA synapses, showing that, in fact, fear memories rely on conditioning-induced activity changes of thalamic and cortical inputs to LA (Kim et al. 2013b). Kim et al. (2016) investigated how the competitive interactions within LA govern the fear conditioning stimulus specificity. They showed that principal-to-principal potentiation increases, whereas interneuron-to-principal synapses decrease stimulus generalization. Similarly, a study by Feng et al. (2016) created a biophysical model of the lateral amygdala and studied the recruitment of its neurons into the explicit-cue fear memory trace. The study revealed that only the principal cells receiving direct tone input were competing for involvement into the fear memory trace regardless of the intrinsic excitability and that the number of recruited prinicipal cells relies on the level of inhibition within the network (Feng et al. 2016). While these studies provide insights into the neurocircuitry of the amygdala and the initial fear formation, they neglect the contributions of other brain areas involved in fear memory and extinction processing.

Li et al. (2009) model of auditory fear conditioning and extinction in the lateral amygdala became the basis for a couple of models involving cortical structures. Pendyam et al. (2013) created a detailed biophysical model of the amygdala including the lateral, basal and central amygdala as well as prelimbic cortex of the medial prefrontal cortex seen in Figure 7. This model accounted for the effects of monoaminergic neurotransmitters. The model predicted that sustained PL firing relies on lateral division of the basal amygdala-induced release of dopamine and noradrenaline, which was verified physiologically with inactivation of BA by muscimol and blockade of noradrenergic neurotransmission with propranolol. Moreover, the model predicted that variation in PL-BA microcircuits can affect fear

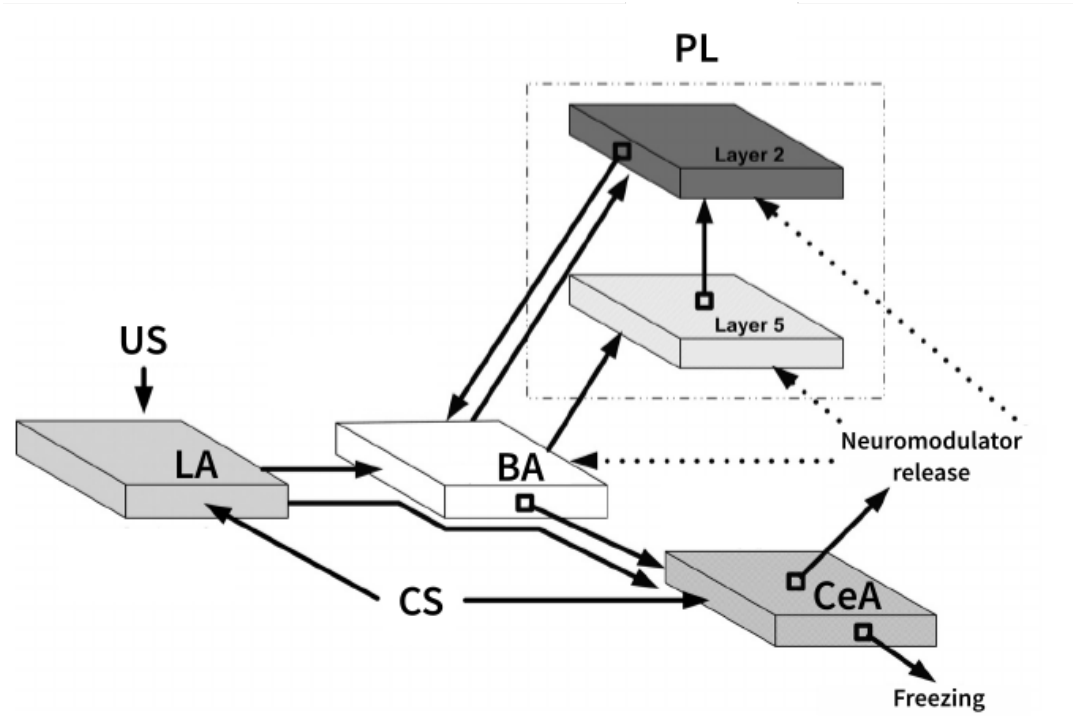

Figure 7 – Model of LA, the lateral division of BA, CeA and PL created by Pendyam et al. (2013). PL was composed of the superficial layer 2 and the deep layer 5. Both layers of PL received inputs from the lateral division of BA, but only layer 2 connection was reciprocal. Shock arrived to LA and tone input arrived to both LA and CeA. Adapted from Pendyam et al. (2013).

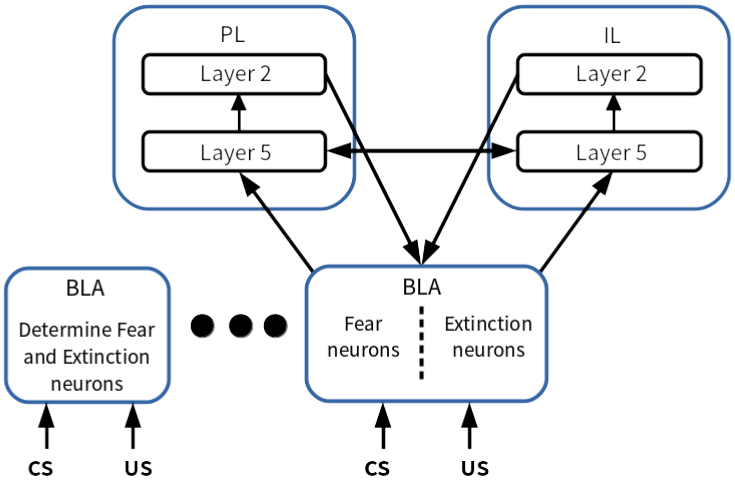

Figure 8 – Model of BLA, PL and IL with superficial layers 2 and deep layers 5, respectively, made by Fenton (2015). The model covers both mPFC areas involved in fear memory processing. Adapted from Fenton (2015).

expression, suggesting that PL's human homologue, dACC, might be a target for the treatment of anxiety disorders.

This model was extended by Fenton (2015) who built both IL and PL of mPFC into the biophysical fear memory network. This model relied on BLA, which upon associating CS and US had segregated inputs to PL and IL, with PL receiving fear and IL receiving extinction inputs (Figure 8). The model was validated by clamping the NMDA-dependent currents which inactivated NMDA neurotransmission. This inactivation reduced neuronal firing during extinction memory retrieval stage, consistent with animal experiment data. Inactivation of PL-IL reciprocal connectivity in the model led to PL firing rates not returing to basal firing rate level during extinction and its recall stages, whereas IL displayed increased activity throughout extinction stages (Fenton 2015). However, the inactivation of PL-IL reciprocal connectivity has not been compared to intact network activity.

Phenomenological models of fear memory network

There is a very limited number of fear memory models using IAF neurons. A model by Vlachos et al. (2011) used leaky IAF neurons to simulate two populations

within the basal amygdala receiving different contextual inputs as well as CS and US. The modelling study proposed that the differently recruited subpopulations of the basal amygdala were involved in encoding of the contextual specificity of fear and extinction memory traces (Vlachos et al. 2011).

Fenton (2015) also used a hybrid model with HH BLA and Izhikevich mPFC neurons and compared the findings with purely biophysical (i.e. HH only) model discussed in section 1.4.3. The hybrid model was broadly able to capture the dynamics of the biophysical fear memory network, but could not reproduce some of the current-related phenomena seen in the biophysical version, namely NMDA inactivation effects in the network. Nevertheless, the model was able to capture the importance of interconnectivity of PL-IL in the medial prefrontal cortex as was seen in the biophysical model. It was also highlighted that the model computation time took a few hours as opposed to 70 hours needed for the biophysical model.

1.4.4 *Summary*

Connectionist models of fear and extinction networks have shown that computational approaches are beneficial in understanding the complex interactions taking place during the paradigm. In addition, these models have addressed several areas beyond the amygdala and the cortex involved in fear memory and extinction processing. However, connectionist models use neuronal approximations. These approximations cannot, for example, represent the individual neuron interactions underpinning synaptic learning. Such model shortcomings are being addressed by spiking neuron networks of fear memory and extinction. These models present a biophysical view of fear memory networks that include synaptic plasticity. However, none of them extended beyond the amygdala and the cortex, unlike some of the earlier connectionist models. Specifically, there has not been a spiking neuron model network addressing the role of the ventral hippocampus in a fear memory processing.

1.5 NEUROCHEMICAL MANAGEMENT OF FEAR MEMORY PROCESSING

There is a lack of interest from Big Pharma to repurpose the existing drugs or study naturally occuring pharmacologically active (ethnopharmacology) compounds since these options are not commercially-viable, with Big Pharma favouring *de novo* drug development (Oprea et al. 2011). Therefore, even if these types of drugs have promising pharmacological activity, not-for-profit, academic research is usually relied upon to bring these promising compounds to the attention of clinicians.

This is the case for cannabis. Its usage can be traced back over 4000 years and is well-tolerated in humans (Li 1973, Bostwick 2012, Devinsky et al. 2014). It contains in excess of a 100 naturally occuring pharmacologically active compounds, phytocannabinoids, one of which, called cannabidiol, is showing promise in the treatment of anxiety disorders (Mehmedic et al. 2010, Campos et al. 2012).

1.5.1 *The case for cannabidiol*

Cannabidiol (CBD) is widely regarded as a major constituent of cannabis sativa that counteracts the psychosis produced by THC in some individuals and has a large anxiolytic potential (Russo & Guy 2006, Campos et al. 2012). Blessing et al. (2015) conducted a metastudy of CBD role in anxiety, concluding that although limited in number, clinical studies support the anxiolytic benefit of cannabidiol. Considering such effects it might not be surprising to see strong evidence of correlation between PTSD, its symptom severity and cannabis use (Bonn-Miller et al. 2011, Cougle et al. 2011, Bonn-Miller et al. 2013). However, as mentioned earlier the clinical data on cannabis and its constituent, cannabidiol, in anxiety and stress disorder patients is very sparse.

Greer et al. (2014) retrospectively applied the PTSD symptom scale on the psychiatric data of the New Mexico Cannabis Program applicants. The scientists revealed a sufficient correlation between cannabis use and PTSD symptom reduction

to warrant a further clinical investigation into cannabis in PTSD treatment (Greer et al. 2014). The authors suggested that the beneficial effects might be attributed to the anxiolytic effect of cannabidiol (Greer et al. 2014).

This lack of clinical studies of CBD in anxiety and stress-related disorders indicates that translationally relevant preclinical data is extremely important. In fact, there are number of studies investigating CBD effects in animal models of fear memory.

1.5.2 *Cannabidiol in fear memory*

Most of the research that tested CBD efficacy was done in contextual fear memory paradigms. CBD administered prior to training reduces fear expression and impairs the formation of contextual fear memory (Levin et al. 2012). A study by Stern et al. (2017) showed that CBD administered immediately after contextual fear acquisition disrupted fear memory consolidation via a DH CB1- and CB2-dependent mechanism. This consolidation disrupting effect is temporally limited by a 6-hour window following acquisition. In fact, CBD administration 24 hours after acquisition, but prior to retrieval only affects fear expression (Resstel et al. 2006). Interestingly, CBD administration on its own or in combination with THC, a partial CB1 agonist, following fear retrieval impairs contextual fear memory re-consolidation and the effect relies on CB1 receptors (Stern et al. 2012, 2014, 2015, Gazarini et al. 2015). These effects seem to rely on how strong the fear conditioning process is as CBD impairs the extinction of weak fear conditioning and facilitates the extinction of strong fear conditioning (Song et al. 2016).

Localised CBD injections in the prelimbic and infralimbic medial prefrontal cortex support functional segregation as intra-IL CBD is associated with increased and intra-PL CBD – with decreased fear expression when administered before fear memory retrieval via 5-HT1A-dependent mechanism (Lemos et al. 2010, Fogaça et al. 2014, Marinho et al. 2015). Conversely, however, Do Monte et al. (2013) showed that a much lower dose of CBD administered to IL prior to extinction facilitated contextual fear extinction via CB1-dependent process. Chronic CBD

administration for 14 days, with CBD administered prior to acquisition and prior to retrieval resulted in increased US-anticipating response and reduced BDNF expression in both the hippocampus and the frontal cortex (ElBatsh et al. 2012). Since BDNF in IL is essential for extinction of fear memory and extinction training increases BDNF in VH it would be interesting to test the pharmacological mechanism underlying this reduction in BDNF expression revealed by ElBatsh et al. (2012).

Considering this literature, CBD efficacy in blocking contextual fear (re)consolidation likely relies on the dorsal hippocampal cannabinoid receptors and has a temporally-restrictive window. Outside of this window CBD effects appear to be limited to modulating conditioned fear expression and facilitating extinction, which seem to have at least partial reliance on IL and PL of mPFC and depend on 5-HT1A receptors in contextual fear memory paradigms.

However, there is very little evidence on CBD efficacy in fear memory related to explicit cues. Das et al. (2013) showed that visually cued fear memory extinction consolidation was facilitated with cannabidiol administration following, but not before, extinction training. A study by Norris et al. (2016) showed that nucleus accumbens shell injections with CBD before training impaired the acquisition of olfactory fear memory via a 5-HT1A-dependent process. This lack of evidence does not indicate the absence of therapeutic potential of cannabidiol, since its benefit is supported by the endocannabinoid system's involvement in explicit cue fear memory with CB1 knockouts and/or CB1 receptor blockade impairing explicit cue fear extinction in animals and with comparable pharmacological effects in humans (Marsicano et al. 2002, Chhatwal et al. 2005, Kamprath et al. 2006, Rabinak et al. 2013).

When it comes to animal fear paradigms the beneficial effects present themselves as an inverted-U shaped dose-response curve (Silveira Filho & Tufik 1981 and Onaivi et al. 1990 cited in de Mello Schier et al. 2012). These effects arise due to the fact that cannabidiol has a low selectivity and, thus, targets many different receptors and other effectors. However, when it comes to innate fear, contextual

and explicit-cue fear memory, a lot of CBD effects can be explained by its actions on the endocannabinoid system and the CB1, 5-HT1A and TRPV1 receptors.

1.5.3 *Endocannabinoids*

Following the identification of cannabinoid receptors, their natural ligands, known as endogenous cannabinoids, or endocannabinoids, were discovered (De Petrocellis et al. 2011). They are highly lipophilic molecules that are synthesised from membrane proteins following post-synaptic depolarisations or the activation of metabotropic glutamate receptors (Fisar 2009).

The two most popular endocannabinoids are the well-studied anandamide (AEA) and the most prevalent 2-Arachidonoylethanol (2-AG) (Fisar 2009). Both of these endocannabinoids have different synthesis pathways, with N-acylphosphatidylethanolamine-specific phospholipase D being responsible for AEA and diacylglycerol lipase α (DAGLα) for 2-AG synthesis (De Petrocellis et al. 2011). These endocannabinoids are broken down by FAAH and monoacyl glycerol lipase (De Petrocelis et al, 2010). Together the receptors, the endocannabinoids and the enzymes form the "endocannabinoid system" (De Petrocellis et al. 2011). This system is important as it functions like any other neurotransmitter system with prominent, albeit short-lived, pharmacological effects at the cannabinoid receptors that mimic some of the effects of exogenous ligands, such as THC (Fisar 2009).

Interestingly, the endocannbinoid effects become behaviourally relevant when endocannabinoid hydrolysis or the cellular uptake is inhibited, as is seen with the administration of CBD (De Petrocellis et al. 2011). This was the case in a study by Morena et al. (2017) who showed that trauma-exposed rats displayed reduced hippocampal anandamide levels and that 2-AG inhibitor, URB597, facilitated extinction consolidation and restored social interaction deficits, which was not seen with extinction training alone. This makes CB1 receptors an interesting target as the majority of the endocannabinoid system pharmacological manipulation effects manifest via these receptors.

1.5.4 *CB1 receptors*

CB1 receptors are seven transmembrane-domain spanning $G_{i/o}$-protein coupled receptors that inhibit adenylate cyclase (Hosking & Zajicek 2008). The areas of CB1 expression in the brain include the hippocampus, the amygdala and the neocortex (Pagotto et al. 2006).

This receptor is important in contextual fear memory as SR141716A, an antagonist at CB1 receptors, attenuated the reduction in freezing, a passive fear expression measure, and facilitation of extinction seen with intracerebrovascular CBD infusion (Bitencourt et al. 2008). Similar effect was seen with a low dose CBD infusion into IL, which facilitated fear extinction (Do Monte et al. 2013). This effect was abolished with pharmacological CB1 blockade, suggesting indirect CB1 activation via the endocannabinoid reuptake inhibition being responsible for extinction facilitation (Do Monte et al. 2013). However, it seems that SR141716A itself could have anxiogenic activity not seen with AM251, suggesting a non-orthodox cannabinoid pharmacology being the possible culprit behind the anxiogenesis (Thiemann et al. 2009). Nevertheless, CB1 receptor's function is key to the facilitation of extinction learning as pharmacological blockade or knockouts show inhibited extinction (Marsicano et al. 2002). Interestingly, these effects are DH CB1 receptor-dependent since antagonism of these receptors in the dorsal hippocampus blocked fear extinction and facilitation of extinction was achieved with anandamide infusion into the same area (de Oliveira Alvares et al. 2008). Therefore, the contextual fear memory extinction process relies at least in part on the dorsal hippocampal CB1 receptors, with CB1 agonism facilitating extinction and antagonism at the receptor impairing it.

However, CB1 involvement is not limited to extinction facilitation. Two experiments by Stern et al. (2012, 2014) where systemic CBD was administered following fear retrieval disrupted fear memory reconsolidation. This effect was blocked by a systemic CB1 receptor antagonist, AM251 (Stern et al. 2012). Direct infusion of CB1 antagonist into PL prevented this CBD effect as well (Stern et al. 2014). This effect seems to depend on the DH CA1 receptors, as infusion of AM251 facilitates fear

memory reconsolidation and infusion of endocannabinoid anandamide blocks it (de Oliveira Alvares et al. 2008). Therefore, fear memory reconsolidation is modulated in DH CB1-dependent manner with its agonism impairing fear memory reconsolidation and antagonism facilitating it.

1.5.5 *5-HT1A receptors*

5-HT1A receptors are $G_{i/o}$-protein coupled seven transmembrane domain spanning receptors that are found in the cortex, the hippocampus, the septum, the amygdala and the dorsal raphe nuclei (Rojas & Fiedler 2016, Burnet et al. 1995, Pompeiano et al. 1992). They are usually called "somatodendritic autoreceptors" as they are found extrasynaptically on serotonergic neurons and their activation leads to the inhibition of firing and reduced synthesis and release of serotonin (Blier et al. 1998). These receptors are also found post-synaptically on non-serotonergic neurons to mediate signalling in response to the neurotransmitter (Albert et al. 2014). Considering their abundance in fear memory circuitry and presence on functionally antagonistic pyramidal cells and interneurons, their pre- and post-synaptic expression phenotype could influence the development of anxiety-prone behaviour (Albert et al. 2014).

As mentioned before, CBD facilitates 5-HT1A receptor activity even at low concentrations, thus inhibiting serotonergic neurons from conducting signals through synaptic terminals. The behavioural manifestations of this effect were tested in innate fear paradigms where CBD produced anxiolytic effects in one study, which was confirmed with an experiment by another group using restraint as a method of anxiogenesis (Campos & Guimarães 2008, Resstel et al. 2009). Interestingly, the first group also showed that injection of WAY-100635, an antagonist at 5-HT1A receptors, in the dorsolateral periaqueductal grey (dlPAG), a midbrain area involved in the mediation of anxiety-related behaviour, blocked the anxiolytic property of CBD (Campos & Guimarães 2008). It seems that these receptors are dependent on intact CB1 signalling as it was shown that CB1 KO mice have impaired 5-HT1A function in the hippocampus and the fronto-parietal cortex, which

is likely due to an impairment of the latter receptors coupling to their G-protein (Mato et al. 2007). This suggests, that 5-HT1A receptors could be affected by CBD in a multi-layered fashion.

5-HT1A involvement in fear memory depends on the nature of the paradigm. In contextual fear memory, intra-PL CBD-induced reduction in fear expression and the opposing effect of intra-IL CBD-induced facilitation of fear expression in contextual fear trained animals both rely on 5-HT1A receptor activation as 5-HT1A-specific antagonism abolished these effects (Fogaça et al. 2014, Marinho et al. 2015). Similar 5-HT1A dependence was observed with CBD infusions into BNST, which reduced contextual fear expression and 5-HT1A antagonist blocked this effect (Gomes et al. 2012). On the other hand, when it comes to explicit cue fear memory, CBD infused into the nucleus accumbens shell blocked consolidation of olfactory fear memory and this effect was not CB1, but 5-HT1A dependent (Norris et al. 2016). Consolidation in contextual fear memory is governed by CB1 receptors suggesting pharmacological differences underpining the contextual and explicit-cue fear paradigms with potentially larger involvement of 5-HT1A in explicit cue fear paradigms (see Section 1.5.4).

1.5.6 *TRPV1 receptors*

The TRPV1 channel is a six transmembrane-domain protein that assembles into tetramers forming a non-selective pore that conducts depolarising Na^{+} and Ca^{2+} cation currents (Gunthorpe & Chizh 2009). This channel is gated by ambient temperatures above 43°C and perhaps the best known agonist of this channel is the chilli pepper constituent capsaicin. Among the other agonists of the channel are the endocannabinoid anandamide and CBD (Vriens et al. 2009, Bisogno et al. 2001).

TRPV1 is responsible for the release of glutamate in dlPAG, which in turn results in anxiogenesis (de Mello Schier et al. 2012). It was shown that whilst low doses of CBD activate 5-HT1A (see above) and produce anxiolysis, increased doses activate TRPV1 receptors, causing anxiogenesis, and result in an inverted-U shaped

dose-response curve for CBD anxiolytic effect (de Mello Schier et al. 2012). This was confirmed with the injection of capsazepine, a TRPV1 antagonist, into dlPAG prior to the administration of a high dose of CBD. The antagonism made high doses of CBD anxiolytic, suggesting that TRPV1 acts as the anxiogenic counterpart to the anxiolytic 5-HT1A activation by the CBD (Campos & Guimarães 2009). In summary, an increase in CBD dose above the anxiolytic level could potentially be inducing innate anxiety via subcortical regions, such as dlPAG through TRPV1-dependent mechanism.

When it comes to contextual fear memory, TRPV1 receptor activation was found to positively modulate the contextual fear expression at the ventromedial prefrontal cortex and antagonism of TRPV1 at the area had the opposite effect (Terzian et al. 2014). Mice that underwent an explicit-cue fear memory training exhibited reduced explicit-cue fear expression with AM404, an endocannabinoid reuptake and breakdown inhibitor and TRPV1 agonist (Llorente-Berzal et al. 2015). This effect was reversed by both CB1 antagonism and TRPV1 antagonism (Llorente-Berzal et al. 2015). These findings suggest a potentially opposing activity of TRPV1 in contextual and auditory fear paradigms, with TRPV1 agonism being responsible for anxiogenesis in the former and anxioysis in the latter.

1.5.7 *Summary*

To sum up, cannabidiol shows anxiolytic effects in innate fear paradigms. CBD also reduces contextual fear expression and facilitates contextual fear extinction. This effect depends on the CB1, 5-HT1A and TRPV1 receptors, specifically CB1 is responsible for extinction facilitation, 5-HT1A governs the anxiolytic effect and TRPV1 agonism by CBD causes anxiogenesis at higher doses. However, there is little to no data on cannabidiol in explicit-cue fear memory.

1.6 AIMS AND HYPOTHESES

The aim for the experimental and computational modelling parts of my PhD is to investigate the role of systemic CBD in auditory fear memory paradigm, the mPFC-VH interaction during fear and extinction recall stages as well as to design a computational model of simplified amygdala-mPFC-VH and test the effect of VH inactivation in the network. The project will address each question with behavioural pharmacology, electrophysiology and computational modelling experiments, respectively.

1.6.1 *Behavioural Pharmacology*

There is a plethora of data to suggest that CBD can be beneficial in contextual fear memory by promoting fear extinction and reducing fear expression as well as innate fear where it is anxiolytic (see Section 1.5). However, no studies so far have looked at systemic CBD effects in auditory fear memory paradigm. To address this we tested the effects of CBD in auditory fear conditioning and extinction. CBD was expected to facilitate extinction learning process in a dose-dependent manner with an inverted-U shaped dose-response curve as seen in contextual fear conditioning experiments. The experiment is discussed in Chapter 2.

1.6.2 *Computational Modelling*

Previous biophysical modelling studies of fear memory and extinction mostly focused on the amygdala, with a few studies including cortical areas (see Section 1.4). The model in this thesis extended the previous modelling studies by Pendyam et al. (2013) and Fenton (2015) with an addition of ventral hippocampus, to probe its role in the network. PL-IL inactivation results would be compared to VH inactivation. We predicted that VH inactivation would disrupt the activity of the cortical areas in a pro-anxiolytic manner, whereas PL-IL connectivity inactivation

would decrease the differences between PL and IL activity. The modelling study is described in detail in Chapter 3.

1.6.3 *Electrophysiology*

It is established that PL is involved in fear retrieval and IL in fear extinction, whereas the ventral hippocampus appears to play a role in both processes (see Section 1.3). Determining the interaction between these areas during fear recall and extinction recall stages would address the lack of understanding when it comes to the interaction of these areas at different fear and extinction stages present currently. We used intra-PL/IL and intra-VH LFP recordings during learned fear retrieval and extinction retrieval. VH-PL was expected to show high theta coherence, reflecting high fear state during fear retrieval, which would be replaced by high VH-IL coherence during low fear, extinction recall stage. The details of the experiment can be found in Chapter 4.

2

EFFECT OF CANNABIDIOL ON AUDITORY FEAR EXPRESSION AND EXTINCTION

2.1 INTRODUCTION

Anxiety and stress-related disorders, such as phobias and post-traumatic stress disorder (PTSD) are highly prevalent, reportedly endured by up to 1 in 10 or 15 people, for social and specific phobias, and PTSD, respectively (Kessler et al. 2005). They are characterized by an expression of defensive, avoidant behaviours when facing the situation associated with the phobia or trauma, or endurance of them in distress (Baldwin et al. 2014).

The recommended treatment options are SSRIs or exposure therapy, both having similar efficacy, problems with a significant portion of patients not responding to treatment and issues sustaining the therapeutic benefit over longer term (Baldwin et al. 2014). Moreover, SSRIs take several weeks before reaching a full therapeutic effect and this loading period can coincide with a worsening of the symptoms (Baldwin et al. 2014).

An alternative approach is combining the pharmacological interventions with exposure therapy to treat these disorders. Norberg et al. (2018) demonstrated that patients who endured more intense exposure sessions had increased fear reduction and ability to tolerate the fear upon renewal with a change of context. Helping patients endure intense fear exposure sessions would be beneficial, however not all anxiolytic drugs are compatible with exposure therapy. In fact, benzodi-

azepines, while reducing symptoms of anxiety impair fear extinction, the process underlying exposure therapy (Pereira et al. 1989, Hart et al. 2014). On the other hand, d-cycloserine is a drug which does not have an anxiolytic effect targeting fear expression, but facilitates fear extinction learning in animal models and shows clinical potential in several specific phobias and PTSD (Richardson et al. 2004, Ressler et al. 2004, Lee et al. 2006, de Kleine et al. 2012, Nave et al. 2012). However, it has considerable limitations, including lack of efficacy when co-administered with tricyclic antidepressants and the potential for fear memory reconsolidation (Werner-Seidler & Richardson 2007, Lee et al. 2006). In other words, d-cycloserine cannot be used for anxiety patients with depression, two highly co-morbid conditions, as well as having a risk of reactivating an old fear memory and transitioning it from a short-term memory into long-term memory.

A drug that could be compatible with psychological interventions is cannabidiol (CBD), a phytocannabinoid anxiolytic. Early studies indicated that systemic administration of cannabidiol can produce anxiolysis in innate fear paradigms (Guimarães et al. 1990, Onaivi et al. 1990, Moreira et al. 2006). Similar anxiolytic effect was noted in restraint stress prior to several innate fear paradigms, including exposure to a natural predator (Resstel et al. 2009, Casarotto et al. 2010, Uribe-Marino et al. 2012).

A pro-anxiolytic effect of CBD is also seen in a contextual fear memory paradigm. CBD administered prior to conditioning impairs fear expression and contextual fear memory formation (Levin et al. 2012). Administration of it immediately after fear training impairs contextual fear memory consolidation (Stern et al. 2017). If CBD is administered following contextual fear conditioning, it results in a reduced fear expression (Resstel et al. 2006). CBD was also shown to block contextual fear memory reconsolidation after its retrieval (Stern et al. 2012, 2014, 2015, Gazarini et al. 2015). Finally, CBD facilitates contextual fear memory extinction learning (Bitencourt et al. 2008). Taken together, CBD has been shown to have both anxiolytic and extinction-facilitating effects in contextual fear memory paradigm.

There is little data on CBD effects in fear memory related to explicit cues. A study of visual fear memory in humans revealed that CBD enhances extinction

when given immediately after, but not before fear extinction (Das et al. 2013). Another study by Norris et al. (2016) showed that CBD infusions into the shell of the nucleus accumbens impaired fear memory encoding. Since CBD has both an anxioytic and extinction-facilitating effect in contextual fear memory paradigm, we hypothesized that this dual effect could be present in auditory fear memory paradigm as well. To test this hypothesis and address the lack of data on CBD in fear memory related to explicit cues we tested the effects of systemic cannabidiol admistration prior to auditory fear extinction on extinction learning and recall, and compared these data to CBD effect on contextual fear at both stages.

2.2 MATERIALS AND METHODS

2.2.1 *Animals*

Adult male Lister-Hooded rats (Charles River, UK; 280-400 g) were housed in groups of 4 with unrestricted access to food and water. All of the experiments were conducted during the light phase of the cycle. All of the procedures strictly adhered to the guidelines set out by the ethical review of by the Animal Welfare and Ethical Review Board at the University of Nottingham and the Animals (Scientific Procedures) Act, 1986.

2.2.2 *Drugs*

Cannabidiol (STI Pharmaceuticals, UK) was suspended in 0.9% sterile saline (Vetivex TM; Dechra Pharmaceuticals PLC, UK) with 2% Tween 80® (Aldrich Chemical Company Ltd., UK) on the day of use and administered at 1 mL/kg injection volume 30 minutes prior to the start of the auditory fear extinction stage (see below). The said combination of solvents was used as a vehicle solution. The doses of CBD (5, 10 or 20 mg/kg) were selected based on the finding that 10 mg/kg should be the optimal dose to see the anxiolytic fear modulating effect of CBD in

learned contextual fear (Lemos et al. 2010). CBD and its vehicle were administered intraperitoneally. All of the drug doses were calculated as a freebase.

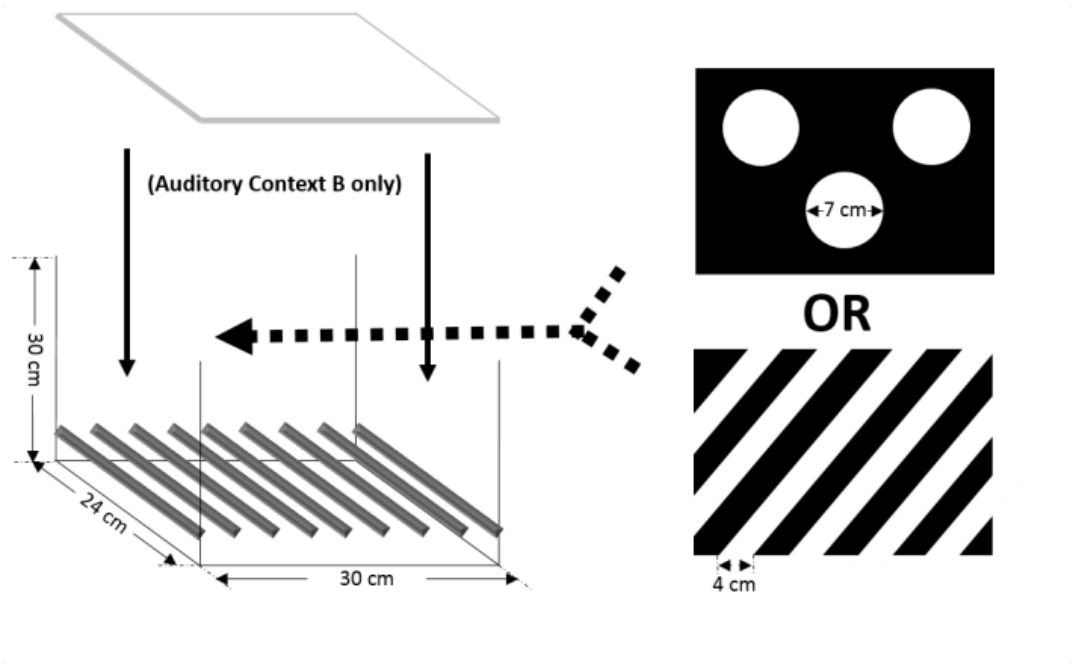

Figure 9 – The arena used for the behavioural testing. It is comprised of a 30×24×30 cm box with electro-conductive metal floor bars connected to an external electric scrambler responsible for delivering alternating current shock of a set amplitude. Two walls of the boxes are covered by a 'spots' or 'stripes' pattern (Box 1 and 2, respectively). There is a secondary Perspex floor used to cover the metal bars in Context B-employing stages of the experiment (see below).

2.2.3 *Testing arena and contexts*

The fear conditioning kit containing the testing arena (Figure 9; Med Associates Inc., USA) and a camera kit (Tracksys Ltd., UK) was used to record the behaviour during the experiments. All of the arena parameters were set and the recordings were done using a computer with the relevant manufacturers' software in Windows XP operating system.

2.2.4 *Auditory fear memory experiments*

Auditory fear conditioning experiments employed two contexts to environmentally differentiate conditioning (Context A) and extinction sessions (Context B), and to allow for the testing of extinction recall outside of the fear conditioning context, respectively (Table 1).

On the first day animals were habituated to both contexts for 10 minutes each. Next day the rats were placed in their respective fear contexts (Context A) and presented with 5 auditory tones (CS; 4 kHz, 30 second, 80 dB) followed by 5 CS that co-terminated with a foot-shock (US; 0.5 sec, 0.5 mA) with 2 minute inter-trial interval (ITI) between the presentation of CS. On the third day animals were injected with CBD or vehicle and after 30 minutes underwent extinction training (Context B) where 15 CS (1 min ITI) were presented. This is a weaker, or partial, extinction training paradigm compared to other studies, like Fenton et al. (2014a), and was purposely intended to be shorter in order to investigate CBD effects on extinction learning facilitation. On the fourth and final day of the experiment the animals underwent a brief extinction recall (Context B, 2 CS, 1 min ITI).

On all of the days the animals were in the testing chambers for 2 minutes before the tone presentations started. Contextual fear was assessed during these two minutes for both extinction and extinction recall stages. After the experiments were completed, the animals were culled using a chamber with an increasing level of CO_2 (2 l/min) and the culling was confirmed with cervical dislocation.

2.2.5 *Behavioural data collection and scoring*

Behavioural data were recorded using overhead cameras. The videos were scored on a mixed-blind basis by two scientists, with one scientist being aware of the administered treatments (i.e. single-blind) and another scientist not being aware of the administered treatments (i.e. double-blind). During scoring, each tone was subdivided into ten blocks of 3 seconds. This was then transformed into

	Context A	Context B
Light	On	Off
Arena (visual cue)	Either 'spots' or 'stripes'	Opposite to Context A
Floor	Metal bars	Perspex floor
Cleaning solution	40% ethanol	
Olfactory cue	1% acetic acid	40% ethanol

Table 1 – The comparison of the differences between the contexts A and B used in auditory fear conditioning experiments. The contexts differ in visual cues by having each of the arenas for the same animal associated with the each of the contexts, tactile cues by changes in the floor, the presence or absence of artificial light inside the arena and differences in odour.

the percentage of time spent freezing per each tone (Stevenson et al. 2009). The score sets by the two scientists were compared to ensure a lack of bias before the analysis was done.

The behaviour of the fear conditioning session was scored and animals were separated into groups of matching mean freezing levels. This was done to ensure there were no biases in animal behaviour across the groups prior to drug administration.

The contextual fear was scored in twenty 3 second blocks to generate the percentage of time spent freezing per minute for the two minutes, as opposed to 30 second tone blocks used for scoring fear during tone presentations.

2.2.6 *Statistical analysis*

The data was analysed using GraphPad Prism v6 and v7 statistical analysis software. Two-factor mixed-measures ANOVA with one between subjects factor (CBD dose) and another within-subjects factor (Stage of Extinction) and One-way ordinary ANOVA with Tukey's post hoc test for multiple comparisons were used where appropriate. The signficance level was set as 0.05. From extinction onwards

the outliers were determined and excluded if they were more than 2 x SD away from their respective group's mean, leaving n=10-11 animals per group.

2.3 RESULTS

2.3.1 *Conditioning*

Fear conditioning resulted in increased freezing behaviour. Mean freezing behaviour during fear conditioning was significantly affected by the stage of fear conditioning, represented as tone-shock pairings ($F_{(4,176)}$= 16.28, p<0.0001; Two-way mixed-measures ANOVA). There was no significant difference in mean freezing behaviour due to CBD dose or its interaction with tone-shock pairing stage during conditioning ($F_{(3, 44)}$ = 0.2209, p=0.88, and $F_{(12, 176)}$ = 0.4204, p=0.95, respectively). The subject matching was effective ($F_{(44, 176)}$ = 2.604, p<0.0001). Taken together this suggests that auditory fear training affected the observed freezing level and there was a lack of bias between the tested drug groups prior to drug administration (see Figure 10A).

2.3.2 *Extinction*

Mean freezing behaviour during extinction was significantly affected by the stage of extinction ($F_{(2, 78)}$ = 119.4, p<0.0001) and its interaction with CBD dose ($F_{(6, 78)}$ = 3.983, p=0.0016) as determined by the Two-way mixed-measures ANOVA. The CBD dose factor accounted for only 1.8% variation in mean freezing level and was not deemed significant ($F_{(3, 39)}$ = 0.8674, p=0.47). Interestingly, however, post hoc analysis revealed that 20 mg/kg CBD significantly reduced mean freezing behaviour compared to the vehicle group (p=0.049) and 5 mg/kg CBD at the first block of five tones during extinction (p=0.0025, Tukey's post hoc, see Figure 10B). The effect was not sustained during later blocks of extinction. It appears that only

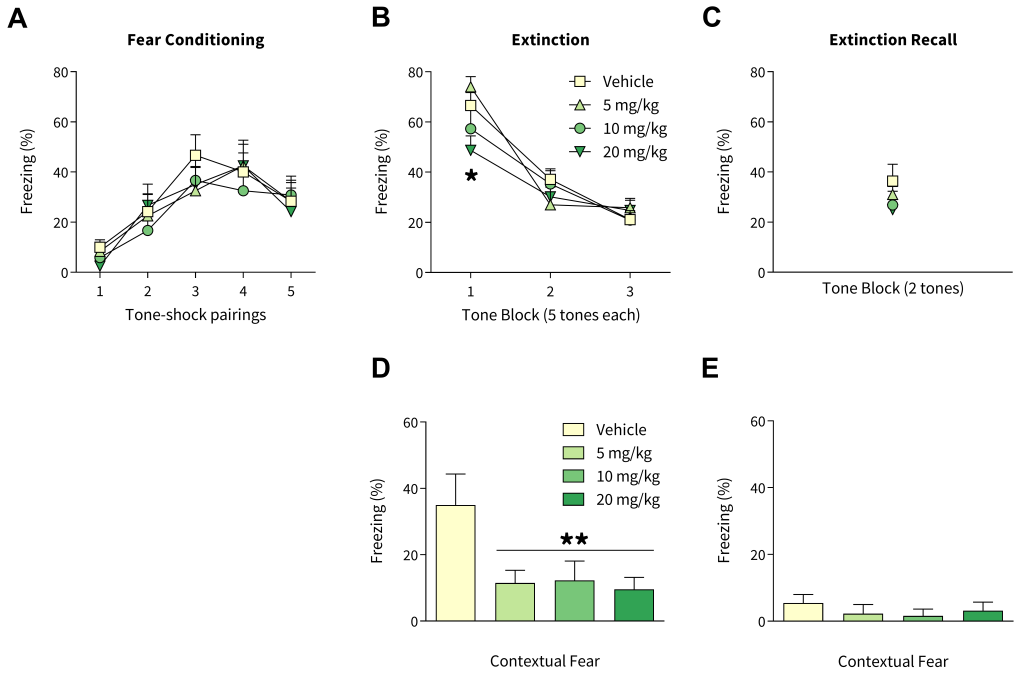

Figure 10 – The results of the auditory fear conditioning experiment using three different, systemically administered, doses of CBD. (A) Fear conditioning resulted in fear response in response to CS and there was no bias between the different groups (n=10-11 per group) prior to drug administration. (B) Only the 20 mg/kg reduced fear expression during the initial stage of extinction training (p=0.049 v Vehicle; p=0.0025 v 5 mg/kg CBD; Two-way mixed-measures ANOVA with Tukey's post hoc). (C) The freezing behaviour during auditory extinction recall did not differ between the drug groups. (D) All doses of CBD reduced contextual fear expression 2 minutes prior to auditory fear extinction training (p<0.01). (E) The contextual fear expression 2 minutes before auditory extinction recall did not differ among drug groups. Asterisks indicate the significance level, where * represents $p < 0.05$ and ** represents $p < 0.01$. All graphs are presented as mean ± SEM.

the highest dose of CBD is able to reduce the initial fear, but does not affect the extinction process.

2.3.3 *Extinction Recall*

There was no significant difference in mean freezing behaviour due to CBD dose (One-way ANOVA: $F_{(3, 39)} = 0.5468$, p=0.65). This means that CBD did not have a detectable effect during extinction recall.

2.3.4 *Contextual Fear before Extinction and Extinction Recall*

Animal freezing was recorded for two minutes prior to the presentation of the first auditory tone indicating the beginning of auditory fear extinction training, or its recall next day, respectively. Two-way mixed-measures ANOVA revealed that the day, CBD dose and day × CBD dose interaction significantly affected the mean freezing level ($F_{(1,44)} = 27.53$, p<0.0001; $F_{(3,44)} = 4.101$, p=0.012 and $F_{(3,44)} = 2.894$, p=0.046, respectively). Tukey's post hoc test revealed that all of the CBD doses had lower mean freezing level than vehicle prior to the first tone presentation of auditory extinction training (p=0.0017, p=0.0036 and p=0.0012; Fig 2D). No such effect was seen in mean freezing behaviour prior to auditory extinction recall (Fig 10E). Interestingly, the matching of subjects was not effective in this analysis ($F_{(44, 44)} = 1.243$, p=0.24). Taking the lack of CBD dose effect on mean freezing levels prior to auditory extinction recall and matching not being effective, it could be a result of low freezing levels of contextual fear prior to extinction recall (Fig 10E) that are masking the effect.

The CBD dose effect on mean freezing prior to extinction training is different to the effects seen during auditory fear extinction, where only the highest dose affected the freezing level. On the other hand, it is in agreement with the published data on CBD effects on contextual fear memory extinction.

2.4 DISCUSSION

2.4.1 *CBD is an anxiolytic that spares extinction of auditory fear memory*

In this experiment we tried to investigate CBD effects in fear memory paradigm relying on explicit cues. The animals successfully learned explicit-cue association with a foot shock. For the first time we have shown that only the highest dose of CBD reduced initial fear to the CS during extinction training, with extinction learning and memory left unaffected. This anxiolytic effect that spares extinction process is a very interesting observation that warrants further investigation. Anxiolytic drugs, such as benzodiazepines are known to impair extinction process while reducing the symptoms of anxiety (Rothbaum et al. 2014). D-cycloserine, on the other hand, has an opposite effect to CBD reported here since it does not have an anxiolytic effect but facilitates learned fear extinction (Graham et al. 2011). Moreover, the current first line treatment of anxiety disorders, SSRIs, have a loading period associated with transient anxiogenesis (Baldwin et al. 2014). Therefore, CBD should be investigated further to gather more robust evidence, since it could potentially be used in combination with exposure therapy.

2.4.2 *Contextual and auditory fear memory pharmacology*

Another interesting facet is the discrepancy in the effective doses between contextual and auditory fear memory. Considering the lack of published studies available it was natural to assume 10 mg/kg dose being most effective in auditory paradigms as highlighted by contextual fear memory studies in rodents, indicating an inverted-U shaped dose-response curve (Lemos et al. 2010). However, this was not the case as only the maximal dose used in our experiment elicited an anxiolytic effect. It would be interesting to see if increasing the doses of CBD in auditory fear memory paradigm could reveal this parabolic phenomena. However, it must be noted that alternative methods of preparing CBD injection solution might

have to be considered, since it is rather troublesome to get high concentrations of the drug into 2% Tween 80/Sterile saline vehicle preparation. In addition to increasing doses of CBD, further experiments involving the blockade of CB1 and 5-HT1A receptors using SR141716 and WAY100,635, respectively, could reveal pharmacological differences that could potentially underlie the dose differences seen in contextual and auditory fear memory anxiolysis.

2.4.3 *Potential brain areas responsible for the CBD effect*

The observed effect of CBD was anxiolytic and not extinction-memory facilitating, leading to question the potential brain areas responsible for this action. Innate fear studies indicate the dorsal part of the periaqueductal grey (DPAG) as injections of CBD into it are anxiolytic and depend on 5-HT1A receptors (Campos & Guimarães 2008, de Paula Soares et al. 2010). Innate and contextual fear memory studies using CBD injections into the bed nucleus of the stria terminalis showed anxiolytic effect dependent on 5-HT1A receptors as well (Gomes et al. 2011, 2012). Similarly, administration of CBD into the central nucleus of the amygdala produces an anxiolytic effect (Hsiao et al. 2012). Lastly, injection of CBD into the prelimbic cortex of the medial prefrontal cortex reduced fear expression and depends on 5-HT1A receptors (Lemos et al. 2010, Fogaça et al. 2014). A summary of potential areas involved can be seen in Figure 11. In order to find the area or areas responsible for CBD anxiolytic action in auditory fear memory paradigm, the first step would be to find the main receptor responsible for anxiolytic action. This could be the serotonin 5-HT1A receptor, but other receptors should be investigated with systemic antagonist administrations. Once the receptors are found, the antagonists for them can be used in conjuction with localised CBD infusions into the brain areas to determine the locus of the anxiolytic activity of CBD in fear memory associated with explicit cues.

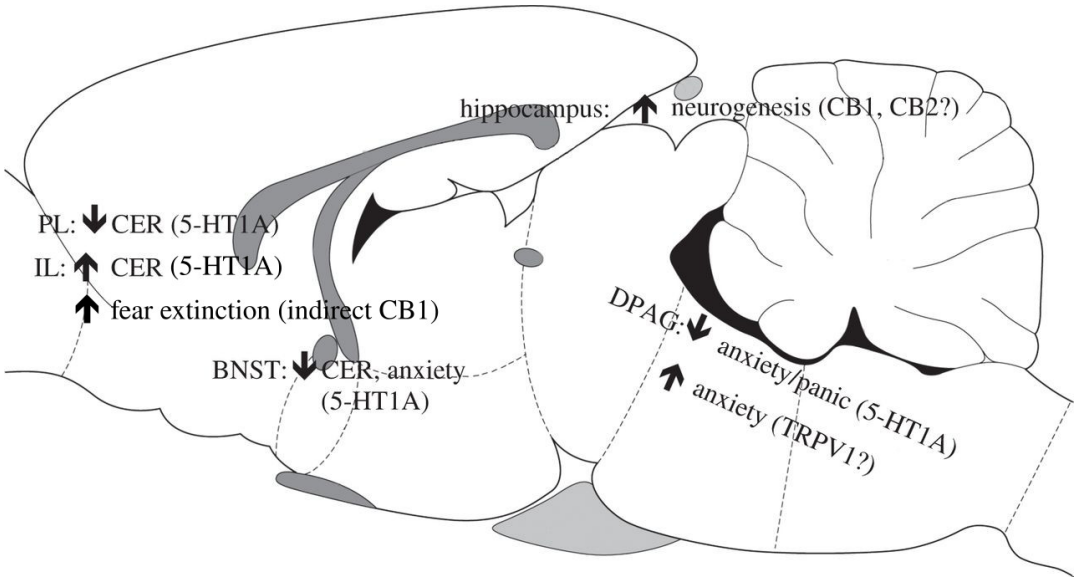

Figure 11 – The brain sites and receptors responsible for the anxiolytic effect of CBD. The vast majority of the anxiolytic effect can be attributed to the 5-HT1A receptor, with BNST, DPAG and PL being the areas responsible for the anxioytic action. BNST, the bed nucleus of the stria terminalis; CER, conditioned emotional response; DPAG, dorsal area of the periaqueductal grey. Adapted from Campos et al. (2012) with additional information from Do Monte et al. (2013) and Marinho et al. (2015).

3

SPIKING MODEL NETWORK OF FEAR MEMORY AND ITS EXTINCTION

3.1 INTRODUCTION

Fear learning and extinction has been studied experimentally for decades with a plethora of disciplines covering its processing by the brain at various different levels. These range from molecular approaches studying synaptic plasticity and histological approaches investigating neuronal projections to electrophyshiological recordings in awake behaving animals and neuroimaging in patients (Blair 2001, Hoover & Vertes 2007, Tovote et al. 2015, Sehlmeyer et al. 2009). However, integrating these multidisciplinary findings into cohesive domains of knowledge is difficult to do intuitively or experimentally due to the complexity of the nervous system and the vast amount of data collected (Nair et al. 2016). This is where computational neuroscience techniques can help.

Spiking neuron fear network models

Fear memory and extinction networks are modelled using various approaches. One of these approaches uses spiking neurons as the basis for the network. These models can be subdivided into highly biophysical spiking neuron models employing a Hodgkin-Huxley (HH) formalism that accounts for various current contributions towards action potential, and phenomenological integrate-and-fire (IAF) models.

Li et al. (2009) created a highly biophysical model of the amygdala consisting of 8 pyramidal cells and 2 interneurons that could learn CS-US associations, highlight key plasticity sites as well as the importance of NMDA receptors in extinction learning. Pendyam et al. (2013) built on this model, creating a large biophysical neuron network of the basal, lateral and central amygdala as well as the prelimbic cortex of the medial prefrontal cortex. The model predicted neurotransmitter involvement in the prelimbic cortex neuronal activity that has been verified biologically. Fenton (2015) extended this model further by incorporating the infralimbic cortex and simplifying the amygdala structure into BLA. The network was designed to investigate the interactions between PL and IL, which are interconnected amongst each other and with BLA. This network had two versions, with one being fully biophysical, and the other mixed with biophysical BLA and phenomenological mPFC, composed of excitatory and inhibitory Izhikevich neurons (Izhikevich 2003). The model used NMDA inactivation as well as PL-IL connectivity inactivation to investigate the validity of the network. While NMDA inactivation experiment generated results consistent with biological experiments in the fully biophysical version, PL-IL inactivation aspects were captured by both biophysical and hybrid model versions. In fact, Fenton (2015) highlighted that the hybrid model was much more computationally efficient, with simulation taking hours as opposed to days.

These spiking neuron models created predictions that can be verified with *in vivo* research findings. However, none of the spiking neuron network models accounted for brain areas beyond the amygdala and the medial prefrontal cortex. In fact, spiking neuron models are yet to address the role of the ventral hippocampus in fear memory and extinction.

The two areas of the medial prefrontal cortex have opposing roles in fear memory and extinction. PL is involved in fear expression, whereas IL is involved in extinction learning and retention (Vidal-Gonzalez et al. 2006, Sierra-Mercado et al. 2011). VH is involved in both of these processes (Sierra-Mercado et al. 2011). Therefore, modelling the ventral hippocampus beside the medial prefrontal cortex and the amygdala might provide a better insight into the neurocircuitry underlying fear learning and extinction.

3.1.1 *Modelling amygdala function*

Several computational models of fear memory and extinction rely on the amygdala undergoing a CS-US association before its neurons can be classified according to their activity and connected to the rest of the network. This is done since inputs to the amygdala create neurons representing fear and extinction traces that have area-specific projections, respectively. Such approaches were used by Pendyam et al. (2013) and Fenton (2015). In contrast, Herry et al. (2008) captured and defined the presence of three populations of neurons within the basolateral amygdala that are recruited during fear conditioning and extinction to represent fear, extinction and extinction resistant memory traces. Vlachos et al. (2011) used a mean-fire rate as well as the integrate-and-fire neuron amygdala models to verify that the recruitment of basolateral amygdala neurons into fear and extinction subpopulations result from CS and US inputs and have a role in encoding contextual specificity of memory traces.

Interestingly, no fear conditioning and extinction network model has made use of this finding to bypass the CS-US association and neuronal classification stage before the amygdala could be connected to the rest of the network and drive its activity. Modelling memory trace populations would not require simulation before they are connected and could drive the rest of fear conditioning and extinction network.

3.1.2 *Aims and hypotheses*

The model considered herein was based on the studies by Pendyam et al. (2013) and Fenton (2015). It extends these works by an addition of the CA1 of the ventral hippocampus to the network of the amygdala and the prelimbic as well as infralimbic cortices of the medial prefrontal cortex. We used integrate-and-fire Izhikevich units to represent the neurons at 1:200 scale interconnected with glutamatergic NMDA and AMPA or inhibitory GABAergic synapses with calcium

concentration-based synaptic learning. We investigated the role of the ventral hippocampus (CA1) on fear learning and extinction by inactivating the area and impeding its inputs on the prelimbic and infralimbic cortices. In addition, this model tests the replacement of the canonical CS-US associating amygdala with three subpopulations of the basolateral amygdala neurons representing fear, extinction and extinction-resistant memory traces.

Specifically, this fear memory neural network model addresses the following 3 aims:

1. Model the full network exclusively using Izhikevich IAF units to test if it can broadly recreate biophysical network activity at a lower computational cost (Fenton 2015).

2. Replace CS-US association learning in the basolateral amygdala by simulating the competitively recruited basal amygdala neuronal populations reflecting all three functionally distinct populations of BA neurons discovered by Herry et al. (2008).

3. Extend the Fenton (2015) model framework, based on Pendyam et al. (2013) and Li et al. (2009) work by adding VH (CA1) and test the impact of its inactivation on the function of the prelimbic and infralimbic activity.

Our VH inactivation approach is compared against intact network as well as inactivation of PL-IL connectivity seen in Fenton (2015). The activity of the prelimbic and infralimbic cortices is monitored and serves as the indicator of the inactivation effects. VH inactivation should be anxiolytic in nature. Therefore, the outcome of VH inactivation is going to verify if the network model is sufficient to reproduce the effect seen in biology.

A secondary objective is to verify if modelling neuronal populations representing fear, extinction and extinction-resistant memort traces is sufficient to reproduce the amygdala functionality seen in other models.

3.2 METHODS

3.2.1 *Overview*

The fear memory and extinction network model, shown in Figure 12, followed the Fenton (2015) BLA-PL-IL model and extended it with the ventral hippocampal (VH) CA1 area due to the increasing focus on its involvement in fear memory processing. The BLA population in Fenton (2015) was replaced with three functionally distinct subpopulations of BA neurons, representing fear, extinction and extinction-resistant memory traces observed biologically by Herry et al. (2008). Lastly, the model relied exclusively on Izhikevich neurons, as opposed to HH and HH/Izhikevich hybrid model networks used by Fenton (2015), since this approach has a very low computational cost.

VH was included to test the effect of its inactivation on the PL and IL activity, and determine its anxiogenic or anxiolytic nature. Since PL activity is correlated with fear expression and IL is involved in fear extinction learning, changes in their activity following VH inactivation would predict anxiogenic and anxiolytic effect.

In addition to this, the Fenton (2015) PL-IL disconnection experiment was conducted to compare the effects of VH inactivation against PL-IL disconnection as well as to validate this model against previous models of fear memory and extinction networks.

3.2.2 *Basic components*

Units

Izhikevich integrate-and-fire spiking unit models were used to model the dynamics in the simulated network (Izhikevich 2003). The notation $\dot{x}$ describes differentiation with respect to time (i.e. $\frac{dx}{dt}$). The two coupled differential equations, governing the membrane potential, $\dot{V}$ and the recovery, or adaptation, current $\dot{u}$,

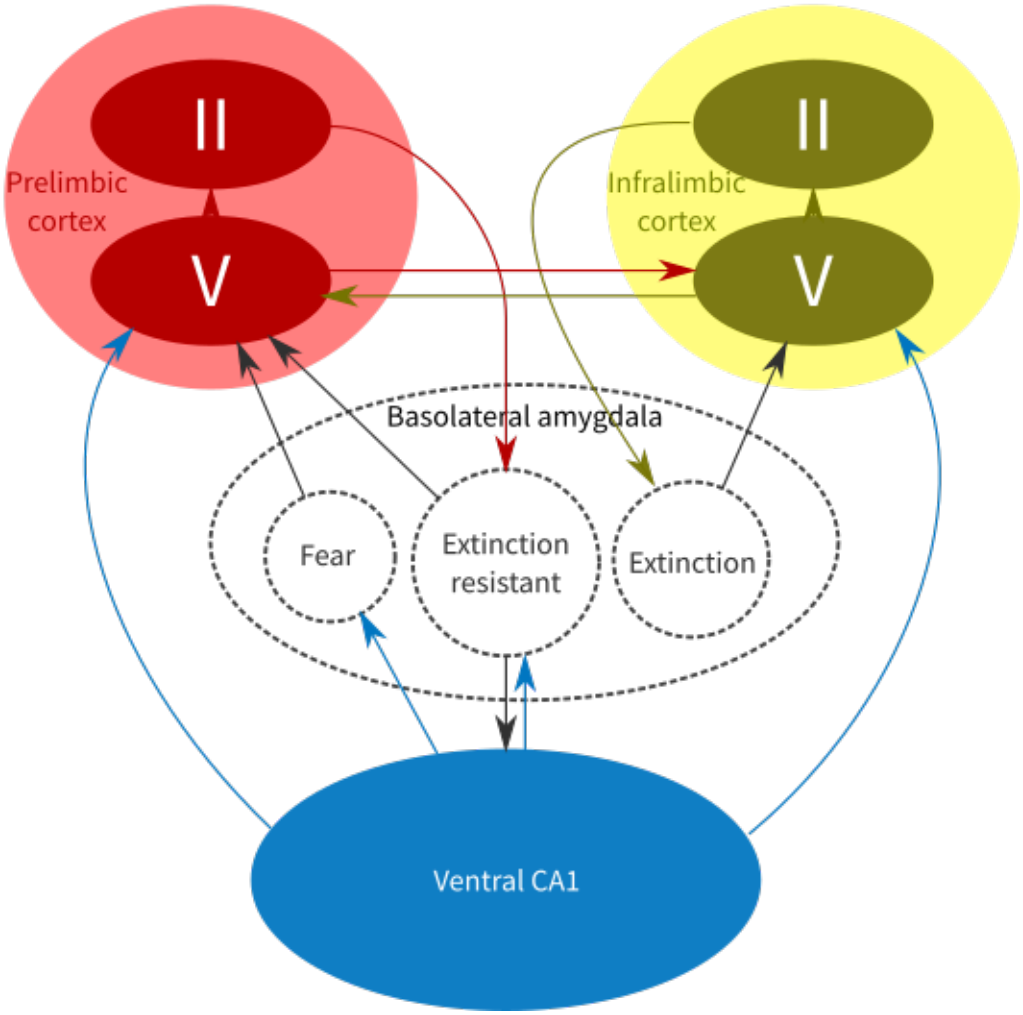

Figure 12 – The framework of the full network. The model was composed of the prelimbic, infralimbic cortices of the medial prefrontal cortex, the ventral hippocampal CA1 area and the populations of basolateral amygdala neurons recruited into fear, extinction and extinction-resistant traces.

respectively, that describe the two dimensional dynamics of Izhikevich neuron at $v < v_{\text{peak}}$ are as follows:

$$C\dot{V} = k(V - V_r)(V - V_t) - u + I, \tag{13}$$

$$\dot{u} = a[b(V - V_r) - u], \tag{14}$$

with reset conditions at $v = v_{\text{peak}}$:

$$V \leftarrow c \qquad \text{when } V > V_{\text{peak}}, \tag{15}$$

$$u \leftarrow u + d \qquad \text{when } V > V_{\text{peak}}. \tag{16}$$

In Eq 13, C is the membrane capacitance, k is the scaling factor, V_r and V_t are resting and threshold potentials, respectively, u is the adaptation variable and I is the input current. In Eq 14, u is the adaptation variable, a is the recovery time constant, b is a constant describing the sensitivity to subthreshold oscillations and determines if u is an amplifying ($b < 0$) or a resonant ($b > 0$) variable. When the neuron fires it is reset according to Eqs 15 and 16, in which c is the reset membrane potential and, d is the final outward current after spike value (for details see Izhikevich (2007) p.273-319).

We used Izhikevich units to describe the spiking activity of the different populations of units within our framework that are involved in fear memory processing. In general these were modelled to be a biologically plausible representation of the neuronal dynamics seen within these areas during *in vivo* and *ex vivo* experiments.

The intrinsically bursting excitatory cell model is the main pyramidal cell in the Pendyam et al. (2013) prelimbic area as well as Fenton (2015) prelimbic and infralimbic areas. This is the most common pyramidal cell in the deep layers (V-VI) of the rat prefrontal cortex (Yang et al. 1996, Durstewitz et al. 2000). In contrast, the regular spiking cell is present in most of the layers of rat neocortex (II - VI) and is the most common cell type encountered during in vivo intracellular recordings (Connors & Gutnick 1990). Therefore, the regular spiking neuron model was chosen

as the main pyramidal cell in the prelimbic and infralimbic areas, activity of which can be seen in Figure 14a.

When it comes to inhibitory units, Kawaguchi & Kubota (1997) suggest that the most common inhibitory neuron in the rat medial prefrontal cortex is the fast spiking (FS) neuron. This type of inhibitory unit was used by both Pendyam et al. (2013) and Fenton (2015) in their Hodgkin-Huxley unit models as the only type of interneuron. However, FS dynamics switch between spiking and subthreshold oscillations when stimulated just above the threshold current and achieves non-frequency adapting fast spiking with stronger inputs (Izhikevich 2007). As seen in Figure 13, this irregular firing at the lower frequency range cannot reliably reproduce the firing rates recorded during fear and working memory experiments, respectively, by Sotres-Bayon et al. (2012) (15-35 Hz) or Fujisawa et al. (2008) (7-8 ± 8 Hz). This is an important drawback of FS interneurons, since our network is

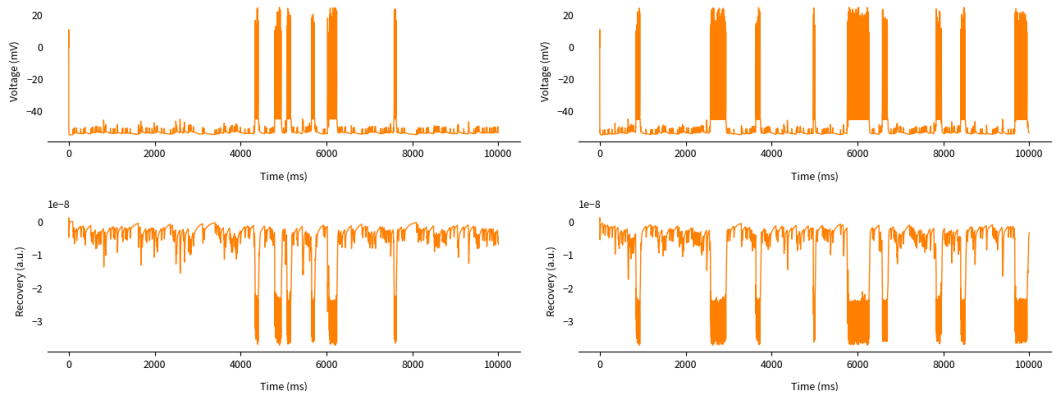

(a) 8.5 Hz mean fire rate of FS interneuron with 25 Hz Poisson input

(b) 26 Hz mean fire rate of FS interneuron with 25 Hz Poisson input

Figure 13 – FS interneurons have no frequency adaptation. A 25 Hz Poisson input used here cannot produce consistent low firing rates. FS model used $20\dot{V} = (V+55)(V+40) - u + I$, $\dot{u} = 0.2\{U(V) - u\}$, if $V \geqslant 25$, then $V \leftarrow -45$. $U(V) = 0$, when $V < -55$, and $U(V) = 0.0025(V+55)^3$, when $V \geqslant -55$. Parameters taken from Izhikevich (2007) p 299.

driven by fear, extinction and extinction-resistant memory trace sub-populations of BLA, as opposed to CS-US association learning in BLA, which in turn produces the said memory trace populations. The former approach provides us with the ability to condense the fear memory paradigm into its main features by deterministically altering the activity of the three memory trace sub-populations, achieving

the activity in the area seen at different stages of the fear memory paradigm in a shorter time that with the latter method. This, in turn, allows us reduce the simulation time provided we can reliably reproduce the basal neuronal activity reported within the different areas of the network. Therefore, a more frequency adaptive interneuron type should be considered. An alternative to FS interneuron is the low-threshold spiking (LTS) interneuron, which electrophysiologically is similar to FS, but lacks a fast potassium current, leading to frequency adaptation that is not present in FS (Izhikevich 2007). In fact, the LTS neuron is a common type of interneuron found in layer 5 of the mPFC besides FS (Bacci et al. 2005). The LTS unit can reliably reproduce the reported inhibitory unit firing rates in vivo within the prelimbic and infralimbic cortices. Lastly, the LTS interneuron is similar to the oriens-lacunosum moleculare (O-LM) interneuron found in the hippocampus that is responsible for the generation of theta oscillations, a frequency band highly implicated in fear memory circuitry and, in the ventral hippocampus, an accurate predictor of an anxiogenic state (Vierling-Claassen et al. 2010, Gloveli et al. 2005, Adhikari et al. 2010, Padilla-Coreano et al. 2016, Yeung et al. 2012). Thus, the LTS neuron, shown in Figure 14b, was used exclusively as the inhibitory unit in our model network Izhikevich (2007).

In order to reflect the neuronal dynamics seen outside of neocortex, the model made use of CA1 units (see Figures 15a and 15b). Izhikevich model parameters for the hippocampal CA1 were constrained by Ferguson et al. (2014) from the cellular properties of CA1 neurons obeserved during ex vivo studies of the rodent hippocampal slicies, revealing two types of pyramidal cells – strongly and weakly adapting. To elicit this property the cells required the replacement of the k scaling constant used in regular pyramidal and LTS inhibitory units with two cases, k_{low} and k_{high}, to scale CA1 membrane potential below and at or beyond membrane potential threshold, respectively:

$$k = \begin{cases} k_{\text{low}} & \text{if } V < V_t, \\ k_{\text{high}} & \text{if } V \geqslant V_t. \end{cases} \tag{17}$$

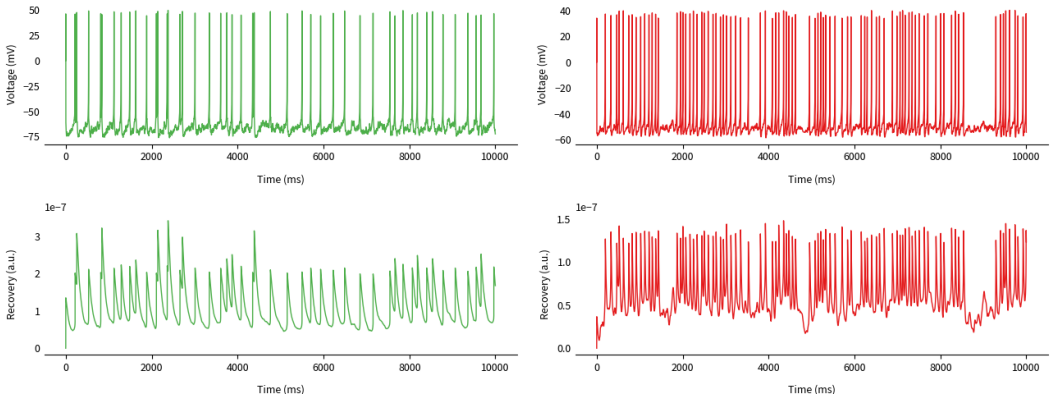

(a) Typical regular Izhikevich neuron (b) Typical LTS Izhikevich neuron

Figure 14 – Example of regular and LTS neuron activity. Top figure shows voltage and bottom figure shows adaption variable evolution over 10 second simulation. Regular unit simulation $150\dot{V} = 1.2(V+75)(V+42) - u + I$, $\dot{u} = 0.015(V+75) - u$, if $V \geqslant 50$, then $v \leftarrow -56$ and $u \leftarrow u + 130$. LTS neuron simulation $100\dot{V} = (V+56)(V+42) - u + I$, $\dot{u} = 0.038(V+56) - u$, if $V \geqslant 40$, then $V \leftarrow -53$ and $u \leftarrow u + 20$. Regular unit received $\lambda = 525$ Hz Poisson process input, whereas LTS unit received $\lambda = 120$ Hz Poisson process input via conductance-based synapses (described below).

The parameters for all of the units used in the model can be found in Table 2.

3.2.3 *Synapses*

The units in this model were interconnected with excitatory and inhibitory synapses. Excitatory synapses were governed by NMDA and AMPA glutamatergic ligand-gated ion channels, since glutamate is the main excitatory neurotransmitter in the brain. Inhibitory synapses relied on GABA ligand-gated ion channels as GABA is the most prominent inhibitory neurotransmitter. Since our model used conductance-based synapses, the postsynaptic unit input current was a sum of NMDA and AMPA cation currents, and GABA anion currents:

$$I = I_{\text{NMDA}} + I_{\text{AMPA}} + I_{\text{GABA}}, \tag{18}$$

where I_{NMDA} was governed by:

$$I_{\text{NMDA}} = \sum G_{\text{NMDA}}(t)\, s(V)\, (V - E_{\text{NMDA}}), \tag{19}$$

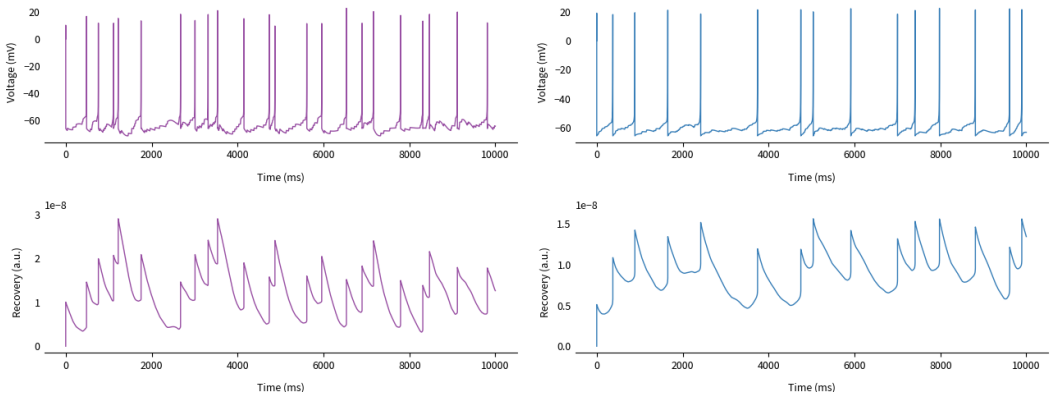

(a) Typical CA1 Strongly-adapting Izhikevich neuron

(b) Typical CA1 Weakly-adapting Izhikevich neuron

Figure 15 – Example of strongly- and weakly- adapting CA1 Izhikevich neuron activity. Top figure shows voltage and bottom figure shows adaption variable evolution over 10 second simulation. Strongly-adapting CA1 simulation $115\dot{V} = (0.1(V < -57) + (3.3(V \geqslant -57))(V + 61.8)(V + 57) - u + I$, $\dot{u} = 0.00123(V + 61.8) - u$, if $V \geqslant 22.6$, then $V \leftarrow -65.8$ and $u \leftarrow u + 10$. Weakly-adapting CA1 simulation $300\dot{V} = (0.5(V < -57) + (3.3(V \geqslant -57))(V + 61.8)(V + 57) - u + I$, $\dot{u} = 0.0013(V + 61.8) - u$, if $V \geqslant 22.6$, then $V \leftarrow -65.8$ and $u \leftarrow u + 5$. Both strongly- and weakly-adapting CA1 neurons received $\lambda = 20$ Hz Poisson process input via conductance-based synapses (descibed below).

Parameter	Regular	LTS	CA1 strong	CA1 weak
C (pF)	150	100	115	300
a (kHz)	0.01	0.03	0.0012	0.001
b (pA/mV)	5	8	3	
c (mV)	-56	-53	-65.8	
d (pA)	130	20	10	5
k (nS/mV)	1.2	1	–	–
k_{low} (nS/mV)	–	–	0.1	0.5
k_{high} (nS/mV)	–	–	3.3	3.3
V_{reset} (mV)	-75	-56	-61.8	
$V_{\text{threshold}}$ (mV)	-45	-42	-57	
V_{peak} (mV)	50	40	22.6	
Reference	Izhikevich (2007)		Ferguson et al. (2014)	

Table 2 – Parameters for four types of units used in the model.

and underwent a voltage-dependent magnesium block, $s(V)$:

$$s(V) = \frac{1.50265}{1 + 0.33 \exp\left(\frac{V}{16\text{mV}}\right)}. \tag{20}$$

In Eq 19, $\sum g_{\text{NMDA}}$ is the sum of NMDA conductances to the target unit, V is the post-synaptic neuron membrane potential and E_{NMDA} is the revesal potential of the NMDA current. I_{AMPA} and I_{GABA} currents in Eq 18, were governed by:

$$I_{\text{AMPA}} = \sum G_{\text{AMPA}}(t)\,(V - E_{\text{AMPA}})\,, \tag{21}$$

$$I_{\text{GABA}} = \sum G_{\text{GABA}}(t)\,(V - E_{\text{GABA}})\,. \tag{22}$$

AMPA-dependent currents in Eq 21 and GABA-dependent currents in Eq 22 were a sum of their respective conductances, $\sum G_{\text{AMPA}}$ and $\sum G_{\text{GABA}}$, due to presynaptic neuron activity, with their currents and direction regulated only by the postsynaptic neuron membrane potential difference from the respective reversal potential for each current (i.e. E_{AMPA} and E_{GABA}) as seen in $V - E_{\text{AMPA}}$ and $V - E_{\text{GABA}}$ terms in Eqs 21 and 22, respectively.

Conductance

Conductance by the 3 neurotransmitters was governed by the following equations:

$$\dot{G} = \frac{\phi h - G}{\tau_{\text{decay}}}, \tag{23}$$

$$\phi = \left(\frac{\tau_{\text{rise}}}{\tau_{\text{decay}}}\right)^{\frac{\tau_{\text{decay}}}{\tau_{\text{rise}} - \tau_{\text{decay}}}}, \tag{24}$$

$$\dot{h} = -\frac{h}{\tau_{\text{rise}}} + \hat{w} G^{\max} \delta(t_0 + \tau_{\text{syn}} - t). \tag{25}$$

Where $\delta(t_0 + \tau_{\text{syn}} - t)$ is a delta function, i.e.:

$$\delta(t_0 + \tau_{\text{syn}} - t) = \begin{cases} 0 & \text{if } t_0 + \tau_{\text{syn}} - t \neq 0, \\ 1 & \text{if } t_0 + \tau_{\text{syn}} - t = 0. \end{cases} \tag{26}$$

This is equivalent to dual exponential conductance dynamics used by Durstewitz et al. (2000), Li et al. (2009), Pendyam et al. (2013) and Fenton (2015). For detailed overview see Roth & van Rossum (2009).

In Eqs 23 – 26 the firing of the presynaptic neuron at time t_0 results in a neurotransmitter release, that after a synapse-specific delay, τ_{syn}, causes the conductance to rise exponentially over a time scale, τ_{rise}, resulting in a peak conductance that is a product of synaptic weight, $\hat{w}$, and the maximal conductance for that neurotransmitter, G^{max}, which in turn decays exponentially over the time scale set by τ_{decay}.

Parameters and constants describing the conductance of each neurotransmitter were used by Pendyam et al. (2013) and have been derived from electrophysiological experiments. The values for them can be found in Table 3. An example simulation of conductance dynamics for each neurotransmitter after a single spike of a pre-synaptic neuron can be seen in Figure 16.

Parameter	NMDA	AMPA	GABA
E (V)	0	0	-75
$\hat{w}$	w_0	w(t)	w(t)
τ_{rise} (ms)	12.7	0.55	0.25
τ_{decay} (ms)	126	2.2	3.75
G^{max} (nS)	0.5	1	0.6

Table 3 – Synaptic conductance parameters. Taken from Pendyam et al. (2013). The synaptic weight governing peak conductance is constant for NMDA and equivalent to the initial synaptic weight for specific synapse (i.e. w_0), whereas it is plastic for both AMPA and GABA (i.e. w_t).

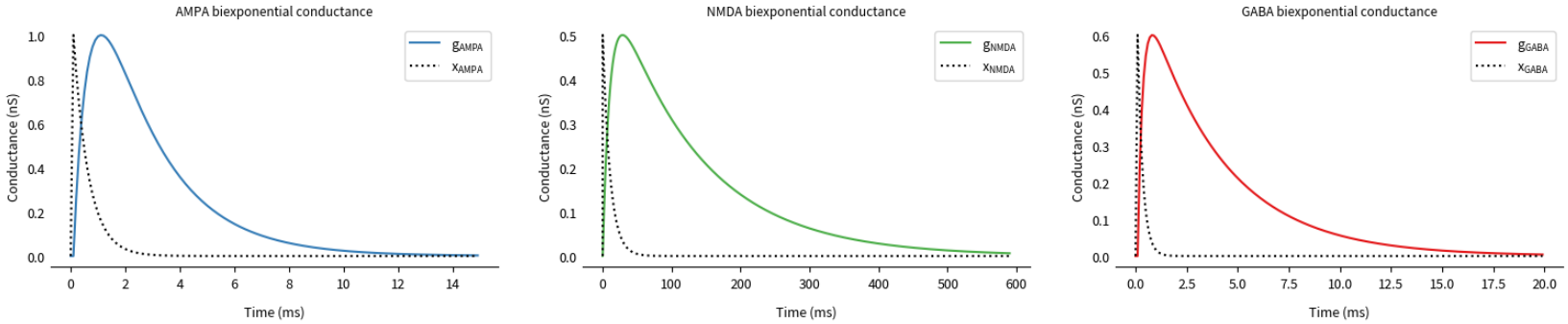

(a) AMPA (b) NMDA (c) GABA

Figure 16 – Biexponential conductance of excitatory glutamatergic AMPA- and NMDA-gated ion channels, as well as inhibitory GABA-gated ion channel. The conductance was modelled with biexponential conductance dynamics $\dot{G} = \frac{\phi h - G}{\tau_{\text{decay}}}$, $\phi = \left(\frac{\tau_{\text{rise}}}{\tau_{\text{decay}}}\right)^{\frac{\tau_{\text{decay}}}{\tau_{\text{rise}} - \tau_{\text{decay}}}}$ and $\dot{h} = -\frac{h}{\tau_{\text{rise}}} + \hat{w} G^{\max} \delta(t_0 + \tau_{\text{syn}} - t)$. AMPA parameters were $\tau_{\text{rise}} = 0.55$ ms, $\tau_{\text{decay}} = 2.2$ ms and $G^{\max} = 1$ nS. NMDA parameters were $\tau_{\text{rise}} = 12.7$ ms, $\tau_{\text{decay}} = 126$ ms and $G^{\max} = 0.5$ nS. GABA_A parameters were $\tau_{\text{rise}} = 0.25$ ms, $\tau_{\text{decay}} = 3.75$ ms and $G^{\max} = 0.6$ nS. $\hat{w}$ was fixed at 1, and $\tau_{\text{syn}} = 0$ for this example.

Plasticity

The bidirectional plasticity of synaptic weights in the model followed Hebbian learning and the calcium-control hypothesis (Bear et al. 1987, Lisman 1989, Shouval et al. 2002a,b). The calcium-control hypothesis states that concentration of calcium in the post-synaptic neuron determines the directionality of plasticity. Specifically, when resting intracellular concentration of calcium is very low, a large influx of Ca^{2+} triggers a signalling cascade leading to a long-term potentiation (LTP) of synapse, or an increase in synaptic weight. Conversely, a moderate influx of calcium leads to long-term depression (LTD), reducing the weight of the synapse. Intracellular calcium concentration was governed by the following differential equation:

$$\dot{[Ca^{2+}]} = -f\frac{I_{Ca^{2+}}}{zFV_{spine}} + \frac{[Ca^{2+}]_{rest} - [Ca^{2+}]}{\tau_{Ca^{2+}}}, \tag{27}$$

where f is the scaling factor for Ca^{2+} influx, $I_{Ca^{2+}}$ is the inward Ca^{2+} current, z is the valence of the Ca^{2+} ion, F is the Faraday constant, V_{spine} is the volume of spinal dendrite, $[Ca^{2+}]_{rest}$ is the resting concentration of Ca^{2+} and $\tau_{Ca^{2+}}$ is the calcium removal constant.

The intracellular calcium concentration governed by Eq 27 changed the weight of a synapse following a biophysical Hebbian plasticity rule in the following way:

$$\dot{w} = \eta\left([Ca^{2+}]\right)\left(\lambda_{rise}\Omega\left([Ca^{2+}]\right) - \lambda_{decay}w\right), \tag{28}$$

where, $\eta([Ca^{2+}]$ is the calcium-dependent learning rate, λ_{rise} is the scaling constant, $\Omega([Ca^{2+}]$ is the two-threshold function underpinning calcium-control hypothesis and λ_{decay} is a decay constant.

The $\eta([Ca^{2+}]$ and $\Omega([Ca^{2+}]$ functions were governed by the following equations:

$$\eta = \begin{cases} \frac{1}{1+\exp 13(-[Ca^{2+}])+5.5} & \text{if } [Ca^{2+}] < 0.389, \\ \frac{1}{1.25+\exp(9.2(-[Ca^{2+}])+4)-0.2} & \text{if } [Ca^{2+}] \geqslant 0.389. \end{cases} \tag{29}$$

$$\Omega = \begin{cases} 0 & \text{if } [Ca^{2+}] \leqslant \theta_d, \\ \alpha\left([Ca^{2+}] - \frac{\theta_p+\theta_d}{2}\right)^4 - 0.1 & \text{if } \theta_d < [Ca^{2+}] < \theta_p, \\ \frac{1.2}{1+\exp(-35(-\theta_p-0.045))-0.2} & \text{if } [Ca^{2+}] \geqslant \theta_p. \end{cases} \tag{30}$$

The two threshold function in Eq 30 uses potentiation, θ_p, and depression, θ_d thresholds that are synapse-specific (Shouval et al. 2002a,b, Li et al. 2009, Vlachos et al. 2011). The α scaling parameter in Eq 30 ensures that θ_p and θ_d represent potentiation and depression boundaries, respectively. The parameter values can be found in Table 4 and simulation of weight-governing functions is shown in Figure 17.

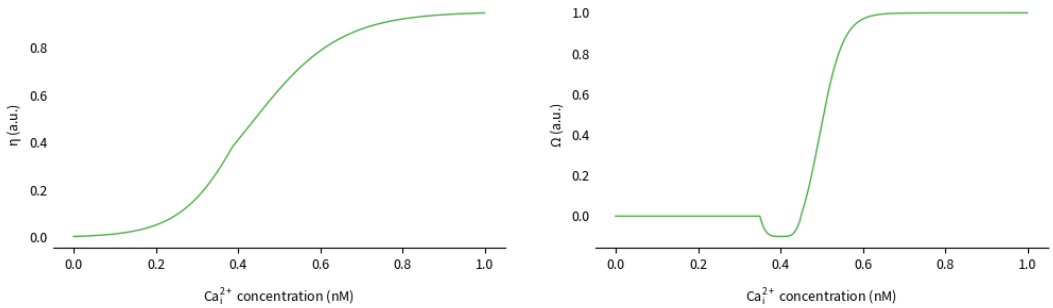

(a) $\eta - Ca^{2+}$-dependent learning rate

(b) Ω – two-threshold function

Figure 17 – η and Ω function example. η is governed by Equation 29, whereas Ω is governed by Equation 30. In this example the θ_d and θ_p are 0.35 and 0.45, respectively.

The influx of calcium in Eq 27 is dependent on the synapse type. This is highlighted by the difference of neurotransmitter-gated channel contribution to $I_{Ca^{2+}}$. Since both AMPA and NMDA are non-selective cation channels, they can directly conduct calcium. Excitatory projections onto excitatory units relied only on NMDA channels for $I_{Ca^{2+}}$ current generation, i.e:

$$I_{Ca^{2+}} = I_{Ca^{2+}}^{NMDA}, \tag{31}$$

$$I_{Ca^{2+}}^{NMDA} = P_0 w G_{NMDA} s(V)\left(V - E_{Ca^{2+}}\right), \tag{32}$$

where P_0 is the fraction of the total current that is calcium current, w is the initial weight of the synapse, G_{NMDA} is the NMDA conductance, $s(V)$ is the voltage-

dependent magnesium block seen in Eq 20, V is the post-synaptic neuron membrane potential and $E_{Ca^{2+}}$ is the calcium current reversal potential.

Excitatory projections onto inhibitory units had both NMDA, described in Eq 32, and AMPA contributions to the $I_{Ca^{2+}}$ current generation:

$$I_{Ca^{2+}} = I_{Ca^{2+}}^{NMDA} + I_{Ca^{2+}}^{AMPA}, \tag{33}$$

$$I_{Ca^{2+}}^{AMPA} = P_0 w_0 G_{AMPA} \left(V - E_{Ca^{2+}}\right). \tag{34}$$

Inhibitory projections onto excitatory units, on the other hand, relied solely on GABA input for $I_{Ca^{2+}}$ current:

$$I_{Ca^{2+}} = I_{Ca^{2+}}^{GABA}, \tag{35}$$

$$I_{Ca^{2+}}^{GABA} = P_0 w(t) G_{GABA} \left(V - E_{Ca^{2+}}\right). \tag{36}$$

In Eqs 34 and 36, the P_0 parameter represents the fraction of the total current of a neurotransmitter that is calcium current. In Eq 34, w_0 is the intial weight for that synapse, G_{AMPA} is the AMPA conductance, V is the post-synaptic neuron membrane potential and $E_{Ca^{2+}}$ is the calcium current reversal potential. In Eq 36, unlike Eqs 32 or 34, calcium influx is frequency (i.e. $w(t)$) dependent, since GABA channel is anion-specific and does not conduct calcium cations. G_{GABA} is the GABA conductance, V is the post-synaptic neuron membrane potential and $E_{Ca^{2+}}$ is the calcium current reversal potential. All of these modelling choices are following Pendyam et al. (2013) and Fenton (2015) work. Parameters for these equations can be found in Table 4.

3.2.4 *Populations*

PL and IL populations

PL and IL are key areas of fear memory processing involved in its expression, or extinction, respectively. These were recreated following Pendyam et al. (2013) and Fenton (2015). The two adjacent areas of the rodent mPFC were constructed

Parameter	Value
f	20
z	2
F[1] (As)	96485.332
V_{spine}[1] (m^3)	$4.1876 * 10^{-18}$
$[Ca^{2+}]_{rest}$[1] (μM)	0.05
τ_{syn}[1] (ms)	50
$E_{Ca^{2+}}$ (mV)	120
P_0 (NMDA)	0.015
P_0 (AMPA)	0.001
P_0 (GABA)	0.15

Table 4 – Universal plasticity constants. Parameters taken from Pendyam et al. (2013), with the exception of V_{spine}, f and P_0 for GABA. We assumed that a dendritic spine is a sphere with a diameter of 2 μm, which required to adjust the f parameter to generate plasticity within our network, whereas, P_0 for GABA was scaled up to account for the lack of I_{Ca} dynamics seen in Pendyam et al. (2013) HH model.

in a similar manner, with both IL and PL subdivided into layer 2 and layer 5 populations (Gabbott et al. 2005). Regular spiking cells represented excitatory units, whereas LTS represented the inhibitory units. The populations were modelled at a 1:200 scale, with PL2, PL5 and IL5 having approximately 1-to-4 excitatory to inhibitory ratio, whereas IL2 had a 1-to-10 excitatory to inhibitory ratio, based on the reported levels of neurons histologically (Gabbott et al. 2005, see Table 5). Each of the PL and IL population layers had their excitatory units interconnected with each unit projecting to four other excitatory units (Fujisawa et al. 2008, see Table 7). Within each layer of PL and IL populations a random 20% of excitatory units projected onto inhibitory units, with one presynaptic neuron projecting to four post-synaptic neurons (Durstewitz & Gabriel 2007, see Table 7). Since the focus was on the excitatory population dynamics in the network, it was important to retain biologically plausible inhibitory input similar to the full scale network. Therefore, it was assumed that all of the inhibitory units project to four random

1 These parameters were used without their respective units in the present model (i.e. dimensionless).

excitatory units (see Table 7). To further ensure the preservation of the inhibitory tone in the network excitatory to inhibitory (E-to-I) and inhibitory to excitatory (I-to-E) synapses had larger weights compared to the excitatory to excitatory (E-to-E) synapses (see Table 6). There were no inhibitory to inhibitory synapses in the network. Figures 18 – 25 show individual simulations of each population activity under basal conditions to visualise the neuronal and synaptic dynamics within PL2, PL5, IL2 and IL5, respectively.

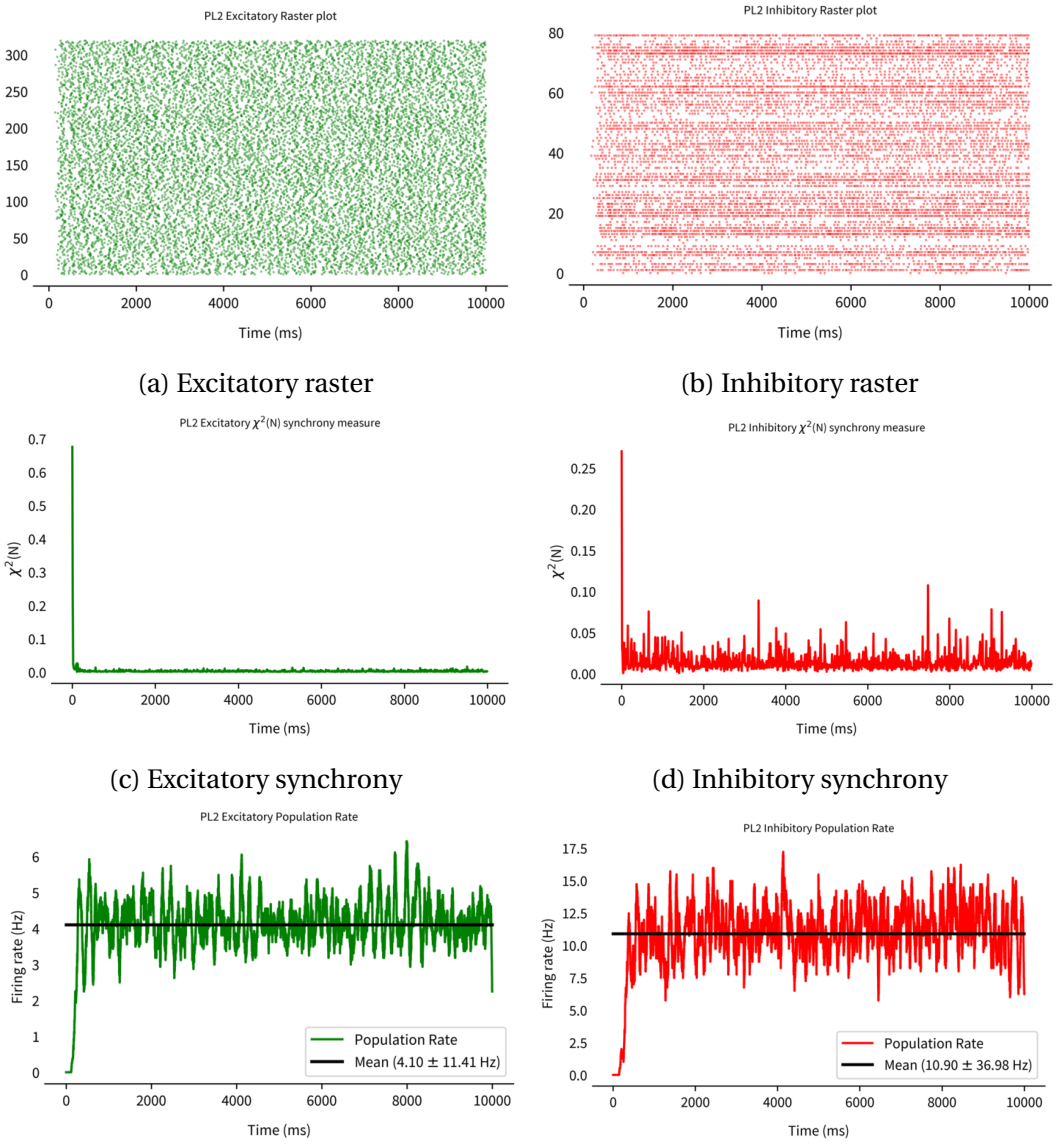

(a) Excitatory raster

(b) Inhibitory raster

(c) Excitatory synchrony

(d) Inhibitory synchrony

(e) Excitatory population rate

(f) Inhibitory population rate

Figure 18 – PL2 population neuronal dynamics. The population was modelled at 1:200 ratio with 320 regular excitatory and 80 inhibitory LTS neurons (Gabbott et al. 2005). All excitatory neurons projected to each other with a fanout of 4. A random 20% of excitatory neurons projected to inhibitory neurons with a fanout of 4. All of the inhibitory neurons projected to excitatory neurons with a fanout of 4. Excitatory units were driven by 480 Hz Poisson input and inhibitory units received 60 Hz Poisson input to recreate the excitatory unit firing rate seen biologically. The synchrony measure was calculated using the method outlined in Golomb (2007). The synchrony was inversely proportional to the population size, where the larger excitatory population had an extremely low synchrony, compared to the very low synchrony of the smaller, inhibitory population. The mean population firing rates are presented as mean ± SD.

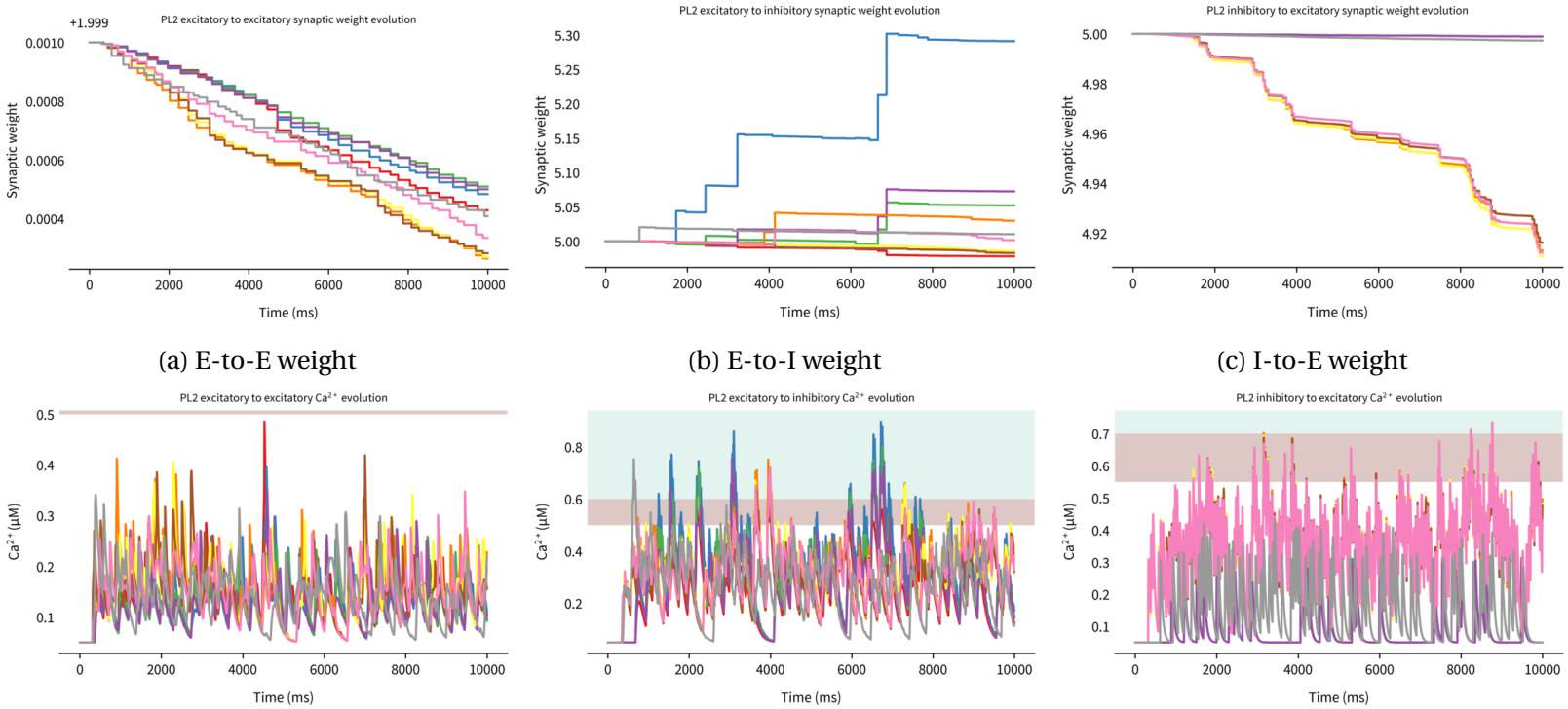

(a) E-to-E weight

(b) E-to-I weight

(c) I-to-E weight

(d) E-to-E Ca^{2+} evolution

(e) E-to-I Ca^{2+} evolution

(f) I-to-E Ca^{2+} evolution

Figure 19 – PL2 population synaptic dynamics. The population was modelled at 1:200 ratio with 320 regular excitatory and 80 inhibitory LTS neurons (Gabbott et al. 2005). All excitatory neurons projected to each other with a fanout of 4. A random 20% of excitatory neurons projected to inhibitory neurons with a fanout of 4. All of the inhibitory neurons projected to excitatory neurons with a fanout of 4. Excitatory units were driven by 480 Hz Poisson input and inhibitory units received 60 Hz Poisson input to recreate the excitatory unit firing rate seen biologically.

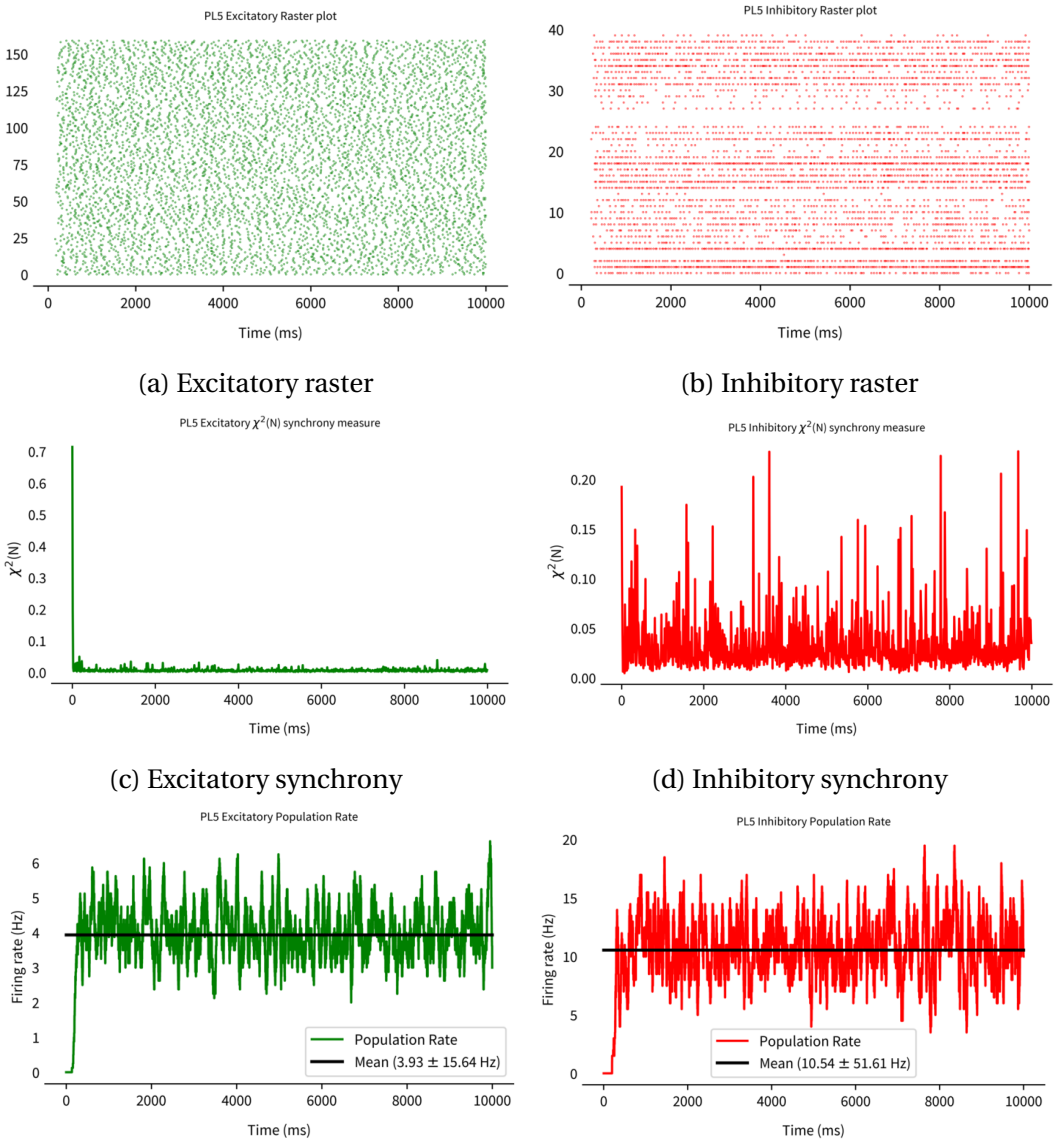

(a) Excitatory raster

(b) Inhibitory raster

(c) Excitatory synchrony

(d) Inhibitory synchrony

(e) Excitatory population rate

(f) Inhibitory population rate

Figure 20 – PL5 population neuronal dynamics. The population was modelled at 1:200 ratio with 160 regular excitatory and 40 inhibitory LTS neurons (Gabbott et al. 2005). All excitatory neurons projected to each other with a fanout of 4. A random 20% of excitatory neurons projected to inhibitory neurons with a fanout of 4. All of the inhibitory neurons projected to excitatory neurons with a fanout of 4. Excitatory units were driven by 480 Hz Poisson input and inhibitory units received 60 Hz Poisson input to recreate the excitatory unit firing rate seen biologically. The synchrony measure was calculated using the method outlined in Golomb (2007). The synchrony was inversely proportional to the population size, where the larger excitatory population had an extremely low synchrony, compared to the low synchrony of the smaller, inhibitory population. The mean population firing rates are presented as mean ± SD.

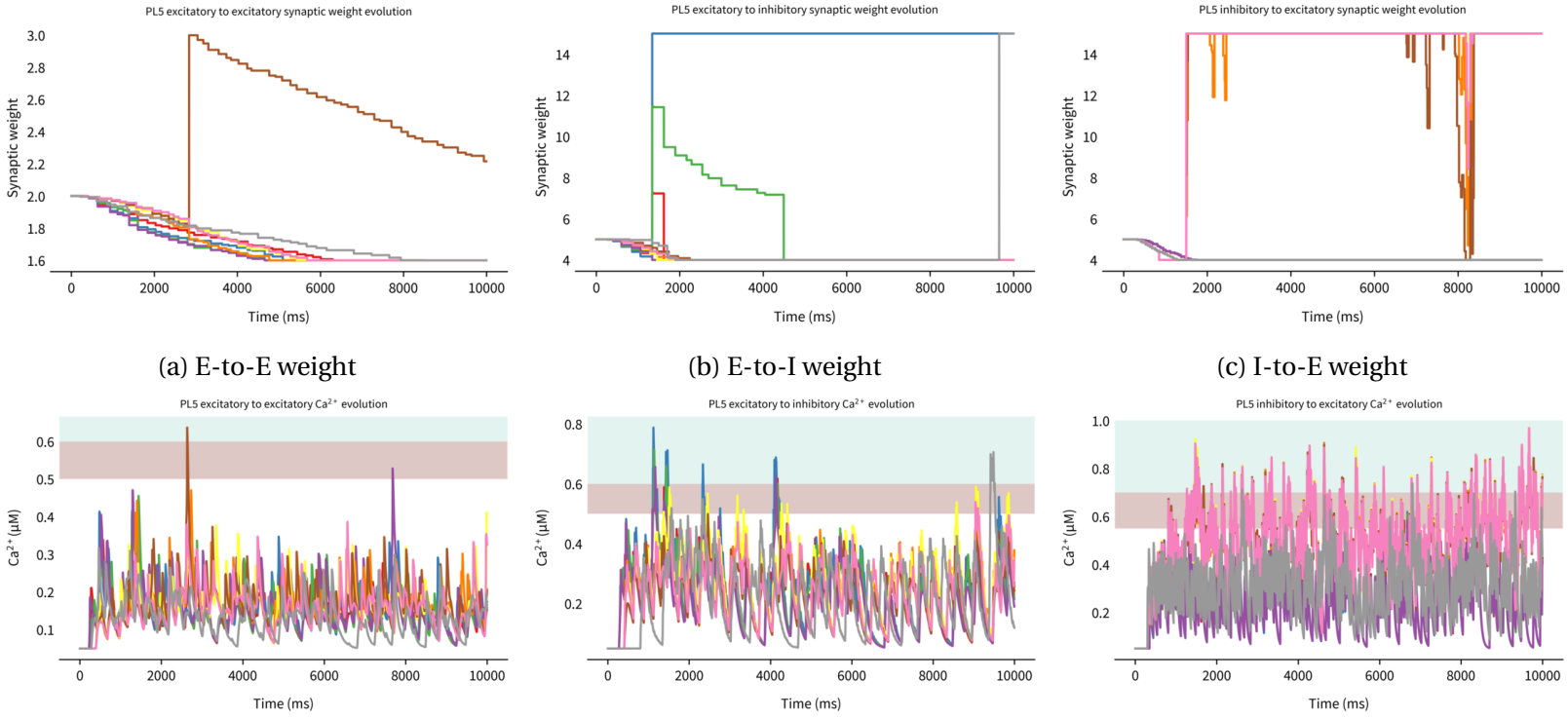

(a) E-to-E weight

(b) E-to-I weight

(c) I-to-E weight

(d) E-to-E Ca^{2+} evolution

(e) E-to-I Ca^{2+} evolution

(f) I-to-E Ca^{2+} evolution

Figure 21 – PL5 population synaptic dynamics. The population was modelled at 1:200 ratio with 160 regular excitatory and 40 inhibitory LTS neurons (Gabbott et al. 2005). All excitatory neurons projected to each other with a fanout of 4. A random 20% of excitatory neurons projected to inhibitory neurons with a fanout of 4. All of the inhibitory neurons projected to excitatory neurons with a fanout of 4. Excitatory units were driven by 480 Hz Poisson input and inhibitory units received 60 Hz Poisson input to recreate the excitatory unit firing rate seen biologically.

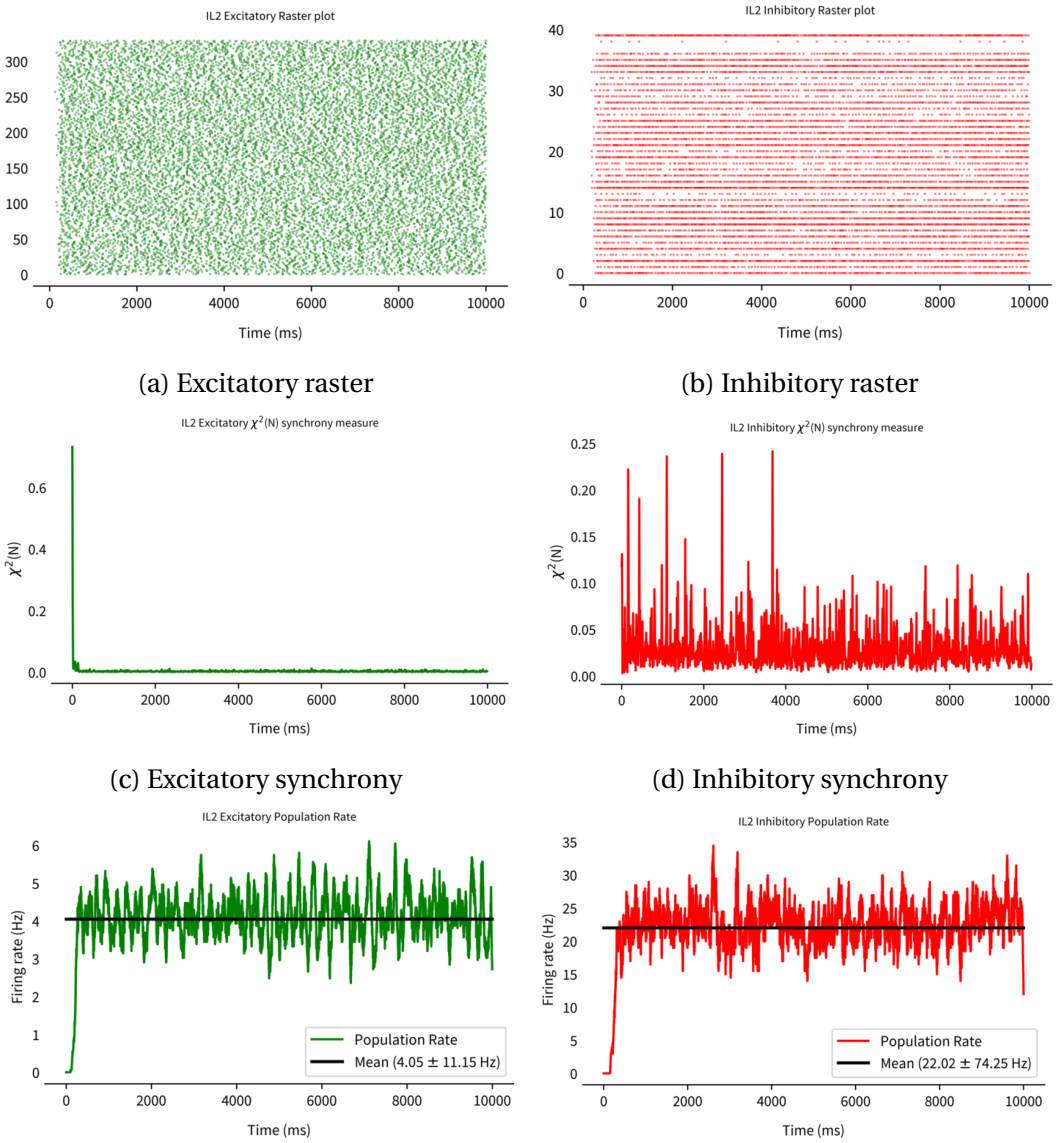

(a) Excitatory raster

(b) Inhibitory raster

(c) Excitatory synchrony

(d) Inhibitory synchrony

(e) Excitatory population rate

(f) Inhibitory population rate

Figure 22 – IL2 population neuronal dynamics. The population was modelled at 1:200 ratio with 330 regular excitatory and 40 inhibitory LTS neurons (Gabbott et al. 2005). All excitatory neurons projected to each other with a fanout of 4. A random 20% of excitatory neurons projected to inhibitory neurons with a fanout of 4. All of the inhibitory neurons projected to excitatory neurons with a fanout of 4. Excitatory units were driven by 480 Hz Poisson input and inhibitory units received 60 Hz Poisson input to recreate the excitatory unit firing rate seen biologically. The synchrony measure was calculated using the method outlined in Golomb (2007). The synchrony was inversely proportional to the population size, where the larger excitatory population had an extremely low synchrony, compared to the low synchrony of the smaller, inhibitory population. The mean population firing rates are presented as mean ± SD.

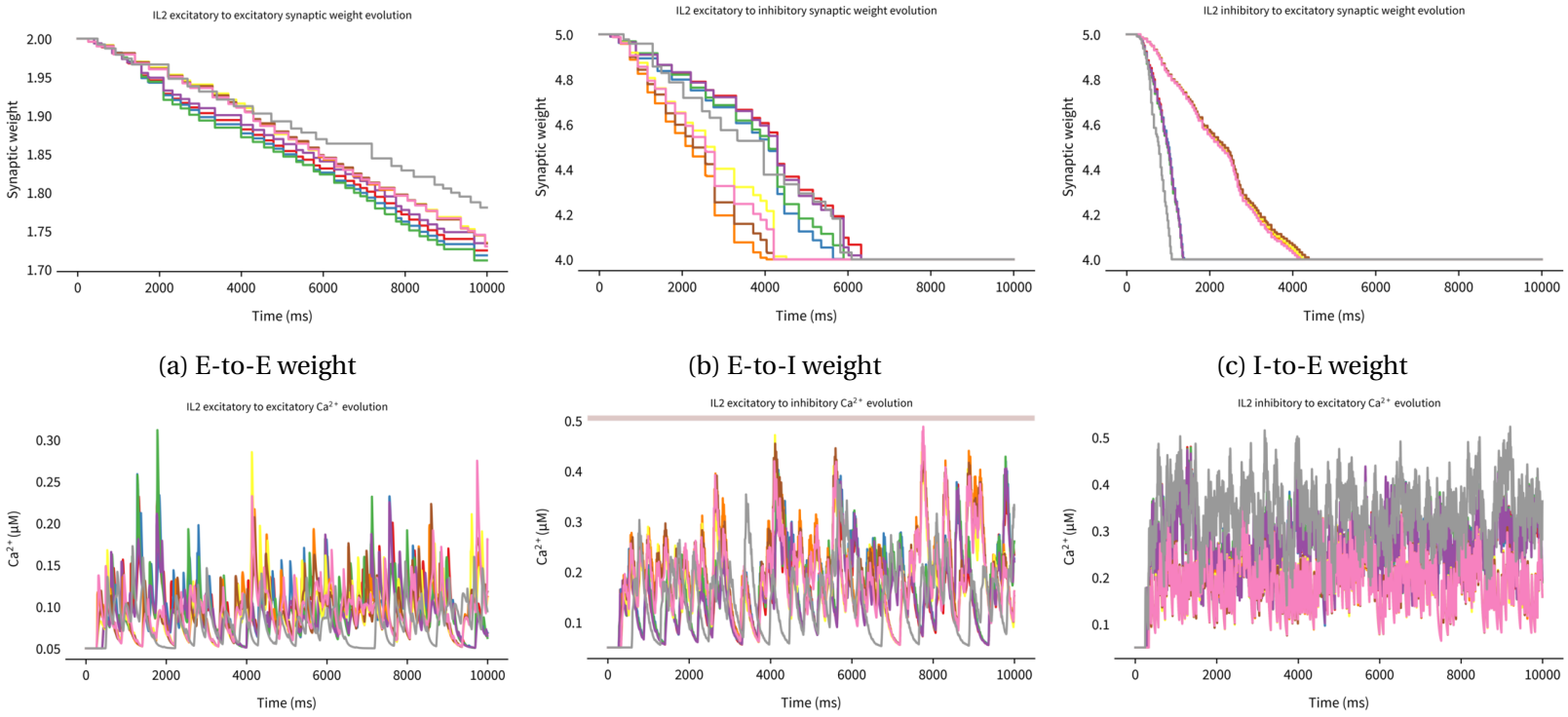

(a) E-to-E weight

(b) E-to-I weight

(c) I-to-E weight

(d) E-to-E Ca^{2+} evolution

(e) E-to-I Ca^{2+} evolution

(f) I-to-E Ca^{2+} evolution

Figure 23 – IL2 population synaptic dynamics. The population was modelled at 1:200 ratio with 330 regular excitatory and 40 inhibitory LTS neurons (Gabbott et al. 2005). All excitatory neurons projected to each other with a fanout of 4. A random 20% of excitatory neurons projected to inhibitory neurons with a fanout of 4. All of the inhibitory neurons projected to excitatory neurons with a fanout of 4. Excitatory units were driven by 480 Hz Poisson input and inhibitory units received 60 Hz Poisson input to recreate the excitatory unit firing rate seen biologically.

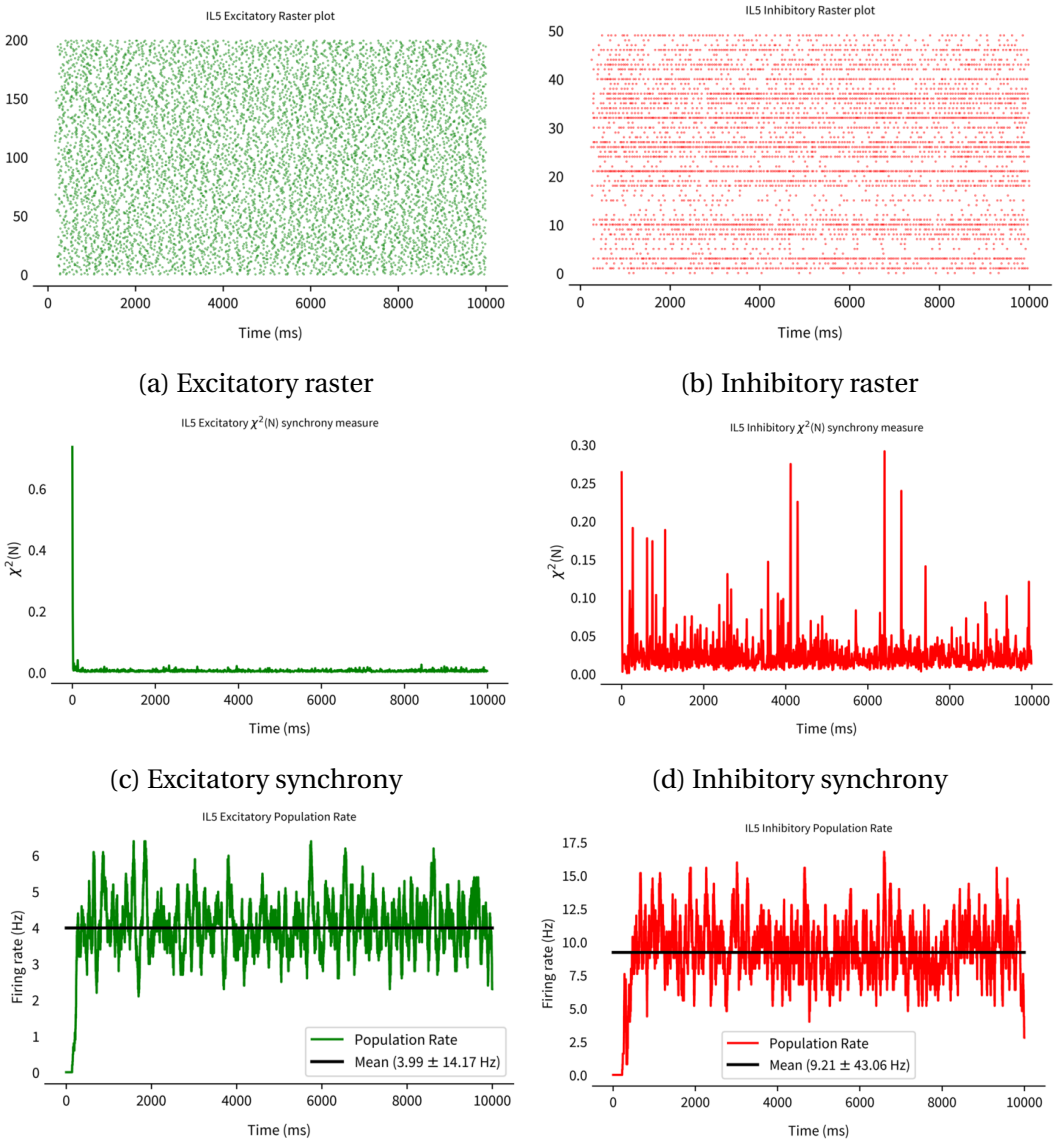

(a) Excitatory raster

(b) Inhibitory raster

(c) Excitatory synchrony

(d) Inhibitory synchrony

(e) Excitatory population rate

(f) Inhibitory population rate

Figure 24 – IL5 population neuronal dynamics. The population was modelled at 1:200 ratio with 200 regular excitatory and 50 inhibitory LTS neurons (Gabbott et al. 2005). All excitatory neurons projected to each other with a fanout of 4. A random 20% of excitatory neurons projected to inhibitory neurons with a fanout of 4. All of the inhibitory neurons projected to excitatory neurons with a fanout of 4. Excitatory units were driven by 480 Hz Poisson input and inhibitory units received 60 Hz Poisson input to recreate the excitatory unit firing rate seen biologically. The synchrony measure was calculated using the method outlined in Golomb (2007). The synchrony was inversely proportional to the population size, where the larger excitatory population had an extremely low synchrony, compared to the low synchrony of the smaller, inhibitory population. The mean population firing rates are presented as mean ± SD.

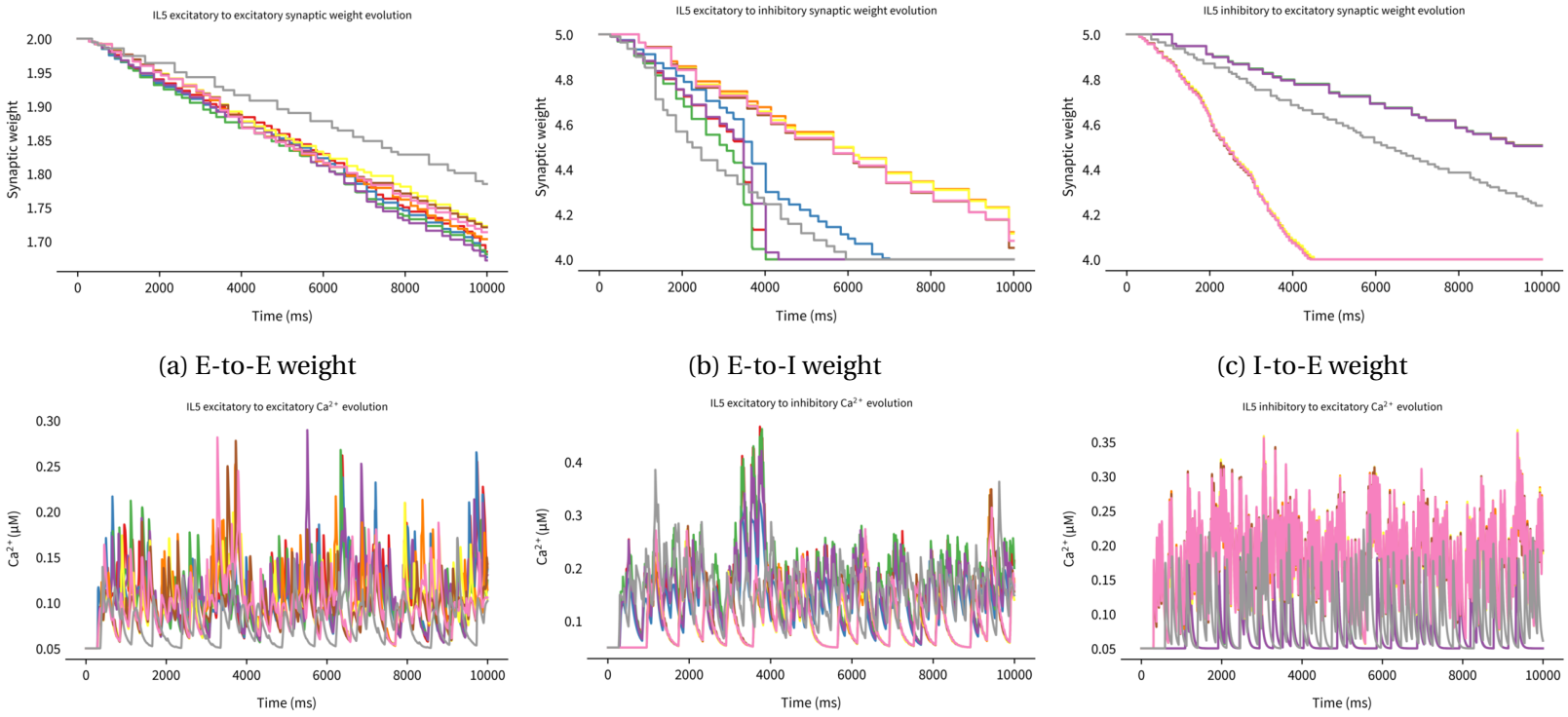

(a) E-to-E weight

(b) E-to-I weight

(c) I-to-E weight

(d) E-to-E Ca^{2+} evolution

(e) E-to-I Ca^{2+} evolution

(f) I-to-E Ca^{2+} evolution

Figure 25 – IL5 population synaptic dynamics. The population was modelled at 1:200 ratio with 200 regular excitatory and 50 inhibitory LTS neurons (Gabbott et al. 2005). All excitatory neurons projected to each other with a fanout of 4. A random 20% of excitatory neurons projected to inhibitory neurons with a fanout of 4. All of the inhibitory neurons projected to excitatory neurons with a fanout of 4. Excitatory units were driven by 480 Hz Poisson input and inhibitory units received 60 Hz Poisson input to recreate the excitatory unit firing rate seen biologically.

Deterministic BLA population

BLA is the key area for fear memory and extinction processing since it is the centre of CS-US association. CS and US inputs elicit synaptic plasticity within the area and lead to the formation BLA neuron sub-populations representing fear and extinction memory traces. In fear memory and extinction network models BLA neurons have to be classified into these sub-populations based on their activity following CS-US association and only then can they be connected to the rest of the network. Such approach was taken by both Pendyam et al. (2013) and Fenton (2015).

However, in this network BLA was modelled as a collection of three pyramidal cell populations representing fear, extinction and extinction-resistant memory traces. These three populations received adjustable Poisson inputs, seen in Figure 26, that would mimic the activity of their biological memory trace counterparts, respectively.

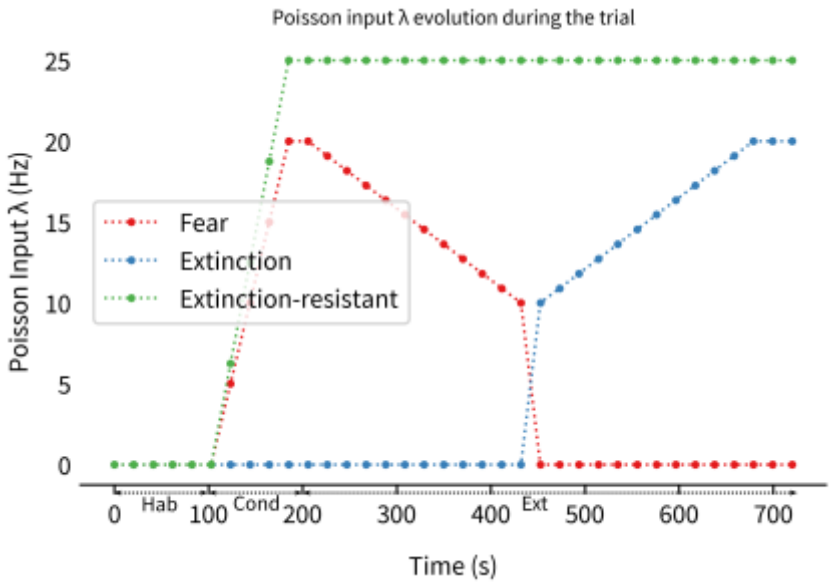

Figure 26 – Poisson inputs driving the three functionally different BLA populations. Inputs modelled BLA activity during habituation (Hab), conditioning (Cond) and extinction (Ext) which are indicated underneath the x-axis.

Strongly adapting cells were used in the three BLA functional populations, since amygdaloid pyramidal neuron biological activity closely resembles that of hippocampal pyramidal cells (Li et al. 2009). To recreate these three populations

Population	Regular	LTS	CA1 (strong)	CA1 (weak)
PL2	320	80	–	–
PL5	160	40	–	–
IL2	330	40	–	–
IL5	200	50	–	–
VH	–	110	270	270
fear	–	–	60	–
ext	–	–	50	–
ext-res	–	–	100	–

Table 5 – Types and numbers of units used in each population. All of the populations, excluding BLA (fear, ext, ext-res) were simulated at a 1:200 scale. The source for PL and IL population numbers and ratios was Gabbott et al. (2005) and used by both Pendyam et al. (2013) and Fenton (2015). VH (CA1) was made to be a minimal representation of the network only using two types of CA1 excitatory units and one type of inhibitory unit, LTS, similar to the hippocampal O-LM interneuron. BLA was not the focus of the study and, thus, represented by three separate strongly-adapting CA1 populations with the ratio of fear:ext:ext-res units corresponding to the ones reported by Herry et al. (2008).

Parameter	E-to-E	E-to-E (CA1)	E-to-I	I-to-E
a	17000	17000	17000	3000
θ_p	0.6	0.6	0.6	0.7
θ_d	0.5	0.5	0.5	0.55
λ_{rise} (Hz)	2	2	1	2
λ_{decay} (Hz)		0.001		
w_0	2	1	5	5
$w_{\min}$		$0.8 \times w_0$		
$w_{\max}$		$3 \times w_0$		
t_{delay} (ms)	6	6	4	4

Table 6 – Synaptic plasticity parameters for synapses within population.

Population	E-to-E	E-to-I	I-to-E
PL2	100% (4)	20% (4)	100% (4)
PL5	100% (4)	20% (4)	100% (4)
IL2	100% (4)	20% (4)	100% (4)
IL5	100% (4)	20% (4)	100% (4)
VH	100% (4)	20% (4)	100% (4)
BLA	0 (0)	0 (0)	0 (0)

Table 7 – Synaptic connectivity rates within each population. The number in parenthesis describes axonal arborizations, or the number of j units receiving an input from one i.

we varied the Poisson inputs, delivered at a constant $w = 5$, so as to obtain the population activity recorded *in vivo* by Herry et al. (2008) (see Figure 26). These three groups consisted of only non-interconnected strongly-adapting excitatory units and served as the main source of information about the fear memory paradigm to the rest of the network (see Tables 5 and 7).

Ventral Hippocampus CA1 population

The ventral hippocampus was modelled as a neuron network composed of two pyramidal cell types and one inhibitory cell type. The ventral hippocampus CA1 construction followed the methodology outlined by Pendyam et al. (2013). Since rats have 390 000 cells in the CA1 of the hippocampus, scaling the area at 1:200 ratio leaves 1950 cells (Rapp & Gallagher 1996). According to Strange et al. (2014), the hippocampus can be organised into dorsal, intermediate and ventral parts. Assuming that each part represents a third of the total CA1 cells, there are 650 ventral CA1 cells at 1:200 scale. However, in contrast to the cortical areas and the often reported 4-to-1 pyramidal cell to GABAergic interneuron ratio, this ratio in the hippocampal CA1 is higher in favour of excitatory cells (Bezaire & Soltesz 2013). Therefore, the ratio of excitatory:inhibitory cells was increased in favour of the excitatory units, resulting in 540 excitatory and 110 inhibitory units. Since LTS is known to be similar to the O-LM hippocampal interneuron, it was used as

the only inhibitory unit type in the area. It was assumed that there was a 1:1 ratio between strongly and weakly adapting CA1 units in the VH area of the model (see Table 5).

When it comes to population inner connectivity, identical connectivity to PL/IL areas was assumed, with all excitatory units projecting to four other excitatory units, a random 20% of excitatory units projecting to inhibitory units and all of the inhibitory units projecting to four excitatory units each (see Table 7). The only difference between the PL/IL and VH connectivity was that E-to-E intial synaptic weights were reduced in order to prevent constant oscillations at basal activity level and match the basal firing rate reported by Hirase et al. (2001) (see Table 6). Figures 27 and 28 show an individual simulation of VH population activity to visualize the neuronal and synaptic dynamics, resepctively.

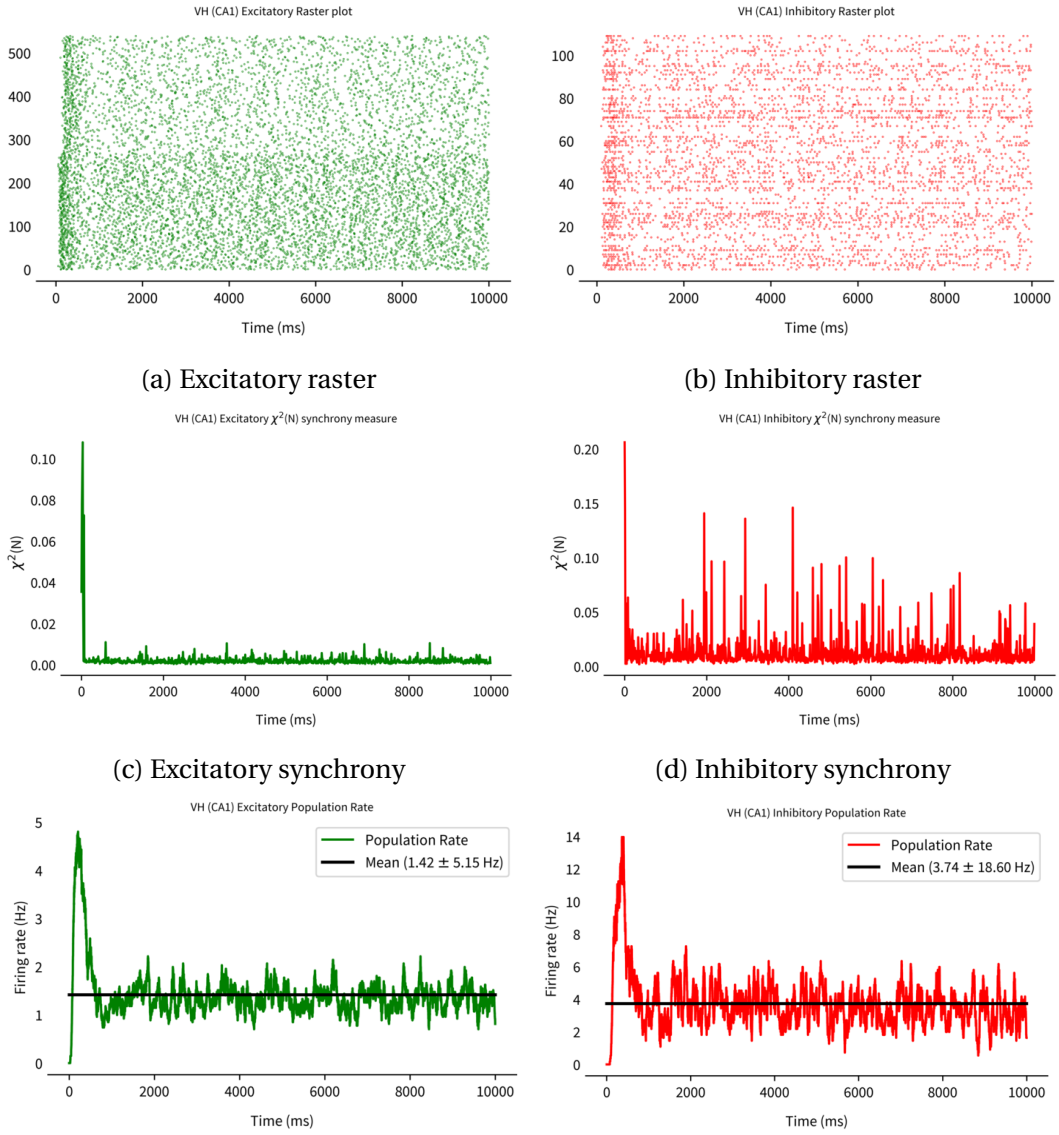

(a) Excitatory raster

(b) Inhibitory raster

(c) Excitatory synchrony

(d) Inhibitory synchrony

(e) Excitatory population rate

(f) Inhibitory population rate

Figure 27 – VH (CA1) population neuronal dynamics. The population was modelled at 1:200 scale (Rapp & Gallagher 1996). A total of 540 CA1 excitatory neurons, with 1:1 strongly- to weakly-adapting ratio, and 110 inhibitory LTS neurons were used. All excitatory neurons projected to each other with a fanout of 4. A random 20% of excitatory neurons projected to inhibitory neurons with a fanout of 4. All of the inhibitory neurons projected to excitatory neurons with a fanout of 4. CA1 neurons received a 10 Hz Poisson input, whereas LTS neurons received a 60 Hz Poisson input, so that CA1 basal activity resembled its biological counterpart seen in Hirase et al. (2001). The synchrony measure was calculated using the method outlined in Golomb (2007). The synchrony was inversely proportional to the population size, where the larger excitatory population had an extremely low synchrony, compared to the low synchrony of the smaller, inhibitory population. The mean population firing rates are presented as mean ± SD.

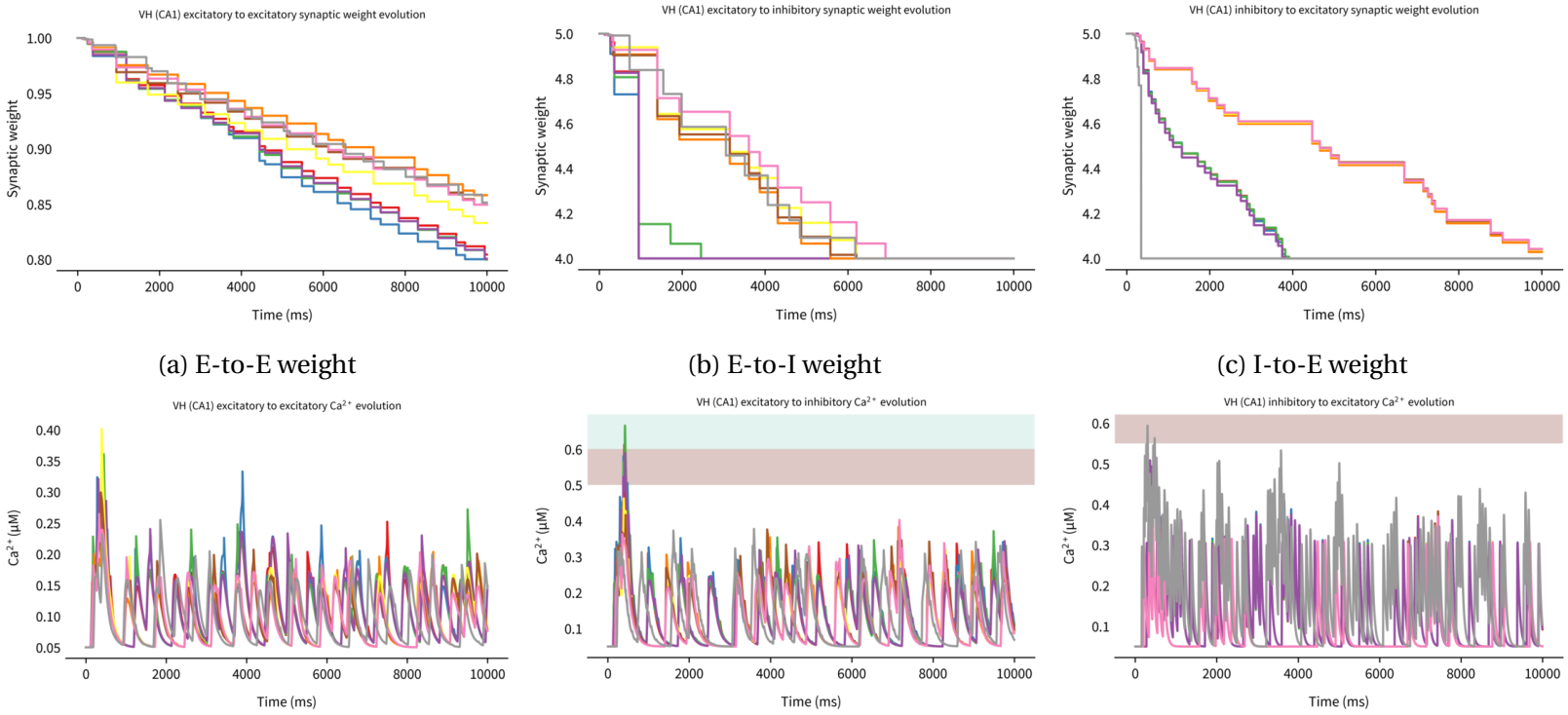

(a) E-to-E weight

(b) E-to-I weight

(c) I-to-E weight

(d) E-to-E Ca^{2+} evolution

(e) E-to-I Ca^{2+} evolution

(f) I-to-E Ca^{2+} evolution

Figure 28 – VH (CA1) population synaptic dynamics. The population was modelled at 1:200 scale (Rapp & Gallagher 1996). A total of 540 CA1 excitatory neurons, with 1:1 strongly- to weakly-adapting ratio, and 110 inhibitory LTS neurons were used. All excitatory neurons projected to each other with a fanout of 4. A random 20% of excitatory neurons projected to inhibitory neurons with a fanout of 4. All of the inhibitory neurons projected to excitatory neurons with a fanout of 4. CA1 neurons received a 10 Hz Poisson input, whereas LTS neurons received a 60 Hz Poisson input, so that CA1 basal activity resembled its biological counterpart seen in Hirase et al. (2001).

Poisson inputs to individual units

Since the populations in this model receive inputs from areas that are not considered in the model, we used Poisson inputs to represent those inputs. Each unit received its own Poisson input via a non-plastic synapse. The Poisson inputs were set so that the mean excitatory unit firing rate was similar to that seen physiologically (see Table 8). An exception was made for the three functionally distinct BLA unit populations, which received individual Poisson inputs that were adjusted in a deterministic fashion over the course of the simulation in order to resemble their biological counterpart activity during fear training and extinction paradigm reported by Herry et al. (2008) (see Figure 26). A summary of the Poisson inputs for each population can be found in Table 9.

Population	Type	Basal firing rate (Hz)	Reference
BLA	Excitatory	2-3	Herry et al. (2008)
PL	Excitatory	3	Burgos-Robles et al. (2009)
IL	Excitatory	4-5	Burgos-Robles et al. (2009)
VH (CA1)	Excitatory	1.5	Hirase et al. (2001)

Table 8 – Examples of basal firing rates of pyramidal (i.e. excitatory) cells seen physiologically for the different populations.

3.2.5 *Full Network of VH, PL, IL and deterministic BA*

Populations were connected in the following way: PL and IL areas followed the framework outlined by Fenton (2015). Specifically, between the layers 2 and 5 of PL there are stronger projections from 5 to 2 (Fujisawa et al. 2008, Pendyam et al. 2013). Therefore, connections between layers 5 and 2 in PL and IL were modelled unidirectionally as a random 10% of layer 5 units projecting to four layer 2 units each (Fujisawa et al. 2008, Pendyam et al. 2013).

PL layer 5 and IL layer 5 are known to be connected reciprocally, with PL layer 5 projecting to both excitatory and inhibitory subpopulations and stimulation

Population	Unit type	Poisson λ (population)	Poisson λ (full-network)
PL2	Regular	480	460
	LTS	60	60
PL5	Regular	480	440
	LTS	60	60
IL2	Regular	480	490
	LTS	60	60
IL5	Regular	480	470
	LTS	60	60
VH	CA1 (Strong)	10	10
	CA1 (Weak)	10	10
	LTS	60	60

Table 9 – Inputs to units in individual populations and the interconnected network.

of IL neurons inhibiting the pyramidal neurons in PL 5 (Vertes 2004, Hoover & Vertes 2007, Van Aerde et al. 2008, Ji & Neugebauer 2012, Fenton 2015). This reciprocal connectivity between PL 5 and IL5 was reconstructed with PL and IL layer 5 excitatory units projecting to both excitatory and inhibitory populations of their counterparts, with a random 10% of units in each population projecting to random four units in its counterpart (Fenton 2015).

Layer 2 pyramidal cells of PL and IL project to BLA, whereas layer 5 pyramidal neurons of IL and PL receive projections from BLA (Little & Carter 2013, Krettek & Price 1977, Orozco-Cabal et al. 2006). Similarly, hippocampal inputs show preference for layer 5 of PL and IL (Parent et al. 2009). Therefore, within PL and IL layer 5 received projections from VH and BLA, and layer 2 sent projections to BLA.

Projections from hippocampus show strong labelling within PL and IL (Hoover & Vertes 2007). Therefore, PL5 and IL5 excitatory units received a random 10% input from VH excitatory units each.

BLA neuron sub-populations representing fear, extinction and extinction resistant memory traces followed the connectivity levels based on the electrophysiological study done by Herry et al. (2008). Since Herry et al. (2008) did not

differentiate between PL and IL areas of mPFC, it was assumed that fear and extinction-resistant memory trace sub-populations would project to PL 5, since PL is responsible for fear expression. Similarly, extinction memory trace sub-population projected to IL 5, since IL is involved in extinction learning.

A random 63% of BLA fear memory trace neurons projected to a random PL5 excitatory unit each. These BLA fear neurons received inputs from a random 36% of VH excitatory units.

A random 50% of extinction units projected to IL5 excitatory units and received projections from 50% of IL2 excitatory units, the later being scaled down since the reported 77% input by Herry et al. (2008) would have been to large.

A random 50% of extinction-resistant units projected to PL 5 and VH excitatory units, and received inputs from 33% of PL2 as well as 40% of VH excitatory units. There was no relationship imposed between the extinction-resistant neurons projecting to PL 5 and VH (Herry et al. 2008, see Table 12).

Due to the differences in population sizes and reported projections weights between populations had to be adjusted accordingly. Generally, excitatory to excitatory (E-to-E) projections within IL and PL had an initial weight of 5.

Inputs arriving to the three BLA sub-populations had an initial weight of 1. Extinction to IL5 projections were initially weighted at 20, while fear-to-PL5 and extinction-resistant-to-PL5 projections started with initial weights of 4 and 1, respectively.

Projections arriving and leaving VH had an initial weight of 1. Excitatory to inhibitory projections between different areas were only used to connect PL5 and IL5. They were set to have an initial weight of 10. A summary of these weights and other synaptic parameters can be seen in Tables 10 and 11.

When interconnecting the different populations Poisson inputs were scaled to maintain the excitatory unit firing rates within range of the ones reported in biological studies (see Table 8 and 9).

Parameter	E-to-E	E-to-I
a	16000	
θ_p	0.45	
θ_d	0.35	
λ_{rise} (Hz)	15	
λ_{decay} (Hz)	0.001	
$w_{\min}$	$0.8 \times w_0$	
$w_{\max}$	$3 \times w_0$	
t_{delay} (ms)	20	30

Table 10 – Universal parameters for synaptic conductance between different populations. The w_0 for each type of synapse are defined in Tables 6 and 11.

Synapses	Type	w_0
Within mPFC	E-to-E	5
To BLA	E-to-E	1
Ext-to-IL5	E-to-E	20
Fear-to-PL5	E-to-E	4
Ext-res-to-PL5	E-to-E	1
VH (to/from)	E-to-E	1
E-to-I (PL5/IL5 only)	E-to-I	10

Table 11 – Initial weights for synapses between different populations.

Population	PL2	PL5	IL2	IL5	VH	Fear	Ext	Ext-Res
PL2 ⇒	•	–	–	–	–	–	33% (1)	–
PL5 ⇒	10% (4)	•	–	10% (4)$^{E/I}$	–	–	–	–
IL2 ⇒	–	–	•	–	–	–	50% (1)	–
IL5 ⇒	–	10% (4)$^{E/I}$	10% (4)	•	–	–	–	–
VH ⇒	–	10% (4)	–	10% (4)	•	36% (1)	–	40% (1)
Fear ⇒	–	63% (1)	–	–	–	–	–	–
Ext ⇒	–	–	–	50% (1)	–	–	–	–
Ext-Res ⇒	–	50% (1)	–	–	50% (1)	–	–	–

Table 12 – Synaptic connectivity rules for connecting individual populations. Bullets (•) represent intra-population connectivity, details of which are summarized in Table 7. Apart from PL5 and IL5 interconnection to both excitatory and inhibitory units, all other interpopulation projections were assumed to be excitatory-to-excitatory type.

3.2.6 *Simulation software*

The model was simulated using Python 2.7 with Brian2 spiking neuron modelling package (Stimberg et al. 2014). The simulation plots were generated using Matplotlib, NumPy and ColorBrewer packages.

3.2.7 *Experimental Protocol*

In total there were 24 sets of three identical simulations. Each set of three simulations were made identical by applying a seed to the pseudo-random number generator in Python. Out of the three identical simulations, the first was left intact, the second had PL-IL synapses disabled and the third had VH and all related synapses inactivated[2]. This was done to compare the activity of the intact model with VH inactivation and PL-IL disconnection.

3.2.8 *Statistical analysis*

All of the individual unit spike times were recorded in each population. Unit activity during 9–89 seconds of the simulation represented baseline or habituation activity, unit activity recorded during 209–289 seconds of the simulation represented high fear or early extinction stage activity and unit activity recorded during 589–669 seconds of the simulation represented the low fear or late extinction stage activity. These intervals were selected to correspond with the simulated BLA memory trace neuron activity reflecting the habituation stage, early and late parts of the extinction stage seen in Figure 26. The neurons were selected on the basis of input responsiveness. The network was driven by the three subpopulations of BLA, representing fear, extinction and extinction-resistant memory trace neuron populations, with each population having a specific activity pattern during habituation,

2 The disabling was done by passing a boolean value (’`False`’) to the relevant Brian2 synaptic and neuronal objects’ attribute "`object.active`". This would allow all of the units and synapses to be generated, but not integrate their equations, rendering them disabled. Please see section B.1.2 in the Appendix

conditioning and extinction (see Figure 26). Specifically, PL received direct input from the fear and extinction-resistant neurons, whereas IL received direct input from the extinction neurons of BLA (see Figure 12). Therefore, PL neurons were determined to be input responsive if their mean firing rate at early extinction was 2 × standard deviation (SD) higher than habituation, corresponding with its fear and extinction-resistant neuron input activity pattern in BLA. Conversely, IL neurons were determined to be input responsive if their mean firing rate at late extinction was 2 × SD higher than habituation, corresponding with the extinction neuron input activity pattern in BLA. Data processing was performed using Python 2.7 NumPy and Pandas packages. Statistical analysis and the graphical visualization of it was carried out using GraphPad Prism v7.0. Two-way repeated-measures ANOVA with Tukey's post hoc test were used for analysis. The results were visualized as mean ± standard error of the mean (SEM). The signficance level was set as 0.05. The differences between treatments at habituation, early and late extinction stages were quantified using percentage difference.

3.3 RESULTS

3.3.1 *Model activity*

Only PL neurons that were responsive to the input from the fear and extinction memory trace neurons of BLA, and only IL neurons that were responsive to the input from the extinction memory trace neurons of BLA were used for statistical analysis (see Section 3.2.8 for details). An identical number of responsive neurons within PL and IL were found in each matched set of three treatments for all 24 sets (i.e. a total of 72 simulations). In PL, an average of 114.9 ± 2.16 neurons, and in IL, an average of 131.1 ± 2.89 neurons were input responsive. This represented 23.94% of 480 total PL neurons and 24.91% of 530 total IL neurons, respectively. This is similar to the numbers of tone-responsive neurons reported in biological studies (Burgos-Robles et al. 2009, Mueller et al. 2010). The activity of the responsive neu-

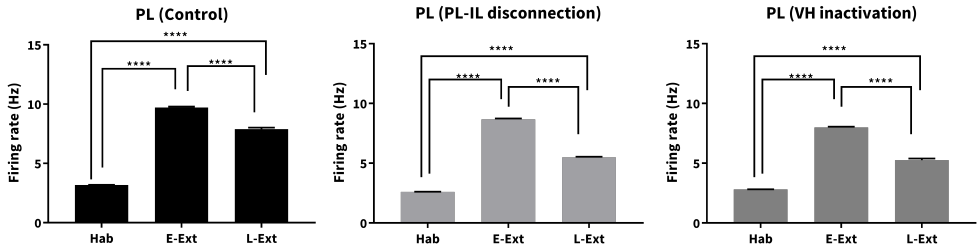

Figure 29 – The effects of stage on the mean PL firing rate in control, PL-IL disconnection and VH inactivation groups. All treatment groups showed a similar trend that was similar to the control group results. Specifically, the mean PL firing rate was low during habituation, increased during early extinction and decreased at late extinction, while staying higher than the habituation firing rate in all of the three treatment groups. Data is presented as mean ± SEM. Astersisks indicate the level of significance, with **** indicating p<0.0001.

rons of each simulation were averaged to represent mean firing rates of PL or IL at habituation, early extinction or late extinction for each treatment of each set.

PL firing rates

Two-way RM ANOVA of PL activity within control, PL-IL disconnection and VH inactivation groups showed that stage (i.e. Hab, E-Ext and L-Ext), treatment (i.e. control, PL-IL disconnection and VH inactivation) and stage × treatment interaction affected the mean PL firing rate ($F(2, 46) = 3697$, $p<0.0001$; $F(2,46) = 275.8$, $p<0.0001$ and $F(4,92) = 159.6$, $p<0.0001$, respectively).

All three treatment groups showed similar results in the Tukey's post hoc test of pairwise comparisons across the simulation stages. In all of the treatment groups PL mean firing rate during habituation was lower than early-extinction or late-extinction firing rate ($p<0.0001$ for all pairwise comparisons). PL had a higher mean firing rate at early-extinction compared to late-extinction in all treatment groups ($p<0.0001$ for all pairwise comparisons). Therefore, the different treatments spared the general PL activity trend during habituation, early and late extinction. These results are shown in Figure 29.

During habituation, both the PL-IL disconnection and the VH inactivation groups had lower mean PL firing rates than the control group (17.95% and 11.85%,

respectively; 2.61 ± 0.01 Hz, 2.81 ± 0.02 Hz and 3.18 ± 0.01 Hz, respectively; p<0.0001 for both comparisons). The VH inactivation group had a higher mean PL firing rate than the PL-IL disconnection group at this stage (7.43%, p=0.019). During early extinction, both the PL-IL disconnection and the VH inactivation groups had lower mean PL firing rates than the control group (10.8% and 17.75%, respectively; 8.67 ± 0.08 Hz, 8 ± 0.06 Hz and 9.72 ± 0.07 Hz, respectively; p<0.0001 for both comparisons). The VH inactivation group had a lower mean PL firing rate than the PL-IL disconnection group (7.78%, p<0.0001). During late extinction, both the PL-IL disconnection and the VH inactivation groups had lower mean PL firing rates than the control group (30.41% and 33.34%, respectively; 5.49 ± 0.05 Hz, 5.26 ± 0.13 Hz and 7.89 ± 0.13 Hz, respectively; p<0.0001 for both comparisons). The VH inactivation group had a lower mean PL firing rate than the PL-IL disconnection group (4.22%, p=0.004). These results are shown in Figure 31 (top).

Mean IL firing rates

Two-way RM ANOVA of IL activity within control, PL-IL disconnection and VH inactivation groups showed that stage, treatment and stage × treatment interaction affected the mean IL firing rate ($F(2,46) = 4585$, $p<0.0001$; $F(2,46) = 226.7$, $p<0.0001$ and $F(4,92) = 116$, $p<0.0001$, respectively).

All three treatment groups showed similar results in the Tukey's post hoc test of pairwise comparisons across the simulation stages. In all of the treatment groups IL mean firing rate during habituation was lower than early-extinction or late-extinction firing rate (p<0.0001 for all pairwise comparisons). Unlike the mean PL firing rate, IL had a lower mean firing rate at early-extinction compared to late-extinction in all treatment groups (p<0.0001 for all pairwise comparisons). Therefore, the different treatments spared the general IL activity trend during habituation, early and late extinction. These results are shown in Figure 30.

During habituation, the PL-IL disconnection group had a lower mean IL firing rate than the control group or the VH inactivation group (6.57% and 3.97%, respectively, 4.4 ± 0.01 Hz, 4.7 ± 0.02 Hz and 4.58 ± 0.01 Hz, respectively; p<0.0001 and p=0.0069, respectively). During early extinction, both the PL-IL disconnection

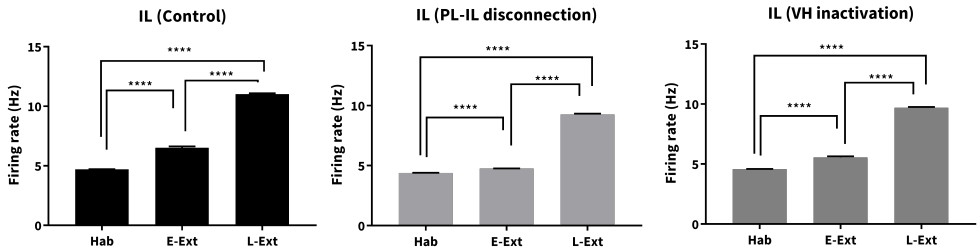

Figure 30 – The effects of stage on the mean IL firing rate in control, PL-IL disconnection and VH inactivation groups. All treatment groups showed a similar trend that was similar to the control group results. Specifically, the mean IL firing rate was low during habituation, it increased at early extinction and was the highest during late extinction in all of the treatment groups. Data is presented as mean ± SEM. Astersisks indicate the level of significance, with **** indicating p<0.0001.

and VH inactivation groups had lower mean IL firing rates than the control group (27.09% and 14.77%, respectively; 4.75 ± 0.02 Hz, 5.56 ± 0.09 Hz and 6.52 ± 0.12 Hz, respectively; p<0.0001 for both comparisons). The PL-IL disconnection group had a lower mean IL firing rate than the VH inactivation group (14.45%, p<0.0001). During late extinction, both the PL-IL disconnection and VH inactivation groups had lower mean IL firing rates than the control group (16.06% and 12.04%, respectively; 9.25 ± 0.08, 9.69 ± 0.07 and 11.02 ± 0.07, respectively; p<0.0001 for both comparisons). The PL-IL disconnection group had a lower mean IL firing rate than the VH inactivation group (4.58%, p<0.0001). The results are shown in Figure 31 (bottom).

3.3.2 *Comparison to previous models*

The model was compared to the Fenton (2015) HH and HH/IAF models. Comparisons between this and both Fenton (2015) models showed that this model had markedly higher PL and IL firing rates, particularly at early extinction and late extinction, regardless of the treatment (Figures 32 and 33).

Control group's mean PL firing rate in this model peaked at early extinction similar to the pattern in both Fenton (2015) models, but did not return to the habituation level at late extinction, whereas it returned to the habituation level

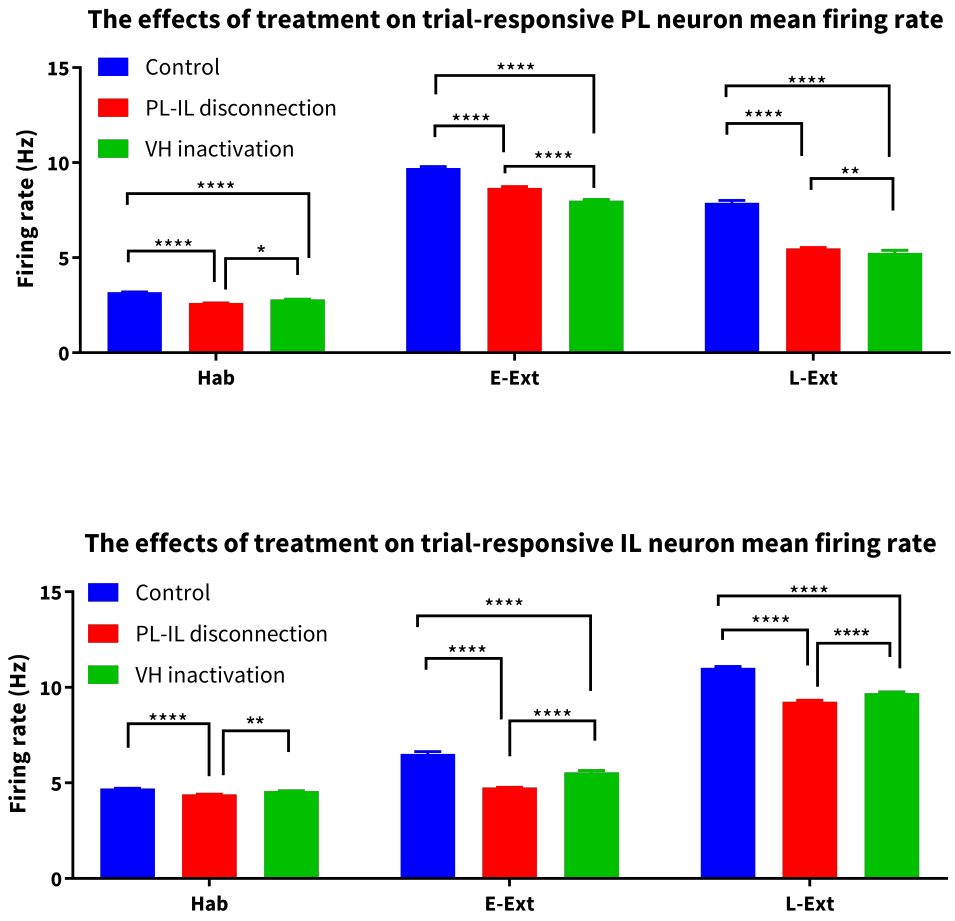

Figure 31 – Results of PL-IL disconnection and VH inactivation. PL-IL disconnection disrupts both PL (top) and IL (bottom) activity in the network, significantly reducing the firing rates in the areas associated with fear expression (PL) and fear extinction (IL). Conversely, VH inactivation disrupts the activity in PL to a larger extent than the previous treatment, while disrupting the activity in IL only during extinction and to a lesser extent than PL-IL disconnection. Data is presented as mean ± SEM. Astersisks indicate the level of significance, with * indicating $p<0.05$, ** indicating $p<0.01$ and **** indicating $p<0.0001$.

after peaking at early extinction in both Fenton (2015) models (Figure 32 (top row) and 33 (top row)). Therefore, the control group's mean PL firing rate pattern showed only partial (i.e. 2 out 3 stages) qualitative match to the Fenton (2015) models, with the mismatch being present at the late extinction stage.

Control group's mean IL firing rates increased from habituation to early to late extinction in this model, whereas Fenton (2015) HH/IAF model habituation and early extinction rates were not significantly different from each other, with only late extinction mean IL firing rate peaking in relation to the previous two stages (Figure 33 (second row)). Therefore, the control group's mean IL firing rate pattern showed a partial qualitative match to the Fenton (2015) HH/IAF model, with the mismatch being present at the early extinction stage.

Mean PL firing rate upon PL-IL disconnection peaked at early extinction, but did not return to the habituation level in this model and a similar pattern of change in the mean PL firing rate upon PL-IL disconnection was reported in both Fenton (2015) models (Figures 32 (middle row) and 33 (third row)). Therefore, the mean PL firing rate upon PL-IL disconnection in this model showed a complete qualitative match to the Fenton (2015) models.

Mean IL firing rate upon PL-IL disconnection increased from habituation to early to late extinction in this model, whereas in both Fenton (2015) models habituation and early extinction rates were not significantly different from each other, with only late extinction mean IL firing rate peaking in relation to the previous two stages (Figure 32 (bottom row) and 33 (bottom row)). Therefore, the PL-IL disconnection group's mean IL firing rate pattern showed a partial qualitative match to the Fenton (2015) models, with the mismatch being present at the early extinction stage.

3.3.3 *Comparison to the biological PL and IL activity*

Comparisons of control group's mean PL firing rates in this model to the PL activity in rodents reported by Burgos-Robles et al. (2009) revealed that this model had a markedly higher mean PL firing rates at early and late extinction compared

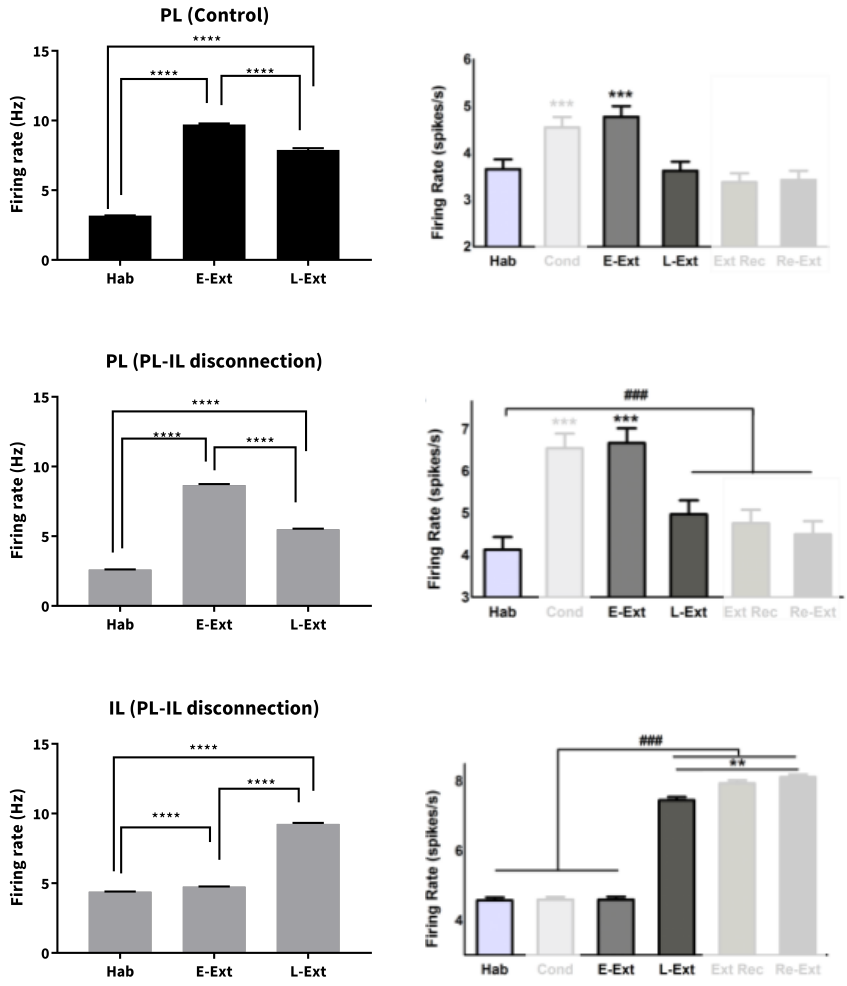

Figure 32 – Comparison between this IAF model (left column) and Fenton (2015) Hodgkin-Huxley model (right column). The left column panels were taken from Figure 29 (left) and Figure 30 (left and middle), respectively. The right column panels were adapted from Fenton (2015). Transparent stages in Fenton (2015) model on the right column were not assessed in the present model. Overall, the present model had markedly higher firing rates at early and late extinction compared to the Fenton (2015) HH model. There was a partial qualitative match of control PL activity between the two models, with only late extinction (L-Ext) being different (top row). A complete qualitative match was found between the models when it came to PL activity upon PL-IL disconnection (middle row). A partial qualitative match of IL activity upon PL-IL disconnection was found between the models, with only early extinction (E-Ext) being different (bottom row).

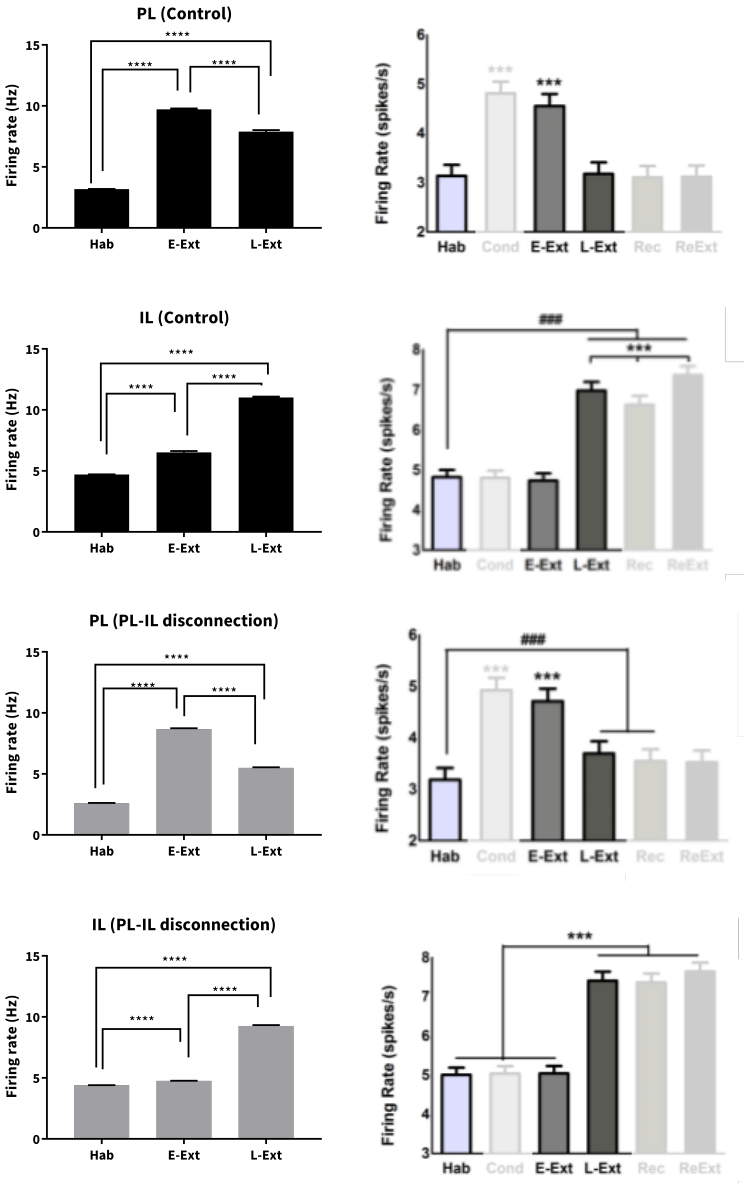

Figure 33 – Comparison between this IAF model (left column) and Fenton (2015) Hodgkin-Huxley/IAF hybrid model (right column). The left column panels were taken from Figure 29 (left and middle) and Figure 30 (left and middle), respectively. The right column panels were adapted from Fenton (2015). Transparent stages in Fenton (2015) model on the right column were not assessed in the present model. Overall, the present model had markedly higher firing rates at early and late extinction compared to the Fenton (2015) HH/IAF model. There was a partial qualitative match of control PL activity between the two models, with only late extinction (L-Ext) being different (top row). There was a partial qualitative match of control IL activity between the two models, with only early extinction (E-Ext) being different (second row). A complete qualitative match was found between the models when it came to PL activity upon PL-IL disconnection (third row). A partial qualitative match of IL activity upon PL-IL disconnection was found between the models, with only early extinction (E-Ext) being different (bottom row).

to the mean PL rates recorded in rats. The mean PL firing rate in this model peaked at early extinction similar to the pattern in the biological data, but did not return to baseline, whereas the mean PL firing rate returned to habituation level after peaking at early extinction in rats (Figure 34A and B). Therefore, this model had only a partial match to the biological PL data, with the mismatch being present at the late extinction stage. Interestingly, however, both Fenton (2015) models showed activity pattern than was very similar to the PL activity in rats, suggesting a complete qualitative match between these models and the biological PL activity (Figure 34, panels B, C and D).

The control group's mean IL firing rate in the model increased from habituation to early to late extinction, whereas in biological IL data the habituation and post-conditioning (i.e. early extinction) did not significantly differ from each other, with only post-extinction session 1 activity being markedly higher than the previous two stages. Therefore, this model had a partial qualitative match with the biological IL data, with the mismatch being present at the post-conditioning (i.e. early extinction) stage (See Figure 35 panels A and B). Interestingly, however, Fenton (2015) IAF/HH model mean IL firing rate was higher only at late extinction, compared to habituation or early extinction. This pattern of activity change matches the one reported by An et al. (2017), suggesting a complete qualitative match between the two models and the biological IL data (See Figure 35 panels B and C).

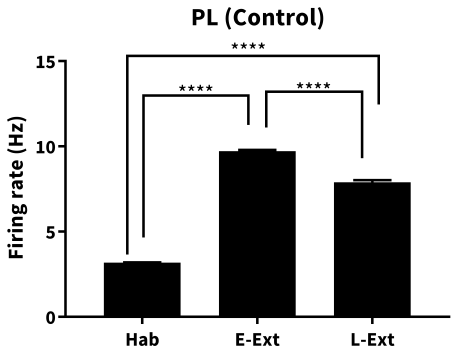

(a) PL activity in the model

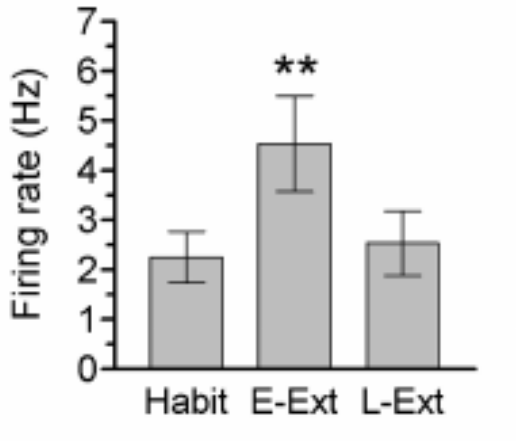

(b) PL activity in rodents

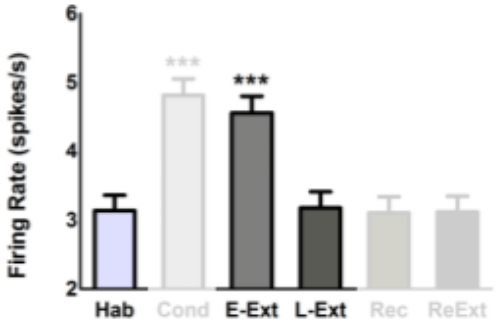

(c) PL activity in Fenton (2015) HH/IAF model

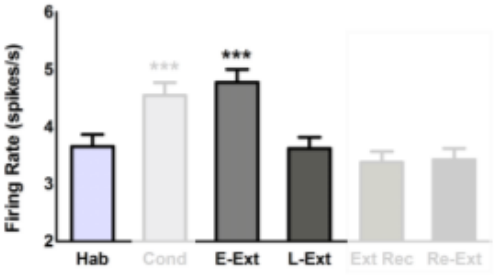

(d) PL activity in Fenton (2015) HH model

Figure 34 – Comparison of simulated PL activity in this model and Fenton (2015) HH and HH/IAF models, and biological PL activity in rats. Figure 34a was taken from Figure 29 (left), Figure 34b was adapted from Burgos-Robles et al. (2009), whereas Figures 34c and 34d were adapted from Fenton (2015). The firing rates in this model were markedly higher at early and late extinction compared to the biological data. There was a partial qualitative match between this model and the biological data, with only the late extinction stage being different (panels 34a and 34b). Conversely, both Fenton (2015) models showed a very similar pattern of activity to the biological data, suggesting a complete qualitative match (panels 34b, 34c and 34d).

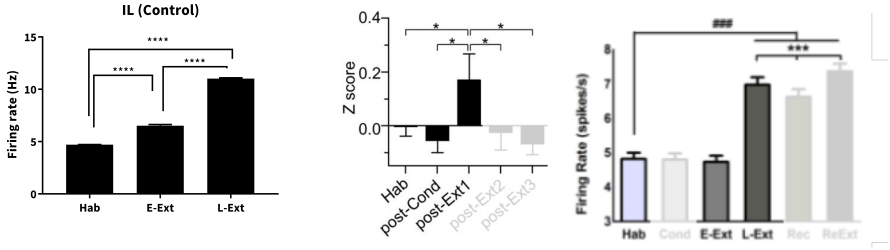

(a) IL activity in the model (b) IL activity in rodents (c) IL activity in Fenton (2015) HH/IAF model

Figure 35 – Comparison of simulated IL activity in this model, Fenton (2015) HH/IAF model and biological IL activity in rats. Figure 35a was taken from Figure 30 (left), Figure 35b was adapted from An et al. (2017) and Figure 35c was adapted from Fenton (2015). The early extinction stage in the models correspond to the post-conditioning stage in the rodent data. The late extinction stage in the models does not exactly map onto the post-extinction stage in the biological data, which is a continuation of the extinction on another day as opposed to the same day, but comparisons can be drawn due to the low reported freezing levels at the stage that resemble the levels that would expected during late extinction (An et al. 2017). There was a partial qualitative match between this model and the biological data, with only the post conditioning (i.e. early extinction) stage being different (panels 35a and 35b). Conversely, the activity pattern in Fenton (2015) HH/IAF model was very similar to the biological data, suggesting a complete qualitative match (panels 35b and 35c).

3.4 DISCUSSION

In this chapter, I present the first fear memory and extinction network of VH, PL and IL driven by fear, extinction and extinction-resistant memory trace BLA neurons that is composed solely of Izhikevich IAF units.

3.4.1 *Model verifies anxiolytic role of VH inactivation*

The experiment with 24 iterations of a control condition, PL-IL disconnection and VH inactivation has shown that disruption of PL and IL connectivity slows down the firing rate in both PL and IL during habituation as well as early and late extinction. Conversely, VH inactivation slows down the PL firing rate at only early and late extinction while reducing IL firing rate across all three stages. PL-IL disconnection reduced the mean PL firing rate at habituation to a larger extent than VH inactivation. However, VH inactivation reduced the mean PL firing rate to larger

extent than PL-IL disconnection at early and late extinction. PL-IL disconnection also reduced the mean IL firing rate at both early and late extinction to a larger extent than VH inactivation. A special case was observed when it came to mean IL firing rates during habituation, where PL-IL disconnection reduced the mean IL firing rate at habituation and this firing rate was reportedly lower than the VH inactivation group's firing rate. However, VH inactivation was not significantly different from the control group at this stage. Some of the aforementioned differences between the two treatment groups, however, were very small and biologically negligible (i.e. <5% difference). Specifically, the differences between the mean PL firing rates between the two groups at late extinction as well as the mean IL firing rate differences at habituation and late extinction. Despite these negligible differences between the two treatment groups, the results still show that VH inactivation suppressed PL, the area associated with fear expression, to a larger extent than PL-IL disconnection, whereas it suppressed the activity of IL, the area associated with fear extinction, to a lesser extent than PL-IL disconnection. This suggests that VH inactivation is a better target for anxiolysis than PL-IL disconnection.

The differences between treatments can be explained with the network architecture of this model. PL-IL disconnection removed the communication between a fraction of PL cells projecting to IL pyramidal and IL inhibitory cells respectively, and vice versa. Since this disconnection affects both PL and IL, it is not surprising to see effects on both PL and IL firing rates. On the other hand, VH inactivation removed the inputs of 540 pyramidal cells and 110 inhibitory cells to the rest of the model network. While VH has direct projections to both PL and IL, it also has indirect projections to PL via fear memory trace neurons and extinction-resistant memory trace neurons within BLA. Naturally, inactivation of VH resulted in removal of such inputs which, in turn, had a larger effect on PL as opposed to IL.

IL fires at higher frequency than PL, but the differences disappear once the areas are disconnected (Van Aerde et al. 2008). Moreover, optogenetic activation of IL causes PL pyramidal cell inhibition (Ji & Neugebauer 2012). PL-IL inactivation in this model did not produce effects consistent with biological data as this treatment reduced the activity of both PL and IL. Interestingly, however, excision of VH slowed

down the firing rate of PL, the area associated with fear expression, to a larger extent than IL.

This observation agrees with multiple pieces of biological evidence suggesting VH involvement in the maintenance of fear. Specifically, lesions to the ventral hippocampus reduce innate fear (McHugh et al. 2004). Lesions to VH also impair the acquisition of the conditioned emotional response to tone, or freezing, in rats (Maren & Holt 2004). This finding can be extended to both trace and contextual fear conditioning, both of which are impaired as a result of lesions to the area (Gilmartin et al. 2012). Sierra-Mercado et al. (2011) has shown that pharmacological inactivations of VH lead to impaired fear expression. This VH inactivation result is consistent with the anxiolytic role of VH inactivation seen biologically and confirms that the network model is sufficient to recreate this effect. In addition to this, the model result supports VH as a relevant target for anxiolysis.

3.4.2 *Comparison to previous models and implications*

The model showed markedly higher firing rates at early and late extinction stages compared to the Fenton (2015) models and the biological PL data. Apart from the complete qualitative match found between this model and Fenton (2015) models in PL activity upon PL-IL disconnection, all other comparisons resulted in partial qualitative matches with one of the three stages showing a mismatch. This mismatching stage was the late extinction stage of PL activity and the early extinction stage of IL activity. A similar pattern of partial qualitative matches was found between this model activity and the biological PL and IL data. Similarly to the comparisons to the previous models, the mismatching stage was the late extinction stage of PL activity and the post conditioning, or early extinction, stage of IL activity. Interestingly, both Fenton (2015) models showed a complete qualitative match to the biological PL data, whereas the Fenton (2015) HH/IAF model showed a complete qualitative match to the biological IL data. Therefore, both Fenton (2015) models matched the biological data better than this model. Since Fenton (2015) HH/IAF model was used as the basis for this model and the main differences

between it and this model are a new BLA and the inclusion of VH (CA1), it is natural to assume that parametric optimisation of these elements might yield a complete qualitative match between this model and the biological PL and IL data recorded in rats. A particular focus should be on the three populations of BLA since they are driving the network activity.

Another interesting outcome of the model is that the basolateral amygdala neuronal subpopulations representing fear, extinction and extinction-resistant memory traces, which are based on the experiments by Herry et al. (2008), are sufficient to represent the input from amygdala to the rest of the network. These basolateral amygdala subpopulations do not rely on CS and US association taking place, which has been relied on by other published models (Li et al. 2009, Vlachos et al. 2011, Pendyam et al. 2013, Fenton 2015). The use of memory trace subpopulations allows the shortening of simulation time without sacrificing the inputs to the rest of the network, thus simplifying the fear memory network building and simulation process.

3.4.3 *Limitations*

The model has several limitations. First of all, it did not reproduce PL-IL disconnection results consistent with biological experiments by Van Aerde et al. (2008) and Ji & Neugebauer (2012). This would require a detailed investigation into the projections between PL and IL experimentally before they can be recreated in the network model.

The second limitation is that, for the most part, the PL and IL firing rates show a partial qualitative match to other models and the biological data. In fact, both models by Fenton (2015) have a complete qualitative match to the biological PL activity, whereas Fenton (2015) HH/IAF model has a complete qualitative match to the biological IL activity. Therefore, Fenton (2015) models match the biological data better than this model. It is most likely due to the use of BLA subpopulations representing fear, extinction and extinction-resistant memory traces. In particular, the firing rate of PL neurons in this model does not return to the habituation level at

late extinction. This reduction of PL firing rates at late extinction to the habituation level is present in other models and the biological data (Fenton 2015, Burgos-Robles et al. 2009). Such lack of reduction could be explained by the extinction-resistant memory trace input from BLA being too strong. When it comes to IL firing rates in this model, they do not match the model data or the biological data. The firing rate of IL neurons at early extinction should be similar to or lower than the habituation firing rate, when compared to other models and biological data, respectively. This could be achieved with adjustments to IL driving input arriving from the extinction memory trace population of BLA. Lastly, the overall firing rates in the model are markedly higher than the ones seen biologically or in other models. Most of these shortcomings are expected to be resolved with parameter optimisation of the model. It should focus on BLA and its synaptic parameters governing the strength of input to the rest of the network.

Last but not least, due to the usage of IAF neurons the model cannot be said to be biophysical. While this is not a key issue in fear memory and extinction networks, the use of such approaches when including the pharmacological interventions relying on current dynamics should be carefully considered.

3.4.4 *Future directions*

Compared to previous spiking neuron models, this model is better suited for expansion that would encompass the full fear memory neurocircuitry without a large computational cost. In fact, the model presented here covers only a fraction of the areas involved in fear memory neurocircuitry. An experimentally-based schematic diagram of this neurocircuitry has been designed by Calhoon & Tye (2015) which can be seen in Figure 36.

Overall, the model presented here generated results of VH inactivation that are consistent with biological data, while being computationally cheaper than previous models and using a novel representation of the basolateral amygdala. Therefore, it presents an excellent starting point for larger scale computational fear memory network investigations.

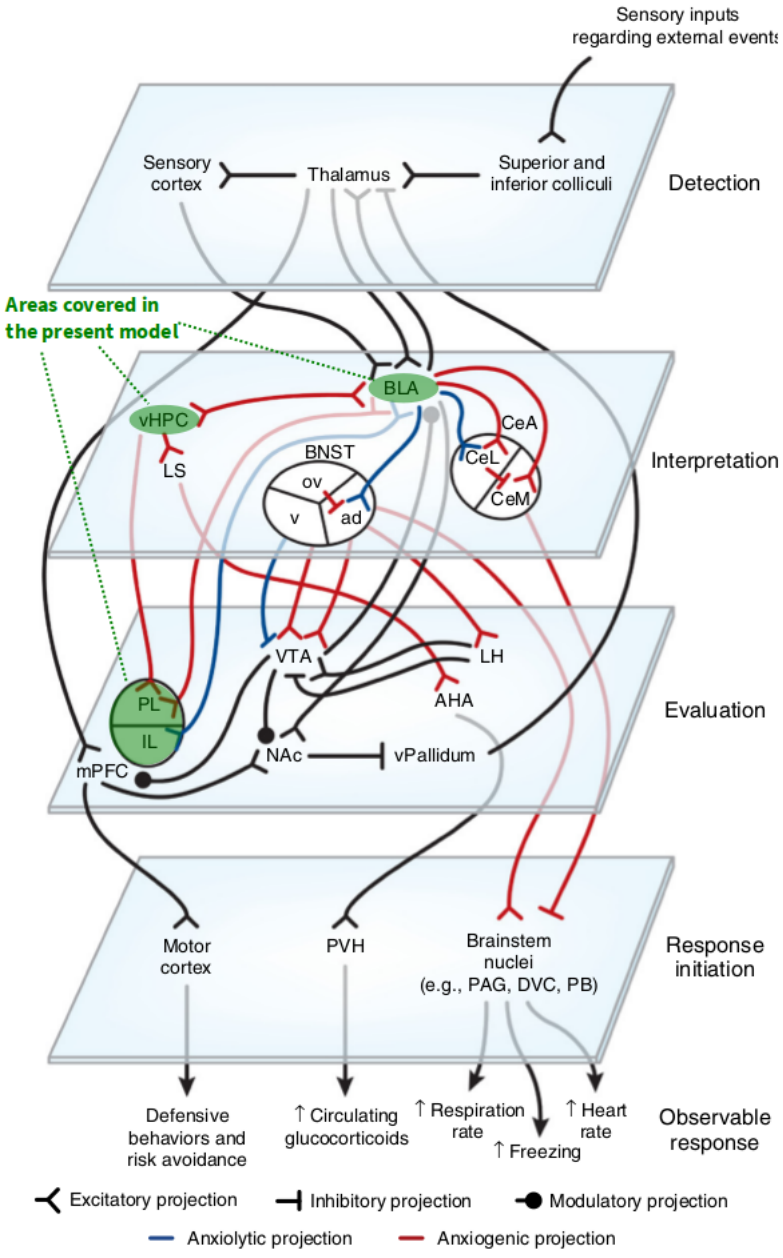

Figure 36 – A schematic diagram of the brain areas involved in fear memory processing based on experimental data. Adapted from Calhoon & Tye (2015).

4

ELECTROPHYSIOLOGICAL INSIGHTS INTO MPFC-VH CIRCUIT FUNCTION DURING LEARNED FEAR EXPRESSION AND EXTINCTION

4.1 INTRODUCTION

The modelling experiment covered in Chapter 3 presented results that are consistent with the anxiolytic role of VH inactivation seen in biology. VH inactivation reduced the PL activity to a larger extent and IL activity to a lesser extent than PL-IL disconnection. These computational model findings highlight the importance of the interaction between the three areas. The inactivation of VH and PL-IL disconnection were performed at the beginning of the simulation in the model. It would be interesting to focus on the activity of these three areas at different stages of auditory fear memory and extinction paradigm to test the temporal features of VH, PL and IL interaction.

PL, IL and VH are involved in various stages of fear conditioning and extinction. IL projects to ITC in the amygdala, which is the locus of extinction plasticity, that, in turn, inhibits the central nucleus of the amygdala and prevents fear expression (Royer & Pare 2002, Quirk et al. 2003). Lesions to ITC impair the expression of extinction and ITC neurons are highly responsive to IL inputs (Likhtik et al. 2008, Amir et al. 2011). Lesions or pharmacological inactivations of IL result in impaired auditory fear retrieval (Quirk et al. 2000, Sierra-Mercado et al. 2011, Santini et al. 2012). Stimulation of IL during the presentation of CS facilitates extinction (Milad et al. 2004, Vidal-Gonzalez et al. 2006, Kim et al. 2010). Electrophysiological and

immunocytochemical data correlates IL activity with extinction retrieval (Milad & Quirk 2002, Holmes et al. 2012, Knapska et al. 2012). However, two recent studies targeting extinction retrieval revealed that silencing IL or electrically stimulating it had no effect on the stage (Do-Monte et al. 2015, Bukalo et al. 2015).

PL plays an opposite role to IL. It projects to LA and indirectly facilitates the output of CeA (Vertes 2004, VanElzakker et al. 2014). It is known to facilitate fear expression, with increased stimulation resulting in increased defensive response (Vidal-Gonzalez et al. 2006, Sierra-Mercado et al. 2011).

The ventral hippocampus, on the other hand, is involved in both fear expression and extinction as pharmacological inactivation of VH impaired both processes (Sierra-Mercado et al. 2011). In addition to this, VH inactivations or lesions lead to impaired auditory fear expression (Maren & Holt 2004, Hunsaker & Kesner 2008). Hippocampal activity is physiologically defined by the presence of synchronous theta oscillations (Buzsáki & Draguhn 2004). Disruption of the hippocampal theta oscillations is an accurate predictor of an anxiolytic effect (Yeung et al. 2012). Ventral hippocampus-led theta synchrony with mPFC predicts anxiety-like behaviour (Adhikari et al. 2010, Padilla-Coreano et al. 2016). Disruptions of this synchrony results in anxiolytic effect (Schoenfeld et al. 2014). IL-LA-DH theta synchrony is involved in fear expression and is disrupted during fear extinction learning, which is replaced by LA-IL and DH-IL synchrony during extinction recall with theta dominance shifting from the hippocampus to IL at this later stage (Lesting et al. 2011, 2013). Fenton et al. (2014a) revealed an opposing high PL and high IL theta activity, during high fear and low fear stages of auditory fear memory, respectively, in addition with low synchrony between the two areas. However, it is not clear if VH theta activity and its interaction with PL or IL is involved in these high and low fear stages. Specifically, VH, PL and IL theta band activity and interaction differences between fear recall and extinction recall have not been addressed.

Prefrontal cortex and ventral hippocampal low gamma oscillations play a role in fear memory too. Hippocampal gamma oscillations are interneuron-dependent and direct its output to other areas (Buzsáki 2001, Gloveli et al. 2005, Hájos & Paulsen 2009, Montgomery & Buzsáki 2007, Buzsáki & Wang 2012). The inhibitory

neurons involved in these oscillations can prevent pyramidal cell firing and contribute to the synchrony in the area (Cobb et al. 1995, Miles et al. 1996, Freund & Buzsáki 1996). Interestingly, fear conditioning and its recall reduce gamma oscillations in the ventral hippocampus of rodent brain slices (Albrecht et al. 2013). However, there is a lack of data on VH low gamma activity at fear recall in awake-behaving animals.

Increased power of low gamma oscillations in PL are seen in fear extinction deficits (Fitzgerald et al. 2014b). In contrast to this, increased gamma oscillations in human homologue of IL signal fear extinction recall, and baseline level oscillations indicate recall failure (Mueller et al. 2010). A study by Fenton et al. (2016) showed reduced PL gamma oscillations during extinction and its recall, while IL had increased gamma oscillations during extinction recall. However, it is not clear if VH interacts with PL and IL at low gamma band at these stages. In fact, VH, PL and IL gamma band activity and interaction differences between fear recall and extinction recall have not been addressed.

PL is involved in fear expression, IL is involved in extinction learning and VH is involved in both processes. While electrophysiological studies suggest the involvement of PL, IL and hippocampus theta band oscillations in fear memory, there are no studies addressing VH theta band activity and its interaction with PL and IL at fear recall and extinction recall stages.

In this study we use local-field potential recordings from PL, IL and VH (CA1) of awake behaving animals in auditory fear memory and extinction paradigm to investigate the VH-IL, VH-PL and PL-IL neural activity interactions during the fear recall and extinction recall stages. We propose that fear recall stage should coincide with high theta synchrony between VH and PL, whereas extinction recall stage should coincide with VH and IL theta synchrony. When it comes to low gamma frequency band oscillation activity, there should be decreased PL and increased IL gamma oscillation power during extinction recall.

4.2 MATERIALS & METHODS

4.2.1 *Animals*

All the animals used in the experiments were adult male Lister-Hooded rats (Charles River, UK) weighing 280-400g at the time of surgery. The rats were housed in groups of 4, singly housed during initial recovery after surgery for 3 days and group housed (up to 4) to recover for 7-10 days prior to the start of the experiments with food and water provided ad libitum. All of the experiments were performed during the light cycle. All of the procedures strictly adhered to the guidelines set out by the Animals (Scientific Procedures) Act, 1986 and the University of Nottingham Animal Welfare and Ethical Review Board.

4.2.2 *Drugs*

The anaesthetic used in the surgeries was isoflurane (Merial Animal Health Ltd., UK). Pre- and post- surgical analgesia was ensured by administering buprenorphine (Vetergesic®; Champion Alstoe Animal Health / Santé Animale Inc., Canada) and meloxicam (Metacam®; Boehringer Ingelheim Vetmedica GmbH, Germany). After the surgery the incision site was treated with local anaesthetic solution – lignocaine with adrenaline (as required; Lignol® - 2% w/v lignocaine, 0.001% w/v adrenaline; Dechra Pharmaceuticals PLC, UK). Buprenorphine and meloxicam administration continued for 2 days after the surgery. Thirty minutes before extinction all of the animals were administered with a 2% Tween 80 in sterile saline solution (i.p.). This was done as the experiment was initially planned to test the effects of cannabidiol on extinction. Since cannabidiol only reduced initial fear expression without affecting extinction the effects of CBD on auditory fear memory and extinction were not tested. At the end of the experiments, the animals were deeply anaesthetised with pentobarbital overdose prior to transcardiac perfusions (Dolethal®, Vetoquinol UK Ltd., UK).

4.2.3 *Electrode implantation surgeries*

Anaesthesia was induced with isolfurane (3.5%, v/v, in O_2) and maintained throughout the surgery (1-2%, v/v, in O_2) ensuring that no hind paw withdrawal reflex was present whilst accounting for the respiratory depressant effect of buprenorphine. The animal was placed into a stereotaxic frame (World Precision Instruments, UK) so that the top of the skull was completely horizontal. Body temperature was maintained by a homeothermic heating blanket (Harvard Apparatus Ltd., UK). The incision area was cleaned with a 4% chlorhexidine antiseptic solution and a single incision along the sagittal suture was made. Five titanium screws were inserted into the skull to allow the fixation of electrodes to the skull with dental cement while also serving as anchor points for the electrode grounding wires. The two microelectrode arrays (NB Labs, USA), consisted of eight 50 µm diameter Teflon-coated stainless steel wires each. The mPFC electrodes had four electrode wires that were 1 mm longer than the remaining four to target both IL and PL, respectively. The electrodes were slowly lowered into the brain using the following coordinates:

Bregma	Brain area		
	PL	IL	VH (CA1)
Anterior-posterior axis	2.7	2.7	-5.2
Medial-lateral axis	-0.3 to -0.5	-0.3 to -0.5	4.8
Dorso-ventral axis	-3.1 to -3.3	-4.1 to -4.3	-6.3 to -6.5

Table 13 – The stereotaxic coordinates of the three brain areas targeted for electrode implantation. The coordinates were taken from Paxinos & Watson (1998).

The electrode arrays and the grounding wires were secured to the screws in the animal's skull with an acrylic resin-based dental cement (Simplex Rapid; Associated Dental Products Ltd., UK). The animals were kept in a recovery chamber for 1-2 hours until the anaesthesia subsided, singly housed during the initial 3 day recovery period and group housed until any behavioural testing was to take place.

4.2.4 *Auditory fear conditioning and extinction experiments*

Auditory fear conditioning experiments employed two contexts to differentiate conditioning (Context A) and extinction as well as its recall sessions (Context B; Table 14). On the first day animals were habituated to both contexts for 10 minutes each. The next day the rats were placed in their respective fear contexts (Context A) and presented with 5 auditory tones (CS; 4 kHz, 30 second, 80 dB) followed by 5 CS that co-terminated with a foot-shock (US; 1 sec, 0.5 mA) with 2 minute inter-trial interval (ITI) between the presentation of CS-US pairing. The duration of the shock was double the one used for psychopharmacology experiments due to the rats having electrode implants, in order to prevent behavioural deficits induced by the surgery (Hart et al. 2009). On the third day animals underwent partial extinction training (Context B) where 15 CS (1 min ITI) were presented. On the fourth and final day the animals underwent a brief extinction recall (Context B, 2 CS, 1 min ITI). This was done since the study intended to look at the effects of CBD on auditory fear conditioning and extinction and not fully extinguish fear so that both extinction facilitating and extinction impairing effects could be detected. Each stage of experiment started with a two minute period prior to the first CS presentation during which animals were allowed to acclimate to the arena.

	Context A	Context B
Light	On	On
Arena (visual cue)	Either spots or stripes	Opposite to Context A
Floor	Metal bars	Perspex floor
Cleaning solution	40% ethanol	40% methanol
Olfactory cue	40% ethanol	40% methanol

Table 14 – The comparison of the differences between the contexts A and B used in auditory fear conditioning experiments. The contexts differ in visual cues by having each of the arenas for the same animal associated with the each of the contexts, tactile cues by changes in the floor and differences in odour.

4.2.5 *Electrophysiology recording*

The electrode arrays were connected to an analog multichannel headstages (Analog 0.050" Pitch Headstages for HIGH Impedance Electrodes; Plexon Inc., USA) attached to a preamplifier (PBX; Plexon Inc., USA). The signal from the preamplifier was fed into a PC and captured using Plexon Recorder/16 software (Plexon Inc., USA). The kit was set up to record a TTL pulse at the start of each tone during auditory fear conditioning experiments. Local-field potentials (LFPs) were filtered with a 2000x gain, 250 Hz low-pass filter threshold and 1.25 kHz sampling rate.

4.2.6 *Histology*

Animals were deeply anaesthetised with pentobarbital and had a DC current passed between electrodes within each of the three electrode placements to deposit iron into each of the recording sites. The rats were transcardially perfused with 0.9% w/v saline followed by a solution of 4% w/v paraformaldehyde and 4% w/v potassium ferrocyanide in PBS. The potassium ferrocyanide reacts with the electrolytically deposited iron salts from the electrodes to result in Prussian Blue staining of the recording sites. The extracted brains were sliced into 100 micron slices until the staining could be seen and stored in a 4% w/v paraformaldehyde solution. The slices that had the staining were imaged under a microscope (see Figures 37a and 37b). This was followed by the visual evaluation of the staining mark location indicating electrode placements. The anterior-posterior coordinate of each stained slice image was identified by comparing its anatomical features with schematic diagrams in a rat brain atlas (Paxinos & Watson 1998). The slices containing staining marks within the medial prefrontal cortex were matched to their corresponding diagrams in the rat brain atlas. This was done to ensure that the staining marks were within the boundaries of PL and IL, respectively. Similarly, the slices containing staining marks within the ventral hippocampus were matched

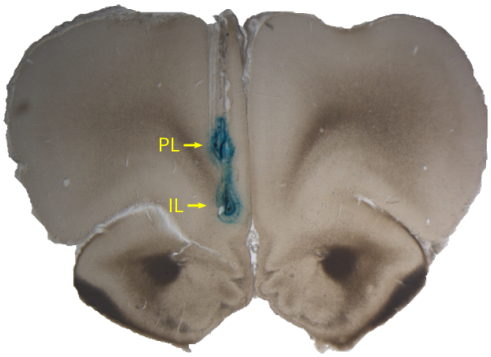

(a) Example of mPFC histology

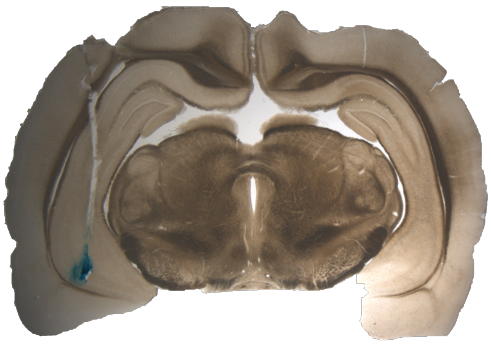

(b) Example of VH (CA1) histology

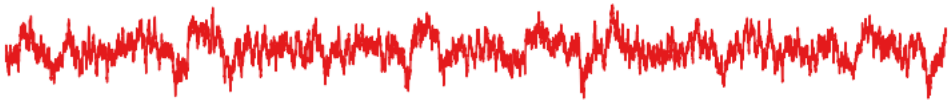

(c) Typical PL recording trace

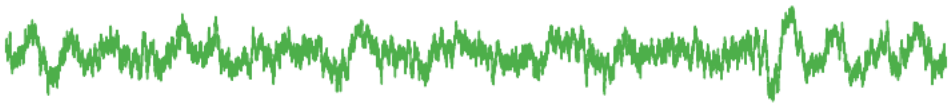

(d) Typical IL recording trace

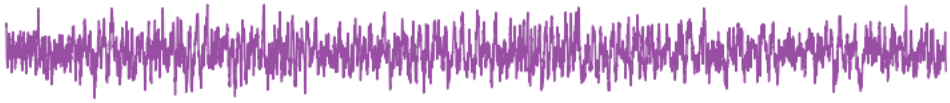

(e) Typical VH (CA1) recording trace

Figure 37 – Typical mPFC and VH histology and recording traces.

to their corresponding diagrams in the rat brain atlas to ensure that the staining marks were within the ventral hippocampal CA1 area.

4.2.7 *Behavioural data collection and scoring*

Behavioural data was recorded by a camera mounted on the ceiling of the arena by the computer running Med Associates software controlling tone and shock presentations. The videos were scored by subdividing each tone into ten 3 second blocks and evaluating freezing during each of these blocks. The result was then transformed into the percentage of time spent freezing per each tone (Stevenson et al. 2009). All of the data sets were checked for adherence to normal

distribution with D'Agostino Pearson test (alpha = 0.05; GraphPad Prism v7). The p = 0.05 was set as a threshold for statistical significance.

4.2.8 *Statistical analysis*

The variances of means between the different groups of conditioning and partial extinction data sets were not identical, so sphericity of the data sets could not be assumed. Therefore, one-way RM ANOVA with Geisser-Greenhouse's correction was used to test the effect of conditioning and extinction stages on freezing behaviour. Paired t-test was used to compare the first block of partial extinction to extinction recall. Subject matching in the paired t-test was assessed using Pearson correlation coefficient (one-tailed), this was done using F-test in one-way RM ANOVA. The data was analysed using GraphPad Prism v7 statistical analysis software. The results were graphed using Python (v2.7), NumPy, Pandas and Matplotlib packages. The asterisk showing the outcome of the paired t-test was added onto the figure using InkScape v0.92 vector graphics editor.

4.2.9 *Electrophysiology analysis*

The recorded LFP traces were extracted as timeseries into MatLab data format using NeuroExplorer software (Plexon, Inc). The timeseries data for each CS was extracted based on the corresponding TTL pulse time captured during the experiment. The CS timeseries data were filtered using 4 Hz high-pass Butterworth filter with default parameters of `elephant.signal.butter`[1] function from the Python 2.7 Elephant package. Each CS of each channel and animal for the Fear Recall and Extinction Recall timeseries data was plotted using Python 2.7, NumPy, SciPy, Matplotlib packages. Noisy or artefact-containing CS recordings were discarded. If there was more than one channel available after this pre-processing, they were selected randomly using `numpy.random.choice`[2] function so that only

1 Please see section B.2.1 in the Appendix for details
2 Please see section B.2.2 in the Appendix for details

one channel per area of a single animal would remain. The channel for Fear Recall and Extinction Recall for each area was kept the same. The data were then analysed for power spectra and coherence, a measure of synchrony, using NeuroSpec2 MatLab package (www.neurospec.org). The CS timeseries for the respective stages were spliced together into a single timeseries per animal in order to increase the accuracy of the spectra estimate. This timeseries was processed using Type 1 analysis (multiple CS per timeseries) with segment power of 10 to convert the data from time domain to frequency domain. The spectra were pooled together using NeuroSpec2 pooling routine. Comparisons of two pooled spectra were performed using Log Ratio test with 99% Confidence Interval. Similarly, comparisons of two pooled coherence measures were performed using a NeuroSpec coherence comparison test (i.e. difference of coherence) with 99% Confidence Interval. This was done to correct for the multiple comparisons in the analysis (Fenton et al. 2014b). The statistical significance threshold for the log ratio of spectra power and the difference of coherence was set to p = 0.01.

4.3 RESULTS

4.3.1 *Histology*

Only the animals with anatomically verified placements in PL, IL and VH were used for behaviour and electrophysiology analysis. A total of 10 animals satisfied these criteria. The diagram depicting these placements can be seen in Figure 38.

4.3.2 *Behaviour*

Conditioning

One-way RM ANOVA with Geisser-Greenhouse correction revealed no significant differences due to CS-US pairing on the mean freezing level ($F(2.748, 24.73) =$

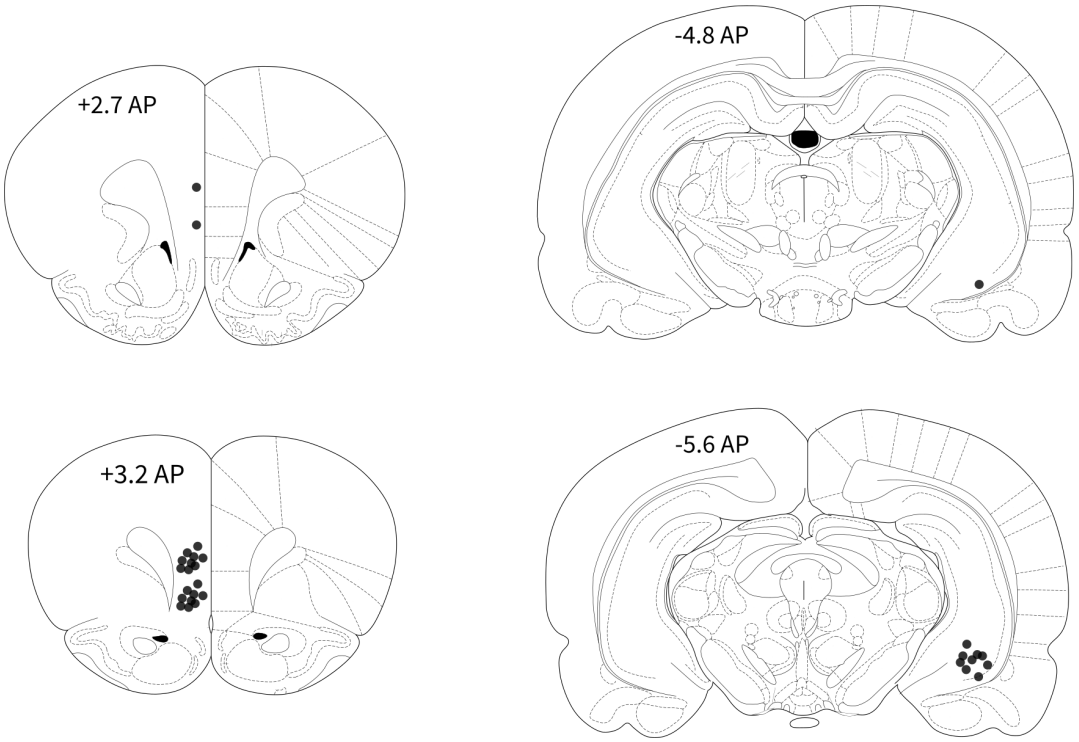

Figure 38 – The diagram depicting the electrode placements verified during histology. AP values indicate a positive or negative distance from Bregma in mm on the anterior-posterior axis. Adapted from Paxinos & Watson (1998).

1.712, p = 0.19, Geisser-Greenhouse epsilon = 0.69, R^2 = 0.16). Subject matching was effective (F(9, 36) = 3.227, p = 0.0057, R^2 = 0.40). Nevertheless, the fear training was successful since the animals expressed learned fear at the start of extinction (see Figure 39).

Partial Extinction

One-way RM ANOVA with Geisser-Greenhouse correction revealed no significant differences in the mean freezing level due to the block of extinction (F(2.206, 19.85) = 1.133, p = 0.35, Geisser-Greenhouse's epsilon = 0.55, R^2 = 0.11). The matching, on the other hand, was effective (F(9, 36) = 5.931, p < 0.0001, R^2 = 0.57). It is very likely that the 15 CS tones used for the partial extinction were too few to result in a sufficient decrease in freezing (see Figure 39).

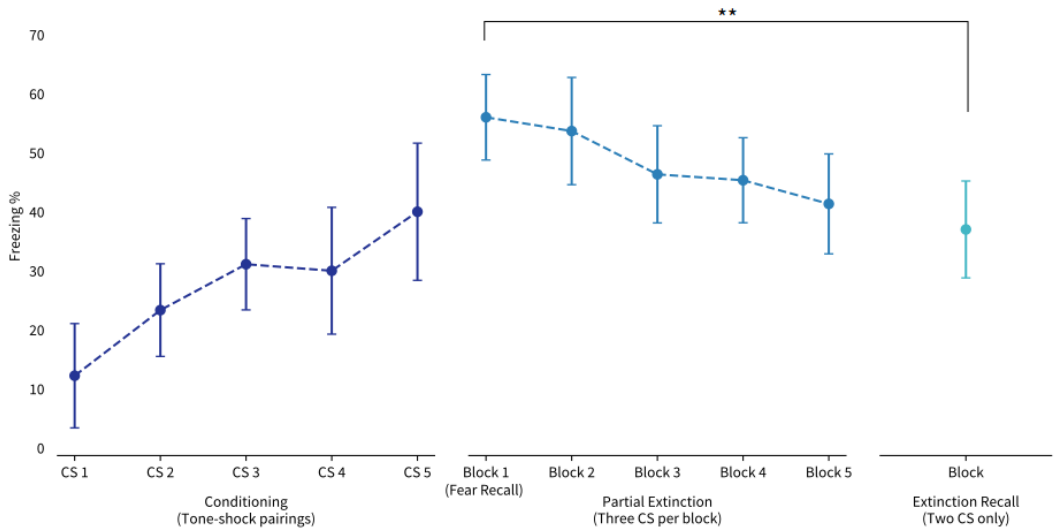

Figure 39 – The behavioural effects of fear conditioning paradigm. There was a significant difference between the the first block of extinction, a measure of fear recall, and extinction recall. Data presented as mean ± SEM. Asterisks indicate the significance level, with ** representing $p<0.01$.

Fear recall versus extinction recall

To detect the differences in freezing behaviour we compared the first block of three tones from extinction, a measure of fear memory recall, against a block of two tones from extinction recall. Paired t-test revealed a significantly reduced freezing level during extinction recall as opposed to fear recall ($t = 3.633$, $df = 9$, $p = 0.0055$, see Figure 39). The pairing of the two data sets was effective (Corr. coefficient (r) = 0.78, $p = 0.004$). This finding shows that even with a low sample size we were able to detect the differences between fear and extinction recall.

4.3.3 *Electrophysiology*

The LFP spectra and coherence estimates in theta frequency band (4 – 12 Hz) including statistical comparisons can be found in Figures 40 and 41. The same estimates in low gamma frequency band (30 – 45 Hz) are presented in Figures 42 and 43.

Spectra power and coherence in the theta frequency band

The ventral hippocampus had about an order of magnitude higher theta band power than either PL or IL at both fear recall and extinction recall stages (Figure 40 top row). At extinction recall VH showed a decrease in theta power at 4 – 7 and 11 – 12 Hz. PL showed a decrease at 4 – 6 Hz theta power and an increase at 7.5 Hz theta power. IL showed a decrease in theta power at 4 – 6.5 Hz and 9.5 – 11.5 Hz ($p<0.01$ for all three areas, Figure 40 bottom row).

Theta band coherence, a measure of synchrony, between VH-PL, VH-IL and PL-IL area pairs was very low (Coherence < 0.10; Figure 41 top row). Since the synchrony between the three pairs of areas was very low, volume conduction of theta oscillations between the three area pairs was negligible. There was a very small increase at 8.5 Hz in VH-PL theta frequency band coherence at extinction recall ($p<0.01$, Figure 41 bottom left). There were no significant changes in VH-IL coherence between extinction recall and fear recall ($p>0.01$, Figure 41 bottom row, middle). PL-IL coherence, on the other hand, decreased at 4 – 7 Hz of the theta frequency band at extinction recall when compared to fear recall ($p<0.01$, Figure 41 bottom row, right).

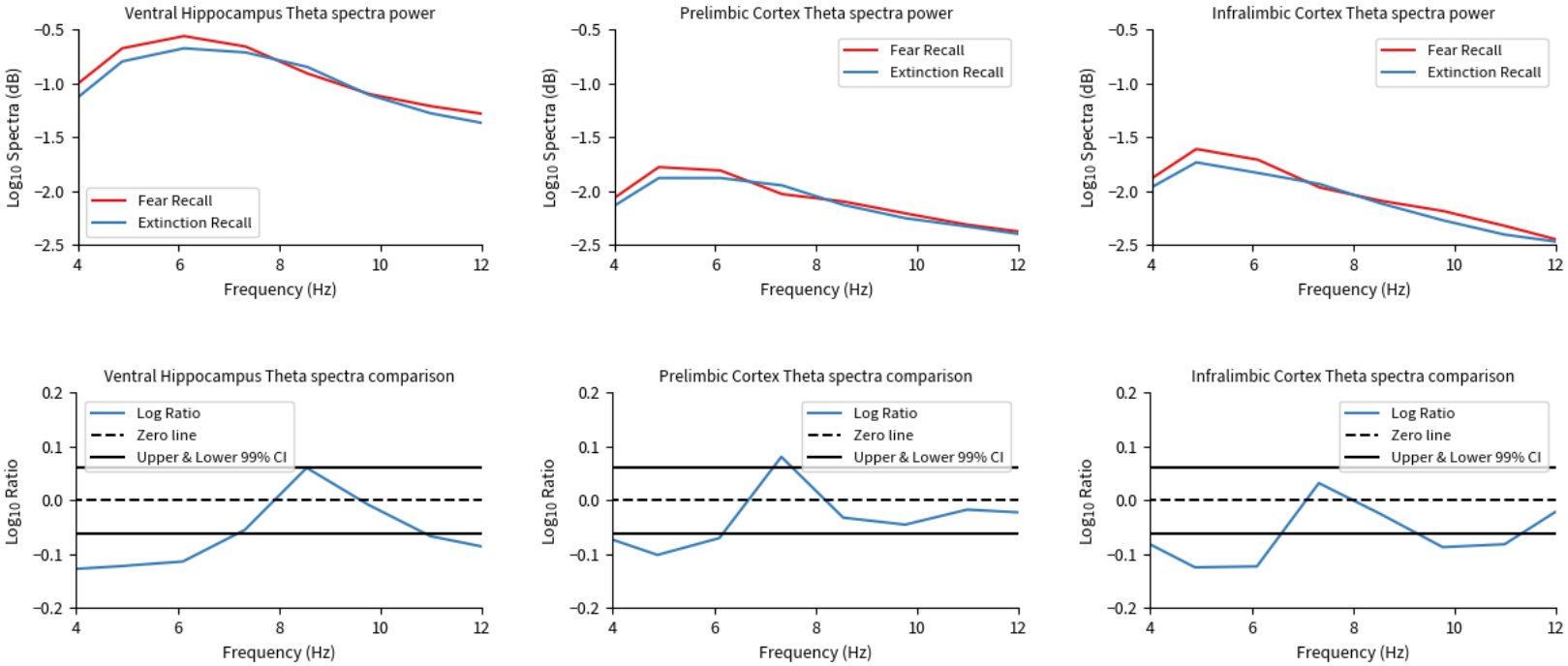

Figure 40 – Pooled theta band (4 – 12 Hz) spectra at Fear and Extinction Recall (top) and its pairwise comparison (bottom) in the VH (left), PL (middle) and IL (right) areas, respectively. Log ratio plots show a 99% confidence interval (solid lines) and a zero (dashed) line. Positive log ratio plot values indicate increased power during extinction recall compared to fear recall, whereas negative log ratio plot values indicate decreased power during extinction recall compared to fear recall. VH power decreased at low and high theta band frequencies at Extinction Recall. PL power decreased at low theta band frequency with a small peak at 7.5 Hz. Finally, IL power decreased at low and high theta frequency range.

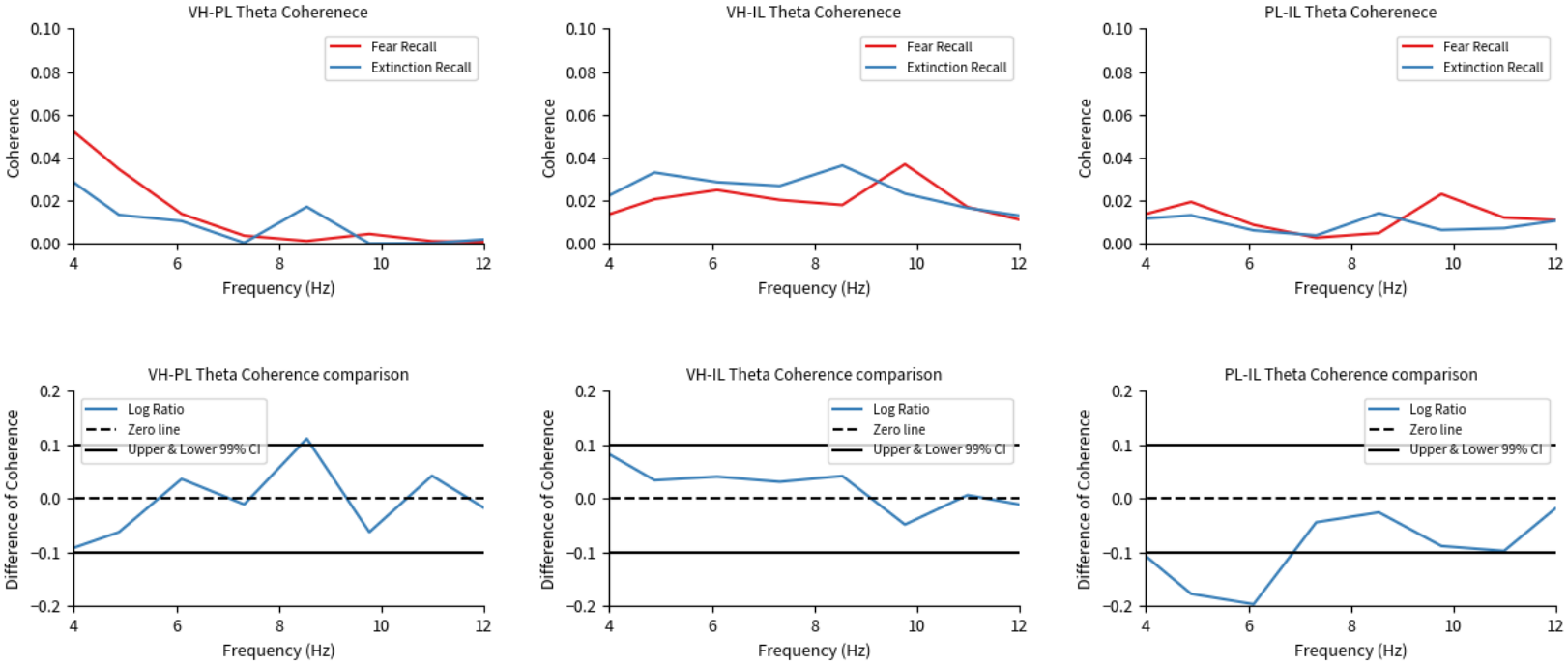

Figure 41 – Pooled theta band (4 – 12 Hz) coherence at Fear and Extinction Recall (top) and its pairwise comparison (bottom) between the VH & PL (left), VH & IL (middle) and PL & IL (right) areas, respectively. Difference of coherence plots show a 99% confidence interval (solid lines) and a zero (dashed) line. Positive difference of coherence plot values indicate increased coherence during extinction recall compared to fear recall, whereas negative difference of coherence plot values indicate decreased coherence during extinction recall compared to fear recall. The coherence estimates between the three area pairs was very low overall (< 0.1 coherence). VH-PL had a slight peak at 8.5 Hz during Extinction Recall. There were no significant changes in theta band coherence between VH and IL. The theta coherence between PL and IL dropped at 4 – 7 Hz.

Spectra power and coherence in the low gamma frequency band

Similar to the observation in the theta band spectra, the ventral hippocampus CA1 had about a magnitude stronger low gamma oscillations compared to either PL or IL (Figure 42 top row). Only the ventral hippocampal low gamma oscillations showed a slight decrease at 32 Hz and small decreases at 37 as well as 40.5 Hz at extinction recall stage compared to fear recall stage ($p<0.01$, Figure 42 bottom row).

Low gamma synchrony in the VH-PL, VH-IL and PL-IL area pairs was extremely low (Coherence < 0.04, Figure 43 top row). Therefore, there is little to no volume conduction of low gamma oscillations between the three area pairs at extinction recall or fear recall. There were no significant changes in low gamma synchrony between the three area pairs at extinction recall compared to fear recall (Figure 43 bottom row).

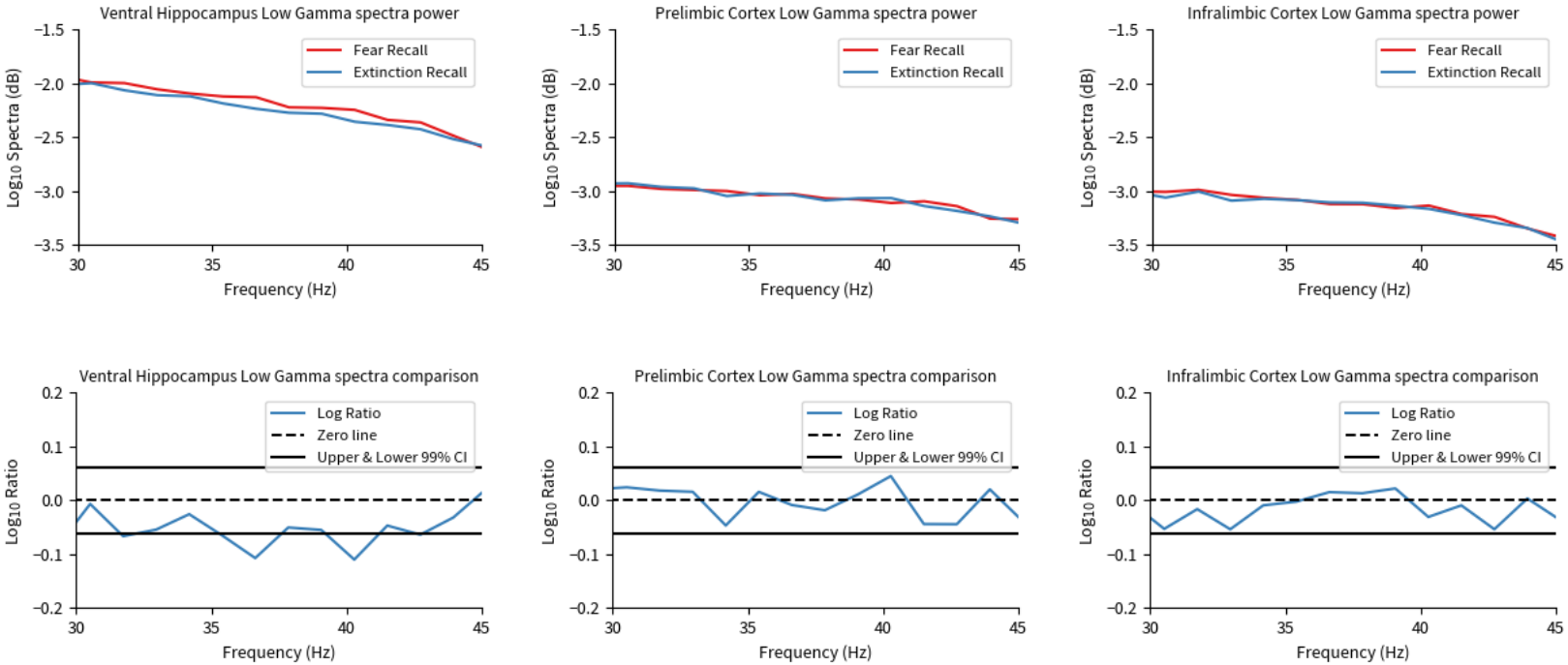

Figure 42 – Pooled gamma band (30 – 45 Hz) spectra at Fear Recall (3 CS) and Extinction Recall (2 CS) stages (top) and its pairwise comparison (bottom) in the VH (left), PL (middle) and IL (right) areas, respectively. Log ratio plots show a 99% confidence interval (solid lines) and a zero (dashed) line. Positive log ratio plot values indicate increased power during extinction recall compared to fear recall, whereas negative log ratio plot values indicate decreased power during extinction recall compared to fear recall. The gamma spectra power changed significantly at Extinction Recall in VH only, showing a slight decrease at 32 Hz and small decreases at 37 as well as 40.5 Hz of the low gamma frequency band.

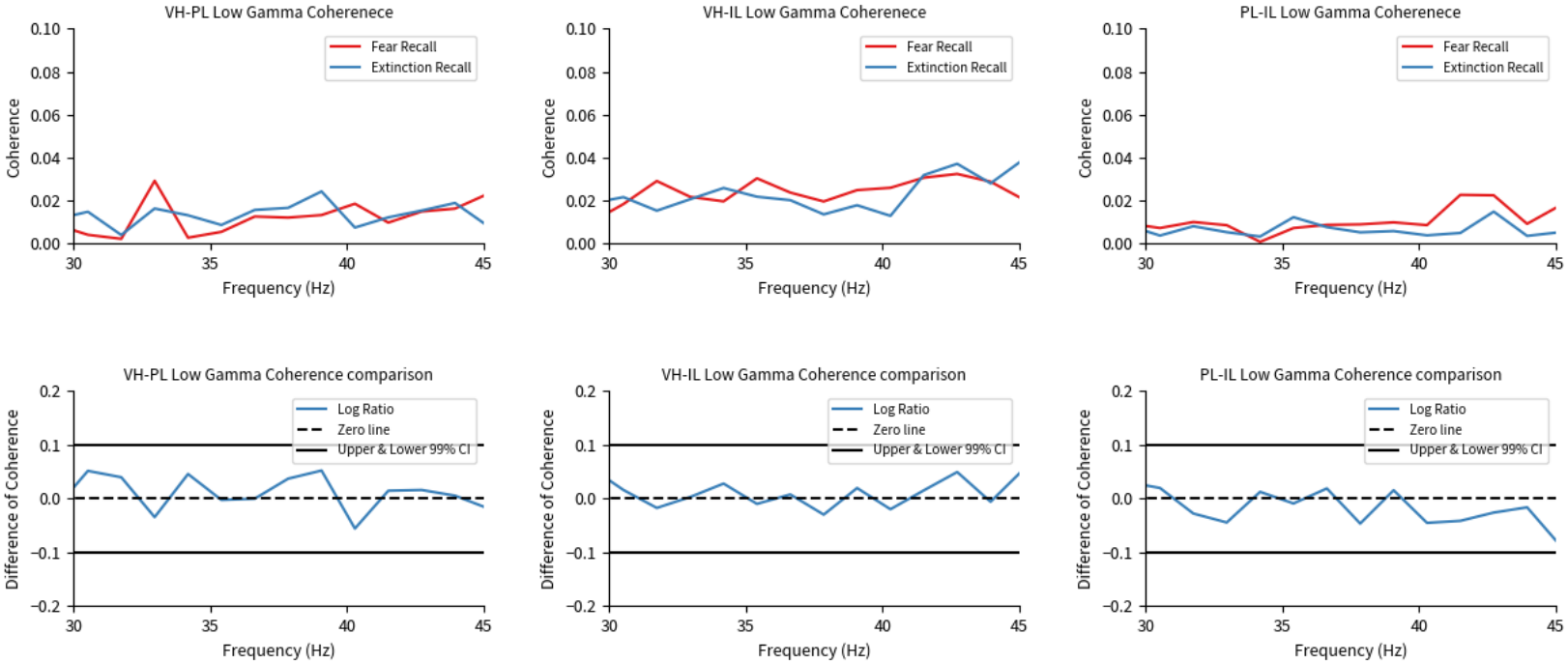

Figure 43 – Pooled low gamma band (30 – 45 Hz) coherence at Fear and Extinction Recall (top) and its pairwise comparison (bottom) between the VH & PL (left), VH & IL (middle) and PL & IL (right) areas, respectively. Difference of coherence plots show a 99% confidence interval (solid lines) and a zero (dashed) line. Positive difference of coherence plot values indicate increased coherence during extinction recall compared to fear recall, whereas negative difference of coherence plot values indicate decreased coherence during extinction recall compared to fear recall. The low gamma frequency band coherence estimates between the three area pairs was very low overall (< 0.1 coherence). The coherence in neither of the three area pairs changed significantly.

4.4 DISCUSSION

In this experiment we investigated the interactions at theta and low gamma frequency bands between VH, PL and IL during fear and extinction recall. The ventral hippocampus had an order of magnitude higher theta and gamma power than PL or IL. The analysis revealed a drop in theta oscillation power in all three areas between fear recall and extinction recall. However, there was negligible volume conductance of theta oscillations among the VH-IL, VH-PL and PL-IL area pairs. Nevertheless, VH-PL coherence showed a a slight peak at 8.5 Hz. PL-IL coherence decreased at low to medium part of the theta frequency band. When it comes to low gamma frequency band, only the ventral hippocampal low gamma oscillations decreased slightly at 32 Hz and more markedly at 37 as well as 40.5 Hz at extinction recall. There was little to no volume conductance of gamma oscillations between VH-PL, VH-IL or PL-IL area pairs.

4.4.1 *Auditory fear conditioning, partial extinction and recall*

There were no changes in mean freezing level due to conditioning. Nevertheless, the animals expressed learned fear indicating successful encoding of fear memory. In addition to this, the experimental parameters have been validated previously (Fenton et al. 2014a). Similarly, there were no changes in freezing level due to extinction. However, there was a reduction in the freezing between fear memory recall and extinction recall, suggesting that both fear training and partial extinction learning were successful. In order to facilitate a larger amplitude of changes in freezing, a full extinction session of 30 CS can be used. Such amplitude should be sufficient to detect significant differences in freezing during extinction.

4.4.2 *Theta power in VH, IL and PL decreased at extinction recall*

VH, IL and PL showed significant decreases in theta power between fear recall and extinction recall. Theta oscillations in the hippocampus have been associated with anxiety-like states in innate fear paradigm and disruption of these oscillations is a predictor of anxiolytic effect (Yeung et al. 2012). Thus, a drop in its power at extinction recall could underpin a reduction in anxiety-like responses. Such phenomena would contribute to significantly reduced fear expression between fear recall and extinction recall observed in the experiment. Indeed, several studies highlighted the involvement of VH in fear expression, with lesions or inactivations leading to fear expression deficits (Sierra-Mercado et al. 2011, Maren & Holt 2004, Hunsaker & Kesner 2008). Therefore, this reduction in theta power can be directly related to fear expression.

The prelimbic cortex is involved in fear expression with increasing activity in the area resulting in increasing fear response (Sotres-Bayon & Quirk 2010). This activity is associated with low theta oscillations in the area, blockade of which impairs fear expression (Dejean et al. 2016). A drop in theta oscillation power at extinction recall suggests a reduced synchrony and/or firing of pyramidal neurons in the prelimbic cortex and, in turn, would lead to reductions in PL-CeA mediated fear expression. Such phenomena would be consistent with the significantly reduced fear expression between fear recall and extinction recall seen in this study.

A plethora of studies indicated IL involvement in fear extinction and retention of extinction memory (Quirk et al. 2000, Sierra-Mercado et al. 2011, Santini et al. 2012, Milad et al. 2004, Vidal-Gonzalez et al. 2006, Kim et al. 2010). Activity in IL has been correlated with extinction recall (Milad & Quirk 2002, Knapska et al. 2012, Holmes et al. 2012). However, optogenetic silencing of IL was shown to have no effect on fear retrieval (Do-Monte et al. 2015). Similarly, Bukalo et al. (2015) revealed that stimulation of IL did not facilitate extinction retrieval. The observations of this experiment could suggest that IL is not involved in extinction recall, as a lack of involvement in extinction recall could explain a reduction in the infralimbic theta oscillation power at this stage compared to fear recall.

4.4.3 *Significant reduction in PL-IL synchrony at extinction recall*

There was a neglible volume conduction of theta oscillations between VH-IL, VH-PL and PL-IL, suggesting very little synchrony between the three area pairs in this frequency band. The low level of synchrony between PL-IL has been reported by Fenton et al. (2014a). However, unlike Fenton et al. (2014a), a significant decrease in already low PL-IL synchrony was observed at extinction recall when compared to fear recall. Higher IL theta power at fear recall compared to extinction recall could explain the higher theta coherence between PL-IL at fear recall. PL and IL are involved in opposing roles of fear expression and extinction, respectively (Vidal-Gonzalez et al. 2006). Therefore, this drop in already low synchrony could suggest a PL-IL cross-communication involvement in auditory fear expression.

4.4.4 *Reduced low gamma oscillations in VH at extinction recall*

There was a significant decrease in low gamma oscillations in VH (CA1) between fear recall and extinction recall. Low gamma oscillations in the hippocampal CA1 rely on parvalbumin-positive (PV) basket cells (Buzsáki & Wang 2012). These neurons participate in local inhibition of the ventral hippocampal CA1 pyramidal cells, reducing their firing and contributing to their synchronisation (Cobb et al. 1995, Miles et al. 1996, Freund & Buzsáki 1996). Therefore, this reduction in VH (CA1) low gamma oscillations during extinction recall compared to fear recall could indicate a decreasing inhibitory tone in the area. However, the reduction of VH low gamma oscillations during extinction recall, compared to fear recall, is not consistent with Albrecht et al. (2013) study showing decreased kainate-induced low gamma oscillations in the ventral hippocampus slices following fear conditioning and its recall.

4.4.5 *No change in PL or IL low gamma oscillations at extinction recall*

There were no changes in PL or IL low gamma oscillation power at extinction recall compared to fear recall. Fenton et al. (2016) showed reduced PL low gamma oscillations and increased IL low gamma oscillations at extinction recall. This difference in findings is most likely due to the difference in extinction training protocol used since Fenton et al. (2016) used a 30 CS extinction training, whereas this study used a 15 CS partial extinction training paradigm. Therefore, it could be possible that extinction training in this study was too short to induce changes in low gamma oscillation activity in PL and IL during extinction recall compared to fear recall.

4.4.6 *Summary*

The findings presented in this study add support to the involvement of VH, PL and IL in auditory fear memory and its extinction recall. In particular, changes in VH and PL activity support the involvement of both areas in fear expression, whereas the observed IL activity could support the notion that it does not participate in extinction retrieval. In addition to this, we present data on PL-IL synchrony, which, albeit low, suggests participation in fear expression. Lastly, our finding of VH low gamma activity decrease during extinction retrieval is not consistent with the data suggesting that fear conditioning and its retrieval induces a reduction in low gamma oscillations.

5

GENERAL DISCUSSION

Fear conditioning and extinction are two psychological processes believed to be dysfunctional in several anxiety and trauma-related disorders. Therefore, a better understanding of the neurophysiological underpinings and pharmacological means of regulating these processes to reduce anxiety is crucial for improving the outcomes of the aforementioned disorders. We set out to investigate auditory fear conditioning and extinction from three perspectives. First, we aimed to determine the effect of cannabidiol on auditory fear memory expression and extinction. Second, we created a spiking neuron fear memory network model that extends previous computational models with the addition of VH to investigate the influence of this area on the activity of PL and IL during auditory fear memory expression and extinction. Third, we aimed to investigate the interactions between the VH, PL and IL during auditory fear memory and extinction recall by recording LFP activity within each area during behavioural testing.

5.1 MAIN FINDINGS AND THEIR IMPLICATIONS

5.1.1 *CBD reduces auditory fear memory expression*

We investigated the effect of systemic CBD administration prior to auditory fear extinction to test its effects on auditory fear memory expression, extinction facilitation, as well as contextual fear memory prior to tone presentations, described in Chapter 2. We found that the highest dose of CBD we used significantly reduced

fear memory expression without affecting extinction learning or encoding. Interestingly, however, all three doses of CBD reduced contextual fear prior to extinction, broadly confirming previous findings (see below). However, our experiment had several limitations. The observed levels of freezing were low throughout the experiment. This could suggest that our conditioning parameters were too strong or too weak. Fear conditioning that is too weak would not lead to CS-US association. In this case, the animals would not be freezing (i.e. expressing learned fear) in response to CS during conditioning or extinction. Since we saw fear behaviour during extinction, this is not likely to be the case. We used five 0.5 second 0.5 amp shocks as our unconditioned stimulus that co-terminated with a tone. If the fear training parameters are too strong, the animal behaviour switches from passive to active fear expression. Such behaviour would result in a reduced amount of time spent freezing, and thus, could potentially explain our observation of low freezing levels. Moreover, we did not see evidence of extinction learning, a reduction in freezing at the end of extinction compared to the beginning. This could be explained by the partial extinction protocol used in the experiment. We used a 15 CS partial extinction paradigm to be able to account for the potential extinction facilitating effects of CBD. A full, 30 CS extinction paradigm should produce evidence of extinction learning (Fenton et al. 2014a). Since CBD did not affect auditory extinction learning or encoding in a partial extinction paradigm, a full extinction training paradigm should be used in future experiments testing the effect of CBD on auditory fear memory and extinction.

Cannabidiol is a phytocannabinoid anxiolytic found in *Cannabis Sativa* plant that has a large anxiolytic potential (Campos et al. 2012). CBD has anxiolytic, extinction facilitating, and fear memory consolidation and reconsolidation disrupting effects in contextual fear paradigms. Administration of CBD prior to fear conditioning reduces fear expression and impairs fear memory consolidation (Levin et al. 2012). If CBD is administered immediately after fear conditioning, it disrupts fear memory consolidation (Stern et al. 2017). Administration of CBD after fear retrieval disrupts its reconsolidation (Stern et al. 2012, 2014, 2015, Gazarini et al. 2015). CBD also impairs extinction of a weak fear memory and facilitates extinction of a strong

fear memory (Song et al. 2016). These effects show that CBD has a multi-faceted anxiolytic and extinction-promoting effect in contextual fear memory.

However, there is very little data on CBD effects in fear memory related to explicit cues. CBD facilitated visually-cued fear extinction consolidation when administered following extinction training (Das et al. 2013). Infusions of CBD into nucleus accumbens shell impaired olfactory fear memory acquisition (Norris et al. 2016). Nevertheless, there were no studies that addressed the effect of CBD in auditory fear memory. Therefore, this is the first report of CBD effects in an auditory fear memory paradigm. The observed CBD effects on contextual fear prior to tone presentations are in line with the previously published studies investigating CBD effects in contextual fear memory.

There are three implications with regards to our findings. First, we did not see the inverted-U shaped dose-response curve associated with CBD anxiolytic effect, where increasing doses of CBD beyond the 10 mg/kg optimal dose result in anxiogenesis in animals and beyond 300 mg in humans (Guimarães et al. 1990, Lemos et al. 2010, Stern et al. 2012, Zuardi et al. 2017). Our highest dose of CBD at 20 mg/kg was the only dose to reduce auditory fear expression, suggesting that higher doses of CBD should be tested in the paradigm. This could be due to the differences in paradigms, since the inverted-U shaped dose-response curve of cannabidiol is reported in innate fear (Guimarães et al. 1990). Moreover, Guimarães et al. (1990) used Wistar strain of rat, whereas we used Lister hooded rats. The inverted-U effect observed by Lemos et al. (2010) transpired from intra-IL and intra-PL CBD administration during a contextual fear memory paradigm. We used CBD systemically during an auditory fear memory paradigm. Therefore, CBD activity at other areas could have masked the inverted-U shaped dose-reponse effect. Lastly, Stern et al. (2012) used Wistar rats in contextual fear memory paradigm. The rat strain and paradigm differences could underlie the lack of inverted-U shaped dose-response curve in our experiment. In fact, Chang & Maren (2010) showed rat strain differences in the extinction of auditory fear memory. Alternative explanation could be that the strength of fear conditioning in our paradigm was not suitable to precipitate this effect. Specifically, if the fear conditioning we used was too strong,

it could have masked anxiogenic effects of a high dose of CBD. In fact, Song et al. (2016) showed that CBD facilitates extinction of strong contextual fear conditioning and impairs the extinction of weak contextual fear conditioning.

Second implication of our finding is that the anxiolytic effects of CBD on auditory fear memory expression together with its effects in contextual fear memory supports CBD use in the treatment of anxiety disorders. In particular, CBD does not seem to impair auditory fear memory extinction, while reducing fear expression, suggesting it could be beneficial as an adjunct approach for exposure therapy, a psychological intervention based on fear extinction training. In fact, it has been shown that arachnophobic patients who were able to undergo maximal intensity exposure therapy sessions showed improved clinical outcomes, specifically, a better ability to tolerate fear (Norberg et al. 2018). Clinically used anxiolytics are limited since benzodiazepines impair fear extinction, whereas SSRIs can have serious adverse effects (Rothbaum et al. 2014, Baldwin et al. 2014). Helping the patients undergo intense exposure therapy sessions with adjunct anxiolytic therapy, like CBD, that does not interfere with fear extinction process and is well-tolerated in humans might revolutionise the treatment of anxiety disorders (Devinsky et al. 2014).

Finally, there was a difference in CBD effects on auditory and contextual fear expression. Only the highest dose of CBD reduced auditory fear memory expression, whereas all three doses reduced contextual fear expression. This finding suggests the involvement of different receptors and/or brain areas in mediating CBD effects in auditory fear memory compared to contextual fear. A study in humans by Bhattacharyya et al. (2015) suggests that CBD suppreses the hippocampal-prefrontal connectivity. In addition to this, it is not clear whether CBD was purely anxiolytic, solely affecting fear expression, or if it disrupted the initial fear memory retrieval at the start of extinction in our experiment. Since fear memory consolidation and reconsolidation disrupting as well as extinction facilitating effects of CBD are CB1 receptor-dependent, whereas anxiolytic effects of CBD seem to rely on 5-HT1A receptors, this could be investigated pharmacologically (Stern et al. 2014, Bitencourt et al. 2008, Do Monte et al. 2013, Gomes et al. 2012, Fogaça et al. 2014).

Therefore, further pharmacological characterisation of CBD effects in contextual and auditory fear memory is warranted.

5.1.2 *Computational VH inactivation suppresses PL activity to a larger extent than PL-IL disconnection*

Fear learning and extinction are studied with a variety of approaches ranging from molecular biology to *in vivo* techniques. It is accepted that the sheer amount of data collected with these approaches is difficult to integrate intuitively (Nair et al. 2016). Moreover, biological approaches are expensive, temporally limited, restricted to a domain, such as a neuron, brain area or general animal behaviour, and, in some cases, carry serious ethical concerns. Therefore, computational modelling methods have been used to integrate this multi-dimensional data and bypass the limitations imposed by the biological approaches.

We created a model of auditory fear memory network based on the Fenton (2015) framework described in Chapter 3. We extended the Fenton (2015) framework with an addition of the ventral hippocampus (CA1). BLA in Fenton (2015) was replaced with three sub-populations of BLA neurons that are recruited into fear, extinction and extinction-resistant memory trace representations during fear memory and extinction paradigm. This model of BLA function was based on Herry et al. (2008) biological experiments and Vlachos et al. (2011) modelling study. Izhikevich integrate-and-fire neuron models were used to represent the spiking neuron dynamics within each area (Izhikevich 2004, 2007). We compared the model activity against the two versions of Fenton (2015) model, which differed in the types of neuron models used, and against published biological PL and IL activity. In addition to this, we compared the effects of a simulated VH inactivation and PL-IL disconnection to the activity in the intact model.

Comparisons of this model to the previous models revealed that the only complete qualitative match was between the model's PL activity and Fenton (2015) models upon PL-IL disconnection. The remaining comparisons resulted in partial qualitative matches between the present model and the biophysical and hybrid

biophysical-phenomenological Fenton (2015) models. Similarly, the model had a partial qualitative match to both biological PL and IL data reported by Burgos-Robles et al. (2009) and An et al. (2017), respectively. Interestingly, Fenton (2015) models showed a complete qualitative match to the biological PL and IL data. The VH inactivation in the model resulted in a larger suppression of PL than PL-IL disconnection. Conversely, the PL-IL disconnection resulted in a larger suppression of PL than VH inactivation. This finding is consistent with biological data on VH influence on fear expression in innate fear and auditory fear memory (McHugh et al. 2004, Maren & Holt 2004, Gilmartin et al. 2014, Sierra-Mercado et al. 2011). Biologically, IL fires at higher frequency than PL, but this difference in activity disappears if the areas are disconnected (Van Aerde et al. 2008). Moreover, activation of IL causes PL pyramidal cell inhibition (Ji & Neugebauer 2012). Specifically, NPY+ interneurons from IL project directly to the pyramidal cells in PL and inhibit their activity (Saffari et al. 2017). Our PL-IL inactivation experiment did not produce results consistent with these biological studies. However, both Van Aerde et al. (2008) and Saffari et al. (2017) investigated the activity *ex vivo* which could have removed the afferents driving PL and IL activity and Ji & Neugebauer (2012) kept the animals under anaesthesia throughout the experiment. Therefore, direct comparisons between these studies and our model activity are not appropriate, since the model mimics a fear memory circuit activity of an awake-behaving rodent.

Interestingly, our modelling study indicates that BLA populations representing competitively recruited neurons representing fear, extinction and extinction-resistant memory traces are sufficient to reproduce the input from the amygdala to PL, IL and VH. Previous published models relied on CS-US association taking place in LA or BLA (Li et al. 2009, Vlachos et al. 2011, Pendyam et al. 2013, Fenton 2015). The use of these three sub-populations of BLA, instead of CS-US association, allows the shortening of simulation time without sacrificing inputs to the rest of the network. Therefore, such approach of BLA modelling simplifies auditory fear memory network building and simulation process.

Our finding that verifies the anxiogenic role of VH in the network is consistent with biological studies, since VH inactivation suppressed PL, the area responsible

for fear expression, activity to a larger extent than IL, the area responsible for extinction. This suggests that our network of VH, PL, IL and the three BLA sub-populations is based on experimental data that can, at least in part, explain the anxiogenic role of VH.

The model has several limitations. First of all, the model, for the most part, had only partial qualitative matches to previous auditory fear memory models and biological data. This is probably due to the use of the three sub-populations of BLA used to drive the rest of the network. Parameter optimisation of these elements might result in activity that shows a complete qualitative match to the biological data and computational models. Finally, our network of integrate-and-fire neurons cannot be said to be biophysical since it does not model the currents that generate an action potential in a neuron. Therefore, the model cannot mimic ion current-dependent effects in the neuron accurately. For example, NMDA inactivation in an integrate-and-fire neuron network model cannot recreate the effect seen in biology, unlike a biophysical neuron network model (Fenton 2015).

A number of fear memory and extinction models have been created. Early models have focused on the connections within fear memory and extinction network, while approximating neuronal activity to represent mean firing rate of the area, as opposed to considering the dynamics of individual neurons. Some of these models focused on the amygdala, providing insights about the sensory input processing and association underlying fear conditioning within the area (Armony et al. 1997b, Ball et al. 2012, Vlachos et al. 2011). Other models extended beyond the amygdala to investigate the role of cortical and limbic structure involvement in fear memory processing (Krasne et al. 2011, Navarro-Guerrero et al. 2012, Moustafa et al. 2013). Although these models provide a good general overview of the brain area interactions in fear memory and extinction processing, such models lack biological realism due to neuronal approximations. These approximations are being addressed with spiking neuron fear memory network models.

Several spiking neuron models, like their neuron-approximating counterparts, focused on the amygdala, its different nuclei and the processing of sensory inputs, including their convergence and association within the area (Li et al. 2009,

2011, Vlachos et al. 2011, Kim et al. 2013b,a, 2016, Feng et al. 2016). The insights provided by some of these models lead to a few studies that went beyond the amygdala and considered the involvement of cortical structures in the processing of auditory fear memory and extinction. A model by Pendyam et al. (2013) considered the role of PL interaction with the amygdala and made predictions regarding activity and neurotransmitter involvement that have been verified physiologically. Fenton (2015) extended this model with an addition of IL, creating a biophysical and a hybrid biophysical-phenomenological spiking neuron version of the network. The models tested PL-IL disconnection effects on the activity in both PL and IL, revealing increased PL activity during fear expression that did not reduce to the baseline level following extinction. However, none of the spiking neuron fear memory network models has considered the role of the ventral hippocampus, an area which is involved in both auditory fear memory expression and extinction (Vidal-Gonzalez et al. 2006, Sierra-Mercado et al. 2011). Therefore, our model is the first spiking neuron model to address the function of the ventral hippocampus in auditory fear memory.

5.1.3 *Theta oscillation power decreases in VH, PL and IL during extinction retrieval*

We recorded LFPs from VH, PL and IL during auditory fear memory, partial extinction and extinction recall paradigm. Partial extinction was used since we initially intended the experiment to test CBD effects of extinction facilitation, as predicted from contextual fear memory studies showing such CBD effect (see above). However, CBD did not affect extinction during the pharmacology experiment. Nevertheless, we found that animals expressed learned fear, suggesting successful encoding of fear memory. There was a significant reduction of freezing during extinction recall compared to fear recall, suggesting that fear and extinction training was successful. VH, IL and PL showed significant decreases in theta power during extinction recall compared to fear recall. There was a very low theta synchrony between PL and IL, VH and PL, and, VH and IL. However, there was a significant decrease in synchrony between PL and IL at extinction recall compared to

fear recall. There was also a significant reduction in VH gamma oscillations during extinction recall compared to fear recall and little to no gamma coherence between PL and IL, VH and PL, or VH and IL, which did not change during extinction recall, compared to fear recall.

A major limitation of this study is the lack of single-unit activity recordings. We could not see single-unit activity with the microelectrode arrays used in this study. Therefore, we focused on local field potentials. Another limitation of the experiment is that while electrophysiology shows decreases in VH, PL and IL theta power at extinction recall compared to fear recall, the computational simulation shows increased IL activity at late extinction. This could be explained by the use of partial extinction in electrophysiology and simulation using a full extinction protocol. Another facet of this difference is that the BLA sub-population activity was based on Herry et al. (2008) data, which contained recorded neuronal activity at conditioning and extinction, but not extinction recall.

When it comes to different brain area involvement in auditory fear conditioning and extinction, PL is involved in fear expression, IL is involved in fear extinction learning and its retention, whereas VH is involved in both processes (Quirk et al. 2000, Vidal-Gonzalez et al. 2006, Sierra-Mercado et al. 2011, Maren & Holt 2004, Hunsaker & Kesner 2008). The interaction of these three areas can be studied electrophysiologically. VH-mPFC theta synchrony predicts anxiety-like behaviour, whereas disruption of this synchrony causes anxiolysis (Adhikari et al. 2010, Padilla-Coreano et al. 2016, Schoenfeld et al. 2014). Fear expression coincides with IL-LA-DH theta synchrony, which is replaced by IL-LA and IL-DH synchrony at extinction recall (Lesting et al. 2011, 2013). High theta activity in PL is seen during learned fear recall, whereas high theta activity in IL coincides with extinction and its recall with little synchrony between the areas (Fenton et al. 2014a).

Fear conditioning and extinction also affects gamma oscillations within the areas. Fear conditioning and its retrieval reduce the power of gamma oscillations in the ventral hippocampal brain slices (Albrecht et al. 2013). Fear extinction deficits coincide with increased PL gamma oscillation power during extinction and its retrieval (Fitzgerald et al. 2014b). Increases of gamma oscillations in human

homolog of IL correlate with successful extinction recall, whereas no change in oscillations correlate with extinction recall failure (Mueller et al. 2010). PL shows reduced gamma oscillations during extinction and extinction recall, whereas IL shows increased oscillations during extinction recall (Fenton et al. 2016). However, interactions between VH, PL and IL at both theta and gamma frequency band during learned auditory fear expression and extinction have not been addressed. Therefore, this is the first report on VH, PL and IL activity and synchrony comparison in theta and low gamma frequency band during fear recall and extinction recall.

Our observed reduction of VH theta power is consistent with biological data suggesting that disruption of theta oscillations in innate fear causes anxiolysis and lesions or inactivations of VH result in fear expression deficits (Yeung et al. 2012, Maren & Holt 2004, Hunsaker & Kesner 2008, Sierra-Mercado et al. 2011). The reduction of PL theta power during extinction recall is consistent with experimental data suggesting PL involvement in fear expression (Sotres-Bayon & Quirk 2010, Dejean et al. 2016). Interestingly, the observed reduction in IL theta power during extinction recall suggests lack of oscillations within pyramidal cell assemblies within IL. Do-Monte et al. (2015) showed that silencing IL after extinction does not affect extinction retrieval. Bukalo et al. (2015) stimulated the IL-amygdala pathway, which facilitated extinction, but not extinction retrieval. Therefore, our observation of reduced IL theta oscilations during extinction retrieval compared to fear retrieval could suggest that IL pyramidal cell oscillations are not necessary for extinction retrieval. Alternatively, this could be supporting Giustino et al. (2016) data showing that differences in PL and IL activity, as opposed to PL activity alone determine freezing behaviour. Lack of activity differences in PL and IL were associated with low freezing (Giustino et al. 2016). Therefore, a similar drop in both PL and IL theta power at extinction recall, a low fear stage, could explain the low freezing seen behaviourally in our experiment.

Despite the already low theta oscillation coherence between PL and IL, there was a decrease during extinction recall compared to fear recall. The low recorded coherence is similar to the finding by Fenton et al. (2014a), who looked at coherence

during the early and late extinction as well as early and late extinction recall. However, here we show changes during extinction recall compared to fear recall. Since PL and IL are involved in fear expression and extinction learning, respectively, this finding in our study supports the *ex vivo* and anaesthesized data regarding PL-IL interaction and is one of the first reported observations of such interaction during an auditory fear paradigm (Van Aerde et al. 2008, Ji & Neugebauer 2012, Saffari et al. 2017).

Our observation regarding the decreased VH low gamma oscillations during extinction recall are contradictory to Albrecht et al. (2013) study showing that fear conditioning and its retrieval reduces VH low gamma oscillations in rodent brain slices. However, rodent brain slices have severed afferents to VH, which could have confounded the observation by Albrecht et al. (2013). This could be investigated further by analysing low gamma activity in VH throughout the fear memory paradigm, including conditioning, fear retrieval and extinction retrieval.

Unlike Fenton et al. (2016), we did not find any differences in PL or IL low gamma power during extinction recall compared to fear recall. However, Fenton et al. (2016) investigated the activity at early and late extinction as well as early and late extinction recall. Apart from the differences in the analysis time points, this could also be associated with the difference in extinction protocols used during our study and the one used by Fenton et al. (2016). Specifically, we used a partial extinction protocol of 15 CS, whereas Fenton et al. (2016) used 30 CS. Therefore, extinction training in our study may have been too short to result in low gamma oscillation changes in PL or IL. Using a longer extinction protocol might reveal a similar result to Fenton et al. (2016).

5.2 FUTURE WORK

5.2.1 *Cannabidiol psychopharmacology*

Our study on the effects of CBD in auditory fear memory and its extinction raises the question of the receptors and areas involved in mediating its effect. We

saw that only the highest dose of CBD reduced auditory fear memory expression without affecting its extinction, whereas all doses of CBD reduced the expression of contextual fear prior to extinction. These findings suggest differences in receptor and/or brain area involvement between auditory and contextual fear.

CBD disruption of contextual fear memory reconsolidation following retrieval is CB1 receptor-dependent (Stern et al. 2012, 2014). Specifically, PL CB1 receptors have been shown to mediate this effect (Stern et al. 2014). Intracerebroventricular or intra-IL CBD infusions prior to extinction facilitate contextual fear extinction learning via CB1-mediated process (Bitencourt et al. 2008, Do Monte et al. 2013). Intra-BNST or intra-PL CBD infusions prior to retrieval reduce fear expression via 5-HT1A receptors (Gomes et al. 2012, Fogaça et al. 2014). Conversely, intra-IL CBD infusions prior to retrieval increase fear expression, also via 5-HT1A-dependent process (Marinho et al. 2015). These effects suggest that in contextual fear memory paradigms extinction facilitating and fear memory disrupting effects are CB1 receptor-dependent, whereas anxiolytic effect is mediated via 5-HT1A receptors. However, it is not clear which receptors are involved in mediating CBD effects in auditory fear memory paradigm.

CBD has an indirect action on CB1 receptors since it is an endocannabinoid breakdown inhibitor, whereas it is a direct agonist of both 5-HT1A and TRPV1 receptors (De Petrocellis et al. 2011, Devinsky et al. 2014). The most likely receptor mediating anxiolytic effect of CBD, considering contextual fear evidence, is 5-HT1A. This suggestion is supported by data from innate fear paradigms (de Mello Schier et al. 2012). In fact, innate fear paradigms suggest that TRPV1 is the receptor responsible for anxiogenic effect of CBD at higher doses (de Mello Schier et al. 2012). TRPV1 receptor agonists mediate contextual fear expression when infused into vmPFC and antagonist have an opposite effect (Terzian et al. 2014). Interestingly, however, AM404, an endocannabinoid reuptake and breakdown inhibitor as well as TRPV1 agonist, reduced explicit-cue fear expression, with the effect blocked by either CB1 antagonism or TRPV1 antagonism (Llorente-Berzal et al. 2015). This could suggest TRPV1 agonism mediating the anxiolytic effect of CBD in auditory fear paradigm. Therefore, there are a few receptors that could be involved in CBD

anxiolytic effect mediation in auditory fear memory paradigm. The receptor involvement in anxiolytic effect of CBD in auditory fear memory can be tested by the use of selective antagonists at TRPV1, CB1 and 5-HT1A receptors (de Mello Schier et al. 2012, Llorente-Berzal et al. 2015). Administrations of antagonist before or during CBD administration in an auditory fear memory paradigm should reveal which of the three receptors is responsible for the anxiolytic effect. In addition to this, it would help to determine if the CBD effect we have seen in our experiment was purely anxiolytic, possibly relying on 5-HT1A receptors, or fear memory retrieval disrupting, potentially CB1-dependent effect.

Since we did not see anxiogenic effect with the highest dose of CBD in auditory fear memory paradigm, it would be interesting to test the effects of increased doses of CBD. This experiment should reveal if the inverted-U shape dose-response curve is present in auditory fear memory paradigms.

Fear relapse phenomena has garnered a lot of interest in the recent years. Fear renewal occurs when an extinguished CS is presented outside of extinction context and results in increased fear expression (Marek et al. 2018). This phenomena has clinical implications since fear renewal of patients suffering from phobias has been documented once exposure therapy stops (Norberg et al. 2018). Similarly, spontaneous recovery of fear occurs when an extinguished CS produces increased fear expression over time, even inside extinction context (Tovote et al. 2015).

Since we saw that CBD reduced auditory fear expression without affecting extinction, it would be interesting to test its effects on both contextually-controlled fear renewal and spontaneous recovery of fear. Administering CBD prior to the fear renewal or spontaneous fear recovery session should reveal whether it has an anxiolytic effect at this stage. In addition to this, we could test the effects of CBD administered before extinction session on fear renewal and recovery. Such experiments would help determine if CBD has any other fear and extinction memory-related effects associated with explicit-cues.

Overall, these experiments should help characterise the receptor involvement in mediating CBD effects in auditory fear memory, help determine the most

effective concentration of the drug for anxiolysis and elucidate the effects of CBD on the further stages of auditory fear memory processing.

5.2.2 *Extending the computational model*

Our model could be used to study contextual fear conditioning and extinction with several modifications to the network. Such a model would require the addition of DH, considering that this area is crucial for contextual fear conditioning (Selden et al. 1991, Anagnostaras et al. 2001, Bouton 1993, Rudy & O'Reilly 2001). DH would need to receive input representing contextual information. This contextual information would then need to be associated with US in BLA. Therefore, the three BLA sub-populations used in our model would have to be replaced with a BLA population seen in the previous models (Pendyam et al. 2013, Fenton 2015). However, BLA would need to undergo context-US, as opposed to CS-US association. Such model would help to better understand the network interactions underpinning contextual fear memory and extinction.

Fear renewal involves multiple brain areas. Orsini et al. (2011) findings suggest that an intact network of VH, BA and PL is essential for fear renewal. Jin & Maren (2015) showed that VH neurons projecting to both PL and BA were particularly active following extinction, suggesting a potential VH-mediated synchronisation between PL and BA involvement in fear renewal. Wang et al. (2016) revealed that there are more numerous VH projections to IL than PL, with a small of population of VH neurons projecting to both areas. These VH-mPFC projections are more active during fear renewal, as opposed to extinction. Marek et al. (2018) showed that VH projects to IL pyramidal cells and interneurons. There is a higher number of VH-IL interneuron projections, which impair IL pyramidal projections to the amygdala, impairing extinction recall and leading to fear renewal. Therefore, fear renewal involves VH, PL, IL and BA network.

Our model can be adapted to simulate fear renewal computationally. It would require the replacement of the three BLA populations with CS-US association in BLA and contextual inputs to VH that would represent fear conditioning and

extinction contexts. This is because our inputs are based on a study by Herry et al. (2008) which does not present fear renewal data. Such auditory fear memory and extinction network could test if the data collected by Orsini et al. (2011), Jin & Maren (2015), Wang et al. (2016) and Marek et al. (2018) are sufficient to recreate fear renewal computationally. Alternatively, we could start by extending the model with the framework from Krasne et al. (2011), which can account for aspects of both cued and contextual fear conditioning, including contextually-controlled fear renewal. Moreover, if temporally-induced alterations to the context were modelled, it could also account for the spontaneous recovery of fear (Krasne et al. 2011). This would require the modelling of the hippocampus, thalamus and periaqueductal grey alongside a detailed amygdala representation. Such model could help elucidate the gaps in knowledge regarding the fear renewal process.

Similarly, our model could be used to study other brain areas that are involved in auditory fear memory and extinction, but have not been included in our model. It is composed of computationally efficient integrate-and-fire Izhikevich neurons, allowing for a larger number of neurons to be modelled, in contrast to, for example, Hodgkin-Huxley neurons, without the need for substantial computational resources. Thus, our model could be used to gradually build on one of the experimentally inspired schematic diagrams of the brain areas involved in fear processing, such as the one proposed by Calhoon & Tye (2015). Eventually, it could be combined with pharmacological data from fear paradigms and a pharmacokinetic model of the blood-brain barrier by Yamamoto et al. (2017) to recreate a biologically constrained artificial rat model capable of learning fear and extinction, and responding to anxiolytic medications. However, the lack of modelled neuronal currents in the current model with integrate-and-fire neurons should be considered when attempting to model pharmacological interventions computationally.

5.2.3 *Electrophysiological investigations*

We saw a reduction of low gamma oscillations in VH during extinction recall compared to fear recall. Low gamma oscillations in the hippocampus rely on parvalbumin-positive interneurons (Buzsáki & Wang 2012). These neurons are involved in local inhibition of the VH CA1 pyramidal cells, contributing to their synchrony (Cobb et al. 1995, Miles et al. 1996, Freund & Buzsáki 1996, Buzsáki & Wang 2012). Therefore, a reduction in low gamma activity suggests disinhibition of the ventral hippocampal pyramidal cells and reductions of their synchrony. These hippocampal pyramidal cells have been shown to project to PL, BA and IL (Jin & Maren 2015, Wang et al. 2016, Marek et al. 2018). Specifically, dual projecting VH pyramidal cells are suggested to be synchronising PL and BA activity, since they are highly active during fear renewal (Jin & Maren 2015). Similarly, VH projections to IL inhibitory neurons cause feed-forward inhibition of IL inputs to the amygdala, leading to fear renewal (Marek et al. 2018). Therefore, it could be that the decrease in low gamma oscillations of VH (CA1) at extinction recall is a VH-priming disinhibition process to encourage pyramidal neuron firing necessary to synchronise BA and PL activity while also inhibiting IL projections to the amygdala leading to contextually-controlled fear renewal. Alternatively, the low gamma oscillations in VH during extinction recall, a low fear state, could be replaced by increases in low gamma oscillations during a high fear state, like fear renewal, leading to increased pyramidal cell synchrony within the area. The LFP recordings during an extended auditory fear paradigm, which includes a fear renewal stage, could determine which of these, if any, conjectures are correct. In other words, an increase or a decrease in low gamma VH power during fear renewal, compared to extinction recall, could suggest if an increased synchrony of pyramidal cells or their disinhibition, respectively, contributes to the fear renewal process. Either finding has the potential of revealing new targets in the treatment of anxiety disorders.

Disruptions of VH theta oscillations in innate fear paradigms is a predictively valid method of determining an anxiolytic effect of drugs (Yeung et al. 2012). We could test the effect CBD administration on theta activity within VH, PL, IL and

even BLA, as well as their synchrony during auditory fear memory expression. This would help characterise the effect of CBD and its influence on the aforementioned area interactions during auditory fear memory expression.

5.3 CONCLUSION

The results in this thesis present new evidence on CBD involvement in auditory fear memory and extinction. Our findings also shed light on the VH, PL and IL involvement in auditory fear memory and extinction from computational modelling and electrophysiological perspectives.

The finding of CBD anxiolytic efficacy in auditory fear conditioning is very exciting since it does not impair extinction learning. This finding supports the potential use of CBD in exposure therapy as an adjunct treatment. Moreover, it raises the question of its potential benefit at later stages of fear memory and extinction, namely fear renewal and recovery, that are types of fear relapse in patients. Computational model of fear memory and extinction network is a very good starting point for the investigation of the other areas involved in fear memory and extinction. Computational modelling is able to incorporate multi-modal information and together with quantitative systems pharmacology models might bring a new era of anxiolytic drug development. Electrophysiological characterization of the VH, PL and IL activity and interactions during extinction recall, compared to fear recall support the involvement of VH, PL as well as PL-IL communication in fear expression. Specifically, we are one of the first to report the PL-IL interaction during an auditory fear memory paradigm. Further studies should investigate the effect of anxiolytic drugs on these electrophysiological phenomena during the auditory fear memory paradigm. Such developments could eventually lead to an improvement in the quality of life for the 14% of Europeans suffering from anxiety disorders each year.

A

APPENDIX A

A.1 PIP PLACEMENT REFLECTION PIECE

For my PIP placement I went to work in Dr Sander Bohte's lab at the national research institute for mathematics and computer science, Centrum Wiskunde und Informatica, located at the Amsterdam Science Park. I was working on a machine reinforcement learning neural network model employing error-backpropagation algorithm tasked to mimic primate undergoing a working memory task. In particular, I was tasked with extending the model's framework to turn the critic-only model into an actor-critic model.

I started with learning the basics of machine learning algorithms and programming them in python. Since machine learning is a branch of computer science, it was a completely new discipline for me. Therefore, I had to learn quite a few computer science concepts along the way. I enjoyed the challenge since the placement supervisor gave me tasks of increasing difficulty without making them too demanding to get me used to working with various algorithms. Once I completed this training I went on to improve AGREL and AuGMEnT models. I have completed the work on AGREL model, but AuGMEnT model still requires some finishing touches.

Overall, I enjoyed this experience very much. I put myself out of my comfort zone by picking a quite challenging placement, but managed to do quite well. In fact, the supervisor expressed his wish to work with me in the future. I have found that the PIP placement was a very rewarding experience and would recommend

other students to challenge themselves when picking a placement project since the experience is worth it.

B

APPENDIX B

The source code for the fear memory and extinction network in Chapter 3 can be downloaded from the following link:
https://1drv.ms/f/s!Ak-2Gea626sKhMkQn2ATgf1Se-IhFQ

B.1 MODELLING CHAPTER SCRIPT EXAMPLES

B.1.1 *Model simulation*

The examples of Python 2.7 Brian2 code snippets used in the model scripts are provided below. Some of the examples present the code in a different sequence than it appears in the modelling script. This was done to improve the clarity and readability of the examples.

The model script was initialized by declaring the libraries used for simulation and setting up Brian2 to compile the script into C++ low level instructions:

```
import matplotlib
matplotlib.use('Agg')  # Necessary for headless running
import numpy
from brian2 import *  # Should be last - overwrites some numpy functions

set_device('cpp_standalone')
```

Each of the 72 simulation scripts contained the conditions for the experiment. A seed for the pseudo-random number generator was specified for each matched set together with the model treatment which in this case is PL-IL disconnection:

```
seed = 7
np.random.seed(seed)


pl5_il5_connected = False
```

The sizes of excitatory and inhibitory neuronal populations were declared. Their neuronal objects and Poisson inputs were created and connected using basic synaptic objects. In total there were 10 neuronal populations created using this method, representing excitatory and inhibitory populations of PL2, PL5, IL2, IL5 and VH (CA1). In contrast to other populations, a representation of BLA was composed of only excitatory neurons. The example below shows the construction of PL2 excitatory population:

```
pl2_Ne = 320

# Regular Izhikevich params
Cm_e = 150 * pF
k_e = 1.2 * pA / mV / mV
vr_e = -75 * mV
vt_e = -45 * mV
vpeak_e = 50 * mV
a_e = 0.01 * kHz
b_e = 5 * pA / mV
c_e = -56 * mV
d_e = 130 * pA

eqs_E = '''

dv/dt = (k_e*(v-vr_e)*(v-vt_e) - u - I)/Cm_e   : volt
du/dt = (a_e*(b_e*(v-vr_e)-u))                 : amp
I = I_syn                                      : amp
I_syn = I_NMDA + I_AMPA + I_GABA               : amp

sv=1.50265/(1+0.33*exp(-v/(16*mV)))            : 1
```

```
I_NMDA = g_NMDA*sv*v                              : amp
I_AMPA = g_AMPA*v                                 : amp
I_GABA = g_GABA*(v+75*mV)                         : amp

g_NMDA = g_NMDA_pl2_ex_to_pl2 + g_NMDA_pl5_ex_to_pl2 + g_NMDA_ca1_ex_to_pl5 +
g_NMDA_pl5_ex_to_pl5 + g_NMDA_il5_ex_to_pl5 + g_NMDA_bla_ex_to_pl5 +
g_NMDA_il2_ex_to_il2 + g_NMDA_il5_ex_to_il2 + g_NMDA_ca1_ex_to_il5 +
g_NMDA_pl5_ex_to_il5 + g_NMDA_il5_ex_to_il5 + g_NMDA_bla_ex_to_il5 +
g_NMDA_bkgr_exc_pl2 + g_NMDA_bkgr_exc_pl5 + g_NMDA_bkgr_exc_il2 +
    g_NMDA_bkgr_exc_il5     : siemens

g_NMDA_bkgr_exc_pl2     : siemens
g_NMDA_bkgr_exc_pl5     : siemens
g_NMDA_bkgr_exc_il2     : siemens
g_NMDA_bkgr_exc_il5     : siemens

g_NMDA_pl2_ex_to_pl2    : siemens
g_NMDA_pl5_ex_to_pl2    : siemens

g_NMDA_ca1_ex_to_pl5    : siemens
g_NMDA_pl5_ex_to_pl5    : siemens
g_NMDA_il5_ex_to_pl5    : siemens
g_NMDA_bla_ex_to_pl5    : siemens

g_NMDA_il2_ex_to_il2    : siemens
g_NMDA_il5_ex_to_il2    : siemens

g_NMDA_ca1_ex_to_il5    : siemens
g_NMDA_pl5_ex_to_il5    : siemens
g_NMDA_il5_ex_to_il5    : siemens
g_NMDA_bla_ex_to_il5    : siemens

g_AMPA = g_AMPA_pl2_ex_to_pl2 + g_AMPA_pl5_ex_to_pl2 + g_AMPA_ca1_ex_to_pl5 +
g_AMPA_pl5_ex_to_pl5 + g_AMPA_il5_ex_to_pl5 + g_AMPA_bla_ex_to_pl5 +
g_AMPA_il2_ex_to_il2 + g_AMPA_il5_ex_to_il2 + g_AMPA_ca1_ex_to_il5 +
g_AMPA_pl5_ex_to_il5 + g_AMPA_il5_ex_to_il5 + g_AMPA_bla_ex_to_il5 +
```

```
g_AMPA_bkgr_exc_pl2 + g_AMPA_bkgr_exc_pl5 + g_AMPA_bkgr_exc_il2 +
    g_AMPA_bkgr_exc_il5     : siemens

g_AMPA_bkgr_exc_pl2     : siemens
g_AMPA_bkgr_exc_pl5     : siemens
g_AMPA_bkgr_exc_il2     : siemens
g_AMPA_bkgr_exc_il5     : siemens

g_AMPA_pl2_ex_to_pl2    : siemens
g_AMPA_pl5_ex_to_pl2    : siemens

g_AMPA_ca1_ex_to_pl5    : siemens
g_AMPA_pl5_ex_to_pl5    : siemens
g_AMPA_il5_ex_to_pl5    : siemens
g_AMPA_bla_ex_to_pl5    : siemens

g_AMPA_il2_ex_to_il2    : siemens
g_AMPA_il5_ex_to_il2    : siemens

g_AMPA_ca1_ex_to_il5    : siemens
g_AMPA_pl5_ex_to_il5    : siemens
g_AMPA_il5_ex_to_il5    : siemens
g_AMPA_bla_ex_to_il5    : siemens

g_GABA = g_GABA_pl2_inh_to_ex + g_GABA_pl5_inh_to_ex + g_GABA_il2_inh_to_ex +
g_GABA_il5_inh_to_ex    : siemens

g_GABA_pl2_inh_to_ex    : siemens
g_GABA_pl5_inh_to_ex    : siemens
g_GABA_il2_inh_to_ex    : siemens
g_GABA_il5_inh_to_ex    : siemens
'''
Threshold_E = 'v>=vpeak_e'
Reset_E = '''
v = c_e
u += d_e
'''
```

```
pl2_E = NeuronGroup(pl2_Ne, eqs_E, reset=Reset_E, threshold=Threshold_E,
    method='euler')

bkgr_pl2_E = PoissonGroup(pl2_Ne, rates=460*Hz)

# Synaptic parameters
tau_AMPA_rise = 0.55*ms
tau_AMPA_decay = 2.2*ms
tau_NMDA_rise = 10.7*ms
tau_NMDA_decay = 125*ms
tau_GABA_rise = 0.25*ms
tau_GABA_decay = 3.75*ms

invpeak_NMDA = (tau_NMDA_rise / tau_NMDA_decay) ** \
               (tau_NMDA_decay / (tau_NMDA_rise - tau_NMDA_decay))
invpeak_AMPA = (tau_AMPA_rise / tau_AMPA_decay) ** \
               (tau_AMPA_decay / (tau_AMPA_rise - tau_AMPA_decay))
invpeak_GABA = (tau_GABA_rise / tau_GABA_decay) ** \
               (tau_GABA_decay / (tau_GABA_rise - tau_GABA_decay))
tau_syn = 50 * ms
Ca_rest = 0.05  # in uM or 50 nM
f = 20
z = 2
F = 96485.332 * amp * second
V_spine = 4.1876e-18

g_AMPA_MAX = 1 * nsiemens
g_NMDA_MAX = 0.5 * nsiemens
g_GABA_MAX = 0.6 * nsiemens

syn_bkgr_exc_pl2 = '''
dx_NMDA_syn/dt = -x_NMDA_syn / tau_NMDA_rise  : siemens
dg_NMDA_syn/dt = (invpeak_NMDA * x_NMDA_syn - g_NMDA_syn) / tau_NMDA_decay  :
    siemens
g_NMDA_bkgr_exc_pl2_post = g_NMDA_syn  : siemens (summed)

dx_AMPA_syn/dt = -x_AMPA_syn / tau_AMPA_rise  : siemens
```

```
dg_AMPA_syn/dt = (invpeak_AMPA * x_AMPA_syn - g_AMPA_syn) / tau_AMPA_decay  :
    siemens
g_AMPA_bkgr_exc_pl2_post = g_AMPA_syn  : siemens (summed)
'''

syn_bkgr_exc_pre = '''
w_AMPA = g_AMPA_MAX
w_NMDA = g_NMDA_MAX
x_AMPA_syn += w_AMPA
x_NMDA_syn += w_NMDA
'''

bkgr_exc_pl2_syn = Synapses(bkgr_pl2_E, pl2_E, model=syn_bkgr_exc_pl2,
                            on_pre=syn_bkgr_exc_pre, delay=1*ms, method="
                                linear")
bkgr_exc_pl2_syn.connect(j='i')
```

A specific case was used for the three memory trace neuron populations of BLA, representing fear, extinction and extinction-resistant memory traces. The Poisson input patterns to these three populations had to be declared specifically. This is an example of the fear input to the BLA fear memory trace population:

```
fear_N = 60

fear_mt = 10
fear_baseline = 0

# Fear Poisson Source
habituation_fear = np.zeros(5)
conditioning_fear = np.arange(0, 2.01, 0.5)
ext_fear_early = np.flipud(np.arange(1, 2, 0.0909))
ext_fear_late = np.repeat(0, 12)
ext_fear = np.concatenate((ext_fear_early, ext_fear_late), axis=0)
extrec_fear = np.repeat(0, 2)
fear = np.hstack([habituation_fear, conditioning_fear, ext_fear, extrec_fear])
     * fear_mt + fear_baseline

fear_stimulus = TimedArray(fear * Hz, dt=20000.*ms)
```

```
fear_Poisson = PoissonGroup(fear_N, rates='fear_stimulus(t)')

# Static Fear, Extinction and Extinction-resistant Poisson input weight
input_w = 5

# Poisson background input general equation (inputs arriving into units as
    g_NMDA_bkgr and g_AMPA_bkgr)
syn_fear_exc = '''
dx_NMDA_syn/dt = -x_NMDA_syn / tau_NMDA_rise  : siemens
dg_NMDA_syn/dt = (invpeak_NMDA * x_NMDA_syn - g_NMDA_syn) / tau_NMDA_decay  :
    siemens
g_NMDA_fear_post = g_NMDA_syn  : siemens (summed)

dx_AMPA_syn/dt = -x_AMPA_syn / tau_AMPA_rise  : siemens
dg_AMPA_syn/dt = (invpeak_AMPA * x_AMPA_syn - g_AMPA_syn) / tau_AMPA_decay  :
    siemens
g_AMPA_fear_post = g_AMPA_syn  : siemens (summed)
'''

# Complementary Poisson background input on_pre condition
syn_fear_exc_pre = '''
w_AMPA = input_w * g_AMPA_MAX
w_NMDA = input_w * g_NMDA_MAX
x_AMPA_syn += w_AMPA
x_NMDA_syn += w_NMDA
'''

# Stimuli which input on their corresponding BLA units
fear_syn = Synapses(fear_Poisson, BLA_E, model=syn_fear_exc,
                    on_pre=syn_fear_exc_pre, method="linear")
fear_syn_i = np.arange(fear_N)
fear_syn_j = np.arange(fear_N)
fear_syn.connect(i=fear_syn_i, j=fear_syn_j)
```

Neuronal indices for synaptic connections were generated using two custom functions, one of which is shown below:

```
def conn_tuple(n_fr, fraction_from, spread_to, n_to, connect_to_self=False):
    """
    Takes N of 'i' and 'j' units, fraction of 'i' being connected (1 == all)
```

```
    and a 'spread' to 'j' (e.g. spread = 4, 4 'j' neurons per 'i' being
    connected) and produces a tuple [0] representing 'i' integers and [1]
    representing 'j' integers of neurons for Brian2 format.
    syn_con_gen_v2.py
    """

    if n_fr != n_to:  # Connecting two different areas
        if spread_to <= n_to:  # Check that spread is within the number of to
            fr = np.sort(np.repeat(np.random.choice(n_fr, int(n_fr *
                fraction_from), replace=False), spread_to))
            to = np.array([], dtype=int)
            for _ in np.unique(fr):
                selection = np.random.choice(n_to, spread_to, replace=False)
                to = np.concatenate((to, selection), axis=0)
                #           return np.array([fr,to])
        else:
            print "The spread_to is too high. Please set it lower than n_to"

    else:  # n_fr == n_to (i.e. is self-connected)
        if connect_to_self is False:  # Condition 'i != j'
            if spread_to <= n_to - 1:  # Check that spread is within n_to -
                self
                fr = np.sort(np.repeat(np.random.choice(n_fr, int(n_fr *
                    fraction_from), replace=False), spread_to))
                to = np.array([], dtype=int)
                for each in np.unique(fr):
                    # Create array of n_to range and remove the i value to
                        prevent autoconn
                    # arr_to_temp = np.delete(np.arange(n_to),np.where(n_j ==
                        i)[0])
                    arr_to_temp = np.delete(np.arange(n_to), np.where(np.
                        arange(n_to) == each)[0])
                    selection = np.random.choice(arr_to_temp, spread_to,
                        replace=False)
                    to = np.concatenate((to, selection), axis=0)
            else:
```

```
                print "The_spread_to_is_too_high._Please_set_it_lower_than_
                    n_to_-_1"

        elif connect_to_self:  # Condition 'i == j' possible
            if spread_to <= n_to:
                fr = np.sort(np.repeat(np.random.choice(n_fr, int(n_fr *
                    fraction_from), replace=False), spread_to))
                to = np.array([], dtype=int)
                for _ in np.unique(fr):
                    selection = np.random.choice(n_to, spread_to, replace=
                        False)
                    to = np.concatenate((to, selection), axis=0)
                    #                return np.array([fr,to])
            else:
                print "The_spread_to_is_too_high._Please_set_it_lower_than_
                    n_to"
    return np.array([fr, to])  # i=Tuple[0], j=Tuple[1]
```

Synaptic objects connecting neuronal objects as well as Poisson inputs to them were specified individually. There were 13 synaptic objects for Poisson inputs to neuronal populations, representing Poisson inputs to the excitatory and inhibitory PL2, PL5, IL2, IL5 and VH (CA1) as well as the three memory trace populations of BLA. There were 17 synaptic objects representing excitatory to excitatory projects, 5 synaptic objects representing excitatory to inhbitory projections and 7 synaptic objects representing inhibitory to excitatory projections. The example below shows one synaptic object interconnecting PL2 excitatory to excitatory neurons:

```
# Synaptic parameters
tau_AMPA_rise = 0.55*ms
tau_AMPA_decay = 2.2*ms
tau_NMDA_rise = 10.7*ms
tau_NMDA_decay = 125*ms
tau_GABA_rise = 0.25*ms
tau_GABA_decay = 3.75*ms

invpeak_NMDA = (tau_NMDA_rise / tau_NMDA_decay) ** \
```

```
                (tau_NMDA_decay / (tau_NMDA_rise - tau_NMDA_decay))
invpeak_AMPA = (tau_AMPA_rise / tau_AMPA_decay) ** \
                (tau_AMPA_decay / (tau_AMPA_rise - tau_AMPA_decay))
invpeak_GABA = (tau_GABA_rise / tau_GABA_decay) ** \
                (tau_GABA_decay / (tau_GABA_rise - tau_GABA_decay))
tau_syn = 50 * ms
Ca_rest = 0.05  # in uM or 50 nM
f = 20
z = 2
F = 96485.332 * amp * second
V_spine = 4.1876e-18

g_AMPA_MAX = 1 * nsiemens
g_NMDA_MAX = 0.5 * nsiemens
g_GABA_MAX = 0.6 * nsiemens

within_EE_w0 = 2
within_EE_lambda_rise = 2 * Hz
within_EE_lambda_decay = 0.001 * Hz
within_EE_w_min = 0.8 * within_EE_w0
within_EE_w_max = 3 * within_EE_w0
within_EE_theta_dep = 0.5
within_EE_theta_pot = 0.6
within_EE_a_syn = 17000

syn_eqs_pl2_ex_to_pl2 = '''
w_clip          : 1
w_AMPA          : siemens
w_NMDA          : siemens

w0              : 1 (constant)
lambda_rise     : hertz (constant)
lambda_decay    : hertz (constant)
w_min           : 1 (constant)
w_max           : 1 (constant)
theta_dep       : 1 (constant)
theta_pot       : 1 (constant)
a_syn           : 1 (constant)
```

```
dx_NMDA_syn/dt = -x_NMDA_syn / tau_NMDA_rise  : siemens (clock-driven)
dg_NMDA_syn/dt = (invpeak_NMDA * x_NMDA_syn - g_NMDA_syn) / tau_NMDA_decay  :
    siemens (clock-driven)
g_NMDA_pl2_ex_to_pl2_post = g_NMDA_syn  : siemens (summed)

dx_AMPA_syn/dt = -x_AMPA_syn / tau_AMPA_rise  : siemens (clock-driven)
dg_AMPA_syn/dt = (invpeak_AMPA * x_AMPA_syn - g_AMPA_syn) / tau_AMPA_decay  :
    siemens (clock-driven)
g_AMPA_pl2_ex_to_pl2_post = g_AMPA_syn  : siemens (summed)

sv_syn = 1.50265 / (1 + 0.33 * exp(-v_post / (16 * mV)))  : 1
I_Ca_NMDA = (0.015 / w0) * g_NMDA_syn * sv_syn * (v_post - (120*mV))  : amp
dCa_E/dt = -f * (I_Ca_NMDA / (z * F * V_spine)) + (Ca_rest - Ca_E) / tau_syn
    : 1 (clock-driven)

eta_E_Ca = int(Ca_E < 0.389) * (1 / (1 + exp(13 * -Ca_E + 5.5)))
+ int(Ca_E >= 0.389) * (1 / (1.25 + exp(9.2 * -Ca_E + 4) -0.2))  : 1

omega_E_Ca = int(Ca_E <= theta_dep) * 0 + int(Ca_E > theta_dep and
Ca_E < theta_pot) * (a_syn * (Ca_E-((theta_pot + theta_dep) / 2)) ** 4 - 0.1)
+ int(Ca_E >= theta_pot) * (1.2 / (1 + exp(-35 * (Ca_E - theta_pot
- 0.045))) - 0.2)  : 1

dEwt/dt = eta_E_Ca * ((lambda_rise * omega_E_Ca) - lambda_decay * Ewt)  : 1 (
    clock-driven)
'''

pl2_ex_to_pl2_syn = Synapses(pl2_E, model=syn_eqs_pl2_ex_to_pl2, on_pre=
    pre_eqs_ex,
                             delay=pl2_ex_to_pl2_syn_delay, method='euler')
pl2_ex_to_pl2_syn.connect(i=pl2_ex_to_pl2_syn_conn[0], j=
    pl2_ex_to_pl2_syn_conn[1])

pl2_ex_to_pl2_syn.w0 = within_EE_w0
pl2_ex_to_pl2_syn.lambda_rise = within_EE_lambda_rise
pl2_ex_to_pl2_syn.lambda_decay = within_EE_lambda_decay
```

```
pl2_ex_to_pl2_syn.w_min = within_EE_w_min
pl2_ex_to_pl2_syn.w_max = within_EE_w_max
pl2_ex_to_pl2_syn.theta_dep = within_EE_theta_dep
pl2_ex_to_pl2_syn.theta_pot = within_EE_theta_pot
pl2_ex_to_pl2_syn.a_syn = within_EE_a_syn

pl2_ex_to_pl2_syn.Ewt = within_EE_w0
pl2_ex_to_pl2_syn.w_clip = within_EE_w0
pl2_ex_to_pl2_syn.Ca_E = Ca_rest
```

Neuronal objects were recorded using SpikeMonitor and PopulationRate-Monitor functions, whereas synaptic variables were recorded using StateMonitor function of Brian2 simulation software. There were 14 SpikeMonitor objects, 14 PopulationRateMonitor objects and 29 StateMonitor objects used per simulation. The example below shows one instance of each monitor used in the simulation:

```
pl2_E_mon = SpikeMonitor(pl2_E)

pl2_E_PRM = PopulationRateMonitor(pl2_E)

pl2_ex_to_pl2_syn_mon = StateMonitor(pl2_ex_to_pl2_syn, ['w_clip', 'Ca_E'], dt
    =1*second, record=pl2_ex_to_pl2_syn_ind)
```

The network was assembled and the simulation was run for 680 seconds. A C/C++ function showing the progress in the linux terminal window was included in the simulation script:

```
net = Network(collect())

duration = 680000 * ms
net.run(duration, report='std::cout << (int)(completed*100.) << "% completed" <<
    std::endl;')
```

The recorded data were saved to file using custom scripts depending on the monitor function used and the variable recorded. The example below shows the function processing SpikeMonitor recordings and one instance of this function call:

```
def dump_neuronmon(neuronmon, filename):
    """
```

```
    This script extracts times and indices of neurons from a given
        StateMonitor set up
    for a Brian2 simulation script. It has a naming hack that allows the saved
         file to
    be named after the name of the StateMonitor object used here as a function
         parameter.

    :param neuronmon: A SpikeMonitor recording neuronal population
    :param filename: A desired filename for the data set. Must be a string
        ("")
    :return: Saves spike times and indices for the set neuronal population in
        .npy files
    """
    neuronmon_times = neuronmon.get_states(units=False).get('t')
    neuronmon_index = neuronmon.get_states().get('i')
    filename_times = "%s_times_no_units.npy" % filename
    filename_index = "%s_index.npy" % filename

    # Append file entries to a master list to facilitate restoration
    with open("dump_neuronmon_master.txt", "a") as myfile:
        myfile.write("%s_times_no_units.npy" % filename)
        myfile.write("%s_index.npy" % filename)

    np.save(filename_times, neuronmon_times)
    np.save(filename_index, neuronmon_index)

dump_neuronmon(pl2_E_mon, "PL2_E_mon")
```

B.1.2 *PL-IL disconnection and VH inactivation in the model*

PL-IL was disconnected and VH was inactivated by passing a boolean value `'False'` to the relevant synaptic and neuronal objects' attribute `"object.active"`:

```
pl5_il5_connected = False
VH_intact = True  # If false disables all VH; its inputs and its outputs

CA1_E.active = VH_intact  # Toggle for VH removal
```

```
CA1_I.active = VH_intact

bkgr_CA1.active = VH_intact

bkgr_CA1_I.active = VH_intact

bkgr_inh_ca1_syn.active = VH_intact

bkgr_CA1_syn.active = VH_intact

ca1_ex_to_ca1_syn.active = VH_intact

bla_ex_to_ca1_syn.active = VH_intact

bla_ex_to_ca1_syn.active = VH_intact

il5_ex_to_pl5_syn.active = pl5_il5_connected

bla_ex_to_ca1_syn.active = VH_intact

pl5_ex_to_il5_syn.active = pl5_il5_connected

ca1_ex_to_bla_syn.active = VH_intact

ca1_ex_to_inh_syn.active = VH_intact

ca1_inh_to_ex_syn.active = VH_intact

pl5_ex_to_il5_inh_syn.active = pl5_il5_connected

il5_ex_to_pl5_inh_syn.active = pl5_il5_connected
```

B.1.3 *Model data extraction for analysis*

Model data was extracted using a custom script which extracts only BLA input responsive neuron activity during habituation, early and late extinction:

```
#!bin/python
import numpy as np
import pandas as pd
import os


def find_responsive(seed):
    """
    Needs to be in root dir with simulation folders
    Calculates responsive indices for each seed (treatment groups should have
        identical responsiveness)
    :param seed: 1-30
    :return: resp_ind - a dictionary of indices for PL2, PL5, IL2, IL5
    save .txt with narrative and gen stats in the root folder
    """

    # Folder name for each seed
    folder = 'full_expt_fextres_12_1_seed{}_control'.format(seed)

    # Make (if necessary) new directory and change to it
    current = os.getcwd()  # Get current directory
    newpath = r'{}/{}'.format(current, folder)  # Current dir + new folder
    if not os.path.exists(newpath):
        print('Error - no such directory')
    os.chdir(newpath)

    # Dictionary to store responsive indices per area, with key being the
        spikemon name
    resp_ind = {
        "IL2": [],
        "IL5": [],
        "PL2": [],
```

```
    "PL5": []}

# Stage sampling times in seconds, picked 80 for a good sample size
hab_times = np.arange(9, 89, 1)
eext_times = np.arange(209, 289, 1)
lext_times = np.arange(589, 669, 1)

# Each spikemon indexes neurons from 0 so need to be careful here
for spikemon in resp_ind:
    times = np.load("{}/{}_E_mon_times_no_units.npy".format(newpath,
        spikemon))
    index = np.load("{}/{}_E_mon_index.npy".format(newpath, spikemon))
    unique_index = np.unique(index)
    neurons = {}

    # Generate an empty list to store indices of responsive neurons
    resp_list = []

    # For each unique neuron
    for i in unique_index:
        # For each entry for that unique neuron
        for j in np.where(index == i):
            # Populate each unique neuron with its firing times
            neurons[int(i)] = times[j]

        # Create empty arrays for firing rates per stage with col
            representing unique neurons
        hab_rates = np.zeros([len(hab_times), len(unique_index)])
        eext_rates = np.zeros([len(eext_times), len(unique_index)])
        lext_rates = np.zeros([len(lext_times), len(unique_index)])

        # Bin firing instances per second (T) into the previously
            generated empty arrays
        for idx, T in enumerate(hab_times):
            hab_rates[idx, i] = len(np.where(np.logical_and(neurons[i] >=
                float(T)+0, neurons[i] < float(T)+1))[0])
```

```
            for idx, T in enumerate(eext_times):
                eext_rates[idx, i] = len(np.where(np.logical_and(neurons[i] >=
                    float(T)+0, neurons[i] < float(T)+1))[0])

            for idx, T in enumerate(lext_times):
                lext_rates[idx, i] = len(np.where(np.logical_and(neurons[i] >=
                    float(T)+0, neurons[i] < float(T)+1))[0])

            # Calculate means and hab SD for each unique neuron
            hab_mean = np.average(hab_rates[:, i])
            hab_sd = np.std(hab_rates[:, i])
            base_2sd = hab_mean + 2 * hab_sd
            eext_mean = np.average(eext_rates[:, i])
            lext_mean = np.average(lext_rates[:, i])

            # If the unique neuron is 'tone responsive'
            if spikemon == 'PL2' or spikemon == 'PL5':
                if base_2sd < eext_mean:
                    resp_list.append(i)
            elif spikemon == 'IL2' or spikemon == 'IL5':
                if base_2sd < lext_mean:
                    resp_list.append(i)

            # This is universal - should be eext for PL and lext for IL!
#            if base_2sd < eext_mean or base_2sd < lext_mean:
#                resp_list.append(i)

        # Insert responsive neuron index list into the respective spikemon
            dictionary value
        resp_ind[spikemon] = resp_list

        # Change directory to root and add a narrative output to a txt file
        os.chdir(current)
        with open('narrative.txt', 'a') as myfile:
            myfile.write(folder)
            myfile.write(spikemon)
            myfile.write('\n\t Total Neurons {}'.format(len(unique_index)))
```

```
            myfile.write('\n\t_Responsive_neurons_{}'.format(len(resp_list)))
            myfile.write('\n\t_Fraction_of_responsive_neurons_{}'.format(len(
                resp_list)/len(unique_index)))
            myfile.write('\n_\n')

        # Return to operating directory
        os.chdir(newpath)

    # Save a .npy containing responsive indices to _control folder of the
        respective seed
    np.save('{}_responsive_index.npy'.format(folder), resp_ind)

    os.chdir(current)
    print resp_ind
    return resp_ind


def generate_container():
    firing_rate = {
        'id': [],
        'mean_hab': [],
        'mean_eext': [],
        'mean_lext': [],
        'seed': [],
        'treatment': [],
        'area': [],
        'subdivision': [],
    }
    return firing_rate


def extract_responsive(seed, resp_ind, firing_rate):
    """

    :param seed: seed of the run in question
    :param resp_ind: responsive indices for the respective seed (control
        resp_ind apply to other treatment groups)
```

```
:param firing_rate: dict containing firing rates for neurons to append
    data to
:return: firing_rate
"""
current = os.getcwd()  # Get current directory
treatment_list = ['control', 'no_plil', 'no___vh']

# Area index for spikemons
area = {
    'PL2': 0,
    'PL5': 0,
    'IL2': 1,
    'IL5': 1
}

# Subdivision index for spikemons
subdivision = {
    'PL2': 2,
    'PL5': 5,
    'IL2': 2,
    'IL5': 5
}

# Stage sampling times in seconds, picked 80 for a good sample size
hab_times = np.arange(9, 89, 1)
eext_times = np.arange(209, 289, 1)
lext_times = np.arange(589, 669, 1)

for t_index, treatment in enumerate(treatment_list):
    # Folder name for each seed and treatment
    folder = 'full_expt_fextres_12_1_seed{}_{}'.format(seed, treatment)

    # Make (if necessary) new directory and change to it
    newpath = r'{}/{}'.format(current, folder)  # Current dir + new folder
    if not os.path.exists(newpath):
        print "Error - folder does not exist"
    os.chdir(newpath)
```

```
# Each spikemon indexes from 0 so need to be careful here
for spikemon, val in resp_ind.iteritems():
    times = np.load("{}/{}_E_mon_times_no_units.npy".format(newpath,
        spikemon))
    index = np.load("{}/{}_E_mon_index.npy".format(newpath, spikemon))
    unique_index = np.unique(index)
    resp_list = resp_ind[spikemon]
    neurons = {}

    # Generate a dict of neurons : fire_times
    for i in unique_index:
        for j in np.where(index == i):
            neurons[int(i)] = times[j]

    for i in resp_list:
        # Create empty arrays for binning firing rates
        hab_rates = np.zeros(len(hab_times))
        eext_rates = np.zeros(len(eext_times))
        lext_rates = np.zeros(len(lext_times))

        # Bin firing instances per second (T) into the previously
            generated empty arrays
        for idx, T in enumerate(hab_times):
            hab_rates[idx] = len(np.where(np.logical_and(neurons[i] >=
                 float(T)+0, neurons[i] < float(T)+1))[0])

        for idx, T in enumerate(eext_times):
            eext_rates[idx] = len(np.where(np.logical_and(neurons[i]
                >= float(T)+0, neurons[i] < float(T)+1))[0])

        for idx, T in enumerate(lext_times):
            lext_rates[idx] = len(np.where(np.logical_and(neurons[i]
                >= float(T)+0, neurons[i] < float(T)+1))[0])

        # Calculate means for each responsive neuron and append to the
             list
```

```
                # Treatment [0, 1, 2]; seed [1:30]; area [0,1]; subdivision
                    [2,5];
                firing_rate['id'].append(i)
                firing_rate['mean_hab'].append(np.average(hab_rates))
                firing_rate['mean_eext'].append(np.average(eext_rates))
                firing_rate['mean_lext'].append(np.average(lext_rates))
                firing_rate['seed'].append(seed)
                firing_rate['treatment'].append(t_index)
                firing_rate['area'].append(area[spikemon])
                firing_rate['subdivision'].append(subdivision[spikemon])

    df_fr = pd.DataFrame.from_dict(firing_rate)
    df_fr.to_csv("{}/seed_{}_firing_rates.csv".format(current, seed), mode='a'
        , index=None, header=True)

    with open('readme.txt', 'a') as myfile:
        myfile.write(folder)
        myfile.write('\n Treatment [0, 1, 2]; seed [1:30]; area [0,1];
            subdivision [2,5];')
        myfile.write('\n WARNING: id reflects unique neurons of the same seed
            and same treatment')
        myfile.write('\n That said, neurons should match across treatment
            groups for same seed')

    os.chdir(current)

    return firing_rate


def save_dict(firing_rate):
    df_alt = pd.DataFrame.from_dict(firing_rate)
    df_alt.to_csv('all_firing_rates.csv', mode='w', index=None, header=True)


firing_rate = generate_container()
for seed in xrange(1, 31):
    resp_ind = find_responsive(seed)
```

```
    firing_rate = extract_responsive(seed, resp_ind, firing_rate)

save_dict(firing_rate)
print('Done')
```

The output of this script was used to calculate mean PL and IL firing rates for each seed and treatment at habituation, early and late extinction.

B.2 ELECTROPHYSIOLOGY CHAPTER SCRIPT EXAMPLES

B.2.1 *Electrophysiology data filtering with Butterworth filter*

The CS timeseries data were filtered using 4 Hz high-pass Butterworth filter with default parameters of `elephant.signal.butter` function from the Python 2.7 Elephant package:

```
import scipy.io
import os
import numpy as np
import matplotlib
matplotlib.use('TkAgg')
import matplotlib.pyplot as plt
import cPickle as pickle
import elephant

mat = scipy.io.loadmat('Data/RJ_dat.mat')

"""
mat file has a dat matrix
[dur_CS, area, CS, stage, animal]
dur_CS == 1250*30 = 37500
area : 0 - PL, 1 - IL, 2 - VH;
CS : 0 or 1 only
stage: 0 - fear recall, 1 - ext recall
animal: 0:9
"""
```

```
samp_rate = 1250.0
dur = 30
dur_CS = 1250*30

print mat['dat'][:, 0, 1, 1, 2]
print mat['dat'].dtype

filt_dat = np.zeros([dur_CS, 3, 2, 2, 10])
for area in [0, 1, 2]:
        for CS in [0, 1]:
                for stage in [0 , 1]:
                        for animal in xrange(10):
                                val = mat['dat'][:, area, CS, stage, animal]
                                val = np.ravel(val)
                                filt_val = elephant.signal_processing.butter(
                                    val, highpass_freq=4.0, fs=samp_rate)
                                filt_dat[:, area, CS, stage, animal] =
                                    filt_val

print filt_dat.shape
print mat['dat'][:, 0, 1, 1, 2]
print filt_dat[:, 0, 1, 1, 2]

x = np.linspace(0, 30, 37500)
plt.plot(x,mat['dat'][:, 2, 1, 1, 2], 'k', lw=2)
plt.plot(x,filt_dat[:, 2, 1, 1, 2], 'r', lw=1)
plt.show()

mat['dat'] = filt_dat
scipy.io.savemat('RJ_4filt_dat.mat', mat)
```

B.2.2 *Random picks of electrode channels if multiple ones are present*

Once noisy channels from the data set were removed, the remaining channels were picked randomly if multiple options were available per area of a single animal. This was done using `numpy.random.choice` function:

```
import numpy as np
import cPickle as pickle
import time

timestr = time.strftime('_%Y%m%d_%H%M')

both_clear_3cs = {
#                     PL                                IL
                                    VH                    CS
'S3':  [['ad17',                'ad20'], ['ad21',         'ad23', 'ad24'], ['
    ad26', 'ad28', 'ad30', 'ad32'], [1, 2, 3], [1, 2]],
'S7':  [[               'ad19', 'ad20'], ['ad21',         'ad23', 'ad24'], ['
    ad26', 'ad28', 'ad30', 'ad32'], [1, 2, 3], [1   ]], # Drop CS2 (i.e. CS1
    only)
'S10': [[                       'ad20'], ['ad21', 'ad22'                ], ['
    ad26', 'ad28', 'ad30', 'ad32'], [1, 2, 3], [1, 2]],
'S11': [[               'ad19', 'ad20'], ['ad21', 'ad22', 'ad23'        ], ['
    ad26',         'ad30', 'ad32'], [1, 2, 3], [1, 2]],
'S12': [[                       'ad20'], ['ad21', 'ad22'                ], ['
    ad26',         'ad30', 'ad32'], [1, 2, 3], [1   ]], # Drop CS2 (i.e. CS1
    only)
'S13': [[               'ad19'        ], ['ad21', 'ad22'                ], ['
    ad26', 'ad28', 'ad30'        ], [1, 2, 3], [1, 2]],
'S14': [['ad17', 'ad18', 'ad19'        ], [               'ad23', 'ad24'], ['
    ad26', 'ad28', 'ad30', 'ad32'], [1, 2, 3], [1, 2]],
'S15': [['ad17', 'ad18', 'ad19', 'ad20'], ['ad21', 'ad22',         'ad24'], ['
    ad26', 'ad28'                ], [1, 2, 3], [1, 2]],
'S17': [[               'ad19', 'ad20'], ['ad21', 'ad22'                ], ['
    ad26', 'ad28', 'ad30', 'ad32'], [1, 2, 3], [1, 2]],
'S19': [[       'ad18', 'ad19', 'ad20'], ['ad21', 'ad22', 'ad23', 'ad24'], ['
    ad26', 'ad28', 'ad30', 'ad32'], [1, 2, 3], [1, 2]]
```

```
}


picks = {}
for k in both_clear_3cs.keys():
    picks[k] = [np.random.choice(both_clear_3cs[k][0]), np.random.choice(
        both_clear_3cs[k][1]), np.random.choice(
            both_clear_3cs[k][2]), both_clear_3cs[k][3], both_clear_3cs[k][4]]

with open('ext_cs3_picks{}.pickle'.format(timestr), 'wb') as myfile:
    pickle.dump(picks, myfile, protocol=pickle.HIGHEST_PROTOCOL)

print picks
```

B.2.3 *Data analysis with Matlab NeuroSpec2 package*

The electrophysiological data was analysed individually for VH, PL and IL power spectra comparison at fear recall compared to extinction recall as well as VH-PL, VH-IL and PL-IL coherence comparison at fear recall compared to extinction recall. An example of VH analysis is shown below:

```
clear
load RJ_4filt_dat

[dur_samp, n_chan, n_trig, n_condition, n_fil] = size(dat);
% n_chan = 1 is PL, 2 is IL, 3 is VH
% n_trig is CS
% n_condition 1 is Fear Recall, 2 is Ext Recall
trig_times = [1; 37501];
duration = [37500; 37500];
samp_rate = 1250;
seg_pwr = 10;
opt_str = '';

for ind=1:n_fil
    vals1_cs1 = dat(:,3,1,1,ind);
```

```
vals1_cs2 = dat(:,3,2,1,ind);
vals1_both = [vals1_cs1; vals1_cs2];

vals2_cs1 = dat(:,3,1,2,ind);
vals2_cs2 = dat(:,3,2,2,ind);
vals2_both = [vals2_cs1; vals2_cs2];
% If vals2 has only 1 CS, use type 0 with 1 cs each
if (max(vals2_cs2)==0)
    [f1(:,:,ind),t1(:,:,ind),cl1(ind),sc1(:,:,ind)] = sp2a2_m1(0,vals1_cs1
        ,vals2_cs1,samp_rate,seg_pwr,opt_str);
    cl1(ind).what=['Set: ',num2str(ind)];

     % Pooled analysis
     if (ind==1)
     % Separate call for first set, creates new pooled analysis.
         [plf1,plv1]=pool_scf(sc1(:,:,ind),cl1(ind));
     else
     % Pass pooled variables as arguments for further sets.
         [plf1,plv1]=pool_scf(sc1(:,:,ind),cl1(ind),plf1,plv1);
     end


else % Otherwise use Type 1 analysis with 2 cs each
    [f1(:,:,ind),t1(:,:,ind),cl1(ind),sc1(:,:,ind)] = sp2a2_m1(1,
        vals1_both,vals2_both,trig_times,duration,samp_rate,seg_pwr,
        opt_str);
    cl1(ind).what=['Set: ',num2str(ind)];

     % Pooled analysis
     if (ind==1)
     % Separate call for first set, creates new pooled analysis.
         [plf1,plv1]=pool_scf(sc1(:,:,ind),cl1(ind));
     else
     % Pass pooled variables as arguments for further sets.
         [plf1,plv1]=pool_scf(sc1(:,:,ind),cl1(ind),plf1,plv1);
     end
end
```

```
end


% Plotting parameters
freq=45;
ch_max=1;
lag_tot=100;
lag_neg=50;
chi_max=0;% Will auto scale

% Process pooled spectral coefficients & plot
[f2,t2,cl2,sc2]=pool_scf_out(plf1,plv1);
figure
cl2.what='VH_Fear_Recall_(fa)_vs_Ext_Recall_(fb)';
psp2_theta_pool6(f2,t2,cl2,freq,lag_tot,lag_neg,ch_max,chi_max)


[f4,cl4]=sp2_compf99(sc2,cl2,2,sc2,cl2,1);
cl4.what='VH_Fear_Recall_vs_Ext_Recall_Log_Ratio'
figure
psp_compf199(f4,cl4,45)

save('V3_VH_pool.mat','f2','f4','cl4')
```

An example of VH-PL coherence analysis is shown below:

```
clear
load RJ_4filt_dat

[dur_samp, n_chan, n_trig, n_condition, n_fil] = size(dat);
% n_chan = 1 is PL, 2 is IL, 3 is VH
% n_trig is CS
% n_condition 1 is Fear Recall, 2 is Ext Recall
trig_times = [1; 37501];
duration = [37500; 37500];
samp_rate = 1250;
seg_pwr = 10;
opt_str = '';
```

```
for ind=1:n_fil
    vals1_cs1 = dat(:,3,1,1,ind);
    vals1_cs2 = dat(:,3,2,1,ind);
    vals1_both = [vals1_cs1; vals1_cs2];

    vals2_cs1 = dat(:,1,1,1,ind);
    vals2_cs2 = dat(:,1,2,1,ind);
    vals2_both = [vals2_cs1; vals2_cs2];
    % If vals2 has only 1 CS, use type 0 with 1 cs each
    if (max(dat(:,1,2,2,ind))==0)
        [f1(:,:,ind),t1(:,:,ind),cl1(ind),sc1(:,:,ind)] = sp2a2_m1(0,vals1_cs1
            ,vals2_cs1,samp_rate,seg_pwr,opt_str);
        cl1(ind).what=['Set:␣',num2str(ind)];

         % Pooled analysis
         if (ind==1)
         % Separate call for first set, creates new pooled analysis.
             [plf1,plv1]=pool_scf(sc1(:,:,ind),cl1(ind));
         else
         % Pass pooled variables as arguments for further sets.
             [plf1,plv1]=pool_scf(sc1(:,:,ind),cl1(ind),plf1,plv1);
         end


    else % Otherwise use Type 1 analysis with 2 cs each
        [f1(:,:,ind),t1(:,:,ind),cl1(ind),sc1(:,:,ind)] = sp2a2_m1(1,
            vals1_both,vals2_both,trig_times,duration,samp_rate,seg_pwr,
            opt_str);
        cl1(ind).what=['Set:␣',num2str(ind)];

         % Pooled analysis
         if (ind==1)
         % Separate call for first set, creates new pooled analysis.
             [plf1,plv1]=pool_scf(sc1(:,:,ind),cl1(ind));
         else
         % Pass pooled variables as arguments for further sets.
```

```
            [plf1,plv1]=pool_scf(sc1(:,:,ind),cl1(ind),plf1,plv1);
        end
    end
end


% Plotting parameters
freq=45;
ch_max=1;
lag_tot=100;
lag_neg=50;
chi_max=0;% Will auto scale

% Process pooled spectral coefficients & plot
[f2,t2,cl2,sc2]=pool_scf_out(plf1,plv1);
figure
cl2.what='VH_Fear_Recall_(fa)_vs_PL_Fear_Recall_(fb)';
psp2_theta_pool6(f2,t2,cl2,freq,lag_tot,lag_neg,ch_max,chi_max)


clear plf1, plv1

for ind=1:n_fil
    vals1_cs1 = dat(:,3,1,2,ind);
    vals1_cs2 = dat(:,3,2,2,ind);
    vals1_both = [vals1_cs1; vals1_cs2];

    vals2_cs1 = dat(:,1,1,2,ind);
    vals2_cs2 = dat(:,1,2,2,ind);
    vals2_both = [vals2_cs1; vals2_cs2];
    % If vals2 has only 1 CS, use type 0 with 1 cs each
    if (max(dat(:,1,2,2,ind))==0)
        [f1(:,:,ind),t1(:,:,ind),cl1(ind),sc1(:,:,ind)] = sp2a2_m1(0,vals1_cs1
            ,vals2_cs1,samp_rate,seg_pwr,opt_str);
        cl1(ind).what=['Set:_',num2str(ind)];

         % Pooled analysis
```

```
        if (ind==1)
        % Separate call for first set, creates new pooled analysis.
            [plf1,plv1]=pool_scf(sc1(:,:,ind),cl1(ind));
        else
        % Pass pooled variables as arguments for further sets.
            [plf1,plv1]=pool_scf(sc1(:,:,ind),cl1(ind),plf1,plv1);
        end


    else % Otherwise use Type 1 analysis with 2 cs each
        [f1(:,:,ind),t1(:,:,ind),cl1(ind),sc1(:,:,ind)] = sp2a2_m1(1,
            vals1_both,vals2_both,trig_times,duration,samp_rate,seg_pwr,
            opt_str);
        cl1(ind).what=['Set:_',num2str(ind)];

        % Pooled analysis
        if (ind==1)
        % Separate call for first set, creates new pooled analysis.
            [plf1,plv1]=pool_scf(sc1(:,:,ind),cl1(ind));
        else
        % Pass pooled variables as arguments for further sets.
            [plf1,plv1]=pool_scf(sc1(:,:,ind),cl1(ind),plf1,plv1);
        end
    end
end

% Process pooled spectral coefficients & plot
[f3,t3,cl3,sc3]=pool_scf_out(plf1,plv1);
figure
cl3.what='VH_Ext_Recall_(fa)_vs_PL_Ext_Recall_(fb)';
psp2_theta_pool6(f3,t3,cl3,freq,lag_tot,lag_neg,ch_max,chi_max)

[f4,cl4]=sp2_compcoh99(sc3,cl3,sc2,cl2);
cl4.what='VH-PL_Fear_Recall_coherence_vs_VH-PL_Ext_Recall_coherence_Log_Ratio'
figure
psp_compcoh199(f4,cl4,45)
```

```
save('V3_VHPL_pool.mat','f2', 't2', 'cl2', 'sc2', 'f3', 't3', 'cl3', 'sc3', '
    f4', 'cl4')
```

BIBLIOGRAPHY

Adhikari, A., Topiwala, M. A. & Gordon, J. A. (2010), 'Synchronized activity between the ventral hippocampus and the medial prefrontal cortex during anxiety', *Neuron* **65**(2), 257–269.

Albert, P. R., Vahid-Ansari, F. & Luckhart, C. (2014), 'Serotonin-prefrontal cortical circuitry in anxiety and depression phenotypes: pivotal role of pre-and post-synaptic 5-HT1A receptor expression', *Frontiers in Behavioral Neuroscience* **8**, 199.

Albrecht, A., Çalışkan, G., Oitzl, M. S., Heinemann, U. & Stork, O. (2013), 'Long-lasting increase of corticosterone after fear memory reactivation: anxiolytic effects and network activity modulation in the ventral hippocampus', *Neuropsychopharmacology* **38**(3), 386–394.

Amir, A., Amano, T. & Pare, D. (2011), 'Physiological identification and infralimbic responsiveness of rat intercalated amygdala neurons', *Journal of Neurophysiology* **105**(6), 3054–3066.

An, B., Kim, J., Park, K., Lee, S., Song, S. & Choi, S. (2017), 'Amount of fear extinction changes its underlying mechanisms', *eLife* **6**, e25224.

Anagnostaras, S. G., Gale, G. D., Fanselow, M. S. et al. (2001), 'Hippocampus and contextual fear conditioning: recent controversies and advances', *Hippocampus* **11**(1), 8–17.

Anagnostaras, S. G., Maren, S. & Fanselow, M. S. (1999), 'Temporally graded retrograde amnesia of contextual fear after hippocampal damage in rats: within-subjects examination', *Journal of Neuroscience* **19**(3), 1106–1114.

Antoniadis, E. A. & McDonald, R. J. (2006), 'Fornix, medial prefrontal cortex, nucleus accumbens, and mediodorsal thalamic nucleus: roles in a fear-based context discrimination task', *Neurobiology of Learning and Memory* **85**(1), 71–85.

Armony, J. L., Servan-Schreiber, D., Cohen, J. D. & LeDoux, J. E. (1995), 'An anatomically constrained neural network model of fear conditioning.', *Behavioral Neuroscience* **109**(2), 246–257.

Armony, J. L., Servan-Schreiber, D., Cohen, J. D. & LeDoux, J. E. (1997a), 'Computational modeling of emotion: explorations through the anatomy and physiology of fear conditioning', *Trends in Cognitive Sciences* **1**(1), 28–34.

Armony, J. L., Servan-Schreiber, D., Romanski, L. M., Cohen, J. D. & LeDoux, J. E. (1997b), 'Stimulus generalization of fear responses: effects of auditory cortex lesions in a computational model and in rats.', *Cerebral Cortex* **7**(2), 157–165.

Arszovszki, A., Borhegyi, Z. & Klausberger, T. (2014), 'Three axonal projection routes of individual pyramidal cells in the ventral CA1 hippocampus', *Frontiers in Neuroanatomy* **8**, 53.

Assareh, N., Bagley, E. E., Carrive, P. & McNally, G. P. (2017), 'Brief optogenetic inhibition of rat lateral or ventrolateral periaqueductal gray augments the acquisition of Pavlovian fear conditioning.', *Behavioral Neuroscience* **131**(6), 454–459.

Bacci, A., Huguenard, J. R. & Prince, D. A. (2005), 'Modulation of neocortical interneurons: extrinsic influences and exercises in self-control', *Trends in Neurosciences* **28**(11), 602–610.

Baldwin, D. S., Anderson, I. M., Nutt, D. J., Allgulander, C., Bandelow, B., den Boer, J. A., Christmas, D. M., Davies, S., Fineberg, N., Lidbetter, N., Malizia, A., McCrone, P., Nabarro, D., O'Neill, C., Scott, J., van der Wee, N. & Wittchen, H.-U. (2014), 'Evidence-based pharmacological treatment of anxiety disorders, post-traumatic stress disorder and obsessive-compulsive disorder: a revision of the 2005 guidelines from the British Association for Psychopharmacology', *Journal of Psychopharmacology* **28**(5), 403–439.

Ball, J. M., Hummos, A. M. & Nair, S. S. (2012), 'Role of sensory input distribution and intrinsic connectivity in lateral amygdala during auditory fear conditioning: a computational study', *Neuroscience* **224**, 249–267.

Bandelow, B., Baldwin, D., Abelli, M., Bolea-Alamanac, B., Bourin, M., Chamberlain, S. R., Cinosi, E., Davies, S., Domschke, K., Fineberg, N., Grünblatt, E., Jarema, M., Kim, Y.-K., Maron, E., Masdrakis, V., Mikova, O., Nutt, D., Pallanti, S., Pini, S., Ströhle, A., Thibaut, F., Vaghi, M. M., Won, E., Wedekind, D., Wichniak, A., Woolley, J., Zwanzger, P. & Riederer, P. (2016), 'Biological markers for anxiety disorders, OCD and PTSD: a consensus statement. Part II: neurochemistry, neurophysiology and neurocognition', *The World Journal of Biological Psychiatry* **18**(3), 162–214.

Barot, S. K., Kyono, Y., Clark, E. W. & Bernstein, I. L. (2008), 'Visualizing stimulus convergence in amygdala neurons during associative learning', *Proceedings of the National Academy of Sciences* **105**(52), 20959–20963.

Bast, T., Zhang, W.-N. & Feldon, J. (2001), 'The ventral hippocampus and fear conditioning in rats', *Experimental Brain Research* **139**(1), 39–52.

Bast, T., Zhang, W.-N. & Feldon, J. (2003), 'Dorsal hippocampus and classical fear conditioning to tone and context in rats: effects of local NMDA-receptor blockade and stimulation', *Hippocampus* **13**(6), 657–675.

Bear, M. F., Cooper, L. N. & Ebner, F. F. (1987), 'A physiological basis for a theory of synapse modification', *Science* **237**(4810), 42–48.

Benchenane, K., Tiesinga, P. H. & Battaglia, F. P. (2011), 'Oscillations in the prefrontal cortex: a gateway to memory and attention', *Current Opinion in Neurobiology* **21**(3), 475–485.

Berretta, S., Pantazopoulos, H., Caldera, M., Pantazopoulos, P. & Pare, D. (2005), 'Infralimbic cortex activation increases c-Fos expression in intercalated neurons of the amygdala', *Neuroscience* **132**(4), 943–953.

Bezaire, M. J., Raikov, I., Burk, K., Vyas, D. & Soltesz, I. (2016), 'Interneuronal mechanisms of hippocampal theta oscillations in a full-scale model of the rodent CA1 circuit', *eLife* **5**, e18566.

Bezaire, M. J. & Soltesz, I. (2013), 'Quantitative assessment of CA1 local circuits: knowledge base for interneuron-pyramidal cell connectivity', *Hippocampus* **23**(9), 751–785.

Bhattacharyya, S., Falkenberg, I., Martin-Santos, R., Atakan, Z., Crippa, J. A., Giampietro, V., Brammer, M. & McGuire, P. (2015), 'Cannabinoid modulation of functional connectivity within regions processing attentional salience', *Neuropsychopharmacology* **40**(6), 1343–1352.

Bishop, S. J. (2007), 'Neurocognitive mechanisms of anxiety: an integrative account', *Trends in Cognitive Sciences* **11**(7), 307–316.

Bisogno, T., Hanuš, L., De Petrocellis, L., Tchilibon, S., Ponde, D. E., Brandi, I., Moriello, A. S., Davis, J. B., Mechoulam, R. & Di Marzo, V. (2001), 'Molecular targets for cannabidiol and its synthetic analogues: effect on vanilloid VR1 receptors and on the cellular uptake and enzymatic hydrolysis of anandamide', *British Journal of Pharmacology* **134**(4), 845–852.

Bitencourt, R. M., Pamplona, F. A. & Takahashi, R. N. (2008), 'Facilitation of contextual fear memory extinction and anti-anxiogenic effects of AM404 and cannabidiol in conditioned rats', *European Neuropsychopharmacology* **18**(12), 849–859.

Blair, H. T. (2001), 'Synaptic plasticity in the lateral amygdala: a cellular hypothesis of fear conditioning', *Learning & Memory* **8**(5), 229–242.

Blessing, E. M., Steenkamp, M. M., Manzanares, J. & Marmar, C. R. (2015), 'Cannabidiol as a potential treatment for anxiety disorders', *Neurotherapeutics* **12**(4), 825–836.

Blier, P., Pineyro, G., El Mansari, M., Bergeron, R. & Montigny, C. d. (1998), 'Role of somatodendritic 5-HT autoreceptors in modulating 5-HT neurotransmission', *Annals of the New York Academy of Sciences* **861**(1), 204–216.

Bliss, T. V. & Lømo, T. (1973), 'Long-lasting potentiation of synaptic transmission in the dentate area of the anaesthetized rabbit following stimulation of the perforant path', *The Journal of Physiology* **232**(2), 331–356.

Blythe, D. & Hackett, L. P. (1999), 'Cardiovascular and neurological toxicity of venlafaxine', *Human & Experimental Toxicology* **18**(5), 309–313.

Bonn-Miller, M. O., Boden, M. T., Vujanovic, A. A. & Drescher, K. D. (2013), 'Prospective investigation of the impact of cannabis use disorders on posttraumatic stress disorder symptoms among veterans in residential treatment.', *Psychological Trauma: Theory, Research, Practice, and Policy* **5**(2), 193–200.

Bonn-Miller, M. O., Vujanovic, A. A. & Drescher, K. D. (2011), 'Cannabis use among military veterans after residential treatment for posttraumatic stress disorder.', *Psychology of Addictive Behaviors* **25**(3), 485–491.

Bostwick, J. M. (2012), 'Blurred boundaries: the therapeutics and politics of medical marijuana', *Mayo Clinic Proceedings* **87**(2), 172–186.

Bouton, M. E. (1993), 'Context, time, and memory retrieval in the interference paradigms of Pavlovian learning.', *Psychological Bulletin* **114**(1), 80.

Bukalo, O., Pinard, C. R., Silverstein, S., Brehm, C., Hartley, N. D., Whittle, N., Colacicco, G., Busch, E., Patel, S., Singewald, N. et al. (2015), 'Prefrontal inputs to the amygdala instruct fear extinction memory formation', *Science Advances* **1**(6), e1500251.

Burette, F., Jay, T. & Laroche, S. (1997), 'Reversal of LTP in the hippocampal afferent fiber system to the prefrontal cortex in vivo with low-frequency patterns of stimulation that do not produce LTD', *Journal of Neurophysiology* **78**(2), 1155–1160.

Burgos-Robles, A., Vidal-Gonzalez, I. & Quirk, G. J. (2009), 'Sustained conditioned responses in prelimbic prefrontal neurons are correlated with fear expression and extinction failure', *Journal of Neuroscience* **29**(26), 8474–8482.

Burnet, P., Eastwood, S., Lacey, K. & Harrison, P. (1995), 'The distribution of 5-HT1A and 5-HT2A receptor mRNA in human brain', *Brain Research* **676**(1), 157–168.

Buzsáki, G. (2001), 'Hippocampal GABAergic interneurons: a physiological perspective', *Neurochemical Research* **26**(8-9), 899–905.

Buzsáki, G. & Draguhn, A. (2004), 'Neuronal oscillations in cortical networks', *Science* **304**(5679), 1926–1929.

Buzsáki, G. & Moser, E. I. (2013), 'Memory, navigation and theta rhythm in the hippocampal-entorhinal system', *Nature Neuroscience* **16**(2), 130–138.

Buzsáki, G. & Wang, X.-J. (2012), 'Mechanisms of gamma oscillations', *Annual Review of Neuroscience* **35**, 203–225.

Calhoon, G. G. & Tye, K. M. (2015), 'Resolving the neural circuits of anxiety', *Nature Neuroscience* **18**(10), 1394–1404.

Campos, A. C. & Guimarães, F. S. (2008), 'Involvement of 5HT1A receptors in the anxiolytic-like effects of cannabidiol injected into the dorsolateral periaqueductal gray of rats', *Psychopharmacology* **199**(2), 223–230.

Campos, A. C. & Guimarães, F. S. (2009), 'Evidence for a potential role for TRPV1 receptors in the dorsolateral periaqueductal gray in the attenuation of the anxiolytic effects of cannabinoids', *Progress in Neuro-Psychopharmacology and Biological Psychiatry* **33**(8), 1517–1521.

Campos, A. C., Moreira, F. A., Gomes, F. V., Del Bel, E. A. & Guimaraes, F. S. (2012), 'Multiple mechanisms involved in the large-spectrum therapeutic potential of cannabidiol in psychiatric disorders', *Philosophical Transactions of the Royal Society B: Biological Sciences* **367**(1607), 3364–3378.

Canteras, N., Simerly, R. & Swanson, L. (1992), 'Projections of the ventral premammillary nucleus', *Journal of Comparative Neurology* **324**(2), 195–212.

Casarotto, P. C., Gomes, F. V., Resstel, L. B. & Guimaraes, F. S. (2010), 'Cannabidiol inhibitory effect on marble-burying behaviour: involvement of CB1 receptors', *Behavioural Pharmacology* **21**(4), 353–358.

Cascade, E., Kalali, A. H. & Kennedy, S. H. (2009), 'Real-world data on SSRI antidepressant side effects', *Psychiatry (Edgmont)* **6**(2), 16–18.

Cenquizca, L. A. & Swanson, L. W. (2007), 'Spatial organization of direct hippocampal field CA1 axonal projections to the rest of the cerebral cortex', *Brain Research Reviews* **56**(1), 1–26.

Chang, C.-h. & Maren, S. (2010), 'Strain difference in the effect of infralimbic cortex lesions on fear extinction in rats.', *Behavioral Neuroscience* **124**(3), 391–397.

Chhatwal, J. P., Davis, M., Maguschak, K. A. & Ressler, K. J. (2005), 'Enhancing cannabinoid neurotransmission augments the extinction of conditioned fear', *Neuropsychopharmacology* **30**(3), 516–524.

Cho, J.-H., Deisseroth, K. & Bolshakov, V. Y. (2013), 'Synaptic encoding of fear extinction in mPFC-amygdala circuits', *Neuron* **80**(6), 1491–1507.

Ciocchi, S., Passecker, J., Malagon-Vina, H., Mikus, N. & Klausberger, T. (2015), 'Selective information routing by ventral hippocampal CA1 projection neurons', *Science* **348**(6234), 560–563.

Cipriani, A., Williams, T., Nikolakopoulou, A., Salanti, G., Chaimani, A., Ipser, J., Cowen, P. J., Geddes, J. R. & Stein, D. J. (2018), 'Comparative efficacy and acceptability of pharmacological treatments for post-traumatic stress disorder in adults: a network meta-analysis', *Psychological Medicine* **48**(12), 1975–1984.

Cobb, S., Buhl, E., Halasy, K., Paulsen, O. & Somogyi, P. (1995), 'Synchronization of neuronal activity in hippocampus by individual GABAergic interneurons', *Nature* **378**(6552), 75.

Connors, B. W. & Gutnick, M. J. (1990), 'Intrinsic firing patterns of diverse neocortical neurons', *Trends in Neurosciences* **13**(3), 99–104.

Cougle, J. R., Bonn-Miller, M. O., Vujanovic, A. A., Zvolensky, M. J. & Hawkins, K. A. (2011), 'Posttraumatic stress disorder and cannabis use in a nationally representative sample.', *Psychology of Addictive Behaviors* **25**(3), 554–558.

Craske, M. G., Treanor, M., Conway, C. C., Zbozinek, T. & Vervliet, B. (2014), 'Maximizing exposure therapy: an inhibitory learning approach', *Behaviour Research and Therapy* **58**, 10–23.

Das, R. K., Kamboj, S. K., Ramadas, M., Yogan, K., Gupta, V., Redman, E., Curran, H. V. & Morgan, C. J. (2013), 'Cannabidiol enhances consolidation of explicit fear extinction in humans', *Psychopharmacology* **226**(4), 781–792.

de Kleine, R. A., Hendriks, G.-J., Kusters, W. J., Broekman, T. G. & van Minnen, A. (2012), 'A randomized placebo-controlled trial of d-cycloserine to enhance exposure therapy for posttraumatic stress disorder', *Biological Psychiatry* **71**(11), 962–968.

de Mello Schier, A. R., de Oliveira Ribeiro, N. P., e Silva, A. C. d. O., Hallak, J. E. C., Crippa, J. A. S., Nardi, A. E. & Zuardi, A. W. (2012), 'Cannabidiol, a Cannabis sativa constituent, as an anxiolytic drug', *Revista Brasileira de Psiquiatria* **34**, S104–S117.

de Oliveira Alvares, L., Genro, B. P., Diehl, F., Molina, V. & Quillfeldt, J. (2008), 'Opposite action of hippocampal CB1 receptors in memory reconsolidation and extinction', *Neuroscience* **154**(4), 1648–1655.

de Paula Soares, V., Campos, A. C., de Bortoli, V. C., Zangrossi Jr, H., Guimarães, F. S. & Zuardi, A. W. (2010), 'Intra-dorsal periaqueductal gray administration of cannabidiol blocks panic-like response by activating 5-HT1A receptors', *Behavioural Brain Research* **213**(2), 225–229.

De Petrocellis, L., Ligresti, A., Moriello, A. S., Allarà, M., Bisogno, T., Petrosino, S., Stott, C. G. & Di Marzo, V. (2011), 'Effects of cannabinoids and cannabinoid-enriched cannabis extracts on TRP channels and endocannabinoid metabolic enzymes', *British Journal of Pharmacology* **163**(7), 1479–1494.

Dejean, C., Courtin, J., Karalis, N., Chaudun, F., Wurtz, H., Bienvenu, T. C. & Herry, C. (2016), 'Prefrontal neuronal assemblies temporally control fear behaviour', *Nature* **535**(7612), 420–424.

Devinsky, O., Cilio, M. R., Cross, H., Fernandez-Ruiz, J., French, J., Hill, C., Katz, R., Di Marzo, V., Jutras-Aswad, D., Notcutt, W. G. et al. (2014), 'Cannabidiol: pharmacology and potential therapeutic role in epilepsy and other neuropsychiatric disorders', *Epilepsia* **55**(6), 791–802.

Do-Monte, F. H., Manzano-Nieves, G., Quiñones-Laracuente, K., Ramos-Medina, L. & Quirk, G. J. (2015), 'Revisiting the role of infralimbic cortex in fear extinction with optogenetics', *Journal of Neuroscience* **35**(8), 3607–3615.

Do Monte, F. H., Souza, R. R., Bitencourt, R. M., Kroon, J. A. & Takahashi, R. N. (2013), 'Infusion of cannabidiol into infralimbic cortex facilitates fear extinction via CB1 receptors', *Behavioural Brain Research* **250**, 23–27.

Dording, C. M., Mischoulon, D., Petersen, T. J., Kornbluh, R., Gordon, J., Nierenberg, A. A., Rosenbaum, J. F. & Fava, M. (2002), 'The pharmacologic management of SSRI-induced side effects: a survey of psychiatrists', *Annals of Clinical Psychiatry* **14**(3), 143–147.

Doron, N. N. & Ledoux, J. E. (1999), 'Organization of projections to the lateral amygdala from auditory and visual areas of the thalamus in the rat', *Journal of Comparative Neurology* **412**(3), 383–409.

Durstewitz, D. & Gabriel, T. (2007), 'Dynamical basis of irregular spiking in NMDA-driven prefrontal cortex neurons', *Cerebral Cortex* **17**(4), 894–908.

Durstewitz, D., Seamans, J. K. & Sejnowski, T. J. (2000), 'Dopamine-mediated stabilization of delay-period activity in a network model of prefrontal cortex', *Journal of Neurophysiology* **83**(3), 1733–1750.

ElBatsh, M. M., Assareh, N., Marsden, C. & Kendall, D. (2012), 'Anxiogenic-like effects of chronic cannabidiol administration in rats', *Psychopharmacology* **221**(2), 239–247.

Etkin, A. & Wager, T. D. (2007), 'Functional neuroimaging of anxiety: a meta-analysis of emotional processing in PTSD, social anxiety disorder, and specific phobia', *American Journal of Psychiatry* **164**(10), 1476–1488.

Falls, W. A., Miserendino, M. & Davis, M. (1992), 'Extinction of fear-potentiated startle: blockade by infusion of an NMDA antagonist into the amygdala', *Journal of Neuroscience* **12**(3), 854–863.

Fanselow, M. S. (2000), 'Contextual fear, gestalt memories, and the hippocampus', *Behavioural Brain Research* **110**(1-2), 73–81.

Feng, F., Samarth, P., Paré, D. & Nair, S. S. (2016), 'Mechanisms underlying the formation of the amygdalar fear memory trace: a computational perspective', *Neuroscience* **322**, 370–376.

Fenton, G. E., Halliday, D. M., Mason, R., Bredy, T. W. & Stevenson, C. W. (2016), 'Sex differences in learned fear expression and extinction involve altered gamma oscillations in medial prefrontal cortex', *Neurobiology of Learning and Memory* **135**, 66–72.

Fenton, G. E., Halliday, D. M., Mason, R. & Stevenson, C. W. (2014b), 'Medial prefrontal cortex circuit function during retrieval and extinction of associative learning under anesthesia', *Neuroscience* **265**, 204–216.

Fenton, G. E., Pollard, A. K., Halliday, D. M., Mason, R., Bredy, T. W. & Stevenson, C. W. (2014a), 'Persistent prelimbic cortex activity contributes to enhanced learned fear expression in females', *Learning & Memory* **21**(2), 55–60.

Fenton, G. F. (2015), Neural Network Interactions Underlying Emotional Learning and Memory: Integrating Experimental and Theoretical Approaches, PhD thesis, University of Nottingham. Unpublished doctoral thesis.

Ferguson, K. A., Huh, C. Y., Amilhon, B., Williams, S. & Skinner, F. K. (2014), 'Simple, biologically-constrained CA1 pyramidal cell models using an intact, whole hippocampus context', *F1000Research* **3**, 104.

Fergusson, D. (2005), 'Association between suicide attempts and selective serotonin reuptake inhibitors: systematic review of randomised controlled trials', *The BMJ* **330**(7488), 396.

Ferrara, N. C., Cullen, P. K., Pullins, S. P., Rotondo, E. K. & Helmstetter, F. J. (2017), 'Input from the medial geniculate nucleus modulates amygdala encoding of fear memory discrimination', *Learning & Memory* **24**(9), 414–421.

Fisar, Z. (2009), 'Phytocannabinoids and endocannabinoids', *Current Drug Abuse Reviews* **2**(1), 51–75.

Fitzgerald, P. J., Seemann, J. R. & Maren, S. (2014a), 'Can fear extinction be enhanced? A review of pharmacological and behavioral findings', *Brain Research Bulletin* **105**, 46–60.

Fitzgerald, P. J., Whittle, N., Flynn, S. M., Graybeal, C., Pinard, C. R., Gunduz-Cinar, O., Kravitz, A. V., Singewald, N. & Holmes, A. (2014b), 'Prefrontal single-unit firing associated with deficient extinction in mice', *Neurobiology of Learning and Memory* **113**, 69–81.

Fogaça, M., Reis, F., Campos, A. & Guimaraes, F. (2014), 'Effects of intra-prelimbic prefrontal cortex injection of cannabidiol on anxiety-like behavior: involvement of 5HT1A receptors and previous stressful experience', *European Neuropsychopharmacology* **24**(3), 410–419.

Fontanez-Nuin, D. E., Santini, E., Quirk, G. J. & Porter, J. T. (2011), 'Memory for fear extinction requires mGluR5-mediated activation of infralimbic neurons', *Cerebral Cortex* **21**(3), 727–735.

Frankland, P. W., Cestari, V., Filipkowski, R. K., McDonald, R. J. & Silva, A. J. (1998), 'The dorsal hippocampus is essential for context discrimination but not for contextual conditioning.', *Behavioral Neuroscience* **112**(4), 863–874.

Freund, T. F. & Buzsáki, G. (1996), 'Interneurons of the hippocampus', *Hippocampus* **6**(4), 347–470.

Fujisawa, S., Amarasingham, A., Harrison, M. T. & Buzsáki, G. (2008), 'Behavior-dependent short-term assembly dynamics in the medial prefrontal cortex', *Nature Neuroscience* **11**(7), 823–833.

Gabbott, P. L., Warner, T. A., Jays, P. R., Salway, P. & Busby, S. J. (2005), 'Prefrontal cortex in the rat: projections to subcortical autonomic, motor, and limbic centers', *Journal of Comparative Neurology* **492**(2), 145–177.

Gazarini, L., Stern, C. A., Piornedo, R. R., Takahashi, R. N. & Bertoglio, L. J. (2015), 'PTSD-like memory generated through enhanced noradrenergic activity is mitigated by a dual step pharmacological intervention targeting its reconsolidation', *International Journal of Neuropsychopharmacology* **18**(1), pyu026.

Gilmartin, M. R., Balderston, N. L. & Helmstetter, F. J. (2014), 'Prefrontal cortical regulation of fear learning', *Trends in Neurosciences* **37**(8), 455–464.

Gilmartin, M. R., Kwapis, J. L. & Helmstetter, F. J. (2012), 'Trace and contextual fear conditioning are impaired following unilateral microinjection of muscimol in the ventral hippocampus or amygdala, but not the medial prefrontal cortex', *Neurobiology of Learning and Memory* **97**(4), 452–464.

Giustino, T. F., Fitzgerald, P. J. & Maren, S. (2016), 'Revisiting propranolol and PTSD: memory erasure or extinction enhancement?', *Neurobiology of Learning and Memory* **130**, 26–33.

Giustino, T. F. & Maren, S. (2015), 'The role of the medial prefrontal cortex in the conditioning and extinction of fear', *Frontiers in Behavioral Neuroscience* **9**, 298.

Gloveli, T., Dugladze, T., Rotstein, H. G., Traub, R. D., Monyer, H., Heinemann, U., Whittington, M. A. & Kopell, N. J. (2005), 'Orthogonal arrangement of rhythm-generating microcircuits in the hippocampus', *Proceedings of the National Academy of Sciences* **102**(37), 13295–13300.

Golomb, D. (2007), 'Neuronal synchrony measures', *Scholarpedia* **2**(1), 1347.

Golomb, D., Yue, C. & Yaari, Y. (2006), 'Contribution of persistent Na+ current and M-type K+ current to somatic bursting in CA1 pyramidal cells: combined experimental and modeling study', *Journal of Neurophysiology* **96**(4), 1912–1926.

Gomes, F. V., Reis, D. G., Alves, F. H., Corrêa, F. M., Guimaraes, F. S. & Resstel, L. B. (2012), 'Cannabidiol injected into the bed nucleus of the stria terminalis reduces the expression of contextual fear conditioning via 5-HT1A receptors', *Journal of Psychopharmacology* **26**(1), 104–113.

Gomes, F. V., Resstel, L. B. & Guimarães, F. S. (2011), 'The anxiolytic-like effects of cannabidiol injected into the bed nucleus of the stria terminalis are mediated by 5-HT1A receptors', *Psychopharmacology* **213**(2-3), 465–473.

Graham, B. M., Langton, J. M. & Richardson, R. (2011), 'Pharmacological enhancement of fear reduction: preclinical models', *British Journal of Pharmacology* **164**(4), 1230–1247.

Greer, G. R., Grob, C. S. & Halberstadt, A. L. (2014), 'PTSD symptom reports of patients evaluated for the New Mexico Medical Cannabis Program', *Journal of Psychoactive Drugs* **46**(1), 73–77.

Griebel, G. & Holmes, A. (2013), '50 years of hurdles and hope in anxiolytic drug discovery', *Nature Reviews Drug Discovery* **12**(9), 667–687.

Griffin, A. L. (2015), 'Role of the thalamic nucleus reuniens in mediating interactions between the hippocampus and medial prefrontal cortex during spatial working memory', *Frontiers in Systems Neuroscience* **9**, 29.

Guimarães, F. S., Chiaretti, T., Graeff, F. & Zuardi, A. (1990), 'Antianxiety effect of cannabidiol in the elevated plus-maze', *Psychopharmacology* **100**(4), 558–559.

Gunthorpe, M. J. & Chizh, B. A. (2009), 'Clinical development of TRPV1 antagonists: targeting a pivotal point in the pain pathway', *Drug Discovery Today* **14**(1), 56–67.

Hájos, N. & Paulsen, O. (2009), 'Network mechanisms of gamma oscillations in the CA3 region of the hippocampus', *Neural Networks* **22**(8), 1113–1119.

Hart, G., Harris, J. A. & Westbrook, R. F. (2009), 'Systemic or intra-amygdala injection of a benzodiazepine (midazolam) impairs extinction but spares re-extinction of conditioned fear responses', *Learning & memory Memory* **16**(1), 53–61.

Hart, G., Panayi, M. C., Harris, J. A. & Westbrook, R. F. (2014), 'Benzodiazepine treatment can impair or spare extinction, depending on when it is given', *Behaviour Research and Therapy* **56**, 22–29.

Hartley, C. A. & Phelps, E. A. (2010), 'Changing fear: the neurocircuitry of emotion regulation', *Neuropsychopharmacology* **35**(1), 136–146.

Hashikawa, K., Naka, M., Nakayama, D., Matsumoto, N., Neve, R. & Matsuki, N. (2013), 'Blockade of stimulus convergence in amygdala neurons disrupts taste associative learning', *Journal of Neuroscience* **33**(11), 4958–4963.

Hebb, D. O. (1949), *The Organization of Behaviour: A Neuropsychological Theory*, John Wiley and Sons, Inc.

Heidbreder, C. A. & Groenewegen, H. J. (2003), 'The medial prefrontal cortex in the rat: evidence for a dorso-ventral distinction based upon functional and anatomical characteristics', *Neuroscience & Biobehavioral Reviews* **27**(6), 555–579.

Hermans, E. J., Battaglia, F. P., Atsak, P., de Voogd, L. D., Fernández, G. & Roozendaal, B. (2014), 'How the amygdala affects emotional memory by altering brain network properties', *Neurobiology of Learning and Memory* **112**, 2–16.

Herry, C., Ciocchi, S., Senn, V., Demmou, L., Müller, C. & Lüthi, A. (2008), 'Switching on and off fear by distinct neuronal circuits', *Nature* **454**(7204), 600–606.

Hirase, H., Leinekugel, X., Csicsvari, J., Czurkó, A. & Buzsáki, G. (2001), 'Behavior-dependent states of the hippocampal network affect functional clustering of neurons', *Journal of Neuroscience* **21**(10), RC145.

Hobin, J. A., Ji, J. & Maren, S. (2006), 'Ventral hippocampal muscimol disrupts context-specific fear memory retrieval after extinction in rats', *Hippocampus* **16**(2), 174–182.

Hodgkin, A. & Huxley, A. (1952a), 'The components of membrane conductance in the giant axon of Loligo', *The Journal of Physiology* **116**(4), 473–496.

Hodgkin, A. L. & Huxley, A. F. (1952b), 'Currents carried by sodium and potassium ions through the membrane of the giant axon of Loligo', *The Journal of Physiology* **116**(4), 449–472.

Hodgkin, A. L. & Huxley, A. F. (1952c), 'The dual effect of membrane potential on sodium conductance in the giant axon of Loligo', *The Journal of Physiology* **116**(4), 497–506.

Hodgkin, A. L. & Huxley, A. F. (1952d), 'A quantitative description of membrane current and its application to conduction and excitation in nerve', *The Journal of Physiology* **117**(4), 500–544.

Holmes, A., Fitzgerald, P. J., MacPherson, K. P., DeBrouse, L., Colacicco, G., Flynn, S. M., Masneuf, S., Pleil, K. E., Li, C., Marcinkiewcz, C. A. et al. (2012), 'Chronic alcohol remodels prefrontal neurons and disrupts NMDAR-mediated fear extinction encoding', *Nature Neuroscience* **15**(10), 1359–1361.

Hoover, W. B. & Vertes, R. P. (2007), 'Anatomical analysis of afferent projections to the medial prefrontal cortex in the rat', *Brain Structure and Function* **212**(2), 149–179.

Hosking, R. & Zajicek, J. (2008), 'Therapeutic potential of cannabis in pain medicine', *British Journal of Anaesthesia* **101**(1), 59–68.

Hsiao, Y.-T., Yi, P.-L., Li, C.-L. & Chang, F.-C. (2012), 'Effect of cannabidiol on sleep disruption induced by the repeated combination tests consisting of open field and elevated plus-maze in rats', *Neuropharmacology* **62**(1), 373–384.

Hunsaker, M. R. & Kesner, R. P. (2008), 'Dissociations across the dorsal–ventral axis of CA3 and CA1 for encoding and retrieval of contextual and auditory-cued fear', *Neurobiology of Learning and Memory* **89**(1), 61–69.

Isbister, G. K., Bowe, S. J., Dawson, A. & Whyte, I. M. (2004), 'Relative toxicity of selective serotonin reuptake inhibitors (SSRIs) in overdose', *Journal of Toxicology: Clinical Toxicology* **42**(3), 277–285.

Izhikevich, E. M. (2003), 'Simple model of spiking neurons', *IEEE Transactions on Neural Networks* **14**(6), 1569–1572.

Izhikevich, E. M. (2004), 'Which model to use for cortical spiking neurons?', *IEEE Transactions on Neural Networks* **15**(5), 1063–1070.

Izhikevich, E. M. (2007), *Dynamical systems in neuroscience*, MIT press.

Jay, T., Burette, F. & Laroche, S. (1996), 'Plasticity of the hippocampal-prefrontal cortex synapses', *Journal of Physiology-Paris* **90**(5), 361–366.

Jay, T. M., Thierry, A.-M., Wiklund, L. & Glowinski, J. (1992), 'Excitatory amino acid pathway from the hippocampus to the prefrontal cortex. contribution of AMPA receptors in hippocampo-prefrontal cortex transmission', *European Journal of Neuroscience* **4**(12), 1285–1295.

Jay, T. M. & Witter, M. P. (1991), 'Distribution of hippocampal CA1 and subicular efferents in the prefrontal cortex of the rat studied by means of anterograde transport of Phaseolus vulgaris-leucoagglutinin', *Journal of Comparative Neurology* **313**(4), 574–586.

Ji, G. & Neugebauer, V. (2012), 'Modulation of medial prefrontal cortical activity using in vivo recordings and optogenetics', *Molecular Brain* **5**(1), 36.

Ji, J. & Maren, S. (2005), 'Electrolytic lesions of the dorsal hippocampus disrupt renewal of conditional fear after extinction', *Learning & Memory* **12**(3), 270–276.

Jin, J. & Maren, S. (2015), 'Fear renewal preferentially activates ventral hippocampal neurons projecting to both amygdala and prefrontal cortex in rats', *Scientific Reports* **5**(1), 8388.

Jovanovic, T., Norrholm, S. D., Blanding, N. Q., Davis, M., Duncan, E., Bradley, B. & Ressler, K. J. (2010), 'Impaired fear inhibition is a biomarker of PTSD but not depression', *Depression and Anxiety* **27**(3), 244–251.

Kamprath, K., Marsicano, G., Tang, J., Monory, K., Bisogno, T., Di Marzo, V., Lutz, B. & Wotjak, C. T. (2006), 'Cannabinoid CB1 receptor mediates fear extinction via habituation-like processes', *Journal of Neuroscience* **26**(25), 6677–6686.

Kawaguchi, Y. & Kubota, Y. (1997), 'GABAergic cell subtypes and their synaptic connections in rat frontal cortex.', *Cerebral Cortex* **7**(6), 476–486.

Kerr, G. W. (2001), 'Tricyclic antidepressant overdose: a review', *Emergency Medicine Journal* **18**(4), 236–241.

Kesner, R. P. & Churchwell, J. C. (2011), 'An analysis of rat prefrontal cortex in mediating executive function', *Neurobiology of Learning and Memory* **96**(3), 417–431.

Kessler, R. C., Berglund, P., Demler, O., Jin, R., Merikangas, K. R. & Walters, E. E. (2005), 'Lifetime prevalence and age-of-onset distributions of DSM-IV disorders in the national comorbidity survey replication', *Archives of General Psychiatry* **62**(6), 593–602.

Kim, D., Paré, D. & Nair, S. S. (2013a), 'Assignment of model amygdala neurons to the fear memory trace depends on competitive synaptic interactions', *Journal of Neuroscience* **33**(36), 14354–14358.

Kim, D., Paré, D. & Nair, S. S. (2013b), 'Mechanisms contributing to the induction and storage of Pavlovian fear memories in the lateral amygdala', *Learning & Memory* **20**(8), 421–430.

Kim, D., Samarth, P., Feng, F., Pare, D. & Nair, S. S. (2016), 'Synaptic competition in the lateral amygdala and the stimulus specificity of conditioned fear: a biophysical modeling study', *Brain Structure and Function* **221**(4), 2163–2182.

Kim, J. J. & Fanselow, M. S. (1992), 'Modality-specific retrograde amnesia of fear', *Science* **256**(5057), 675–677.

Kim, M. J., Gee, D. G., Loucks, R. A., Davis, F. C. & Whalen, P. J. (2011), 'Anxiety dissociates dorsal and ventral medial prefrontal cortex functional connectivity with the amygdala at rest', *Cerebral Cortex* **21**(7), 1667–1673.

Kim, S. C., Jo, Y. S., Kim, I. H., Kim, H. & Choi, J.-S. (2010), 'Lack of medial prefrontal cortex activation underlies the immediate extinction deficit', *Journal of Neuroscience* **30**(3), 832–837.

Kim, W. B. & Cho, J.-H. (2017a), 'Encoding of discriminative fear memory by input-specific LTP in the amygdala', *Neuron* **95**(5), 1129–1146.

Kim, W. B. & Cho, J.-H. (2017b), 'Synaptic targeting of double-projecting ventral CA1 hippocampal neurons to the medial prefrontal cortex and basal amygdala', *Journal of Neuroscience* **37**(19), 4868–4882.

Kjelstrup, K. G., Tuvnes, F. A., Steffenach, H.-A., Murison, R., Moser, E. I. & Moser, M.-B. (2002), 'Reduced fear expression after lesions of the ventral hippocampus', *Proceedings of the National Academy of Sciences* **99**(16), 10825–10830.

Klüver, H. & Bucy, P. C. (1937), '"Psychic blindness" and other symptoms following bilateral temporal lobectomy in Rhesus monkeys.', *American Journal of Physiology* **119**, 352–353.

Knapska, E., Macias, M., Mikosz, M., Nowak, A., Owczarek, D., Wawrzyniak, M., Pieprzyk, M., Cymerman, I. A., Werka, T., Sheng, M. et al. (2012), 'Functional anatomy of neural circuits regulating fear and extinction', *Proceedings of the National Academy of Sciences* **109**(42), 17093–17098.

Kopala, L. C., Day, C., Dillman, B. & Gardner, D. (1998), 'A case of risperidone overdose in early schizophrenia: a review of potential complications.', *Journal of Psychiatry and Neuroscience* **23**(5), 305–308.

Krasne, F. B., Fanselow, M. & Zelikowsky, M. (2011), 'Design of a neurally plausible model of fear learning', *Frontiers in Behavioral Neuroscience* **5**, 41.

Krettek, J. & Price, J. (1977), 'The cortical projections of the mediodorsal nucleus and adjacent thalamic nuclei in the rat', *Journal of Comparative Neurology* **171**(2), 157–191.

Laurent, V. & Westbrook, R. F. (2009), 'Inactivation of the infralimbic but not the prelimbic cortex impairs consolidation and retrieval of fear extinction', *Learning & Memory* **16**(9), 520–529.

LeDoux, J. E. (2000), 'Emotion circuits in the brain', *Annual Review of Neuroscience* **23**(1), 155–184.

LeDoux, J. E. (2014), 'Coming to terms with fear', *Proceedings of the National Academy of Sciences* **111**(8), 2871–2878.

LeDoux, J. E., Iwata, J., Cicchetti, P. & Reis, D. (1988), 'Different projections of the central amygdaloid nucleus mediate autonomic and behavioral correlates of conditioned fear', *Journal of Neuroscience* **8**(7), 2517–2529.

LeDoux, J. E. & Pine, D. S. (2016), 'Using neuroscience to help understand fear and anxiety: a two-system framework', *American Journal of Psychiatry* **173**(11), 1083–1093.

Lee, J. L., Milton, A. L. & Everitt, B. J. (2006), 'Reconsolidation and extinction of conditioned fear: inhibition and potentiation', *Journal of Neuroscience* **26**(39), 10051–10056.

Lemos, J. I., Resstel, L. B. & Guimarães, F. S. (2010), 'Involvement of the prelimbic prefrontal cortex on cannabidiol-induced attenuation of contextual conditioned fear in rats', *Behavioural Brain Research* **207**(1), 105–111.

Lesting, J., Daldrup, T., Narayanan, V., Himpe, C., Seidenbecher, T. & Pape, H.-C. (2013), 'Directional theta coherence in prefrontal cortical to amygdalo-hippocampal pathways signals fear extinction', *PLoS One* **8**(10), e77707.

Lesting, J., Narayanan, R. T., Kluge, C., Sangha, S., Seidenbecher, T. & Pape, H.-C. (2011), 'Patterns of coupled theta activity in amygdala-hippocampal-prefrontal cortical circuits during fear extinction', *PLoS One* **6**(6), e21714.

Levin, R., Almeida, V., Fiel Peres, F., Bendlin Calzavara, M., Derci da Silva, N., Akimi Suiama, M., Tamie Niigaki, S., Waldo Zuardi, A., Eduardo Cecilio Hallak, J., Alexandre Crippa, J. et al. (2012), 'Antipsychotic profile of cannabidiol and rimonabant in an animal model of emotional context processing in schizophrenia', *Current Pharmaceutical Design* **18**(32), 4960–4965.

Li, G., Amano, T., Pare, D. & Nair, S. S. (2011), 'Impact of infralimbic inputs on intercalated amygdala neurons: a biophysical modeling study', *Learning & Memory* **18**(4), 226–240.

Li, G., Nair, S. S. & Quirk, G. J. (2009), 'A biologically realistic network model of acquisition and extinction of conditioned fear associations in lateral amygdala neurons', *Journal of Neurophysiology* **101**(3), 1629–1646.

Li, H.-L. (1973), 'An archaeological and historical account of cannabis in China', *Economic Botany* **28**(4), 437–448.

Likhtik, E., Popa, D., Apergis-Schoute, J., Fidacaro, G. A. & Paré, D. (2008), 'Amygdala intercalated neurons are required for expression of fear extinction', *Nature* **454**(7204), 642–645.

Likhtik, E., Stujenske, J. M., Topiwala, M. A., Harris, A. Z. & Gordon, J. A. (2014), 'Prefrontal entrainment of amygdala activity signals safety in learned fear and innate anxiety', *Nature Neuroscience* **17**(1), 106–113.

Lisman, J. (1989), 'A mechanism for the Hebb and the anti-Hebb processes underlying learning and memory', *Proceedings of the National Academy of Sciences* **86**(23), 9574–9578.

Lisman, J., Schulman, H. & Cline, H. (2002), 'The molecular basis of CaMKII function in synaptic and behavioural memory', *Nature Reviews Neuroscience* **3**(3), 175–190.

Little, J. P. & Carter, A. G. (2013), 'Synaptic mechanisms underlying strong reciprocal connectivity between the medial prefrontal cortex and basolateral amygdala', *Journal of Neuroscience* **33**(39), 15333–15342.

Llorente-Berzal, A., Terzian, A. L. B., di Marzo, V., Micale, V., Viveros, M. P. & Wotjak, C. T. (2015), '2-AG promotes the expression of conditioned fear via cannabinoid receptor type 1 on GABAergic neurons', *Psychopharmacology* **232**(15), 2811–2825.

Lovett-Barron, M., Kaifosh, P., Kheirbek, M. A., Danielson, N., Zaremba, J. D., Reardon, T. R., Turi, G. F., Hen, R., Zemelman, B. V. & Losonczy, A. (2014), 'Dendritic inhibition in the hippocampus supports fear learning', *Science* **343**(6173), 857–863.

Mahan, A. L. & Ressler, K. J. (2012), 'Fear conditioning, synaptic plasticity and the amygdala: implications for posttraumatic stress disorder', *Trends in Neurosciences* **35**(1), 24–35.

Mao, S.-C., Hsiao, Y.-H. & Gean, P.-W. (2006), 'Extinction training in conjunction with a partial agonist of the glycine site on the NMDA receptor erases memory trace', *Journal of Neuroscience* **26**(35), 8892–8899.

Marek, R., Jin, J., Goode, T. D., Giustino, T. F., Wang, Q., Acca, G. M., Holehonnur, R., Ploski, J. E., Fitzgerald, P. J., Lynagh, T. et al. (2018), 'Hippocampus-driven feed-forward inhibition of the prefrontal cortex mediates relapse of extinguished fear', *Nature Neuroscience* **21**(3), 384–392.

Maren, S., Aharonov, G. & Fanselow, M. S. (1997), 'Neurotoxic lesions of the dorsal hippocampus and Pavlovian fear conditioning in rats', *Behavioural Brain Research* **88**(2), 261–274.

Maren, S. & Holt, W. G. (2004), 'Hippocampus and Pavlovian fear conditioning in rats: muscimol infusions into the ventral, but not dorsal, hippocampus impair the acquisition of conditional freezing to an auditory conditional stimulus.', *Behavioral Neuroscience* **118**(1), 97–110.

Marinho, A., Vila-Verde, C., Fogaça, M. & Guimarães, F. (2015), 'Effects of intra-infralimbic prefrontal cortex injections of cannabidiol in the modulation of emotional behaviors in rats: contribution of 5HT1A receptors and stressful experiences', *Behavioural Brain Research* **286**, 49–56.

Marquis, J.-P., Killcross, S. & Haddon, J. E. (2007), 'Inactivation of the prelimbic, but not infralimbic, prefrontal cortex impairs the contextual control of response conflict in rats', *European Journal of Neuroscience* **25**(2), 559–566.

Marsicano, G., Wotjak, C. T., Azad, S. C., Bisogno, T., Rammes, G., Cascio, M. G., Hermann, H., Tang, J., Hofmann, C., Zieglgänsberger, W. et al. (2002), 'The endogenous cannabinoid system controls extinction of aversive memories', *Nature* **418**(6897), 530–534.

Mato, S., Aso, E., Castro, E., Martín, M., Valverde, O., Maldonado, R. & Pazos, Á. (2007), 'CB1 knockout mice display impaired functionality of 5-HT1A and 5-HT2A/C receptors', *Journal of Neurochemistry* **103**(5), 2111–2120.

Matus-Amat, P. (2004), 'The role of the dorsal hippocampus in the acquisition and retrieval of context memory representations', *Journal of Neuroscience* **24**(10), 2431–2439.

McCormick, D. A. & Huguenard, J. R. (1992), 'A model of the electrophysiological properties of thalamocortical relay neurons', *Journal of Neurophysiology* **68**(4), 1384–1400.

McGarry, L. M. & Carter, A. G. (2017), 'Prefrontal cortex drives distinct projection neurons in the basolateral amygdala', *Cell Reports* **21**(6), 1426–1433.

McHugh, S., Deacon, R., Rawlins, J. & Bannerman, D. M. (2004), 'Amygdala and ventral hippocampus contribute differentially to mechanisms of fear and anxiety.', *Behavioral Neuroscience* **118**(1), 63.

Mehmedic, Z., Chandra, S., Slade, D., Denham, H., Foster, S., Patel, A. S., Ross, S. A., Khan, I. A. & ElSohly, M. A. (2010), 'Potency trends of Δ9-thc and other

cannabinoids in confiscated cannabis preparations from 1993 to 2008', *Journal of Forensic Sciences* **55**(5), 1209–1217.

Milad, M. R., Orr, S. P., Lasko, N. B., Chang, Y., Rauch, S. L. & Pitman, R. K. (2008), 'Presence and acquired origin of reduced recall for fear extinction in PTSD: results of a twin study', *Journal of Psychiatric Research* **42**(7), 515–520.

Milad, M. R., Pitman, R. K., Ellis, C. B., Gold, A. L., Shin, L. M., Lasko, N. B., Zeidan, M. A., Handwerger, K., Orr, S. P. & Rauch, S. L. (2009), 'Neurobiological basis of failure to recall extinction memory in posttraumatic stress disorder', *Biological Psychiatry* **66**(12), 1075–1082.

Milad, M. R. & Quirk, G. J. (2002), 'Neurons in medial prefrontal cortex signal memory for fear extinction', *Nature* **420**(6911), 70–74.

Milad, M. R. & Quirk, G. J. (2012), 'Fear extinction as a model for translational neuroscience: ten years of progress', *Annual Review of Psychology* **63**, 129–151.

Milad, M. R., Wright, C. I., Orr, S. P., Pitman, R. K., Quirk, G. J. & Rauch, S. L. (2007), 'Recall of fear extinction in humans activates the ventromedial prefrontal cortex and hippocampus in concert', *Biological Psychiatry* **62**(5), 446–454.

Milad, M., Vidal-Gonzalez, I. & Quirk, G. (2004), 'Electrical stimulation of medial prefrontal cortex reduces conditioned fear in a temporally specific manner.', *Behavioral Neuroscience* **118**(2), 389–394.

Miles, R., Tóth, K., Gulyás, A. I., Hájos, N. & Freund, T. F. (1996), 'Differences between somatic and dendritic inhibition in the hippocampus', *Neuron* **16**(4), 815–823.

Montgomery, S. M. & Buzsáki, G. (2007), 'Gamma oscillations dynamically couple hippocampal CA3 and CA1 regions during memory task performance', *Proceedings of the National Academy of Sciences* **104**(36), 14495–14500.

Moreira, F. A., Aguiar, D. C. & Guimarães, F. S. (2006), 'Anxiolytic-like effect of cannabidiol in the rat Vogel conflict test', *Progress in Neuro-Psychopharmacology and Biological Psychiatry* **30**(8), 1466–1471.

Morena, M., Berardi, A., Colucci, P., Palmery, M., Trezza, V., Hill, M. N. & Campolongo, P. (2017), 'Enhancing endocannabinoid neurotransmission augments the efficacy of extinction training and ameliorates traumatic stress-induced behavioral alterations in rats', *Neuropsychopharmacology* **43**(6), 1284–1296.

Moustafa, A. A., Gilbertson, M. W., Orr, S. P., Herzallah, M. M., Servatius, R. J. & Myers, C. E. (2013), 'A model of amygdala–hippocampal–prefrontal interaction in fear conditioning and extinction in animals', *Brain and Cognition* **81**(1), 29–43.

Mueller, D., Bravo-Rivera, C. & Quirk, G. J. (2010), 'Infralimbic D2 receptors are necessary for fear extinction and extinction-related tone responses', *Biological Psychiatry* **68**(11), 1055–1060.

Mueller, E. M., Panitz, C., Hermann, C. & Pizzagalli, D. A. (2014), 'Prefrontal oscillations during recall of conditioned and extinguished fear in humans', *Journal of Neuroscience* **34**(21), 7059–7066.

Muench, J. & Hamer, A. M. (2010), 'Adverse effects of antipsychotic medications', *American Family Physician* **81**(5), 617–622.

Myers, K. M. & Davis, M. (2007), 'Mechanisms of fear extinction', *Molecular Psychiatry* **12**(2), 120–150.

Nair, S. S., Paré, D. & Vicentic, A. (2016), 'Biologically based neural circuit modelling for the study of fear learning and extinction', *NPJ science of learning* **1**, 16015.

Narayanan, R. T., Seidenbecher, T., Kluge, C., Bergado, J., Stork, O. & Pape, H.-C. (2007), 'Dissociated theta phase synchronization in amygdalo-hippocampal circuits during various stages of fear memory', *European Journal of Neuroscience* **25**(6), 1823–1831.

Navarro-Guerrero, N., Lowe, R. & Wermter, S. (2012), A neurocomputational amygdala model of auditory fear conditioning: a hybrid system approach, *in* 'Neural Networks (IJCNN), The 2012 International Joint Conference on', IEEE, pp. 1–8.

Nave, A. M., Tolin, D. F. & Stevens, M. C. (2012), 'Exposure therapy, D-cycloserine, and functional magnetic resonance imaging in patients with snake phobia: a randomized pilot study.', *The Journal of Clinical Psychiatry* **73**(9), 1179–1186.

Nguyen, H.-B., Parent, C., Tse, Y. C., Wong, T. P. & Meaney, M. J. (2017), 'Generalization of conditioned auditory fear is regulated by maternal effects on ventral hippocampal synaptic plasticity', *Neuropsychopharmacology* **43**, 1297–1307.

Norberg, M. M., Newins, A. R., Jiang, Y., Xu, J., Forcadell, E., Alberich, C. & Deacon, B. J. (2018), 'The scarier the better: maximizing exposure therapy outcomes for spider fear', *Behavioural and Cognitive Psychotherapy* **46**(6), 754–760.

Norris, C., Loureiro, M., Kramar, C., Zunder, J., Renard, J., Rushlow, W. & Laviolette, S. R. (2016), 'Cannabidiol modulates fear memory formation through interactions with serotonergic transmission in the mesolimbic system', *Neuropsychopharmacology* **41**(12), 2839–2850.

Onaivi, E. S., Green, M. R. & Martin, B. R. (1990), 'Pharmacological characterization of cannabinoids in the elevated plus maze.', *Journal of Pharmacology and Experimental Therapeutics* **253**(3), 1002–1009.

Oprea, T. I., Bauman, J. E., Bologa, C. G., Buranda, T., Chigaev, A., Edwards, B. S., Jarvik, J. W., Gresham, H. D., Haynes, M. K., Hjelle, B. et al. (2011), 'Drug repurposing from an academic perspective', *Drug Discovery Today: Therapeutic Strategies* **8**(3-4), 61–69.

Orozco-Cabal, L., Pollandt, S., Liu, J., Vergara, L., Shinnick-Gallagher, P. & Gallagher, J. P. (2006), 'A novel rat medial prefrontal cortical slice preparation to investigate synaptic transmission from amygdala to layer V prelimbic pyramidal neurons', *Journal of Neuroscience Methods* **151**(2), 148–158.

Orsini, C. A., Kim, J. H., Knapska, E. & Maren, S. (2011), 'Hippocampal and prefrontal projections to the basal amygdala mediate contextual regulation of fear after extinction', *Journal of Neuroscience* **31**(47), 17269–17277.

Padilla-Coreano, N., Bolkan, S. S., Pierce, G. M., Blackman, D. R., Hardin, W. D., Garcia-Garcia, A. L., Spellman, T. J. & Gordon, J. A. (2016), 'Direct ventral hippocampal-prefrontal input is required for anxiety-related neural activity and behavior', *Neuron* **89**(4), 857–866.

Pagotto, U., Marsicano, G., Cota, D., Lutz, B. & Pasquali, R. (2006), 'The emerging role of the endocannabinoid system in endocrine regulation and energy balance', *Endocrine Reviews* **27**(1), 73–100.

Paré, D., Quirk, G. J. & Ledoux, J. E. (2004), 'New vistas on amygdala networks in conditioned fear', *Journal of Neurophysiology* **92**(1), 1–9.

Parent, M. A., Wang, L., Su, J., Netoff, T. & Yuan, L.-L. (2009), 'Identification of the hippocampal input to medial prefrontal cortex in vitro', *Cerebral Cortex* **20**(2), 393–403.

Paxinos, G. & Watson, C. (1998), *The Rat Brain in Stereotaxic Coordinates, Fourth Edition*, Academic Press.

Pendyam, S., Bravo-Rivera, C., Burgos-Robles, A., Sotres-Bayon, F., Quirk, G. J. & Nair, S. S. (2013), 'Fear signaling in the prelimbic-amygdala circuit: a computational modeling and recording study', *Journal of Neurophysiology* **110**(4), 844–861.

Pereira, M. E., Rosat, R., Huang, C. H., Godoy, M. G. C. & Izquierdo, I. (1989), 'Inhibition by diazepam of the effect of additional training and of extinction on the retention of shuttle avoidance behavior in rats.', *Behavioral Neuroscience* **103**(1), 202–205.

Pompeiano, M., Palacios, J. M. & Mengod, G. (1992), 'Distribution and cellular localization of mRNA coding for 5-HT1A receptor in the rat brain: correlation with receptor binding', *Journal of Neuroscience* **12**(2), 440–453.

Popa, D., Duvarci, S., Popescu, A. T., Léna, C. & Paré, D. (2010), 'Coherent amygdalocortical theta promotes fear memory consolidation during paradoxical sleep', *Proceedings of the National Academy of Sciences* **107**(14), 6516–6519.

Purvis, L. K. & Butera, R. J. (2005), 'Ionic current model of a hypoglossal motoneuron', *Journal of Neurophysiology* **93**(2), 723–733.

Quirk, G. J. & Beer, J. S. (2006), 'Prefrontal involvement in the regulation of emotion: convergence of rat and human studies', *Current Opinion in Neurobiology* **16**(6), 723–727.

Quirk, G. J., Likhtik, E., Pelletier, J. G. & Paré, D. (2003), 'Stimulation of medial prefrontal cortex decreases the responsiveness of central amygdala output neurons', *Journal of Neuroscience* **23**(25), 8800–8807.

Quirk, G. J. & Milad, M. R. (2010), 'Neuroscience: editing out fear', *Nature* **463**(7277), 36–37.

Quirk, G. J., Russo, G. K., Barron, J. L. & Lebron, K. (2000), 'The role of ventromedial prefrontal cortex in the recovery of extinguished fear', *Journal of Neuroscience* **20**(16), 6225–6231.

Rabinak, C. A., Angstadt, M., Sripada, C. S., Abelson, J. L., Liberzon, I., Milad, M. R. & Phan, K. L. (2013), 'Cannabinoid facilitation of fear extinction memory recall in humans', *Neuropharmacology* **64**, 396–402.

Rapp, P. R. & Gallagher, M. (1996), 'Preserved neuron number in the hippocampus of aged rats with spatial learning deficits', *Proceedings of the National Academy of Sciences* **93**(18), 9926–9930.

Remick, R. A., Froese, C. & Keller, F. (1989), 'Common side effects associated with monoamine oxidase inhibitors', *Progress in Neuro-Psychopharmacology and Biological Psychiatry* **13**(3-4), 497–504.

Ressler, K. J., Rothbaum, B. O., Tannenbaum, L., Anderson, P., Graap, K., Zimand, E., Hodges, L. & Davis, M. (2004), 'Cognitive enhancers as adjuncts to psychotherapy: use of D-cycloserine in phobic individuals to facilitate extinctionof fear', *Archives of General Psychiatry* **61**(11), 1136–1144.

Resstel, L. B., Joca, S. R., Moreira, F. A., Corrêa, F. M. & Guimarães, F. S. (2006), 'Effects of cannabidiol and diazepam on behavioral and cardiovascular responses induced by contextual conditioned fear in rats', *Behavioural Brain Research* **172**(2), 294–298.

Resstel, L., Tavares, R. F., Lisboa, S. F., Joca, S. R., Correa, F. & Guimarães, F. S. (2009), '5-HT1A receptors are involved in the cannabidiol-induced attenuation of behavioural and cardiovascular responses to acute restraint stress in rats', *British Journal of Pharmacology* **156**(1), 181–188.

Richardson, R., Ledgerwood, L. & Cranney, J. (2004), 'Facilitation of fear extinction by D-cycloserine: theoretical and clinical implications', *Learning & Memory* **11**(5), 510–516.

Riediger, C., Schuster, T., Barlinn, K., Maier, S., Weitz, J. & Siepmann, T. (2017), 'Adverse effects of antidepressants for chronic pain: a systematic review and meta-analysis', *Frontiers in Neurology* **8**, 307.

Rogan, M. T., Stäubli, U. V. & LeDoux, J. E. (1997), 'Fear conditioning induces associative long-term potentiation in the amygdala', *Nature* **390**(6660), 604–607.

Rojas, P. S. & Fiedler, J. L. (2016), 'What do we really know about 5-HT1A receptor signaling in neuronal cells?', *Frontiers in Cellular Neuroscience* **10**, 272.

Romanski, L. M. & LeDoux, J. E. (1993), 'Information cascade from primary auditory cortex to the amygdala: corticocortical and corticoamygdaloid projections of temporal cortex in the rat', *Cerebral Cortex* **3**(6), 515–532.

Rosas-Vidal, L. E., Do-Monte, F. H., Sotres-Bayon, F. & Quirk, G. J. (2014), 'Hippocampal–prefrontal BDNF and memory for fear extinction', *Neuropsychopharmacology* **39**(9), 2161–2169.

Rosen, J. B. & Schulkin, J. (1998), 'From normal fear to pathological anxiety.', *Psychological Review* **105**(2), 325–350.

Rosen, R. C., Lane, R. M. & Menza, M. (1999), 'Effects of SSRIs on sexual function: a critical review', *Journal of Clinical Psychopharmacology* **19**(1), 67–85.

Roth, A. & van Rossum, M. C. (2009), Modeling synapses, *in* E. D. Schutter, ed., 'Computational modeling methods for neuroscientists', MIT Press Cambridge, MA, chapter 6, pp. 139–160.

Rothbaum, B. O., Price, M., Jovanovic, T., Norrholm, S. D., Gerardi, M., Dunlop, B., Davis, M., Bradley, B., Duncan, E. J., Rizzo, A. & Ressler, K. J. (2014), 'A randomized, double-blind evaluation of d-cycloserine or alprazolam combined with virtual reality exposure therapy for posttraumatic stress disorder in Iraq and Afghanistan war veterans', *American Journal of Psychiatry* **171**(6), 640–648.

Royer, S. & Pare, D. (2002), 'Bidirectional synaptic plasticity in intercalated amygdala neurons and the extinction of conditioned fear responses', *Neuroscience* **115**(2), 455–462.

Rudy, J., Huff, N. & Matus-Amat, P. (2004), 'Understanding contextual fear conditioning: insights from a two-process model', *Neuroscience & Biobehavioral Reviews* **28**(7), 675–685.

Rudy, J. W. & O'Reilly, R. C. (2001), 'Conjunctive representations, the hippocampus, and contextual fear conditioning', *Cognitive, Affective, & Behavioral Neuroscience* **1**(1), 66–82.

Russo, E. & Guy, G. W. (2006), 'A tale of two cannabinoids: the therapeutic rationale for combining tetrahydrocannabinol and cannabidiol', *Medical Hypotheses* **66**(2), 234–246.

Saffari, R., Teng, Z., Zhang, M., Kravchenko, M., Hohoff, C., Ambrée, O. & Zhang, W. (2017), 'NPY+-, but not PV+-GABAergic neurons mediated long-range inhibition from infra-to prelimbic cortex', *Translational Psychiatry* **6**(2), e736.

Sah, P., Faber, E. L., De Armentia, M. L. & Power, J. (2003), 'The amygdaloid complex: anatomy and physiology', *Physiological Reviews* **83**(3), 803–834.

Santini, E., Quirk, G. J. & Porter, J. T. (2008), 'Fear conditioning and extinction differentially modify the intrinsic excitability of infralimbic neurons', *Journal of Neuroscience* **28**(15), 4028–4036.

Santini, E., Sepulveda-Orengo, M. & Porter, J. T. (2012), 'Muscarinic receptors modulate the intrinsic excitability of infralimbic neurons and consolidation of fear extinction', *Neuropsychopharmacology* **37**(9), 2047–2056.

Schoenfeld, T. J., Kloth, A. D., Hsueh, B., Runkle, M. B., Kane, G. A., Wang, S. S.-H. & Gould, E. (2014), 'Gap junctions in the ventral hippocampal-medial prefrontal pathway are involved in anxiety regulation', *Journal of Neuroscience* **34**(47), 15679–15688.

Sehlmeyer, C., Schöning, S., Zwitserlood, P., Pfleiderer, B., Kircher, T., Arolt, V. & Konrad, C. (2009), 'Human fear conditioning and extinction in neuroimaging: a systematic review', *PLoS One* **4**(6), e5865.

Seidenbecher, T., Laxmi, T. R., Stork, O. & Pape, H.-C. (2003), 'Amygdalar and hippocampal theta rhythm synchronization during fear memory retrieval', *Science* **301**(5634), 846–850.

Selden, N., Everitt, B., Jarrard, L. & Robbins, T. (1991), 'Complementary roles for the amygdala and hippocampus in aversive conditioning to explicit and contextual cues', *Neuroscience* **42**(2), 335–350.

Senn, V., Wolff, S. B., Herry, C., Grenier, F., Ehrlich, I., Gründemann, J., Fadok, J. P., Müller, C., Letzkus, J. J. & Lüthi, A. (2014), 'Long-range connectivity defines behavioral specificity of amygdala neurons', *Neuron* **81**(2), 428–437.

Sherin, J. E. & Nemeroff, C. B. (2011), 'Post-traumatic stress disorder: the neurobiological impact of psychological trauma', *Dialogues in Clinical Neuroscience* **13**(3), 263–278.

Shouval, H. Z., Bear, M. F. & Cooper, L. N. (2002a), 'A unified model of NMDA receptor-dependent bidirectional synaptic plasticity', *Proceedings of the National Academy of Sciences* **99**(16), 10831–10836.

Shouval, H. Z., Castellani, G. C., Blais, B. S., Yeung, L. C. & Cooper, L. N. (2002b), 'Converging evidence for a simplified biophysical model of synaptic plasticity', *Biological Cybernetics* **87**(5-6), 383–391.

Sierra-Mercado, D., Padilla-Coreano, N. & Quirk, G. J. (2011), 'Dissociable roles of prelimbic and infralimbic cortices, ventral hippocampus, and basolateral amygdala in the expression and extinction of conditioned fear', *Neuropsychopharmacology* **36**(2), 529–538.

Silveira Filho, N. G. & Tufik, S. (1981), 'Comparative effects between cannabidiol and diazepam on neophobia, food intake and conflict behavior.', *Research Communications in Psychology, Psychiatry & Behavior* **6**, 25–26.

Sinclair, L. I., Christmas, D. M., Hood, S. D., Potokar, J. P., Robertson, A., Isaac, A., Srivastava, S., Nutt, D. J. & Davies, S. J. C. (2009), 'Antidepressant-induced jitteriness/anxiety syndrome: systematic review', *British Journal of Psychiatry* **194**(06), 483–490.

Sirota, A., Montgomery, S., Fujisawa, S., Isomura, Y., Zugaro, M. & Buzsáki, G. (2008), 'Entrainment of neocortical neurons and gamma oscillations by the hippocampal theta rhythm', *Neuron* **60**(4), 683–697.

Song, C., Stevenson, C. W., Guimaraes, F. S. & Lee, J. L. (2016), 'Bidirectional effects of cannabidiol on contextual fear memory extinction', *Frontiers in Pharmacology* **7**, 493.

Sotres-Bayon, F. & Quirk, G. J. (2010), 'Prefrontal control of fear: more than just extinction', *Current Opinion in Neurobiology* **20**(2), 231–235.

Sotres-Bayon, F., Sierra-Mercado, D., Pardilla-Delgado, E. & Quirk, G. J. (2012), 'Gating of fear in prelimbic cortex by hippocampal and amygdala inputs', *Neuron* **76**(4), 804–812.

Squire, L. R. & Zola, S. M. (1996), 'Structure and function of declarative and nondeclarative memory systems', *Proceedings of the National Academy of Sciences* **93**(24), 13515–13522.

Stahl, S. M., Grady, M. M., Moret, C. & Briley, M. (2005), 'SNRIs: the pharmacology, clinical efficacy, and tolerability in comparison with other classes of antidepressants', *CNS Spectrums* **10**(09), 732–747.

Steckler, T. & Risbrough, V. (2012), 'Pharmacological treatment of PTSD–established and new approaches', *Neuropharmacology* **62**(2), 617–627.

Stern, C. A., da Silva, T. R., Raymundi, A. M., de Souza, C. P., Hiroaki-Sato, V. A., Kato, L., Guimarães, F. S., Andreatini, R., Takahashi, R. N. & Bertoglio, L. J. (2017), 'Cannabidiol disrupts the consolidation of specific and generalized fear memories via dorsal hippocampus CB1 and CB2 receptors', *Neuropharmacology* **125**, 220–230.

Stern, C. A., Gazarini, L., Takahashi, R. N., Guimaraes, F. S. & Bertoglio, L. J. (2012), 'On disruption of fear memory by reconsolidation blockade: evidence from cannabidiol treatment', *Neuropsychopharmacology* **37**(9), 2132–2142.

Stern, C. A., Gazarini, L., Vanvossen, A. C., Zuardi, A. W., Galve-Roperh, I., Guimaraes, F. S., Takahashi, R. N. & Bertoglio, L. J. (2015), 'Δ 9-tetrahydrocannabinol alone and combined with cannabidiol mitigate fear memory through reconsolidation disruption', *European Neuropsychopharmacology* **25**(6), 958–965.

Stern, C., Gazarmi, L., Vanvossen, A., Zuardi, A., Guimarães, F., Takahashi, R. & Bertoglio, L. (2014), 'Involvement of the prelimbic cortex in the disruptive effect of cannabidiol on fear memory reconsolidation', *European Neuropsychopharmacology* **24**, S322.

Stevenson, C. W., Spicer, C. H., Mason, R. & Marsden, C. A. (2009), 'Early life programming of fear conditioning and extinction in adult male rats', *Behavioural Brain Research* **205**(2), 505–510.

Stewart, C. L. & Wrobel, T. A. (2009), 'Evaluation of the efficacy of pharmacotherapy and psychotherapy in treatment of combat-related post-traumatic stress disor-

der: a meta-analytic review of outcome studies', *Military Medicine* **174**(5), 460–469.

Stimberg, M., Goodman, D. F., Benichoux, V. & Brette, R. (2014), 'Equation-oriented specification of neural models for simulations', *Frontiers in Neuroinformatics* **8**, 6.

Strange, B. A., Witter, M. P., Lein, E. S. & Moser, E. I. (2014), 'Functional organization of the hippocampal longitudinal axis', *Nature Reviews Neuroscience* **15**(10), 655–669.

Strobel, C., Marek, R., Gooch, H. M., Sullivan, R. K. & Sah, P. (2015), 'Prefrontal and auditory input to intercalated neurons of the amygdala', *Cell Reports* **10**(9), 1435–1442.

Tamam, L. & Ozpoyraz, N. (2002), 'Selective serotonin reuptake inhibitor discontinuation syndrome: a review', *Advances in Therapy* **19**(1), 17–26.

Tamura, M., Spellman, T. J., Rosen, A. M., Gogos, J. A. & Gordon, J. A. (2017), 'Hippocampal-prefrontal theta-gamma coupling during performance of a spatial working memory task', *Nature Communications* **8**(1), 2182.

Taylor, S., Thordarson, D. S., Maxfield, L., Fedoroff, I. C., Lovell, K. & Ogrodniczuk, J. (2003), 'Comparative efficacy, speed, and adverse effects of three PTSD treatments: exposure therapy, EMDR, and relaxation training.', *Journal of Consulting and Clinical Psychology* **71**(2), 330–338.

Terzian, A. L. B., dos Reis, D. G., Guimarães, F. S., Corrêa, F. M. & Resstel, L. B. (2014), 'Medial prefrontal cortex Transient Receptor Potential Vanilloid Type 1 (TRPV1) in the expression of contextual fear conditioning in Wistar rats', *Psychopharmacology* **231**(1), 149–157.

Thiemann, G., Watt, C. A., Ledent, C., Molleman, A. & Hasenöhrl, R. U. (2009), 'Modulation of anxiety by acute blockade and genetic deletion of the CB1 cannabinoid receptor in mice together with biogenic amine changes in the forebrain', *Behavioural Brain Research* **200**(1), 60–67.

Tierney, P. L., Degenetais, E., Thierry, A.-M., Glowinski, J. & Gioanni, Y. (2004), 'Influence of the hippocampus on interneurons of the rat prefrontal cortex', *European Journal of Neuroscience* **20**(2), 514–524.

Tovote, P., Fadok, J. P. & Lüthi, A. (2015), 'Neuronal circuits for fear and anxiety', *Nature Reviews Neuroscience* **16**(6), 317–331.

Uribe-Marino, A., Francisco, A., Castiblanco-Urbina, M. A., Twardowschy, A., Salgado-Rohner, C. J., Crippa, J. A. S., Hallak, J. E. C., Zuardi, A. W. & Coimbra, N. C. (2012), 'Anti-aversive effects of cannabidiol on innate fear-induced behaviors evoked by an ethological model of panic attacks based on a prey vs the wild snake Epicrates cenchria crassus confrontation paradigm', *Neuropsychopharmacology* **37**(2), 412–421.

Uylings, H. B. & van Eden, C. G. (1990), 'Qualitative and quantitative comparison of the prefrontal cortex in rat and in primates, including humans', *Progress in Brain Research* **85**, 31–62.

Van Aerde, K. I., Heistek, T. S. & Mansvelder, H. D. (2008), 'Prelimbic and infralimbic prefrontal cortex interact during fast network oscillations', *PLoS One* **3**(7), e2725.

Van de Kar, L., Piechowski, R. A., Rittenhouse, P. A. & Gray, T. S. (1991), 'Amygdaloid lesions: differential effect on conditioned stress and immobilization-induced increases in corticosterone and renin secretion', *Neuroendocrinology* **54**(2), 89–95.

VanElzakker, M. B., Dahlgren, M. K., Davis, F. C., Dubois, S. & Shin, L. M. (2014), 'From Pavlov to PTSD: the extinction of conditioned fear in rodents, humans, and anxiety disorders', *Neurobiology of Learning and Memory* **113**, 3–18.

Varela, C., Kumar, S., Yang, J. & Wilson, M. (2014), 'Anatomical substrates for direct interactions between hippocampus, medial prefrontal cortex, and the thalamic nucleus reuniens', *Brain Structure and Function* **219**(3), 911–929.

Vertes, R. P. (2004), 'Differential projections of the infralimbic and prelimbic cortex in the rat', *Synapse* **51**(1), 32–58.

Vertes, R. P. (2006), 'Interactions among the medial prefrontal cortex, hippocampus and midline thalamus in emotional and cognitive processing in the rat', *Neuroscience* **142**(1), 1–20.

Vertes, R. P., Hoover, W. B., Szigeti-Buck, K. & Leranth, C. (2007), 'Nucleus reuniens of the midline thalamus: link between the medial prefrontal cortex and the hippocampus', *Brain Research Bulletin* **71**(6), 601–609.

Vervliet, B., Craske, M. G. & Hermans, D. (2013), 'Fear extinction and relapse: state of the art', *Annual Review of Clinical Psychology* **9**, 215–248.

Vidal-Gonzalez, I., Vidal-Gonzalez, B., Rauch, S. L. & Quirk, G. J. (2006), 'Microstimulation reveals opposing influences of prelimbic and infralimbic cortex on the expression of conditioned fear', *Learning & memory Memory* **13**(6), 728–733.

Vierling-Claassen, D., Cardin, J., Moore, C. I. & Jones, S. R. (2010), 'Computational modeling of distinct neocortical oscillations driven by cell-type selective optogenetic drive: separable resonant circuits controlled by low-threshold spiking and fast-spiking interneurons', *Frontiers in Human Neuroscience* **4**, 198.

Vlachos, I., Herry, C., Lüthi, A., Aertsen, A. & Kumar, A. (2011), 'Context-dependent encoding of fear and extinction memories in a large-scale network model of the basal amygdala', *PLoS Computational Biology* **7**(3), e1001104.

Vriens, J., Appendino, G. & Nilius, B. (2009), 'Pharmacology of vanilloid transient receptor potential cation channels', *Molecular Pharmacology* **75**(6), 1262–1279.

Wang, M. E., Yuan, R. K., Keinath, A. T., Álvarez, M. M. R. & Muzzio, I. A. (2015), 'Extinction of learned fear induces hippocampal place cell remapping', *Journal of Neuroscience* **35**(24), 9122–9136.

Wang, Q., Jin, J. & Maren, S. (2016), 'Renewal of extinguished fear activates ventral hippocampal neurons projecting to the prelimbic and infralimbic cortices in rats', *Neurobiology of Learning and Memory* **134**, 38–43.

Werner-Seidler, A. & Richardson, R. (2007), 'Effects of D-cycloserine on extinction: consequences of prior exposure to imipramine', *Biological Psychiatry* **62**(10), 1195–1197.

White, N. C., Litovitz, T. & Clancy, C. (2008), 'Suicidal antidepressant overdoses: a comparative analysis by antidepressant type', *Journal of Medical Toxicology* **4**(4), 238–250.

Wiltgen, B. J. (2006), 'Context fear learning in the absence of the hippocampus', *Journal of Neuroscience* **26**(20), 5484–5491.

Wittchen, H.-U., Jacobi, F., Rehm, J., Gustavsson, A., Svensson, M., Jönsson, B., Olesen, J., Allgulander, C., Alonso, J., Faravelli, C. et al. (2011), 'The size and burden of mental disorders and other disorders of the brain in Europe 2010', *European Neuropsychopharmacology* **21**(9), 655–679.

Wolitzky-Taylor, K. B., Horowitz, J. D., Powers, M. B. & Telch, M. J. (2008), 'Psychological approaches in the treatment of specific phobias: a meta-analysis', *Clinical Psychology Review* **28**(6), 1021–1037.

Yamamoto, Y., Välitalo, P. A., van den Berg, D.-J., Hartman, R., van den Brink, W., Wong, Y. C., Huntjens, D. R., Proost, J. H., Vermeulen, A., Krauwinkel, W. et al. (2017), 'A generic multi-compartmental CNS distribution model structure for 9 drugs allows prediction of human brain target site concentrations', *Pharmaceutical Research* **34**(2), 333–351.

Yang, C. R., Seamans, J. K. & Gorelova, N. (1996), 'Electrophysiological and morphological properties of layers V-VI principal pyramidal cells in rat prefrontal cortex in vitro', *Journal of Neuroscience* **16**(5), 1904–1921.

Yeung, M., Treit, D. & Dickson, C. T. (2012), 'A critical test of the hippocampal theta model of anxiolytic drug action', *Neuropharmacology* **62**(1), 155–160.

Young, S. L., Bohenek, D. L. & Fanselow, M. S. (1994), 'NMDA processes mediate anterograde amnesia of contextual fear conditioning induced by hippocampal

damage: immunization against amnesia by context preexposure.', *Behavioral Neuroscience* **108**(1), 19–29.

Zelinski, E. L., Hong, N. S., Tyndall, A. V., Halsall, B. & McDonald, R. J. (2010), 'Prefrontal cortical contributions during discriminative fear conditioning, extinction, and spontaneous recovery in rats', *Experimental Brain Research* **203**(2), 285–297.

Zhang, W.-N., Bast, T., Xu, Y. & Feldon, J. (2014), 'Temporary inhibition of dorsal or ventral hippocampus by muscimol: distinct effects on measures of innate anxiety on the elevated plus maze, but similar disruption of contextual fear conditioning', *Behavioural Brain Research* **262**, 47–56.

Zhu, H., Pleil, K. E., Urban, D. J., Moy, S. S., Kash, T. L. & Roth, B. L. (2014), 'Chemogenetic inactivation of ventral hippocampal glutamatergic neurons disrupts consolidation of contextual fear memory', *Neuropsychopharmacology* **39**(8), 1880–1892.

Zuardi, A. W., Rodrigues, N. P., Silva, A. L., Bernardo, S. A., Hallak, J. E., Guimarães, F. S. & Crippa, J. A. (2017), 'Inverted U-shaped dose-response curve of the anxiolytic effect of cannabidiol during public speaking in real life', *Frontiers in Pharmacology* **8**, 259.